UNIVERSITY OF INSUBRIA

Department of Science and High Technology

Como, Italy

Ph.D. Course in Environmental Sciences and Chemistry

XXXV Cycle

Development of temporal and spatial models for predicting the fate of chemicals in a multimedia environment

Parisa Falakdin

Supervisor: Prof. Antonio DI GUARDO

Co-supervisor: Prof. Elisa TERZAGHI

January 2023

To Parvin, Manouchehr, Pouya & Obada

Table of Contents

1. INTRODUCTION

1.1. Spatial environmental fate modeling

Environmental fate models (EFM) or Mackay-type models (Mackay, 2001) are important tools to assess the fate of organic chemicals in the environment. They perform mass balance calculations for various environmental processes from the release of a contaminant into the environment incorporating chemical and environmental properties. Therefore, they provide the prediction of contamination levels in various environmental compartments such as soil, water, vegetation, and air. These models were also used for the risk assessment of chemicals (ECHA, 2020; RIVM, 2004). Figure 1 shows the "unit of world" as explained by Mackay, (1979) and illustrates different environmental media within a box model.

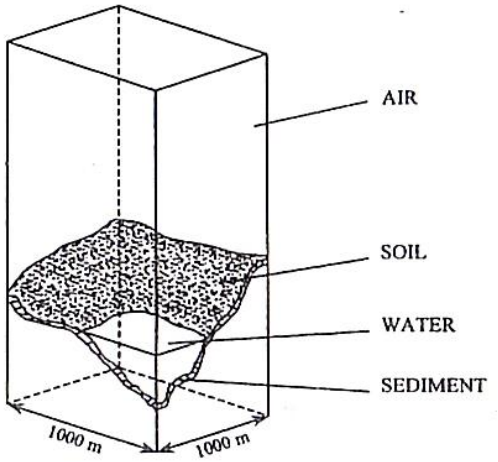

Figure 1 unite of world (Mackay, 1979).

Challenges and advancements regarding environmental modelling were reviewed in a recent paper (Di Guardo et al., 2018). A common assumption in EFMs is spatial homogeneity. Even though this assumption is useful in a variety of scenarios where

the spatial variation does not play a considerable role in the fate and transport of contaminants, in an environment where these variations are significant, this assumption will result in under/overestimation of the real world. Therefore, there is a need for including higher ecological realism in current modeling structures and simulation scenarios. Among all the incorporation of spatial inhomogeneity into modeling (Di Guardo et al., 2018; Di Guardo and Hermens, 2013) is of utmost importance.

Spatial variation can be due to source strength (i.e., the proximity and accessibility of locations from an emission source) as well as environmental characteristics (e.g., organic carbon, soil texture, vegetation cover, etc.) that causes differences in fate processes and results in non-uniform distribution of concentrations in the environment (Wania, 1996).

Different approaches in modeling have been performed so far to target spatial variations in multimedia fate models. For example, the integration of an atmospheric model into an EFM to account for advection and dispersion processes in the atmosphere. The most common example of this type of model is the Gaussian model which calculates the concentration of a chemical released from a point source emission where the emission rate and meteorological conditions are constant.

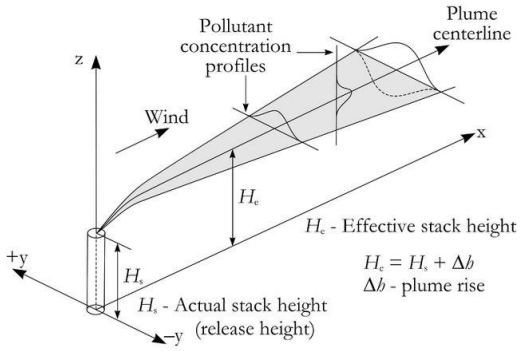

Figure 2 Scheme of a Gaussian model (Leelossy et al., 2014).

Atmospheric models can predict a high temporal and spatial resolution of chemical concentrations in the air. The results can be incorporated within an EFM system for further calculation concerning multimedia processes.

Another way to address spatial variability within an EFM model is the integration of a Geographical Information System (GIS) to allocate different geographic features for different locations. Examples of such models are two versions of spatial SoilPlus (Falakdin et al., 2022; Ghirardello et al., 2014).

Finally, a spatial multimedia fate model accounts for spatial variability within the EFM framework. For example, IMPACT-2002 (Pennington et al., 2005), A multimedia multi-pathway model that estimates the concentration and level of contaminants in the air, water, soil, sediments, and vegetation.

Different modelling approaches implemented so far that account for the spatial heterogeneity of environments were studied. A chronological revision was performed to explore their major features and characteristics. Additionally, the models were evaluated in three different aspects of spatial, temporal, and chemical domains. This was the focus of my first paper (i.e., **Paper I**) titled “Spatially resolved environmental fate models: A review” published in Chemosphere journal.

1.2. Model development

During their lifetime in the global environment, chemicals such as persistent organic pollutants (POPs) undergo various processes of volatilization, diffusion, advection, deposition, and runoff that occur among environmental compartments. POPs' behaviour and their fate processes have been subject to various fate models in order to predict their movements and assess their environmental concentration levels. Advances in this concept achieved such as accounting for temporal and spatial variabilities, incorporation of plant-related processes, and integration with other environmental models and platforms.

SoilPlusVeg (SPV) is a dynamic multimedia fugacity-based model that characterized vegetation compartments such as roots, stems, and leaves along with their corresponding processes within the multimedia fate modelling framework. SPV includes air, vegetation, and soil media that each consist of a number of compartments. For each compartment, a fugacity capacity is considered and is described by Z values (mol/m^3 Pa). Additionally, transport and transformation processes are described using D values (mol/Pa h) (Ghirardello et al., 2010; Terzaghi et al., 2017). SPV model performance and sensitivity analysis were previously explained (Terzaghi et al., 2017).

SPV model was developed in Visual Basic version 6.0 and integrates a GIS tool (MapWindow v. 5.6.3, MapWindow.org) to interrogate and retrieve geographical information. Figure 3 illustrates the SPV model as well as the different compartments and processes that occur among them.

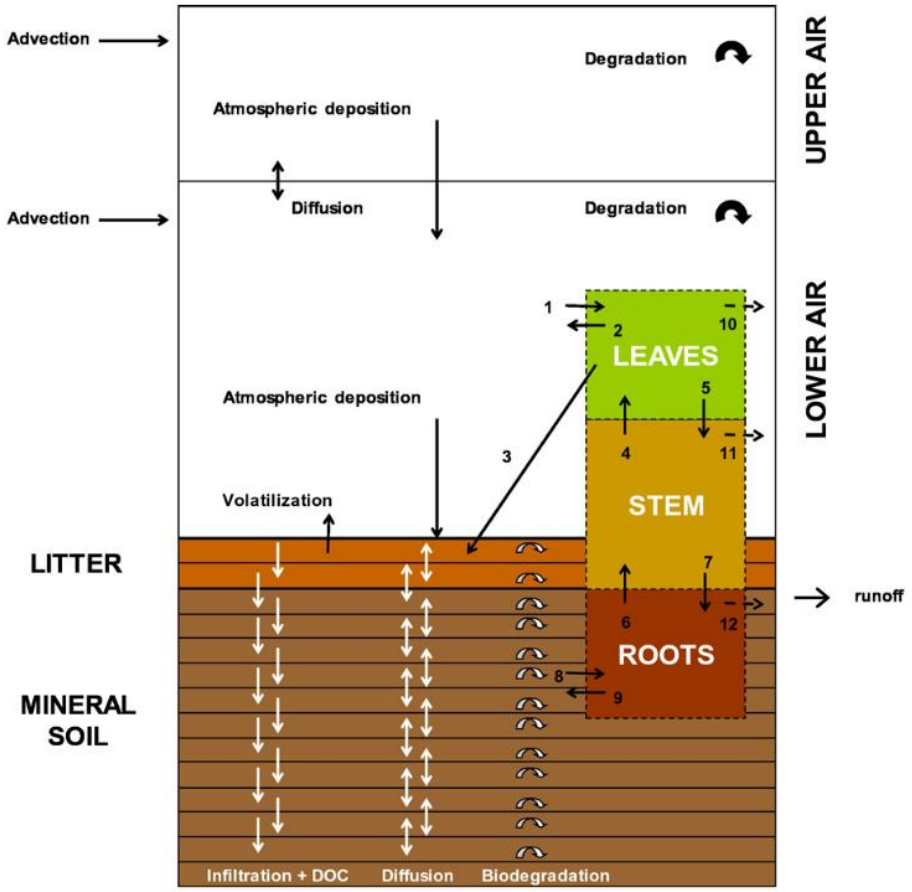

Figure 3 Compartments and processes included in the mass-balance calculations of SPV (Terzaghi et al., 2017).

As mentioned in section 1.1., one of the objectives of environmental modelling advancements is the inclusion of spatial differences within the models in order to increase the realism of modelling and simulation scenarios. Therefore, the SPV model was further developed, in this Ph.D. project, into a spatially and temporally resolved multimedia fate model by adding a grid system where each grid cell acts as an SPV unit. This new version of the model is called Gridded-SoilPlusVeg (GSPV).

In GSPV one of the the spatial featured of the environment is introduced by adding directional advective wind and its propagation within the grid to account for the effect of source strength and dynamic and multi-directional atmospheric transport. Moreover, the GIS system was used to introduce different vegetation cover properties for each cell. The GSPV model is dynamic (similar to SPV) in input environmental parameters such as meteorological data, vegetation parameters, and emission rates. Mass-balance calculations are performed up to a temporal resolution of a second and the results are provided on an hourly basis.

The primary implementation of the GSPV model was for the simulation of a contaminated site of national relevance (SIN Pieve Vergonte) in Ossola Valley. The levels of DDTs found in fish species in one of the largest lakes in northern Italy, Lake Maggiore during a monitoring campaign, were higher than the legal threshold of food (up to mg/kg fresh weight) (Ceschi et al., 1996). The reason for this elevated level of contamination was related to the discharge of a chemical plant that produced DDTs for around 50 years (1948 to 1996). Some of these contaminants were directly discharged into the Toce river (one of the tributaries of Lake Maggiore). The production of DDTs was stopped in 1996 after the ban on DDTs production by Italian regulations. However, the area surrounding the chemical plant along with Lake Maggiore were heavily affected and the passive emission of DDTs into the atmosphere was not stopped for the following decades.

Therefore, the area surrounding the chemical plant was considered for the simulation using the GSPV model. The objective was to predict the fate and transport of DDT for 100 years starting from the year of production (1948) within

the local scale region in order to know how the fate of this contaminant has evolved during the years of DDT production as well as following years. Plus, to estimate the time required for the contamination to clean up through degradation.

Several sampling campaigns were conducted between 2001 and 2011 and various samples of soil, leaves, and litter was collected. Samples were analyzed for DDTs concentrations and used for the comparison and validation with model predictions for the corresponding years. The results of this work, including model development, simulation, and result comparisons were published in Science of the Total Environment journal, **Paper II**, titled "Predicting the regional contamination evolution of DDT for 100-years with a new gridded spatial and dynamic multimedia fate model".

Moreover, the regional environment, an area of 200km X 200km, including an area of southern Switzerland and Northern Italy was simulated for further validation of the model and to predict the fate of a local DDT contamination source on a larger scale. The objective of this second simulation was also to calculate the amount of DDT deposition fluxes over years into the lakes located in the study area (i.e., Lake Maggiore, Lake Lugano, and Lake Como). The deposition value relating to Lake Maggiore was then utilized for a dynamic Lake model simulation in order to identify the potential lake contamination level caused by atmospheric transport and deposition. The results of simulations were compared with the monitoring and literature data. This study is in preparation and the manuscript is provided under section **Paper III**, titled "Predicting the contribution of a local emission source in

mid-range transport of DDTs and their deposition in terrestrial and aquatic ecosystems".

1.3. Microplastic measurements and analysis

Microplastics (MPs) have become a global concern since plastic production has been increasing in the last 60 years and reached up to 367 million tons in 2020 (PlasticsEurope, 2021). Plastic materials smaller than 5 mm have been considered as "Microplastics" (Barnes et al., 2009). Different sources of MPs include the corrosion of larger plastics as secondary source of microplastics as well as the produced microplastics (e.g., cosmetics) as the primary source. Various studies have been conducted to investigate reliable methodologies to analyse and quantify microplastics in marine environments (López-Rosales et al., 2022a, 2022b, 2021), however, a few are accounting for the impact of these pollutants in other environmental media such as the atmosphere and terrestrial vegetation. This is while MPs are considered an emerging airborne pollutant and exposure through inhalation can have a great impact on human health. Amato-Lourenço et al., (2020) have reviewed microplastics as airborne inhalant toxicants and pathogens with indoor and outdoor sources and their effect on human health. There is still a vast need for further investigation of these particles in the atmosphere and their behaviour such as deposition, transport, and distribution in the environment.

Due to the large number of MPs in environmental samples, quantifying the characteristics of these particles reliably and in a reasonable amount of time is a challenging task. It can take plenty of time to quantify microplastics using traditional infrared (IR) spectroscopy and/or microspectroscopy. This method

which involves the collection of the full spectrum at specific points is not time efficient for the levels of microplastics found in the environmental samples.

Recently, a device called ‘Laser Direct Infrared Imaging’ (LDIR) was developed by Agilent company (USA) that can provide a good resolution for the detection of very thin particles in a matter of a second (Hildebrandt et al., 2020).

Agilent 8700 LDIR instrument, integrated with Agilent Clarity software, automatically identifies and measures particles up to 10 μm in diameter. The number of the total particles along with information about the length, width, height, diameter, aspect ratio, area, perimeter, eccentricity, circularity, and solidity are extracted. Different libraries, including the library provided by Agilent itself, can be used for the identification of particles. Additionally, the software provides the quality of the matching spectra for each detected particle as a percentage.

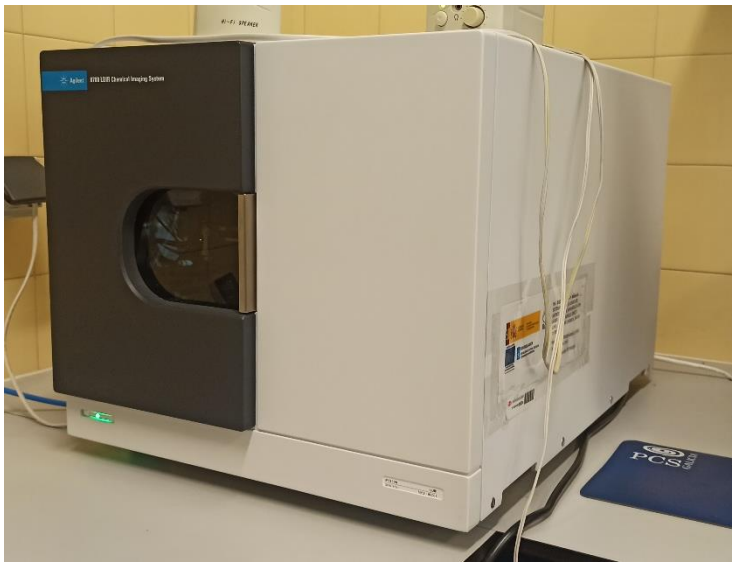

Figure 4 Agilent 8700 LDIR Chemical Imaging System.

A research project is carried out by the *University of A Coruña* on the measurements of atmospheric depositions of microplastics using bulk depositors.

Several air samples were collected using bulk samplers in a remote area. Samples were collected including total suspended particles, dry and wet deposition, and dust deposition, and went through pre-treatment and identification processes. Additionally, samples of leaves were collected as passive air samplers for comparison reasons.

Since the analysis of airborne microplastics is a relatively new topic and identification of these particles on leaves has not been performed previously, this work is considered as a preliminary investigation on sample pre-treatments and analysis of these polymers in air and leaf media.

The **Paper IV** provides information about air and leaves samples from preparations to identification and characterization of microplastics conducted during my stay at the *University of A Coruña* as a visiting Ph.D.

1.4. Collaborative papers

In collaboration with other researchers of the Environmental Modeling Group (EMG), a study was performed with the objective of investigating rain samples, as a proxy of air concentrations, and SPME analysis as a tool to study the spatial and temporal variability of atmospheric levels of PAHs in an urban environment. A historical data collection for temporally and spatially resolved PAH concentration in air and rainfall was performed as an initial dataset for model calibration and validation of the results. This study was published in the Science of the Total Environment journal, **Paper V**, titled "Estimating temporal and spatial levels of PAHs in the air using rain samples and SPME analysis: Feasibility evaluation in an urban scenario".

Another collaboration on newly discovered soil contaminants (i.e., sulfonated and hydroxy-sulfonated PCBs) by the EMG was performed. Collaboration was done as part of the laboratory analysis of soil samples. This paper was published in Environmental Pollution journal, titled "Bioaccumulation of PCBs and their hydroxy and sulfonated metabolites in earthworms: Comparing lab and field results", **Paper VI.**

2. OBJECTIVE OF THE THESIS

Some of the important challenges in the prediction of risk for ecological systems are considered as:

a) the use of temporally and spatially resolved data for the chemical emissions instead of generic annual (or steady) values.

b) incorporating different environmental properties depending on the characteristics of each geographical location;

c) the development of environmental fate models capable of predicting time and space variable chemical concentrations. The current study focus on the following goals:

1. To perform an overview of the spatially resolved environmental models in order to highlight their importance and to survey the methods and advancements carried out so far in accounting for spatial variations in environmental models.
2. The development of a gridded spatial and temporal dynamic fate model for the prediction of organic chemicals in the environment where different representative environmental characteristics (e.g., vegetation cover) can be allocated to each grid. Moreover, to account for the effects of directional advective wind on the spread of contamination in the regional environment.
3. To apply the model developed on different real-world scenarios and predict the fate of organic chemicals in time and space. The simulation results must agree with the monitoring data of the corresponding time and location.
4. To utilize the latest available technology for the growing issue of microplastics

in the atmosphere. Moreover, to implement an initial sample treatment method for terrestrial leaves, as passive air sampler and an index of atmospheric contamination.

3. STRUCTURE OF THE THESIS

This thesis is based on the following papers, referred to in the text by their Roman numerals:

I. Falakdin P., Terzaghi E., Di Guardo A., 2022. Spatially resolved environmental fate models: A Review. Chemosphere. 290, 0045-6535. https://doi.org/10.1016/j.chemosphere.2021.133394

II. Falakdin P., Terzaghi E., Raspa G., Di Guardo A., 2022. Predicting the regional contamination evolution of DDT for 100-years with a new gridded spatial and dynamic multimedia fate model. Sci. Total Environ. 845, 0048-9697. http://dx.doi.org/10.1016/j.scitotenv.2022.157190

III. Falakdin P., Terzaghi E., Di Guardo A. Predicting the contribution of a local emission source in mid-range transport of DDTs and their deposition in terrestrial and aquatic ecosystems. Submitted to Science of the Total Environment.

IV. Falakdin P., Lopez-Rosales A., Muniategui Lorenzo S.N., Andrade J., Di Guardo A., Characterization of microplastics in atmospheric and foliage samples. In preparation.

V. Terzaghi E., Falakdin P., Fattore E., Di Guardo A., 2020. Estimating

temporal and spatial levels of PAHs in air using rain samples and SPME analysis: Feasibility evaluation in an urban scenario. Sci. Total Environ. 762, 0048-9697. https://doi.org/10.1016/j.scitotenv.2020.144184

VI. Palladini J., Bagnati R., Passoni A., Davoli E., Lanno A., Terzaghi E, Falakdin P., Di Guardo A., 2022. Bioaccumulation of PCBs and their hydroxy and sulfonated metabolites in earthworms: Comparing lab and field results. Environ. Pollut. 293, 0269-7491. https://doi.org/10.1016/j.envpol.2021.118507

4. SUMMARY OF RESULTS

PAPER I

Spatially resolved environmental models are important tools to introduce and highlight the spatial variability of the real world into modeling. Although various spatial models have been developed so far, yet the development and evaluation of these models remain a challenging task due to several difficulties related to model setup, computational cost, and obtaining high-resolution input data (e.g., monitoring and emission data). For example, atmospheric transport models can be used when high resolution predicted concentrations in atmospheric compartments are required, while spatial multimedia fate models may be preferred for regulatory risk assessment, life cycle impact assessment of chemicals, or when the partitioning of chemical substances in a multimedia environment is considered. The goal of this paper is to review and compare different spatially resolved environmental models, according to their spatial, temporal and chemical domains, with a closer insight into spatial multimedia fate models, to achieve a better understanding of their strengths and limitations. This review also points out several requirements for further improvement of existing models as well as for their integration.

PAPER II

In 1996 high dichlorodiphenyltrichloroethane (DDT) concentrations were found in Lake Maggiore (Italy) fish and sediments. DDT was produced by a chemical company located in a subalpine valley (Ossola valley, Piedmont Region, Italy), and ended up in the Toce River, a tributary of Lake Maggiore. In the area surrounding the chemical plant, high DDT concentrations in soil and vegetation were found after subsequent investigations. The quantification of the release from contaminated soil and the following migration toward downwind areas, deposition to the soil, and further evaporation plays an important role in understanding future DDT trends in soil and the atmosphere. To study this phenomenon, soil, and vegetation from Ossola Valley were monitored in 2001 and 2011. The concentration values obtained (soils: 0.05 to 1 μg/g; vegetation 2–100 ng/g), allowed to reconstruct the contamination gradient in the valley and were used to develop and calibrate a spatially resolved multimedia fugacity model. The model accounts for spatial and temporal dynamicity of environmental characteristics such as wind speed and direction, variable air compartment height etc., and simulates the fate and transport of chemicals on a local scale. The dynamic emission of DDT (about 13,000 kg for the 50 y production time) to the air was estimated and utilized for a 100-year simulation (from 1948 to 2048). The results obtained allowed to understand the temporal and spatial pattern of DDT contamination for a long period at a local scale as well as the potential contribution as a source potentially affecting sites at larger distances.

PAPER III

A recently developed dynamic multiple box multimedia fate model (Gridded-SoilPlusVeg) was developed and implemented to account for the environmental variation and the effect of directional advective transport of chemicals towards different compartments and geographical locations. A chemical plant located in Pieve Vergonte in Ossola valley produced and emitted DDTs for around 50 years. In the previous study the fate and transport of p,p'-DDT emitted from the chemical plant were evaluated in nearby areas (up to 12 km). In this paper, the Gridded-SoilPlusVeg model was run for p,p'-DDT during and decades after the cease of production (a total of 100 years) for a larger study area (200 km x 200 km) in order to evaluate the contribution of a local source on a larger scale. Additionally, the deposition fluxes into the lakes were calculated and were used as input into a dynamic fugacity-based aquatic model to calculate DDT concentration in water and sediments of Lake Maggiore. The results of the simulations were compared with the monitoring and literature data. The results obtained from the spatial fate model, Gridded-SoilPlusVeg, allowed to estimate the atmospheric deposition fluxes and identify a potential cause for the high level of contamination in terrestrial and aquatic ecosystems on a regional scale.

Paper IV

The growing trend of plastic production in recent years has raised concerns regarding microplastic-related environmental issues. Microplastic particles go through transport and deposition processes and end in different environmental media and food chains. In this report, atmospheric and leaf samples were collected and analyzed for the presence and quantity of identified microplastics. This work represents the methodologies used for pre-treatments and identification of microplastic using laser direct infrared spectroscopy. The pre-treatment process included washing, extraction, concentration, and transfer of the samples into the reflective slides. Microplastics then were identified by infrared spectroscopy based on their features such as size (area, width, height, and diameter), circularity, solidity, polymer composition, and matching quality. The results are illustrated for each sample, and in comparison, with each other indicating a good agreement between atmospheric and leaf samples despite the fact that they were collected at different times and locations.

PAPER V

There is a growing interest in evaluating the role of concentration changes of contaminants in temporal and spatial gradients. This is often relevant for fast moving environmental phases such as air and water. In this paper, small volumes of rainwater were sampled as a proxy for air concentrations of Polycyclic Aromatic Hydrocarbons (PAHs): rain was collected in three sampling sites (high traffic, restricted traffic and a low traffic zone) in Como. Solid phase microextraction (SPME) was used for the extraction to reduce required sample volumes, allowing the acquisition of more samples in time. Rain samples highlighted a spatial and temporal variability along a traffic gradient in the Como city, especially for the most abundant PAH, e.g., phenanthrene. Air concentrations were then estimated from rain concentrations. The results show that this is a cheap and promising method, although requiring rainfall/snowfall conditions, that can be used to perform monitoring campaigns of air concentrations at a higher temporal and spatial resolution than the adopted standard methods (e.g., high-volume air samplers). The results could be employed for evaluation of the exposure, emission profiles and calibration of fate models.

PAPER VI

Sulfonated and hydroxy-sulfonated PCBs were recently discovered by our group as new PCB soil contaminants, constituting about 1% of their parent compounds in soil. Here we investigate for the first time the bio accumulation of these metabolites as well as hydroxy-PCBs and native PCBs in earthworms. A sequence of three experiments, at increasing complexity and ecological realism, were performed with four different earthworm species (*Eisenia foetida* Savigny*, Lumbricus terrestris* L, *Allolobophora chlorotica* Savigny and *Aporrectodea caliginosa* Savigny) exposed to contaminated soils. The first experiment confirmed that when exposing earthworms to soil contaminated with a single hexa-chlorinated congener (PCB 155), no formation of polar metabolites in earthworms could be detected. This allowed to plan the following two experiments, using a soil from a PCB contaminated site and rich in relatively high levels (10–130 μg kg^{-1}) of hydroxy-, sulfonated-, and hydroxysulfonated-PCBs. Bioaccumulation factors (BAFs) and bioconcentration factors (BCFs) were then obtained in the second and third experiments, to compare the accumulation behavior of these chemicals in laboratory and natural conditions. Regressions between BAF/BCF and Log Kow/Log D, produced a variety of results, being generally significant between BCF and PCBs and not significant in the other cases. In general, the metabolites accumulated in earthworms with detectable concentrations in their tissues (8–115 μg kg^{-1}), although sulfonated and hydroxy-sulfonated PCBs showed BAF and BCF values lower (up to two orders of magnitude) than those calculated for the parent PCBs, given their lower lipophilicity.

5. ACKNOWLEDGEMENTS

First, I would like to thank Prof. Di Guardo for allowing me to carry out my Ph.D. with a scholarship, for believing in me, and for giving me the opportunity to continue the path that was quite different than my background.

Thanks to Prof. Terzaghi who guided me through these three years offering me her scientific supervision and guidance from laboratory experiments to research documentation.

I thank the Environmental Modeling Group's students and friends (Gianmaria, Alessia, and Jessica) for their friendship and support during these years as well as their collaborations in sample analysis and laboratory experiments.

I would like to thank the University of A Coruña (UDC) Department of Science, Prof. Muniategui Lorenzo, and Prof. Andrade, for hosting me as a visiting Ph.D. student and providing me with the necessary materials, instructions, and assistance for my experiments on microplastics.

Thanks to Adrian for all the guidance and training with laboratory protocols and results analysis of microplastics during my stay at UDC.

Last but not least, thanks to all my family for always being there during these years, for their continuous support and endurance of not being able to visit them. No matter what happened in the world, the pandemic, the unstable situation of my country, and other problems along the way, they did everything they could to always charge me with positive energy and gave nothing but love and support. Special thanks to Obada for having "endured" me for the entirety of this journey, and for his courage and love.

Thanks to my best friends Samin and Sanaz, even though we haven't seen each other for years, you've always been there in times of need.

6. References

Allen, S., Allen, D., Phoenix, V.R., Le Roux, G., Durántez Jiménez, P., Simonneau, A., Binet, S., Galop, D., 2019. Atmospheric transport and deposition of microplastics in a remote mountain catchment. Nat. Geosci. 12, 339–344. https://doi.org/10.1038/s41561-019-0335-5

Amato-Lourenço, L.F., dos Santos Galvão, L., de Weger, L.A., Hiemstra, P.S., Vijver, M.G., Mauad, T., 2020. An emerging class of air pollutants: Potential effects of microplastics to respiratory human health? Sci. Total Environ. 749, 141676. https://doi.org/10.1016/j.scitotenv.2020.141676

Barnes, D.K.A., Galgani, F., Thompson, R.C., Barlaz, M., 2009. Accumulation and fragmentation of plastic debris in global environments. Philos. Trans. R. Soc. B Biol. Sci. 364, 1985–1998. https://doi.org/10.1098/rstb.2008.0205

Ceschi, M., De Rossa, M., Jaggli, M., 1996. Contaminanti organici, inorganici e radionuclidi nell'ittiofauna dei laghi Ceresio e Verbano (bacini svizzeri). Trav Chim Aliment Hyg 87, 189–211.

Di Guardo, A., Gouin, T., MacLeod, M., Scheringer, M., 2018. Environmental fate and exposure models: advances and challenges in 21 st century chemical risk assessment. Environ. Sci. Process. Impacts 20, 58–71. https://doi.org/10.1039/C7EM00568G

Di Guardo, A., Hermens, J.L., 2013. Challenges for exposure prediction in ecological risk assessment: Challenges in Exposure Prediction. Integr. Environ. Assess. Manag. 9, e4–e14. https://doi.org/10.1002/ieam.1442

Falakdin, P., Terzaghi, E., Raspa, G., Di Guardo, A., 2022. Predicting the regional contamination evolution of DDT for 100-years with a new gridded spatial and dynamic multimedia fate model. Sci. Total Environ. 845, 157190. https://doi.org/10.1016/j.scitotenv.2022.157190

Ghirardello, D., Morselli, M., Otto, S., Zanin, G., Di Guardo, A., 2014. Investigating the need for complex vs. simple scenarios to improve predictions of aquatic ecosystem exposure with the SoilPlus model. Environ. Pollut. 184, 502–510. https://doi.org/10.1016/j.envpol.2013.10.002

Ghirardello, D., Morselli, M., Semplice, M., Di Guardo, A., 2010. A Dynamic Model of the Fate of Organic Chemicals in a Multilayered Air/Soil System: Development and Illustrative Application. Environ. Sci. Technol. 44, 9010–9017. https://doi.org/10.1021/es1023866

Hermsen, E., Mintenig, S.M., Besseling, E., Koelmans, A.A., 2018. Quality Criteria for the Analysis of Microplastic in Biota Samples: A Critical Review. Environ. Sci. Technol. 52, 10230–10240. https://doi.org/10.1021/acs.est.8b01611

Hernandez-Gonzalez, A., Saavedra, C., Gago, J., Covelo, P., Santos, M.B., Pierce, G.J., 2018. Microplastics in the stomach contents of common dolphin (Delphinus delphis) stranded on the Galician coasts (NW Spain, 2005–2010). Mar. Pollut. Bull. 137, 526–532. https://doi.org/10.1016/j.marpolbul.2018.10.026

Hildebrandt, L., Gareb, F.E., Zimmermann, T., Klein, O., Emeis, K.-C., 2020. Fast, Automated Microplastics Analysis Using Laser Direct Chemical Imaging 8.

Khalid, N., Aqeel, M., Noman, A., Khan, S.M., Akhter, N., 2021. Interactions and effects of microplastics with heavy metals in aquatic and terrestrial environments. Environ. Pollut. 290, 118104. https://doi.org/10.1016/j.envpol.2021.118104

Leelossy, Á., Molnár, F., Izsák, F., Havasi, Á., Lagzi, I., Mészáros, R., 2014. Dispersion modeling of air pollutants in the atmosphere: a review. Cent. Eur. J. Geosci. 6, 257–278. https://doi.org/10.2478/s13533-012-0188-6

Li, Y., Shao, L., Wang, W., Zhang, M., Feng, X., Li, W., Zhang, D., 2020. Airborne fiber particles: Types, size and concentration observed in Beijing. Sci. Total Environ. 705, 135967. https://doi.org/10.1016/j.scitotenv.2019.135967

López-Rosales, A., Andrade, J., Fernández-González, V., López-Mahía, P., Muniategui-Lorenzo, S., 2022a. A reliable method for the isolation and characterization of microplastics in fish gastrointestinal tracts using an infrared tunable quantum cascade laser system. Mar. Pollut. Bull. 178, 113591. https://doi.org/10.1016/j.marpolbul.2022.113591

López-Rosales, A., Andrade, J.M., Grueiro-Noche, G., Fernández-González, V., López-Mahía, P., Muniategui-Lorenzo, S., 2021. Development of a fast and efficient method to analyze microplastics in planktonic samples. Mar. Pollut. Bull. 168, 112379. https://doi.org/10.1016/j.marpolbul.2021.112379

López-Rosales, A., Andrade, J.M., López-Mahía, P., Muniategui-Lorenzo, S., 2022b. Development of an analytical procedure to analyze microplastics in edible macroalgae using an enzymatic-oxidative digestion. Mar. Pollut. Bull. 183, 114061. https://doi.org/10.1016/j.marpolbul.2022.114061

Luo, X., Wang, Z., Yang, L., Gao, T., Zhang, Y., 2022. A review of analytical methods and models used in atmospheric microplastic research. Sci. Total Environ. 828, 154487. https://doi.org/10.1016/j.scitotenv.2022.154487

Mackay, D., 2001. Multimedia Environmental Models: The Fugacity Approach, Second Edition, 0 ed. CRC Press. https://doi.org/10.1201/9781420032543

Mackay, D., 1979. Finding fugacity feasible. Environ. Sci. Technol. 13, 1218–1223. https://doi.org/10.1021/es60158a003

Munyaneza, J., Jia, Q., Qaraah, F.A., Hossain, M.F., Wu, C., Zhen, H., Xiu, G., 2022. A review of atmospheric microplastics pollution: In-depth sighting of sources, analytical methods, physiognomies, transport and risks. Sci. Total Environ. 822, 153339. https://doi.org/10.1016/j.scitotenv.2022.153339

Novillo, O., Raga, J.A., Tomás, J., 2020. Evaluating the presence of microplastics in striped dolphins (Stenella coeruleoalba) stranded in the Western Mediterranean Sea. Mar. Pollut. Bull. 160, 111557. https://doi.org/10.1016/j.marpolbul.2020.111557

Pennington, D.W., Margni, M., Ammann, C., Jolliet, O., 2005. Multimedia Fate and Human Intake Modeling: Spatial versus Nonspatial Insights for Chemical Emissions in Western Europe. Environ. Sci. Technol. 39, 1119–1128. https://doi.org/10.1021/es034598x

Plastics Europe, 2021. Plastics-the Facts 2021. An Analysis of European Plastics Production, Demand And Waste Data.

Shao, L., Li, Y., Jones, T., Santosh, M., Liu, P., Zhang, M., Xu, L., Li, W., Lu, J., Yang, C.-X., Zhang, D., Feng, X., BéruBé, K., 2022. Airborne microplastics: A review of current perspectives and environmental implications. J. Clean. Prod. 347, 131048. https://doi.org/10.1016/j.jclepro.2022.131048

Terzaghi, E., Morselli, M., Semplice, M., Cerabolini, B.E.L., Jones, K.C., Freppaz, M., Di Guardo, A., 2017. SoilPlusVeg: An integrated air-plant-litter-soil model to predict organic chemical fate and recycling in forests. Sci. Total Environ. 595, 169–177. https://doi.org/10.1016/j.scitotenv.2017.03.252

Terzaghi, E., Wild, E., Zacchello, G., Cerabolini, B.E.L., Jones, K.C., Di Guardo, A., 2013. Forest Filter Effect: Role of leaves in capturing/releasing air particulate matter and its

associated PAHs. Atmos. Environ. 74, 378–384. https://doi.org/10.1016/j.atmosenv.2013.04.013

Thompson, R.C., Olsen, Y., Mitchell, R.P., Davis, A., Rowland, S.J., John, A.W.G., McGonigle, D., Russell, A.E., 2004. Lost at Sea: Where Is All the Plastic? Science 304, 838–838. https://doi.org/10.1126/science.1094559

Wania, F., 1996. Spatial variability in compartmental fate modelling: Linking fugacity models and GIS. Environ. Sci. Pollut. Res. 3, 39–46. https://doi.org/10.1007/BF02986813

Paper I

Chemosphere 290 (2022) 133394

Contents lists available at ScienceDirect

Chemosphere

journal homepage: www.elsevier.com/locate/chemosphere

Spatially resolved environmental fate models: A review

Parisa Falakdin, Elisa Terzaghi, Antonio Di Guardo *

Department of Science and High Technology, University of Insubria, Via Valleggio 11, 22100, Como, CO, Italy

HIGHLIGHTS

- Spatial atmospheric transport models and multimedia fate models were reviewed.
- More than 50 spatial models were described including their applications.
- Their spatial, temporal, and chemical domains were investigated for comparison.
- Further developments especially their integration is suggested.

GRAPHICAL ABSTRACT

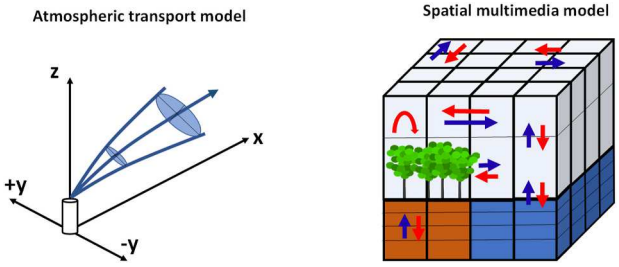

ARTICLE INFO

Handling Editor: Volker Matthias

Keywords:
Spatially explicit models
Atmospheric models
Multimedia chemical fate models
GIS
Mathematical models
Spatio-temporal resolution

ABSTRACT

Spatially resolved environmental models are important tools to introduce and highlight the spatial variability of the real world into modeling. Although various spatial models have been developed so far, yet the development and evaluation of these models remain a challenging task due to several difficulties related to model setup, computational cost, and obtaining high-resolution input data (e.g., monitoring and emission data). For example, atmospheric transport models can be used when high resolution predicted concentrations in atmospheric compartments are required, while spatial multimedia fate models may be preferred for regulatory risk assessment, life cycle impact assessment of chemicals, or when the partitioning of chemical substances in a multimedia environment is considered. The goal of this paper is to review and compare different spatially resolved environmental models, according to their spatial, temporal and chemical domains, with a closer insight into spatial multimedia fate models, to achieve a better understanding of their strengths and limitations. This review also points out several requirements for further improvement of existing models as well as for their integration.

1. Introduction

Environmental fate models are important tools to assess the environmental cycle of contaminants. They can be used to perform the mass balance of a chemical discharged into the environment (Mackay, 2001). For this reason, they are also used in the context of risk assessment of chemicals (ECHA, 2020; RIVM, 2004) and were the object of a recent review (Di Guardo et al., 2018). Throughout the evolution of environmental fate models, plenty of challenges were faced and addressed that are worth considering for further advancement of the existing models and development of new predictive models. In particular, the need to include more ecological realism in the current scenarios and to develop models capable of incorporating and handling such complexity. One of the most important challenges is the inclusion of spatial variability of the real environment into the models (Di Guardo et al., 2018; Di Guardo and Hermens, 2013). An example of such need is

* Corresponding author.
E-mail addresses: pfalakdin@uninsubria.it (P. Falakdin), elisa.terzaghi@uninsubria.it (E. Terzaghi), antonio.diguardo@uninsubria.it (A. Di Guardo).

https://doi.org/10.1016/j.chemosphere.2021.133394
Received 23 May 2021; Received in revised form 13 December 2021; Accepted 20 December 2021
Available online 22 December 2021

the requirement of being able to compare predicted to monitoring concentrations in the environment. Such measured concentration (in water, soil, air, biota, etc.) often depend not only on physical-chemical properties, partitioning, and emission strength but also on the pure variability of the natural environment (e.g., texture and organic carbon in soil, particulate and dissolved organic carbon (POC and DOC) in water, uptake rate for different plant species, bioavailability of chemicals in water and soil, etc.).

In the 1990s, atmospheric transport models (ATMs) were used to provide spatially resolved chemical concentrations, however, these models were only applicable for air modeling. On the other hand, multimedia box models were mostly applied for long-lived substances for which relatively small temporal and often spatial changes were expected, additionally, the measurements used to have a low spatial and temporal resolution (Di Guardo et al., 2018). As a result, in the simulations, long-term average and often homogeneous phase conditions were used to describe environmental characteristics. This was due to the need to reduce complexities, develop models in a tiered strategy, and introduce complexity (e.g., new compartments, processes, or details) only when required (Mackay et al., 1996a, 1996b; Mackay, 2001). Since the 1990s, the mobility of chemicals in a spatially variable environment was more appreciated (Scott et al., 1998; Wania and Mackay, 1993). Wania (1996) described two main sources of spatial variability in environmental systems; 1) different proximity and accessibility of locations from an emission source which causes variation in source strength and incomplete mixing processes. 2) variability in environmental characteristics (e.g., organic carbon, soil texture, etc.) that causes the different intensity of fate processes which results in non-uniform distribution of concentrations in the environment (Wania, 1996). Additionally, new contaminants found in monitoring campaigns along with spatially different discharges of chemicals in the environment (such as pesticides) imposed to address the evolution and variability of concentrations at different locations in space (Ippolito and Fait, 2019; Mishra et al., 2012; Morselli et al., 2018c; Shen et al., 2005). Throughout the time, environmental fate models were challenged with the need to introduce higher flexibility for spatial and temporal variations, also related to the advances in analytical chemistry which provided a higher spatio-temporal resolution of measurements to support model-measurement comparisons (Di Guardo et al., 2018). Thus, modelers started to apply different approaches aiming to improve the spatial resolution of the models. This is particularly important for models such as the compartmental fate models, which assume well-mixing within a compartment and therefore a prevailing concentration representing the phase studied. Therefore, in such models, spatial differences were not present within each compartment so new visions and techniques had to be adopted in order to perceive such differences. Spatially resolved models are also very useful in bioaccumulation studies (Gobas et al., 2016; van den Brink et al., 2016), especially when food chain enrichment is involved and depends on many organisms at different levels, possibly feeding in very different spots and/or ecosystems (for example, where the predator feeds on terrestrial and aquatic species at the same time).

This paper aims to review two common spatial modeling approaches that specifically deal with the quantitative impact of distance and spatial variability of environmental features on chemical concentrations; namely atmospheric transport models and spatial multimedia models (SMMs) with a particular focus on the latter. This study will not treat in great depth spatial models that do not mathematically calculate a distance-concentration relationship. Major model development features plus the evaluation of their spatial, temporal, and chemical domains were assessed in order to provide a historical and evolutionary perspective on the most common approaches available. Several reviews have been previously conducted on spatial models (Leelossy et al., 2018; Li, 2019; Pistocchi et al., 2010; Pistocchi and Galmarini, 2010), however, a comprehensive survey on ATMs and SMMs that recapitulates their characteristics, applications, advantages, and limitations in analogy with each other yet has not been carried out. This review, which includes examples of their application to specific cases, allows comparison of their structure and features, as well as their potential developments.

2. Spatially resolved models

2.1. Atmospheric transport models

ATMs mathematically describe how the atmosphere affects the emitted pollutants due to the combination of advection (transport due to the wind) over large spatial ranges and dispersion (due to turbulent eddy motions and dilution by wind) within short distances. They may also consider the plume rise, wind shear, and physical and chemical transformations (Turner, 1979). ATMs require information about meteorology and emission. They are mostly utilized for the impact assessment of emissions and accidently released hazardous substances on air quality, under varying meteorological conditions. Besides, ATMs are also used at nuclear and chemical plants for emergency responses (Shankar Rao, 2007).

Atmospheric transport and dispersion of the pollutants can be mainly described by two categories of models namely Eulerian and Lagrangian. The fundamental equation (1) (Zannetti, 1990) is based on the conservation of mass of a single pollutant concentration c(x,y,z,t), as a function of space (along x, y, and z axes) and time (t). Different processes, such as horizontal and vertical mixing due to the turbulence, deposition, chemical reaction, radioactive decay, and physical transformation, can be described by the following equation:

$$\frac{\partial c}{\partial t} = -V.\nabla c + D.\nabla^2 c + S \quad (1)$$

where c is the pollutant concentration, V is the velocity, D is the molecular diffusivity, $\nabla^2 = \frac{\partial^2}{\partial x^2} + \frac{\partial^2}{\partial y^2} + \frac{\partial^2}{\partial z^2}$ is the Laplacian operator, ∇ is the gradient operator, and S represents the sources and sinks. Leelossy et al. (2018) describe the sources and sinks as the sum of three terms of emissions, chemical reactions, and deposition.

As described by (Zannetti, 1990), Eulerian modeling considers a fixed coordinate frame with respect to the Earth, and each air parcel is treated within the same frame. In this modeling approach, the velocity compound in equation (1) includes two resolvable (obtained from measurements or meteorological models) and unresolvable (including turbulent atmospheric diffusion eddies which should be minimized) components. Likewise, the concentration and the sources and sinks terms are explained by theoretical mean and unresolvable components. The Eulerian equation is eventually solved either analytically or numerically (Zannetti, 1990). A well-known Eulerian approach that solves the aforesaid equation analytically for relatively short distances is the Gaussian Plume model. The Gaussian method assumes a continuous point source emission together with uniform wind flow and homogeneous turbulence to generate a 3-dimensional concentration field. Even though these assumptions are against the inhomogeneous nature of the wind and turbulence in the Planetary Boundary Layer (PBL), the simplicity of this method, its consistency with the random turbulence, and the fact that the method has been evaluated with a large number of experimental data justifies the use of these models (Demael and Carissimo, 2008).

In Lagrangian modeling, the reference system follows the average atmospheric motion, and the dispersion of the chemical is considered as the transport of an air parcel (or "puff") along a trajectory assuming to keep its identity during the path. In the Lagrangian equation for atmospheric dispersion, a probability density function defines the movement of the air parcel from a certain location and time to another. The sources and sinks term is also a function of time and space, and for each variable, a fluctuation term due to the uncertainties is considered. Finally, the average concentration is calculated as an integration over the entire

atmospheric domain (Zannetti, 1990).

Several types of ATMs (e.g., dispersion models, particle models, photochemical models, meteorological models, etc.) can be found, depending on the purpose of a model and the type of chemicals simulated. For example, relatively inert pollutants such as CO and SO_2 can be modeled by dispersion models, while more chemically reactive pollutants such as O_3 and NO_2, which may react to form secondary pollutants can be modeled by photochemical models (Turner, 1979). In the following sections, several types of ATMs with a number of examples are explained in brief.

Dispersion models are mathematical equations that describe atmospheric dispersion and physical and chemical processes that occur within the plume to calculate the concentration of the pollutant in different locations. These models can be generally applied to local situations (a few km from the source), although some can be applied also at regional, and global scales (Holmes and Morawska, 2006). AERMOD (Cimorelli et al., 2005) is an example of a dispersion model that incorporates air dispersion based on PBL parameters such as mixing height, stability, turbulence, etc. AERMOD is a steady-state and follows the Gaussian plume formulation. CALPUFF (Scire et al., 2000) is another example of the dispersion model that is based on Lagrangian Gaussian puff model formulation and dynamically simulates the transport of the contaminants by incorporating temporal and spatial variations in the meteorological field during the simulation period. The model accounts for chemical removal, wet and dry deposition, complex terrain algorithms, building downwash, plum fumigation, etc. The two-dimensional meteorological fields (e.g., mixing height, surface characteristics, and dispersion properties) were incorporated into the model by a meteorological model (CALMET) while the processes of dispersion and transformation for a "puff" of emitted material are calculated by CALPUFF.

Particle models simulate the transport of particles in the atmosphere within a Lagrangian system and represent the plume using a certain number of "fictitious" particles that move in semi-random trajectories to simulate the dynamic of specific parameters such as mass, heat, electrical charge density, etc. (Zannetti, 1992). The advantage of using the Lagrangian method for particle dispersion over the Eulerian method is its extremely fine resolution which is due to the independence of the emitted tracer from the computational grid, while, in the Eulerian approach, the emitted tracer immediately is mixed within the grid cells (Stohl et al., 2005). An example of these models is FLEXPART (Stohl et al., 1998) that calculates the trajectories of a large number of particles (each representing a parcel of tracer material) and atmospheric transport processes, turbulent diffusion, dry and wet deposition, decay, and linear chemistry that can be applied from local to global scale.

Photochemical models are air quality models that account for the description of the atmospheric chemistry, reactions, and transformation of the chemicals towards secondary pollutants after their emission into the air. They have been formulated mostly in Lagrangian and Eulerian reference frames and are applicable for local, regional, and global spatial scales (Russell, 2000; Tesche, 1983). Photochemical dispersion models were initially built to simulate the transport, transformation, and dispersion of ozone and its photochemical oxidants (Tesche, 1983). For example, MOZART is a global three-dimensional model for tropospheric ozone and its precursors that accounts for surface emission, formation, and the fate of photo-oxidants and provides dynamic distribution of up to 56 chemical mixing ratios (e.g., O3, NOx, CO, etc.) (Brasseur et al., 1998). CMAQ (Byun and Ching, 1999) is a photochemical air quality model that simulates the concentration of airborne gases such as ozone, particulates, toxic and acid depositions. In this model, the simulation of reactivity of organic compounds in the atmosphere using different species, grouped based on their carbon bond type (Whitten et al., 1980), along with a module for the simulation of aerosol physics was implemented.

Some types of ATMs are supported by meteorological (sub)models, used to provide resolved input data on meteorological fields. For example, CALMET is a meteorological model that provides a 3-dimensional diagnostic gridded wind field required for CALPUFF simulations (Scire et al., 1999). Another example is AERMET which is the meteorological pre-processor for the AERMOD model; AERMET requires surface characteristics, cloud cover, upper air temperature, near-surface wind speed, wind direction, and temperature to calculate hourly PBL heights and other input parameters for AERMOD (Cimorelli et al., 2005).

There is a broad range of ATMs to survey (Table 1 reports a brief comparison between ATMs and SMMs, and Table 2 shows a list of models and some of their major features, as well as their applications to different scenarios or chemicals). In the interest of brevity, it is preferred to discuss their general characteristics as well as their pros and cons rather than detailed model structures.

Limitations concerning ATMs can be different for each approach depending on the modeling assumptions. Several limitations are discussed concerning particle dispersion models by Holmes and Morawska (2006). For instance, Gaussian models work under the steady-state assumption, they only account for diffusion and advection processes, and they are unconcerned about the inner-plume interactions. In urban areas, they neglect the effects of multiple buildings. They are neither suitable for the low-wind conditions and distances less than 100 m nor for far-field modeling (up to a few kilometers). Additionally, the homogeneous wind-field assumption is regardless of meteorological variations over long distances (Holmes and Morawska, 2006).

As mentioned earlier, Lagrangian models can provide fine spatial resolution, however, for simulation of long-range transport of chemicals, calculations must be performed for a large number of trajectories which can increase computational cost. One solution to this issue is the implementation of nested models, for example, to use a Lagrangian model close to the source and interpolate the obtained concentration field to a Eulerian grid to perform long-range Eulerian simulation (Leelossy et al., 2014). A different approach to solve the aforementioned problem was implemented by Asman (2001) for the atmospheric transport and deposition of ammonia and ammonium using the TREND model, a Lagrangian plume-type model. The model is applied for Denmark and surrounding sea areas on a 5 km $\times$ 5 km grid and can implement different types of formulation depending on the spatial scale. In local scales, a Gaussian formulation is used because the plume has not been spread entirely over the mixing layer, while at longer distances a one-layer model that assumes the plume is well-mixed over the mixing layer and accounts for the vertical concentration profile due to the dry deposition can be used (Asman, 2001).

On the other hand, among the advantages of ATMs is their ability to provide a high spatial and temporal resolution while maintaining a low to moderate computational effort. ATMs can have a horizontal spatial resolution of up to several meters and a temporal resolution of under an hour. However, different factors can affect the transport of chemicals in the air where high spatial resolution is desired. For example, the effect of the geometry of natural and artificial objects (such as micrometeorological effects of urban geometry). A review has been surveyed by Vardoulakis et al. (2003) on the air quality modeling in the

Table 1
General comparison between ATM and SMM modeling approaches.

Atmospheric transport models (ATMs)	Spatial multimedia models (SMMs)
• ATMs usually calculate only processes and concentrations of chemicals associated with the **atmospheric compartments.** • They typically deal with **airborne chemicals** (NO_x, O_3, PAHs, …). • They provide spatial resolution up to **several meters.** • They use resolved **meteorological data (less than 1 h).**	• Processes and concentrations are calculated for **different environmental media** (e.g., air, water, soil, sediment, vegetations, …) • They can deal with **chemicals that are present in the different types of media** (e.g., PCBs, pesticides, PAHs, …) • They provide a spatial resolution of up to hundreds of **meters.** • They use **hourly to yearly average meteorological data.**

Table 2
Spatially resolved multimedia models and atmospheric transport models developed during the last decades and their major characteristics.

	Model name	SS[a]	D[b]	Scale	Chemicals	Compartments	Features	Authors	Model Applications
Atmospheric transport models (ATMs)	CTDMPLUS	✔	×	R[c]	SO_2	air	**Gaussian**, simulation of dispersion for point-source emissions and complex terrain topography.	US EPA. (Paumier et al., 1992; Perry, 1992)	Venkatram et al. (2001)
	DEHM	×	✔	R	SO_2, S O_4^{-2}, HCH [(1)], PCB [(2)] congeners.	air	**Eulerian**, for long-range transport of air pollution in the Arctic.	Christensen (1997)	(Christensen et al., 2004; Hansen et al., 2015; Skov et al., 2020)
	FLEXPART	×	✔	R	PDCHs [(3)], PTCHs [(4)], BC [(5)]	air	**Lagrangian**, particle-dispersion model used for emergency responses in Austria with a sub-grid scale parametrization for PBL height.	Stohl (1998)	(Eckhardt et al., 2017; Pisso et al., 2019)
	MOZART	×	✔	G[d]	O_3, NO_x, HNO_3, N_2O_5, CH_4, $CO{\cdot}N_2O$	air	**Semi-Lagrangian,** 3D model for studying the global budget of tropospheric ozone and its precursor.	Brasseur et al. (1998)	(Emmons et al., 2010; Horowitz et al., 2003)
	MATCH	×	✔	L[e] to G	Tracers like CO_2	air	**Eulerian**, offline, and limited-area atmospheric transport model with three vertical layers	Robertson et al. (1999)	Lawrence et al. (2007)
	CMAQ	×	✔	R	Atrazine, Benzene, Diesel particles, BAP [(6)], Dust, Trace metals, NH3	air	**Eulerian** model based on "1-atm" approach (multi-pollutant chemistry and multi-scale dynamics and thermodynamics)	Byun and Ching (1999)	(Appel et al., 2013; Aulinger et al., 2011; Cooter et al., 2002, 2012; Cooter and Hutzell, 2002; Golden et al., 2010; Karl et al., 2019a; Seigneur et al., 2003)
	CALPUFF	×	✔	L to R	NO_x (NO and NO_2)	air	**Lagrangian and Gaussian (puff model)**, meteorological and air quality modeling system.	Scire et al. (2000)	Oleniacz and Rzeszutek (2018)
	GEOS-CHEM	×	✔	G	Ozone-NO_x-hydrocarbon, O_3, CO, H_2O	air	**Eulerian**, global 3D model for simulation of tropospheric ozone-NOx-hydrocarbons based on assimilated meteorological observations from Goddard Earth Observing System.	Bey et al. (2001)	(Han et al., 2020; Nassar et al., 2009; Wagner et al., 2019)
	MITgcm	×	✔	L to G	Hg, PCBs	air, water	Global circulation model for different scales in ocean and atmosphere	Adcroft et al. (2004)	(Wagner et al., 2019; Zhang et al., 2019)
	AERMOD	✔	×	R	SO_2, SF_6 [(7)], PAHs	air	**Gaussian** air dispersion model to improve the formulation of the planetary boundary layer.	(Cimorelli et al., 2005; Perry et al., 2005)	Morselli et al. (2012)
	CAMx	×	✔	L to C[f]	FTOH [(8)], PFCA [(9)], O_3, PM	air	**Eulerian**, a photochemical dispersion "1-atm" regional model for gaseous and particulate air pollution.	ENVIRON (2005)	(Nopmongcol et al., 2012; Tesche et al., 2006; Yarwood et al., 2007)
	ADEPT	✔	×	C	NO_x, SO_x, Benzene	air	A simplified model like **Gaussian**, Atmospheric deposition, and transport model for risk assessment	Roemer et al. (2005)	(Hollander et al., 2008; Pistocchi and Galmarini, 2010)
	WRF/Chem	×	✔	R	O_3, CO, NO_x, Hg, Fine particles	air	**Eulerian**, Implementation of chemical processes into Weather Research and Forecasting (WRF).	Grell et al. (2005)	(Gencarelli et al., 2014; Sicard et al., 2021)
	MPI-MCTM	×	✔	G	HCH, DDT, PCBs	air, soil, water, vegetation, snow, land ice	Multicompartmental chemistry transport model coupled with several sub-models to account for many environmental media.	Guglielmo et al. (2009)	Lammel and Stemmler (2012)
	[Li]	×	✔	R	PAHs	air	Advection–diffusion model with high resolution coupled with the emissions inventory.	(B. Li et al., 2018)	
	NJUCPL	×	✔	G	Hg	air, water	Online coupled model (GEOS-Chem, MITgcm) to assess air-sea exchange fluxes of Hg.	Zhang et al. (2019)	
	EPISODE-CityChem	×	✔	R	NO_2, O_3, PM	air	**Eulerian** air dispersion model for urban air quality that can be applied for a variety of airborne pollutants.	(Hamer et al., 2020; Karl et al., 2019b)	Karl et al. (2019b)

(*continued on next page*)

Table 2 (*continued*)

	Model name	SS[a]	D[b]	Scale	Chemicals	Compartments	Features	Authors	Model Applications
Spatial multimedia models (SMMs)	Globo-POP	×	✔	G	PCBs, PBDEs [(10)], DDT [(11)], α-HCH	air, water, soil, sediments	A global model that divides the environment into nine latitudinal zones to obtain concentrations as a function of time.	Wania and Mackay (1993)	(Scheringer and Wania, 2003; Wania and Dugani, 2003; Wania and Mackay, 1995, 1996)
	SoilFug	×	✔	L	Pesticides (metolachlor, terbuthylazine, fenitrothion)	soil and receiving surface water	A multimedia model that was used for the prediction of runoff at the catchment scale.	Di Guardo et al. (1994a)	(Barra et al., 2000; Di Guardo et al., 1994b)
	ChemCAN	✔	×	R	CB [(12)], LAS [(13)], TCE [(14)], PCB, α-HCH, B[*a*]P, HCB, Atrazine	air, water, soil, sediment	One of the primary multimedia models to simulate the fate of organic chemicals parametrized for Canada	Mackay et al. (1996b)	Webster et al. (2004)
	CliMoChem	×	✔	G	PCBs, CCl_4 [(15)], α-HCH, mirex, atrazine	air, water, soil	A global model that considers the influence of temperature on fate and transport of chemicals. The model consists of a variable number of latitudinal zones.	Scheringer et al. (2000)	(Fenner et al., 2007; Hollander et al., 2008; Scheringer et al., 2004; Scheringer and Wania, 2003)
	BETR North America	✔	✔	C	Toxaphene, γ-HCH, PBDEs, PAHs, HCB [(16)], DecaBDE [(17)], BC, PCBs, PFOS [(18)], D5 [(19)]	air, freshwater, freshwater sediments, coastal water, soil, vegetation	Regionally segmented multimedia fate model for North America	MacLeod et al. (2001)	BETR North America, Evn-BETR: (Armitage et al., 2007; Earnshaw et al., 2015; Hauck et al., 2008; Hollander et al., 2008; Liu et al., 2015, 2014; Konstantinos Prevedouros et al., 2004; K. Prevedouros et al., 2004)
	[Coulibaly]	×	✔	L	TCE	air, water, soil, sediments, vegetation, roots, vadose	GIS-based multimedia model for the fate of chemicals in the watershed.	Coulibaly et al. (2004)	
	POPsME	×	✔	C	PAHs, PCDD/F [(20)]	air, water, soil, sediments	A multimedia model to describe changes in concentrations. The model considers the relative concentration of each medium over soil concentration.	Lee et al. (2004)	Lee et al. (2007)
	G-CIEMS	×	✔	C	Benzene, Dioxins, 1,3-Butadiene, Herbicides	air, water, forest canopy, soil	Grid catchment model developed on GIS to benefit from geo-referenced river model and spatially resolved multimedia fate model in the same system.	Suzuki et al. (2004)	(Hayashi et al., 2016; Hollander et al., 2008; Imaizumi et al., 2018)
	IMPACT 2002	✔	×	R	PeCDF [(21)], PAHs, HCB, BC	air, water, soil, sediments, vegetation	A multimedia multi-pathway model to estimate concentration and level of contaminants in food.	Pennington et al. (2005)	(Armitage et al., 2007; Hauck et al., 2008; Manneh et al., 2010)
	BETR Global	✔	✔	G	PCBs	air, water, soil, vegetation	A global model that integrates global climate data from the National Centres. The globe is represented with 288 multimedia regions on a 15° grid.	MacLeod et al. (2005)	MacLeod et al. (2011)
	BasinBox	✔	×	L	3175 hypothetical organic chemicals	air, water, soil, sediment	Generic multimedia fate model for river catchments to assess the risks of new and existing chemicals.	Hollander et al. (2006)	Hollander et al. (2009)
	CoZMo-POP 2	×	✔	R	POPs	air, water, soil, sediments, forest	A multimedia model to describe the long-term fate of chemicals in coastal environments or drainage basins of large lakes	Wania et al. (2006)	Choi and Wania (2011)
	GLOBOX	✔	×	G	Nitrobenzene	air, soil, water, sediment	A global model for life-cycle assessment toxicity characterization factors. Multimedia processes are based on EUSES.	Wegener Sleeswijk (2006)	Wegener Sleeswijk and Heijungs (2010)
	[Luo]	×	✔	R	B[*a*]P, HCB	air, water, soil, sediments, vegetation	Extension of Monte Carlo analysis in a multimedia fate model. Stochastic simulations	Luo and Yang (2007)	Luo et al. (2007)

(*continued on next page*)

Table 2 (*continued*)

Model name	SS[a]	D[b]	Scale	Chemicals	Compartments	Features	Authors	Model Applications
						are run to demonstrate uncertainties.		
IMPACT North America	✔	×	C	B[*a*]P, TCDD [22], Hg	air, water, soil, sediments, vegetation	A multimedia multi-pathway air and exposure model extended to include the indoor and urban environment.	Humbert et al. (2009)	
COHERN	×	✔	L	PCBs, PAHs, PCDD/Fs	air, water, sediments	A 3D hydrodynamic model coupled with a contaminant fate and ecological model for the distribution of chemicals in water bodies.	Dueri et al. (2010)	
SDMFM	✔	✔	R	Toluene	air, water, soil, organic film, vegetation, sediments	Development of a spatial model based on a finite-difference method that is applied to a uniform grid.	Kim et al. (2010)	
LSRMFM	✔	×	L	benzene, toluene, xylene, styrene	air, water, soil, organic film, vegetation, sediments	Spatially refined multimedia fate model combined with GIS, for human carcinogenic and non-carcinogenic inhalation risk assessments. The model has a 0.5 × 0.5-km segment resolution.	Kim et al. (2011)	
SO-MUM	×	✔	R	PCBs, PBDEs	air, water, soil, sediments, vegetation, film	A spatial model with 5 × 5 km2 cell resolution to back-calculate air emissions from measured concentrations.	Csiszar et al. (2013)	Csiszar et al. (2014)
Spatial SoilPlus	×	✔	R	pesticides	air, soil, water	The model is GIS integrated and it includes spatial soil layers, dynamic air, and catchment runoff.	Ghirardello et al. (2014)	
ECORAME	×	✔	L	PAHs	air, water, sediment, vegetation	A model for aquatic ecological exposure that treats each water segment as an independent cell to increase the accuracy of assessments.	Jung et al. (2014)	
SESAMe	✔	×	R & C	B[*a*]P, ACE [23], TCS [24], DF [25]	air, water, soil, sediments, vegetation	A model to investigate the influence of environmental parameters on chemical overall persistence and long-range transport potential.	Zhu et al. (2014)	SESAMe v3.3: (Zhu et al., 2016, 2019)
ChimERA fate	×	✔	R	PCBs	water, sediments, macrophyte, TSP [30], DOM [31]	The fate of organic chemicals in dynamic water-sediment systems, layered sediments, and water segments is investigated.	Morselli et al. (2015)	Improved ChimERA: (Di Guardo et al., 2017)
[Ligaray]	×	✔	R	PAHs	air, water, soil	A multimedia model coupled with a hydrological model (SWAT) is used to simulate the spatial and temporal distribution of PAHs in the watershed.	Ligaray et al. (2016)	
INCA-Contaminants	×	✔	R	PCBs, Metaldehyde	air, water, soil, sediments	Hydrological, biogeochemical, and multimedia fate model to simulate the fate of contaminants at catchment scale.	Nizzetto et al. (2016)	Lu et al. (2017)
POPsLTEA	×	✔	C	PAHs	air, water, soil, sediments	Effect of climate change on fate and transport of PAHs	(J.H. Song et al., 2016)	
BETR-UR	✔	×	R	PAHs, PFOA/PFO [26]	air, water, soil, sediments, vegetation	Land cover information is included in the model to simulate the fate of PAHs between urban and rural area	(S. Song et al., 2016)	Modified BETR-UR: (Su et al., 2018)
BC-Model	✔	×	R	Phe [27], Pyr [28], B[*a*]P	air, water, soil, sediments, vegetation, organic film	In the multimedia model, organic matter was replaced by black carbon to simulate PAHs distribution.	Wang et al. (2017)	
SoilPCA	×	✔	R	150 organic chemicals	air, soil, vegetation	Multimedia model to determine surface soil pollution potential due to accidental release of chemicals.	Kim et al. (2018)	
PeCHREM	×	✔	C	Pesticide	air, water, soil	The model is applied together with G-CIEMS to estimate	Imaizumi et al. (2018)	Misaki et al. (2019)

(*continued on next page*)

Table 2 (*continued*)

	Model name	SS[a]	D[b]	Scale	Chemicals	Compartments	Features	Authors	Model Applications
							spatially and temporally variable emissions of pesticides for risk assessment.		
	DynaPlus	×	✔	R	Pesticides, Insecticides, Fungicides	air, litter, soil, water, DOM	The model is used to improve the predictions of pesticide fate in cultivated mountain basins.	Morselli et al. (2018c)	Morselli et al. (2018b)
	Pangea framework	✔	×	L to G	HPC, LAS, TCS, MeP [(29)], D5	agricultural and natural land, air, water, sediments	Comparison between the global impacts versus local impacts resulting from point source emissions.	Wannaz et al. (2018c)	(Jolliet et al., 2020; Wannaz et al., 2018a, 2018b)
	RSEMM	×	✔	L	antibiotics	air, water, soil, sediments	Integration of an environmental multimedia method (EMM) and a water quality model for assessing the risk of chemicals in a river basin	Dong (2019)	
	[Huang]	✔	×	L	PAHs	air, water, soil, sediments, vegetation, film	Level III fugacity multimedia model to assess the mass flux variation of PAHs in Shanghai	Huang et al. (2019)	
	NEM	×	✔	G	PCBs and other organic chemicals	air, water, soil, sediments, vegetation	A nested global multimedia model to achieve high spatial user-defined resolution	Breivik et al. (2021)	
Other spatial models	USEtox	✔	×	L to G	Organic chemicals	air, water, soil, sediments	Fate and exposure model for chemical impact characterization for human toxicity and freshwater ecotoxicity	Rosenbaum et al. (2008)	(Belyanovskaya et al., 2019; Fantke et al., 2016; Kounina et al., 2014; Sala et al., 2011)
	PiFs	✔	×	L	Organic chemicals	air, water, soil	A flexible mass balanced based model to quantify cumulative transfer fractions and exposure pathways of products consumed by human	Fantke et al. (2016)	
	PROTEX	×	✔	R	Organic chemicals	air, water, soil, sediments, vegetation, indoor compartments	First dynamic nested multimedia indoor, urban, rural chemical fate model to assess the distribution and concentrations and pathways of contaminants.	Li et al. (2018a)	(Li et al., 2019; L. Li et al., 2018b, 2020)

[a] Steady-state.
[b] Dynamic.
[c] Regional.
[d] Global.
[e] Local.
[f] Continental.[g] for models without a specific name, the name of the developer is mentioned within the brackets.
(1) Hexachlorocyclohexane.
(2) Polychlorinated biphenyl.
(3) Perfluoro-dimethylcyclohexane.
(4) Perfuoro-trimethyl cyclohexane.
(5) Black carbon.
(6) Benzo[*a*]pyrene.
(7) Sulfur hexafluoride.
(8) Fluorotelomer alcohol.
(9) Perfluorononanoic acid.
(10) Polybrominated diphenyl ethers.
(11) Dichlorodiphenyltrichloroethane.
(12) Chlorobenzene.
(13) Linearalkylbenzene sulfonates.
(14) Tetrachloroethylene.
(15) Tetrachloromethane.
(16) Hexachlorobenzene.
(17) Decabromodiphenyl ether.
(18) Perfluorooctanesulfonic.
(19) Decamethylcyclopentasiloxane.
(20) Polychlorinated Dibenzo-p-Dioxins/Polychlorinated Dibenzofurans.
(21) Pentachlorodibenzofuran.
(22) Tetrachlorodibenzodioxin.
(23) Acenaphthene.
(24) Triclosan.
(25) Dibenzofuran.
(26) Perfluorooctanoic acid.
(27) Phenanthrene.

(28) Pyrene.
(29) Methyl paraben.
(30) Total suspended particles.
(31) Dissolved organic matter.

urban environment where the impacts of the above-mentioned factors on the air quality of street canyons were discussed.

2.2. Spatial multimedia models

Spatial multimedia models are mass balance partitioning models, also called 'box' or 'compartmental models' or 'Mackay type' models (Mackay, 1979), which have been widely used to evaluate the complex interaction between chemicals and the environment. These types of models are usually composed of several connected environmental compartments (e.g., air, water, soil, sediments, vegetation, etc.), for which different processes such as emission, transport, and degradation are being calculated. An important issue about such models is that they often provide sufficient information without demanding a huge amount of input data and producing outputs that cannot be evaluated (McKone and MacLeod, 2003). Therefore, the art of environmental modeling, according to Mackay (2001), includes the selection of the "best" or "least-worst" set of assumptions in such a way that the model could be simple and understandable and yet maintain realism and usefulness (Mackay, 2001). A common assumption in multimedia fate modeling, as recommended by Mackay (1979), is the homogeneity of the compartments, also called the continuous stirred tank reactor (CSTR) assumption, and as a result the allocation of one concentration value to each environmental compartment. This assumption has been adequate and convenient for early model applications (Wania and Mackay, 1993) as well as scenarios where the compartments are well-mixed and the spatial condition is close to uniform (e.g., QWASI model (Mackay and Diamond, 1989)). However, as the scale of a study area increases the spatial resolution of the model decreases and this is even more troublesome where the environmental heterogeneity is not negligible and is not describable with only one concentration value.

Cohen et al. (1990) discussed the importance of using spatially resolved compartments in environmental models and developed a spatial multimedia compartmental model as a combination of uniform (air, water, biota, suspended solids) and non-uniform compartments (soil and sediment) (Cohen et al., 1990). Cohen and Cooter (2002) categorized the multimedia models based on the spatial variation of their compartments into (a) *Integrated spatial multimedia models* where transport and fate of the chemicals are described by spatial models considering intermedia boundary conditions and a set of medium-specific transport equations, (b) *Linked spatial single-medium models* where a collection of single-media spatial models interacts with each other and the output of one model is used as the input to the others, (c) *Compartmental "well-mixed" media models (both fugacity-based and concentration-based)* where the assumption of homogeneity is applied and all compartments are considered as well-mixed, and (d) *Integrated spatial-multimedia-compartmental models* where a combination of uniform and nonuniform compartments are considered to calculate the transport of the pollutant within such system (Cohen and Cooter, 2002). The need of including the variation of environmental characteristics in multimedia fate models was further discussed in a workshop organized by the Society of Environmental Toxicology and Chemistry (SETAC) in 1994 which was later published as a book (Cowan et al., 1995). In this workshop, the use of Uniform Geographical Units (UGUs) was suggested, and they were defined as "areas of geographic surface, fairly uniform in their physical and biological characteristics, such that they can be represented by a specific set of transport and characterization parameters". Such definition put the bases for sectioning the environmental media of aquatic and terrestrial ecosystems. In this workshop, the need of using appropriate scales in space and time was also underlined in order to predict chemical differences in a region, for example, depending on different sources present.

A five-stage strategy was then illustrated to compare chemical fate in evaluative (EQC model), regional (ChemCAN), near-field (SoilFug and QWASI) (Mackay et al., 1996a, 1996b, 1996c, 1996a). The purpose was to show the importance of chemical properties in ruling fate in an evaluative environment, then the role of regional characteristics (e.g., compartment sizes, specific mass-transfer coefficients, air and water residence times, etc.) in influencing the fate, and the need of local (near-field) models for specific studies. In this comparison, the increasing complexity of the simulations started to evaluate the role of spatial properties at different scales.

During the years, modelers have increasingly included the spatial variation of the real environment for several or all of the simulated compartments in a variety of multimedia fate models (Barra et al., 2000; Csiszar et al., 2013; Ghirardello et al., 2010; MacLeod et al., 2001; Suzuki et al., 2004).

To increase the spatial resolution of multimedia fate models, different approaches have been implemented. One of these approaches is the multiple connected multimedia fate models where the study area is divided into several multimedia sub-models and each of them is representative of a homogenous (multimedia) environment. Such settings allow environmental characteristics and input parameters to be different for each sub-model. Average concentrations are calculated for each sub-model for different compartments, based on intermedia partitioning, transport, and degradation processes. The horizontal (or vertical) connections among the boxes of each environment can be performed with advective flows of air and/or water. Examples are the global multimedia fate models (Scheringer, 1996; Scheringer et al., 2000; Wania and Mackay, 1996). An example of the multiple box model, applied dynamically on a local scale (watershed), is the one of Luo et al. (2007) where the region of interest can be divided into a number of connected boxes. The model uses fugacity-based equations to calculate the transport of chemicals in a Eulerian system (Luo et al., 2007). In the multi-homogeneous box approach, several issues must be addressed. For example, considering a well-mixed environment within each box can be suitable for screening-level models, however, the instantaneous mixing assumption can cause errors, which should not be neglected especially when modeling environmental systems in which only limited mixing processes such as diffusion or dispersion are present. Warren et al. (2009) discussed this issue and recommended approaches to avoid mathematical errors caused by deviations from CSTR. For example, when a multi-box CSTR is used, it is important to account for the fraction of the chemical that is removed from each box within the time step, therefore, the size of the boxes must be set accordingly (Warren et al., 2009). Additionally, the CSTR assumption for chemicals with high partitioning ratios (Kow or Koa) may not be adequate since kinetic delays may occur in achieving thermodynamic equilibrium. For this reason, very slow partitioning may occur for these chemicals. The complex transport processes of these types of chemicals were addressed by Mackay et al. (2019) and several methods are suggested to quantify these processes.

The integration of geographic information system (GIS) into a multimedia fate model was first suggested by Wania (1996) where the QWASI model was divided into four separate units in a heterogeneous environment under steady-state assumptions. This GIS integration assisted to incorporate more homogeneous sub-models hence maintaining the simplicity. Models prior to this were not calculating regions differently, for example, the regions of Canada in the ChemCAN model were calculated one at a time (Mackay et al., 1996c).

Such integration provides an important tool to create maps of chemical concentrations and process rates, find the correlation between

contamination patterns and GIS data in order to perform risk analysis (Wania, 1996). This method is used in a variety of studies to include different territorial and cartographic information such as landscape characterization and hydrographic networks. In GIS integrated models, the spatial division of a study area can be performed depending on the geographical characteristics, therefore, multimedia fate and transport processes are applied for each division. For example the model developed by Barra et al. (2000), a multimedia fugacity fate model (SoilFug) coupled with GIS, was the first GIS-integrated model that was applied to a catchment area in order to predict pesticide pollution in surface water. Several uniform geographical units (UGU) were allocated for the field area. The model could provide the capability of studying the environment in three levels of detail; eleven UGU, three major sub-basins of sampling stations, and the entire study area (Barra et al., 2000).

Each grid cell or geographical unit may contain features that differ from other units, for example, the stream segments and catchments. In an SMM coupled with GIS, the geographical units may be connected by water flow from upper to lower river segments in the GIS component as well as advective air in the multimedia fate model component. An example of this approach is the spatial SoilPlus, model, a dynamic model fully integrated with GIS, providing a link between the site-specific layered soil model to a GIS. The model was applied for the prediction of runoff of pesticides in an agricultural watershed using a field-based database of properties (soil texture, OC, rainfall, pesticides, and half-life in soil, etc.) (Ghirardello et al., 2014).

A common approach in spatial modeling is incorporating two models in one framework in order to take advantage of their specific features in each of the models. For example, a hydrological model integrated with a multimedia fate model can provide a more detailed approach for simulating a river basin environment. Dong (2019) integrated a numerical water quality model that simulates the interactions and processes occurring between water and sediment compartments with an environmental multimedia model consisting of air, soil, and water. The two models were connected through intermedia fluxes of water (Dong, 2019). Similarly, MITgcm (Adcroft et al., 2004), a 3D physically based model, was used in a number of chemical fate simulations such as those of PCB fate in the global oceans (Wagner et al., 2019) where the MITgcm was coupled with GEOS-Chem (Bey et al., 2001) to obtain monthly atmospheric concentrations and deposition of PCBs. The MITgcm model was also coupled to GEOS-Chem to form a new model (NJUCPL) to estimate the air-water exchange at a global scale for mercury (Zhang et al., 2019).

The combination of an SMM with an ATM is another method used in spatially resolved environmental modeling. This method benefits from the high spatial and temporal resolution of atmospheric transport models as well as the inclusion of more environmental compartments in multimedia fate models. Morselli et al. (2012, 2011) first integrated a multimedia fate model (AirFug) with a meteorological preprocessor (AERMET) to calculate PBL heights and later an air dispersion model (AERMOD) (Cimorelli et al., 2005). This modeling approach includes the effect of atmospheric dynamics (i.e. variation of PBL height and meteorological conditions) on soil concentrations in a local scale model (Morselli et al., 2011, 2012). A similar approach was later applied by Csiszar et al. (2013) and a multiple box model (MUM) is coupled to an atmospheric forecast model (BLFMAPS) to predict intraurban scale emission and the fate of chemicals (Csiszar et al., 2013). A recent example of a spatial model created as an integration of several models is Pangea, which is a framework composed of different sets of models for spatial simulation of chemical substances in the environment. This framework includes local to global spatial scales and uses a GIS engine, a set of environmental models (EMs), and a set of environmental processes models (EPMs) which calculate the fate and transport of pollutants within and between different media. Different sets of grids with different resolution and refinement capabilities are embedded in this framework (e.g., background grid, result grid, atmospheric, terrestrial, sediments, and sea/ocean grids). Pangea is applied solely or together with other modeling systems to estimate the environmental exposure of chemicals (Jolliet et al., 2020; Wannaz et al., 2018a, 2018c).

The inclusion of more regions in a spatially resolved model requires more data and involves more computational complications, therefore, the selection of the number and size of the segmentation is important (see Fig. 1). There is often a trade-off between having a higher fidelity to the real system at the cost of complexity and high data requirement or obtaining simplicity, mathematical ease, and transparency while compromising spatial resolution. For instance, Woodfine et al. (2001) provided a framework to link regional segmentations of compartmental fate models for water basins in Canada. According to the authors, a minimum of 3×3 segmentations (9 regions) is required to provide an acceptable level of detail. Therefore, for BETR – North America a 5×5 region scenario was considered and the regions linked to each other, while regional models up to the time of this study were single models applied for the whole region (Woodfine et al., 2001).

Models that are typically used at a large-scale or for the global environment are easier to construct because each grid cell or single box represents a large area (i.e., several thousand square kilometers). A global SMM has generally a low spatial resolution since the spatial inhomogeneities within each cell are not considered (Scheringer and Wania, 2003). The first global model for chemical fate in a multimedia environment was primarily introduced by (Wania and Mackay, 1993, 1995). The initial version of the model was multi-compartmental and unsteady-state where the global environment was characterized by only nine sequentially arranged climatic zones connected to each other by advective and intermedia transport processes. Soon after, Scheringer et al. (2000) presented a new global model (CliMoChem) which was developed based on the two previously built global models (Scheringer, 1996; Wania and Mackay, 1993), increasing the resolution of the model to a variable number of latitudinal zones (10–90), 80 identical cells, 10 climatic zones, and four atmospheric layers. This model was used to evaluate the effect of factors such as chemical properties, temperature, and deposition on the chemical tendency to transport and accumulate at the Poles (cold condensation) (Scheringer et al., 2000).

Another type of global-scale model is the General Circulation Models (GCM), which use mass, energy, and momentum conservation equations, discretized over connected atmospheric, land, and ocean control volumes. These models can provide high spatial and temporal resolutions in calculating fate and transport of POPs, however, they are computationally complex and require detailed model inputs. The Berkeley-Trent (BETR-Global) model is an intermediate approach between multimedia mass balance models and GCMs, therefore, it can benefit from the detailed modeling features of GCMs and transparency of multimedia fate models. It was utilized to assess the effect of climate on the fate and transport of chemicals. The model includes both steady-state and dynamic modes. The entire globe is covered by $15^\circ \times 15^\circ$ regional segmentations (288 multimedia regions) (MacLeod et al., 2005).

Most recently, the nested exposure model (NEM) (Breivik et al., 2021) by adopting two multimedia fate models of CoZMo-POP2 and BETR-Global provided a nested model with a user-defined spatial resolution, incorporating regional, continental, and global scales within one framework. Different grid sizes of $15^\circ \times 15^\circ$, $5^\circ \times 5^\circ$, and $1^\circ \times 1^\circ$ are used to provide an insight into how varying spatial resolution can affect the atmospheric deposition. Another advantage of a global model with an adaptable spatial resolution is that model resolution can be assigned depending on the availability of an emission inventory, since using a high-resolution transport model in a large-scale environment, where the emission inventory data are not as resolved, can cause over-parameterization of the model.

Higher spatial resolution is implemented in models with local or regional scales for risk assessment purposes. Each segment or grid cell covers a smaller area, consequently, more detailed input parameters are required. An example of such models is that of Wang et al. (2017), who developed a regional model for evaluating the spatial distribution of

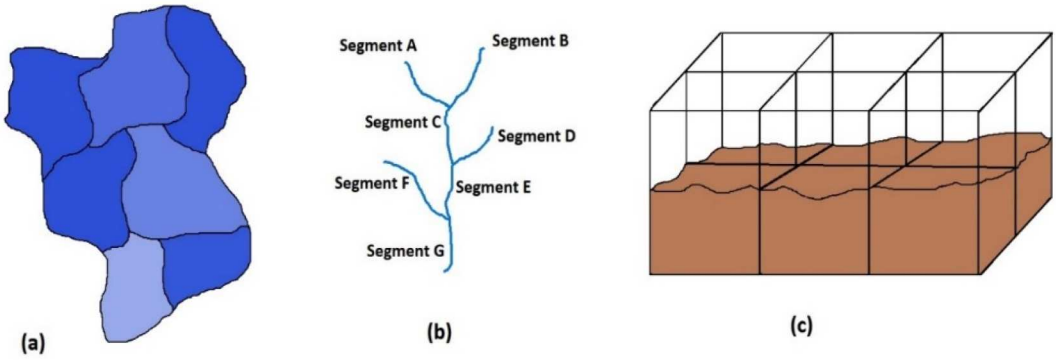

Fig. 1. Different types of spatial segmentations. (a) catchment division (b) river segmentation (c) gridding.

PAH in Nanjing, China. In this model 36 individual cells with 4 × 4 km resolution cover the entire region (Wang et al., 2017). Spatial segmentation may be realized based on the similarity of the physical properties, or general criteria in which an area could be delimited, for example, surface water direction and fluxes in a watershed. This type of segmentation is implemented by Coulibaly et al. (2004) where the Passaic River watershed in New Jersey is divided into 11 sub-watersheds. The model is also integrated with GIS. Assigning similar areas as a sub-watershed facilitates the incorporation of GIS resources into the model because each watershed can be represented as one polygon in the GIS. The connection between these sub-watersheds was set through horizontal water flows (Coulibaly et al., 2004).

A division of geographical catchments was done in G-CIEMS (Suzuki et al., 2004), where a set of hydrologically isolated basins were confined in the geographical boundary and consisting of multiple unit catchments, was connected to a river network segmentation in which each catchment is connected to its corresponding river. The connections between upper to lower river segments were formulated into the database through a node-path structure.

River segmentation was also implemented in the DynaPlus model (Morselli et al., 2018b, 2018c, 2018b) where a dynamic small-scale watershed fugacity model is connected to a river network in order to evaluate the runoff of pesticides in mountain watersheds, where high slopes determine fast chemical movements due to surface runoff, and consequently, sudden chemical loading to surface water.

The spatially oriented MUM (SO-MUM) (Csiszar et al., 2013) model is instead an example of gridded divisions on a regional scale. The model is the extension of a one-box model (MUM) into a multiple box model with a spatial resolution of 5 km × 5 km. The model is loosely coupled with the air pollution transport model BLFMAPS for the simulation of upper air compartment and intercell air transport. The cells were linked by tributaries, the output of an upstream cell was set as the input of a downstream cell (Csiszar et al., 2013). The size of the grids may be equal in all cells like the atmospheric grids of G-CIEMS or can be more refined across the area of interest like the grid system in the Pangea framework (Wannaz et al., 2018a).

Some recent multimedia fate models present spatial features, such as local and regional environments. However, these models cannot be classified as spatially resolved models as specified in the introduction and will not be evaluated in depth in this review since the main focus of this study is on models that calculate a distance-concentration relationship. However, these models are important to allow to calculate the role of different spatial scales on the intake fractions for different population groups and exposure pathways from products to humans through direct exposure, as well as exposures, after indoors and outdoors exchange processes. They are listed in Table 2 as "Other spatial models".

The parametrization of spatial scales in such models is different than spatial models with geographical resolutions. Chemical emission and fate are assessed for indoor, urban, and rural environments where each spatial scale and its role are compared. For example, EUSES (Vermeire et al., 1997) comprises nested local, regional, and continental spatial scales in a steady-state model and is used to perform risk assessment in Europe. Recently, a new model PROTEX (L. Li et al., 2018a, 2018b; Li et al., 2019) was developed as a nested but dynamic, multi-scale, and multi-route fate and exposure model and was applied to study the fate of PCBs and PBDEs at different scales of indoor, urban, and rural environments. The indoor environment consists of compartments such as organic film, air, carpet, and vinyl floor, and it is nested within an urban environment consisting of organic film, air, vegetation, soil, water, and sediment. Additionally, the urban environment is nested within a rural environment. The interaction of these environments and the fate of chemicals are calculated based on Mackay's fugacity formulations and resulted in time-varying indoor and urban emission values. In this model, however, each compartment of each scale has one value (e.g. one value is assigned to the air compartment of urban scale for each time-step. This is the main difference between these models with the spatially resolved ATMs or SMMs where there are spatial divisions (e.g., grids, segmentation, etc.) within the model scale and different concentration values are calculated for each division depending on their distance from the emission source. Similarly, some life cycle assessment models (LCA) such as USEtox (please refer to https://usetox.org/support/publications for a complete list of applications) and later MAPPE (Pistocchi et al., 2011; Rosenbaum et al., 2008) introduced spatial features in the evaluation of organic contaminant fate. Additionally (Fantke et al., 2016), developed a framework that calculates exposure pathway-specific product intake fractions (PiFs) using chemical mass transfer between adjacent compartments. It includes near-field exposures, consisting of compartments that are in direct contact with humans, and far-field exposures, with compartments such as water, ambient air, and soil (Fantke et al., 2016).

3. Comparison between atmospheric transport models and spatial multimedia models

Scheringer and Wania (2003) report that SMMs are easier to understand, more transparent, and their results are simpler to interpret in comparison with the ATMs. A less computational effort is required for these models and they are more flexible to be used for different scenarios. On the other hand, SMMs use average values for model parameters and they typically provide lower spatial and temporal resolutions compared with ATMs (Scheringer and Wania, 2003). ATMs can provide long-range transport simulation of chemicals in the air (leaving out the Gaussian models that, as mentioned before, are specified for short distances) with high temporal resolutions and realistic spatial patterns. They can be used to track the pathways of pollutants in the air and detect a specific emission source (Stohl, 1998). ATMs mainly calculate only the processes occurring in the atmosphere, even though, they may account for emission and depositions from and towards other media such as soil and water, but as a result, they provide the concentration of pollutants in

the atmospheric compartments (Christensen, 1997; Cooter and Hutzell, 2002; Stohl et al., 1998). The addition of other environmental media into an atmospheric model requires more input parameters and processes in order to acquire spatial resolution in all of the simulated media. This generally can make the model computationally expensive and difficult to calibrate. The two types of spatial models (e.g., ATMs and SMMs) are compared in the following sections selecting three aspects: their spatial, temporal, and chemical domains. Table 1 points out several aspects where the two modeling approaches differ from each other.

3.1. Spatial domain

Dungan (2015) describes that the word "scale" refers to different concepts, and due to the potential confusion among various definitions, it is suggested that authors avoid the term "scale" and instead use the specific term (e.g., cartographic ratio, grain, extent, resolution, support, range, variance, and footprint). To refer to the size of a study domain, the word "extent" is recommended to be used, which is defined as the total length, area, or volume that exists or is observed or analyzed (Dungan, 2015). In addition, the classification of geographical and meteorological scales is very subjective; however, a common way of categorizing spatial scales is a range from micro (local) to mega (global) scale (see Fig. 2). A more detailed discussion about the above-mentioned terms and their differentiation is provided by Herod (2009).

Often increasing the spatial domain of a model (from local to global) results in a decrease in spatial resolution. Also, by increasing the spatial resolution of a model, the complexity increases. Therefore, it is important to know the level of detail required in predicting the concentration values to achieve the objective of a model. In the ATMs, the majority of efforts in modeling are put on the characterization of air compartments including vertical and horizontal resolutions (Byun and Ching, 1999; Grell et al., 2005; Oleniacz and Rzeszutek, 2018). Since ATMs generally deal with only one medium (i.e., air), they can considerably increase their spatial resolution. For example, EPISODE-CityChem was developed by Hamer et al. (2020) to be implemented for large populated urban areas where the emission sources are very complex. Therefore, a high spatially resolved approach is considered. The model is based on the Eulerian approach with a horizontal grid resolution of 1 km × 1 km and

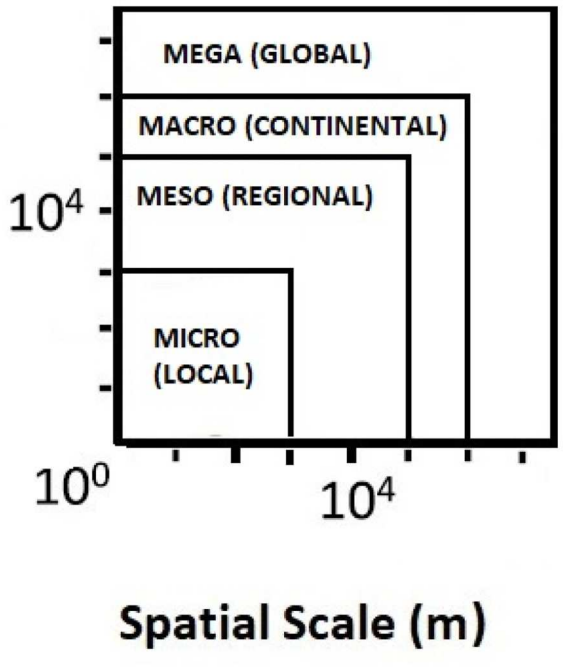

Fig. 2. Different levels of spatial scales (modified from (Shugart et al., 2020)).

sub-grid-scale modules like Gaussian dispersion and photochemistry to account for the point and line sources that increase the spatial resolution to around 100 m. The good performance of this model to show the hourly NO_2 concentrations was related to the effectiveness of sub-grid models (Hamer et al., 2020).

A modeling aspect that is highly emphasized in ATMs is the vertical resolution that according to different studies plays an important role. For example, the MOZART model was developed in the framework of the NCAR Community Climate Model (CCM), the number of vertical levels in CCM was set to 18, however in MOZART, these levels were increased to 25 starting from 70 m above ground level i.e., boundary layer, up to the height of 35700 m in the stratosphere. Increasing vertical levels in MOZART compared to CCM resulted in a better prediction of the vertical profile of ozone in the upper troposphere in comparison with the observations. In the AERMOD model, the objective was mainly focused on modeling vertical atmospheric inhomogeneity that includes PBL variations and vertical meteorological profiles. The model implementation was evaluated for moderate to complex terrain topography and provided reliable results. It was concluded that this was due to the improvement in the characterization of vertical profiles and PBL. Another Example is GEOS-Chem (Bey et al., 2001) that includes 20 to 70 vertical levels from the surface, in different versions of the model, and the meteorological fields are provided for these levels. The importance of vertical resolution of air in SMMs is often neglected or simplified. In some models, these variations are considered by including more compartments for air or integrating an ATM into the multimedia fate model to handle the vertical inhomogeneities. For example (Ghirardello et al., 2010; Morselli et al., 2011), integrated two variable height air compartments (upper air and lower air), varying according to hourly PBL variations, and this allowed to reconstruct, to a better extent hourly concentration variations of chemicals in air. Later on, AERMET and AERMOD sub-models were integrated into the multimedia fate model, AirFug, by Morselli et al. (2012) to account for hourly mixing height and PBL parameters as well as the presence of a point-source (simulated by AERMOD) in the model domain. Diel variation of air concentrations is observed due to PBL variations, wind speed, and wind direction showing that if the effect of a nearby emission source is neglected, daytime concentrations decrease due to the increase of PBL height, and nighttime concentrations increase due to the decrease of atmospheric dilution. Similar behavior is obtained when seasonal variations are accounted for, e.g., in winter, when the PBL height is lower in comparison to summer (Morselli et al., 2012). Also Ghirardello et al. (2010), as mentioned above, incorporated two dynamic air layers, hourly changing with height according to PBL variation, into the SoilPlus model, a layered soil multimedia model (Ghirardello et al., 2010) increasing also the vertical spatial domain in soil. In the study of J. H. Song et al. (2016) the effect of climate change is included in an SMM (POPsLTEA) by considering 4 layers of air with different distances from the surface in order to account for height dependent fate and transport of PAHs (vertical resolution). The model also accounts for horizontal resolution (i.e., 5000 cells of 50 km × 50 km and 1008 cells of 12.5 km × 12.5 km) as well as several environmental compartments (air, surface water, seawater, soil, and sediment). However, in comparison with an ATM, these spatial resolutions are still lower (J. H. Song et al., 2016). Therefore, the ATMs are considered quite free-handed in increasing the spatial resolution, however, the SMMs may have some limitations in increasing the number of segmentation since it also depends on the model capabilities to perform complex calculations. As the size of spatial units decreases, more units are needed to cover the area, therefore, a higher computational effort is required. Since SMMs also perform the flux calculations among different media and different compartments of each media, it is important to design the units (i.e., the number of units covering an area as well as their shape) in a way as to account for the relevant information while maintaining a certain level of simplicity.

Sometimes models focus on a smaller scale to be able to increase their spatial resolutions. For example, the ECORAME model (Jung et al.,

2014) is a multimedia model at local scale (10–10^2 km^2) for the simulation of chemicals in watersheds. The model considered each water segment as an independent cell rather than treating the whole watershed within one cell to be able to capture the variations in each stream. As the results of this study show, the concentration gradient within one stream can vary up to a factor of 10. Another model as such is the SoilPCA model (Kim et al., 2018), a multimedia fate model to evaluate the accidental chemical release, such as spills, on agricultural soil at a local scale. The model deals with the fate of chemicals with a spatial scale of a few kilometers. It is made of 3100 cells: 100 cells along the longitudinal direction and 31 cells along the transverse direction. The emission was considered to one of the atmospheric cells as an accidental release of contaminants. As a result, the model calculates the wind governed temporal variation of atmospheric concentrations by considering unidirectional wind speed.

In the comparison between ATMs and SMMs it is often observed that within a similar domain an ATM provides higher spatial resolution in comparison with a SMM. To give an example, at the global scale, an SMM like BETR-Global (MacLeod et al., 2011), covers the global environment by 15° × 15° grids, while a global ATM like GEOS-Chem (Bey et al., 2001) considers 1° × 1° grid resolution. The importance of spatial variation of environmental characteristics is inevitable. However, under certain conditions, other parameters such as physicochemical properties of the substances may seem to be more influential on the distribution of concentrations in the environment. Hollander et al. (2009) utilized an SMMs level III nested model, BasinBox, to evaluate the effect of substance properties and environmental characteristics (such as mixing height, precipitation intensities, temperature, and wind velocity for air compartment and other soil and water-related parameters) on the variation of concentrations. The concentration range (CR) value, the ratio between the 95th and 5th concentration percentiles, for chemical properties was at least three orders of magnitude greater than the CR of the environmental characteristics showing the higher influence of chemical properties (Hollander et al., 2009). However, their simulated environment was represented by a region of selected average environmental properties and dynamics. The evaluation of the sensitivity of the individual environmental parameters as well as physical-chemical properties was done by changing one parameter at a time. Therefore, their average regional characteristics could not reflect the variability and different association of environmental properties typically found on a spatial scale: for example, a part of the soil environment could have organic carbon and textural properties totally different from another part and the sensitivity analysis performed did not evaluate this variability. A similar conclusion was made by Zhu et al. (2014), who utilized the multimedia SESAMe model over China to account for overall persistence and long-range transport potential accounting for different environmental characteristics (i.e., precipitation, wind speed, temperature, and soil organic carbon) (Zhu et al., 2014). However, among environmental parameters considered for the air compartment, the effect of wind direction is neglected, which is an important factor especially when the emission is not diffuse but comes from a specific direction (Morselli et al., 2012). The effect of spatially resolved emission in the air was also emphasized in the study of Csiszar et al. (2013) by coupling a forecast and air pollution transport model (BLFMAPS) with a dynamic SMM, SO-MUM. The model was used to back-calculate the emission of POPs to air indicating the importance of such information in predicting the spatially variable concentrations of chemicals (Csiszar et al., 2013).

3.2. Temporal domain

The use of a dynamic model can improve the realism of the results especially in presence of episodic changes in emission or environmental conditions. Due to the unstable nature of the atmosphere, ATMs typically provide a high temporal resolution especially for input meteorological data (Christensen, 1997; ENVIRON, 2005; Robertson et al., 1999; Stohl, 1998). Sometimes a meteorological model is embedded within an ATM, as reported before, which provides temporally resolved meteorological data in two ways of offline or online. CMAQ is a "1-atm" model meaning that it couples air quality and meteorology modeling within one framework. The model is offline, so the meteorological data are fed into the model in hourly or several-hour time intervals. CMAQ is used by (Aulinger et al., 2011) to prove the importance of temporally resolved emission and meteorological data in chemical transport and deposition modeling of benzo(*a*)pyrene. The results of three modeling scenarios were compared: in the first one emission rate is constant during the year, in the second one, the emission rates vary seasonally, and hourly varying emission rates are compared with the measured data. In the third scenario where hourly emission rates are used, the indexes of agreement (IOA), a representation of the agreement between predicted and measured data, increased for most of the sites, representing better results. However, in the scenario where the emission is constant during the year, the result concentrations still follow the seasonal variation, similarly to the measurements, which indicate that the predicted concentration values are also dependent on the variation of meteorological conditions (e.g., PBL height) (Aulinger et al., 2011). The inclusion of meteorological models in an ATM has also been used in WRF/Chem (Grell et al., 2005) model, however, through an online approach so the meteorological data can be used in the model within the time scales of much less than 1 h. The study shows that the model provides a good forecasting skill for O_3 and its precursors (CO and NO_x) which was related to the model capability to include high-resolution physical meteorology within an air quality model. ATMs may implement a steady-state approach when the effect of temporal variations is not significant in order to maintain simplicity. For example, the AERMOD plume dispersion model requires a large number of parameters to represent these complexities; therefore, a steady-state Gaussian approach is implemented (Cimorelli et al., 2005; Perry et al., 2005). This approach makes the model suitable for small spatial domains. Similar logic is applied for SMMs; for example, IMPACT North America (Humbert et al., 2009) is capable of covering three different spatial scales including urban indoors and regional scales, several hundred zones of a continental scale located in a global box, hence the model is under the steady-state assumption to preserve simplicity. Therefore, depending on the objective of a model, the temporal resolution can be selected. For example, the response times of emission change of decamethylcyclopentasiloxane (D5) and PCB-180 in water and sediment under both steady-state and dynamic assumptions were investigated by Kim et al. (2017) using the Quantitative Water Air Sediment Interactive model (QWASI). Under both assumptions, the model provided a reliable estimation of the emission rates, an important factor to predict accurate concentration values. From the comparison between the simulations it was concluded that even though a dynamic model would provide a realistic insight into the environmental conditions, however, when the variations are known, also a steady-state model could provide reliable results while maintaining simplicity and transparency (Kim et al., 2017). Apart from simplicity, the steady-state assumption results in one concentration value which can simply be compared to predicted no-effect concentration (PNEC) and toxicity/exposure ratio (TER) for environmental risk assessment (ERA) purposes, while, for unsteady-state models where more than one concentration value is obtained, there is a need for further interpretation of the results (European Community, 2003). Examples of steady-state spatially resolved models are some fugacity models such as ChemCAN (Mackay et al., 1996b), where many regions of Canada were described and could be individually used as spatial scenarios for the simulation, the BETR North America (MacLeod et al., 2001), also capable of unsteady-state calculations, which includes 24 linked regional environment, and more recently a model developed to simulate the fate of PAHs in Shanghai (Huang et al., 2019).

However, recent studies (Di Guardo and Hermens, 2013; Morselli et al., 2015) called for more realistic peak exposure prediction which requires the evaluation of unsteady-state approaches in compartments

such as water (or air) and their significance in terms of risk assessment. The necessity to use high temporal resolution in SMMs in presence of sudden changes in environmental conditions is confirmed by several models which have adopted dynamic approaches. For example, the dynamic CoZMo_POP2 was developed for predicting the long-range fate of POPs in the coastal environment or drainage basin of large lakes. The model can utilize user-defined and time-variant emissions and environmental parameters (Wania et al., 2006). As another example, in the study of Morselli et al. (2018c) it is shown that the application of plant protection products (PPPs) imposes episodic peaks in watersheds with steep slopes: in such conditions the use of a dynamic model is a necessity (Morselli et al., 2018c). Pesticide applications are just a typical example of peak emission. The importance of assessing the relevance of unsteady (peak) emission on human exposure was recently underlined (D. Li et al., 2020) who compared their impact on human health by using a steady-state vs. an unsteady-state model. Likewise, the dynamicity of meteorological conditions in SMMs that are dealing with the most unstable compartment (i.e., air) must be considered. The influence of environmental dynamics such as PBL variation and vegetation on the prediction of exposure of some PCBs for terrestrial systems is investigated by Morselli et al. (2018a) using a multimedia dynamic model; (SoilPlusVeg). Results of the SoilPlusVeg simulation indicated the maximum PCB diel concentration variation due to PBL cycle, temperature-driven volatilization, and wind speed. The dynamic vegetation compartments also showed the daily variation of concentrations due to the uptake and release behavior of leaves (Morselli et al., 2018a). These short-term variations are not detectable with standard (e.g., periodic) monitoring campaigns or steady-state assumptions.

3.3. Chemical domain

Atmospheric transport models were initially used for ozone and its precursors. They mostly dealt with atmospheric chemicals such as O_3, SO_x, NO_x, dust, metals, and later PAHs (Appel et al., 2013; Nassar et al., 2009; Oleniacz and Rzeszutek, 2018; Robertson et al., 1999; Seigneur et al., 2003). Even though these models typically neglect the processes that occur in other environmental media, they simulate detailed processes for one or several chemicals in the air. These processes can be physical (e.g., dispersion characteristics in complex urban geometry (Vardoulakis et al., 2003)) or chemical (e.g., detailed chemical reactions). These processes are not usually accounted for in a multimedia fate model. For example, the CTDMPLUS model (Paumier et al., 1992; Perry, 1992) considers the dispersion due to a terrain when a chemical is released from a point source and passing over and around a three-dimensional complex terrain. The result of the SO_2 simulation with CTDMPLUS for near distances away from an emission source (2–3 km) showed top 25 hourly predictions of SO_2 concentrations, paired by rank with observations, is within a factor of 2. Another example is the extension of CityChem to EPISODE v10.0 model (Karl et al., 2019b) that accounts for complex atmospheric chemistry on an urban scale where there are complex anthropogenic traffic-related emissions. A larger number of chemicals such as NO_x, O_3, VOCs, SO_2, and secondary pollutants can be considered. Atmospheric models may provide mechanisms for a higher number of chemicals, for example, the GEOS-Chem model (Bey et al., 2001) includes 80 atmospheric chemicals, over 300 reactions for the troposphere, while adopting simpler reaction chemistry for the stratosphere.

Spatial multimedia fate models, especially those not coupled with atmospheric models, consider atmospheric processes in a much simpler way (often they only deal with advection and reaction of chemicals in the air). For example, in the G-CIEMS model (Suzuki et al., 2004), air compartments (lower air and upper air) are considered in a multiple box gridded model. The contribution of advective wind is incorporated using the directional average of inflow and outflow wind for each grid cell. Additionally, for large spatial extents like global models, the assumption of mixing the spatial units (i.e., geographical zones) faster than chemical movements may be considered; however, this may ignore small-scale atmospheric processes within each zone (Scheringer et al., 2000).

An example of how chemicals are differently processed in the two approaches is that of PAHs. They are modeled with both atmospheric transport and spatial multimedia fate models because many of them are of concern to human health due to their carcinogenic properties (IARC, 2010) and they are compounds discharged into the atmosphere from anthropogenic and natural sources. They are present in the air as vapor or associated with particle phase and can move to the soil by absorption, dry and wet depositions, and forest filter effect (McLachlan and Horstmann, 1998). Each model type considers different processes depending on the medium or media that are described, for example, for an atmospheric model, deposition processes are calculated only as removal processes, however, a multimedia fate model provides information about where chemicals end up after being removed from the atmosphere, therefore, investigating their further multimedia path (e.g., towards soils and sediment) (Ligaray et al., 2016; Wang et al., 2017). In a dynamic ATM, PAHs were modeled by Li et al. (2018) with a high spatial resolution of 1 km^2 for an industrialized and populated city. Processes accounted for PAHs in the air include advection, diffusion, the reaction of gaseous PAHs with OH radicals, and dry and wet depositions, coupled with emission inventory (B. Li et al., 2018). On the other hand, the spatially resolved Berkeley-Trent-Urban-Rural Fate Model (BETR-UR), also implemented for simulation of PAHs (S. Song et al., 2016), uses similar processes but being a box model neglects concentration differences within the box. This model implements intercompartmental transfer, degradation, and advection in the air in the urban and rural areas at a much larger scale (regional), but includes processes taking place in other media as well as fluxes from the air towards vegetation, soil, and freshwater.

Different studies were performed to improve the knowledge of chemical emission sources, pathways, and processes and their impact on the partitioning, distribution, and spatio-temporal variability. For example, Dueri et al. (2010) developed a 3D coupled hydrodynamic fate model for the fate of polychlorinated dibenzo-p-dioxins and dibenzofurans (PCDD/Fs) in a lagoon in order to identify the possible sources, seasonality of loads, and the role of atmospheric deposition (Dueri et al., 2010). Another example is the method of Imaizumi et al. (2018) for estimation of spatiotemporal variable emissions of herbicides from paddy fields (PeCHREM). The PeCHREM method is based on the published information on pesticide formulations. PeCHREM was used along with G-CIEMS, and a Japanese GIS dataset to calculate daily concentration changes of 25 herbicides in the whole Japan (Imaizumi et al., 2018).

This is particularly important for persistent and hydrophobic chemicals like POPs, especially evaluating their mobility on a global scale (Scheringer et al., 2000; Wania and Mackay, 1993). Among the driving parameters in regulating partitioning, we can list K_{aw} and K_{oa}. Chemicals with Log K_{aw} within the range of −5 to −1 and Log K_{oa} in the range of 6–13 tend to partition towards water and octanol (where octanol is representative of organic carbon in biota and solid phases), respectively, rather than air (Scheringer and Wania, 2003). This tendency has encouraged modelers to include additional elements that are effective in retaining organic chemicals such as terrestrial plants, macrophytes, and phytoplankton, as well as DOC, into multimedia fate models (Ghirardello et al., 2010; McLachlan and Horstmann, 1998; Morselli et al., 2015, 2018b; Terzaghi et al., 2017).

PCBs and some pesticides are among chemicals with relatively high K_{ow}. As shown in Table 2, these chemicals are mostly modeled by multimedia fate models due to their presence in compartments that are rich in organic carbon such as soil, sediments, and suspended solids (Csiszar et al., 2013; Di Guardo et al., 1994a; Fenner et al., 2007; Morselli et al., 2015; Nizzetto et al., 2016). Models may provide the long-term simulation of PCBs (up to decades) (MacLeod et al., 2005); their persistence, especially in a media like soil, followed by evaporation, and further deposition makes soil act as a long-term emission

source of PCBs to air. ATMs may also be implemented to simulate compounds like PCBs. For this purpose, it is required to include other environmental media and their corresponding processes. For example, the effect of climate change on the transport of POPs (HCH and PCBs) to Arctics is considered using an ATM model, DEHM (Hansen et al., 2015). The model includes air, water, soil, vegetation, and snow compartments. Processes such as two-way air-surface gas exchange as well as intra-compartmental processes were incorporated into the model (Hansen et al., 2004). Another example is the implementation of a multicompartmental chemistry transport model (MPI-MCTM) (Guglielmo et al., 2009) for the global distribution of different persistent chemicals (e.g., HCH, DDT, and PCBs). The model is made of different sub-models such as a three-dimensional atmosphere-ocean circulation model, an atmospheric aerosol model, marine biogeochemistry, and a two-dimensional top-soil and vegetation surfaces model. Embedding different sub-models enables the model to account for the fate of chemicals in other environmental compartments (e.g., air, soil, water, vegetation, snow, and land ice) (Guglielmo et al., 2009; Lammel and Stemmler, 2012).

While the models outlined above deal with mostly non-polar chemicals, not many models are capable to predict the fate of polar and ionizable chemicals, particularly on a spatial scale. The need of developing models for these chemicals was recently outlined (Di Guardo et al., 2018; Di Guardo and Hermens, 2013). While some predictive partitioning schemes are available for these chemicals (Franco and Trapp, 2010; Trapp et al., 2010), only some models were developed to account for spatial variability. One of such models is SESAMe v3.3 (Zhu et al., 2016) which adds the capability of predicting chemical fate at variable environmental pHs. However, considering that many substances (e.g., perfluoroalkyl substances such as PFOS and PFOA), given their high solubility and limited volatility, may undergo long-range aqueous transport, (instead of atmospheric transport), new models and approaches should be probably implemented, while a few are available (Kong et al., 2018; Li et al., 2017; Liu et al., 2015).

4. Conclusions

This study reviewed two types of spatially explicit environmental models namely ATMs and SMMs. Depending on the chemical properties, environmental characteristics, the type, and the number of media intended for simulation, the required spatial and temporal resolution, and the objective of the study, a model or a combination of different spatial models may be used. ATMs have been proven to be important tools for high-resolution simulation of contaminants in the atmosphere. Some of these models however include other environmental media as well as some of their processes (e.g., deposition and accumulation of contaminants from the atmosphere into the soil (Cheng, 2020)) but the spatial resolution of these additional media are mainly lower than the atmospheric compartments. SMMs consider different processes in multiple environmental media (e.g., air, water, soil, etc.). They can provide a closer insight into the interaction and fate of substances within and between these media, however, they may attain a lower spatial and sometimes temporal resolution in comparison to ATMs since obtaining an infinitesimal high spatial resolution for several environmental media (each consists of several compartments) requires high computational efforts and a large amount of input and monitoring data. Therefore, the choice of a suitable spatial scale and segmentation method is recommended to improve the accuracy of such models. After all, every modeling approach that is focusing in detail on one aspect may require to compromise in other aspects which might not be within the indispensable scopes. Both ATMs and SMMs play an important role in the risk assessment of chemicals and the prediction of exposure concentrations. Hence, they provide a basis for developing and testing different hypotheses such as risk evaluation of new chemicals and their large-scale transport mechanisms. The development of hybrid ATM-SMMs to account for a closer insight (or integration) into the modeling of horizontal and vertical atmospheric resolutions is therefore recommended to capture the complexity of environmental simulations.

Author contribution

Parisa Falakdin Investigation, Writing - original draft, Reviewing and Editing; Elisa Terzaghi: Writing- Reviewing and Editing; Antonio Di Guardo: Funding Acquisition, Resources, Writing- Reviewing and Editing, Supervision.

Declaration of competing interest

The authors declare that they have no known competing financial interests or personal relationships that could have appeared to influence the work reported in this paper.

Acknowledgments

University of Insubria is acknowledged for granting the PhD salary of P.F.

References

Adcroft, A., Hill, C., Campin, J.M., Marshall, J., Heimbach, P., 2004. Overview of the formulation and numerics of the MIT GCM. Proceedings of the ECMWF Seminar Series on Numerical Methods, Recent Developments in Numerical Methods for Atmosphere and Ocean Modelling. ECMWF.

Appel, K.W., Pouliot, G.A., Simon, H., Sarwar, G., Pye, H.O.T., Napelenok, S.L., Akhtar, F., Roselle, S.J., 2013. Evaluation of dust and trace metal estimates from the Community Multiscale Air Quality (CMAQ) model version 5.0. Geosci. Model Dev 6, 883–899. https://doi.org/10.5194/gmd-6-883-2013.

Armitage, J.M., Cousins, I.T., Hauck, M., Harbers, J.V., Huijbregts, M.A.J., 2007. Empirical evaluation of spatial and non-spatial European-scale multimedia fate models: results and implications for chemical risk assessment. J. Environ. Monit. 9, 572. https://doi.org/10.1039/b700680b.

Asman, W., 2001. Modelling the atmospheric transport and deposition of ammonia and ammonium: an overview with special reference to Denmark. Atmos. Environ. 35, 1969–1983. https://doi.org/10.1016/S1352-2310(00)00548-3.

Aulinger, A., Matthias, V., Quante, M., 2011. An approach to temporally disaggregate benzo(a)pyrene emissions and their application to a 3D eulerian atmospheric chemistry transport model. Water Air Soil Pollut. 216, 643–655. https://doi.org/10.1007/s11270-010-0559-x.

Barra, R., Vighi, M., Maffioli, G., Di Guardo, A., Ferrario, P., 2000. Coupling SoilFug model and GIS for predicting pesticide pollution of surface water at watershed level. Environ. Sci. Technol. 34, 4425–4433. https://doi.org/10.1021/es000986c.

Belyanovskaya, A., Laratte, B., Perry, N., Baranovskaya, N., 2019. A regional approach for the calculation of characteristic toxicity factors using the USEtox model. Sci. Total Environ. 655, 676–683. https://doi.org/10.1016/j.scitotenv.2018.11.169.

Bey, I., Jacob, D.J., Yantosca, R.M., Logan, J.A., Field, B.D., Fiore, A.M., Li, Q., Liu, H.Y., Mickley, L.J., Schultz, M.G., 2001. Global modeling of tropospheric chemistry with assimilated meteorology: model description and evaluation. J. Geophys. Res. Atmos. 106, 23073–23095. https://doi.org/10.1029/2001JD000807.

Brasseur, G.P., Hauglustaine, D.A., Walters, S., Rasch, P.J., Müller, J.-F., Granier, C., Tie, X.X., 1998. MOZART, a global chemical transport model for ozone and related chemical tracers: 1. Model description. J. Geophys. Res. Atmos. 103, 28265–28289. https://doi.org/10.1029/98JD02397.

Breivik, K., Eckhardt, S., McLachlan, M.S., Wania, F., 2021. Introducing a nested multimedia fate and transport model for organic contaminants (NEM). Environ. Sci. Process. Impacts 23, 1146–1157. https://doi.org/10.1039/D1EM00084E.

Byun, D.W., Ching, J.K.S., 1999. In: Science Algorithms of the EPA Models-3 Community Multiscale Air Quality (CMAQ) Modeling System. US Environ. Prot. Agency Off. Res. Dev. Wash. DC EPA/600/R-99/030.

Cheng, Z., 2020. Mercury accumulation in soil from atmospheric deposition in temperate steppe of Inner Mongolia, China. Environ. Pollut. 269–7491. https://doi.org/10.1016/j.envpol.2019.113692.

Choi, S.-D., Wania, F., 2011. On the reversibility of environmental contamination with persistent organic pollutants. Environ. Sci. Technol. 45, 8834–8841. https://doi.org/10.1021/es2017544.

Christensen, J.H., 1997. The Danish eulerian hemispheric model — a three-dimensional air pollution model used for the arctic. Atmos. Environ. 31, 4169–4191. https://doi.org/10.1016/S1352-2310(97)00264-1.

Christensen, J.H., Brandt, J., Frohn, L.M., Skov, H., 2004. Modelling of mercury in the arctic with the Danish eulerian hemispheric model. Atmos. Chem. Phys. 4, 2251–2257. https://doi.org/10.5194/acp-4-2251-2004.

Cimorelli, A.J., Perry, S.G., Venkatram, A., Weil, J.C., Paine, R.J., Wilson, R.B., Lee, R.F., Peters, W.D., Brode, R.W., 2005. AERMOD: a dispersion model for industrial source applications. Part I: general model formulation and boundary layer characterization. J. Appl. Meteorol. 44, 682–693. https://doi.org/10.1175/JAM2227.1.

Cohen, Y., Cooter, E.J., 2002. Multimedia environmental distribution of toxics (MendTox). I: hybrid compartmental-spatial modeling framework. Pract. Period. Hazard. Toxic, Radioact. Waste Manag. 6, 70–86. https://doi.org/10.1061/(ASCE)1090-025X(2002)6:2(70).

Cohen, Y., Tsai, W., Chetty, S.L., Mayer, G.J., 1990. Dynamic partitioning of organic chemicals in regional environments: a multimedia screening-level modeling approach. Environ. Sci. Technol. 24, 1549–1558. https://doi.org/10.1021/es00080a015.

Cooter, E.J., Hutzell, W.T., 2002. A regional atmospheric fate and transport model for atrazine. 1. Development and implementation. Environ. Sci. Technol. 36, 4091–4098. https://doi.org/10.1021/es011371y.

Cooter, E.J., Hutzell, W.T., Foreman, W.T., Majewski, M.S., 2002. A regional atmospheric fate and transport model for atrazine. 2. Evaluation. Environ. Sci. Technol. 36, 4593–4599. https://doi.org/10.1021/es011372q.

Cooter, E.J., Bash, J.O., Benson, V., Ran, L., 2012. Linking agricultural crop management and air quality models for regional to national-scale nitrogen assessments. Biogeosciences 9, 4023–4035. https://doi.org/10.5194/bg-9-4023-2012.

Coulibaly, L., Labib, M.E., Hazen, R., 2004. A GIS-based multimedia watershed model: development and application. Chemosphere 55, 1067–1080. https://doi.org/10.1016/j.chemosphere.2004.01.014.

Cowan, C.E., Mackay, D., Feijtel, T.C.J., van de Meent, D., Di Guardo, A., Davies, J., Mackay, N. (Eds.), 1995. The Multi-Media Fate Model: a Vital Tool for Predicting the Fate of Chemicals. SETAC Press, Pensacola, Fla.

Csiszar, S.A., Daggupaty, S.M., Verkoeyen, S., Giang, A., Diamond, M.L., 2013. SO-MUM: a coupled atmospheric transport and multimedia model used to predict intraurban-scale PCB and pbde emissions and fate. Environ. Sci. Technol. 47, 436–445. https://doi.org/10.1021/es3033023.

Csiszar, S.A., Diamond, M.L., Daggupaty, S.M., 2014. The magnitude and spatial range of current-use urban PCB and PBDE emissions estimated using a coupled multimedia and air transport model. Environ. Sci. Technol. 48, 1075–1083. https://doi.org/10.1021/es403080t.

Demael, E., Carissimo, B., 2008. Comparative evaluation of an eulerian CFD and Gaussian plume models based on prairie grass dispersion experiment. J. Appl. Meteorol. Climatol. 47, 888–900. https://doi.org/10.1175/2007JAMC1375.1.

Di Guardo, A., Hermens, J.L., 2013. Challenges for exposure prediction in ecological risk assessment: challenges in Exposure Prediction. Integrated Environ. Assess. Manag. 9, e4–e14. https://doi.org/10.1002/ieam.1442.

Di Guardo, A., Calamari, D., Zanin, G., Consalter, A., Mackay, D., 1994a. A fugacity model of pesticide runoff to surface water: development and validation. Chemosphere 28, 511–531. https://doi.org/10.1016/0045-6535(94)90295-X.

Di Guardo, A., Williams, R.J., Matthiessen, P., Brooke, D.N., Calamari, D., 1994b. Simulation of pesticide runoff at Rosemaund Farm (UK) using the SoilFug model. Environ. Sci. Pollut. Res. 1, 151–160. https://doi.org/10.1007/BF02986938.

Di Guardo, A., Morselli, M., Morabito, G., Semplice, M., Van den Brink, P.J., De Laender, F., 2017. European environmental scenarios of chemical bioavailability in freshwater systems. Sci. Total Environ. 580, 1237–1246. https://doi.org/10.1016/j.scitotenv.2016.12.084.

Di Guardo, A., Gouin, T., MacLeod, M., Scheringer, M., 2018. Environmental fate and exposure models: advances and challenges in 21 st century chemical risk assessment. Environ. Sci. Process. Impacts 20, 58–71. https://doi.org/10.1039/C7EM00568G.

Dong, J., 2019. A regional spatial environmental multimedia modeling (RSEMM) approach for assessing the risk of antibiotics in river basin system – a China case study. Sustain. Cities Soc. 50, 2210–6707. https://doi.org/10.1016/j.scs.2019.101624.

Dueri, S., Marinov, D., Fiandrino, A., Tronczyński, J., Zaldívar, J.-M., 2010. Implementation of a 3D coupled hydrodynamic and contaminant fate model for PCDD/fs in thau lagoon (France): the importance of atmospheric sources of contamination. Int. J. Environ. Res. Publ. Health 7, 1467–1485. https://doi.org/10.3390/ijerph7041467.

Dungan, J.L., 2015. Christopher D. Lloyd: exploring spatial scale in geography. Math. Geosci. 47, 885–887. https://doi.org/10.1007/s11004-015-9608-8.

Earnshaw, M.R., Jones, K.C., Sweetman, A.J., 2015. A first European scale multimedia fate modelling of BDE-209 from 1970 to 2020. Environ. Int. 74, 71–81. https://doi.org/10.1016/j.envint.2014.09.011.

ECHA, 2020. ECHA. Chem. Saf. Assess. Report. Tool CHESAR. https://chesar.echa.europa.eu/en, 12.22.20.

Eckhardt, S., Cassiani, M., Evangeliou, N., Sollum, E., Pisso, I., Stohl, A., 2017. Source–receptor matrix calculation for deposited mass with the Lagrangian particle dispersion model FLEXPART v10.2 in backward mode. Geosci. Model Dev. (GMD) 10, 4605–4618. https://doi.org/10.5194/gmd-10-4605-2017.

Emmons, L.K., Walters, S., Hess, P.G., Guenther, A., Kinnison, D., Laepple, T., Orlando, J., Tie, X., Tyndall, G., Wiedinmyer, C., Baughcum, S.L., Kloster, S., 2010. Description and evaluation of the model for ozone and related chemical tracers, version 4 (MOZART-4). Geosci. Model Dev. (GMD) 3, 43–67. https://doi.org/10.5194/gmd-3-43-2010.

ENVIRON, 2005. ENVIRON, User's Guide. Comprehensive Air Quality Model with Extensions Version 4.20. ENVIRON International Corporation, Novato, CA.

European Community, 2003. Technical Guidance Document on Risk Management. Institute for Health and Consumer Protection. https://echa.europa.eu/documents/10162/16960216/tgdpart2_2ed_en.pdf.

Fantke, P., Ernstoff, A.S., Huang, L., Csiszar, S.A., Jolliet, O., 2016. Coupled near-field and far-field exposure assessment framework for chemicals in consumer products. Environ. Int. 94, 508–518. https://doi.org/10.1016/j.envint.2016.06.010.

Fenner, K., Lanz, V.A., Scheringer, M., Borsuk, M.E., 2007. Relating atrazine degradation rate in soil to environmental conditions: implications for global fate modeling. Environ. Sci. Technol. 41, 2840–2846. https://doi.org/10.1021/es061923i.

Franco, A., Trapp, S., 2010. A multimedia activity model for ionizable compounds: validation study with 2,4-dichlorophenoxyacetic acid, aniline, and trimethoprim. Environ. Toxicol. Chem. 29, 789–799. https://doi.org/10.1002/etc.115.

Gencarelli, C.N., De Simone, F., Hedgecock, I.M., Sprovieri, F., Pirrone, N., 2014. Development and application of a regional-scale atmospheric mercury model based on WRF/Chem: a Mediterranean area investigation. Environ. Sci. Pollut. Res. 21, 4095–4109. https://doi.org/10.1007/s11356-013-2162-3.

Ghirardello, D., Morselli, M., Semplice, M., Di Guardo, A., 2010. A dynamic model of the fate of organic chemicals in a multilayered air/soil system: development and illustrative application. Environ. Sci. Technol. 44, 9010–9017. https://doi.org/10.1021/es1023866.

Ghirardello, D., Morselli, M., Otto, S., Zanin, G., Di Guardo, A., 2014. Investigating the need for complex vs. simple scenarios to improve predictions of aquatic ecosystem exposure with the SoilPlus model. Environ. Pollut. 184, 502–510. https://doi.org/10.1016/j.envpol.2013.10.002.

Gobas, F.A., Burkhard, L.P., Doucette, W.J., Sappington, K.G., Verbruggen, E.M., Hope, B.K., Bonnell, M.A., Arnot, J.A., Tarazona, J.V., 2016. Review of existing terrestrial bioaccumulation models and terrestrial bioaccumulation modeling needs for organic chemicals. Integrated Environ. Assess. Manag. 12, 123–134. https://doi.org/10.1002/ieam.1690.

Golden, H.E., Knightes, C.D., Cooter, E.J., Dennis, R.L., Gilliam, R.C., Foley, K.M., 2010. Linking air quality and watershed models for environmental assessments: analysis of the effects of model-specific precipitation estimates on calculated water flux. Environ. Model. Software 25, 1722–1737. https://doi.org/10.1016/j.envsoft.2010.04.015.

Grell, G.A., Peckham, S.E., Schmitz, R., McKeen, S.A., Frost, G., Skamarock, W.C., Eder, B., 2005. Fully coupled "online" chemistry within the WRF model. Atmos. Environ. 39, 6957–6975. https://doi.org/10.1016/j.atmosenv.2005.04.027.

Guglielmo, F., Lammel, G., Maier-Reimer, E., 2009. Global environmental cycling of γ-HCH and DDT in the 1980s – a study using a coupled atmosphere and ocean general circulation model. Chemosphere 76, 1509–1517. https://doi.org/10.1016/j.chemosphere.2009.06.024.

Hamer, P.D., Walker, S.-E., Sousa-Santos, G., Vogt, M., Vo-Thanh, D., Lopez-Aparicio, S., Schneider, P., Ramacher, M.O.P., Karl, M., 2020. The urban dispersion model EPISODE v10.0 – Part 1: an Eulerian and sub-grid-scale air quality model and its application in Nordic winter conditions. Geosci. Model Dev. (GMD) 13, 4323–4353. https://doi.org/10.5194/gmd-13-4323-2020.

Han, H., Wu, Y., Liu, J., Zhao, T., Zhuang, B., Wang, H., Li, Y., Chen, H., Zhu, Y., Liu, H., Wang, Q., Li, S., Wang, T., Xie, M., Li, M., 2020. Impacts of atmospheric transport and biomass burning on the inter-annual variation in black carbon aerosols over the Tibetan Plateau. Atmos. Chem. Phys. 20, 13591–13610. https://doi.org/10.5194/acp-20-13591-2020.

Hansen, K.M., Christensen, J.H., Brandt, J., Frohn, L.M., Geels, C., 2004. Modelling atmospheric transport of α-hexachlorocyclohexane in the Northern Hemispherewith a 3-D dynamical model: DEHM-POP. Atmos. Chem. Phys. 4, 1125–1137. https://doi.org/10.5194/acp-4-1125-2004.

Hansen, K.M., Christensen, J.H., Geels, C., Silver, J.D., Brandt, J., 2015. Modelling the impact of climate change on the atmospheric transport and the fate of persistent organic pollutants in the Arctic. Atmos. Chem. Phys. 15, 6549–6559. https://doi.org/10.5194/acp-15-6549-2015.

Hauck, M., Huijbregts, M.A.J., Armitage, J.M., Cousins, I.T., Ragas, A.M.J., van de Meent, D., 2008. Model and input uncertainty in multi-media fate modeling: Benzo [a]pyrene concentrations in Europe. Chemosphere 72, 959–967. https://doi.org/10.1016/j.chemosphere.2008.03.014.

Hayashi, T.I., Imaizumi, Y., Yokomizo, H., Tatarazako, N., Suzuki, N., 2016. Ecological risk assessment of herbicides in Japan: integrating spatiotemporal variation in exposure and effects using a multimedia model and algal density dynamics models: ecological risk assessment of herbicides in Japan. Environ. Toxicol. Chem. 35, 233–240. https://doi.org/10.1002/etc.3162.

Herod, A., 2009. Scale: the Local and the Global. In: Clifford N., Holloway S., Rice S.P., Valentine G. (Eds): Key Concepts in Geography, 2nd. SAGE, London, UK, pp. 217–235.

Hollander, A., Huijbregts, M.A.J., Ragas, A.M.J., van de Meent, D., 2006. BasinBox: a generic multimedia fate model for predicting the fate of chemicals in river catchments. Hydrobiologia 565, 21–38. https://doi.org/10.1007/s10750-005-1903-9.

Hollander, A., Scheringer, M., Shatalov, V., Mantseva, E., Sweetman, A., Roemer, M., Baart, A., Suzuki, N., Wegmann, F., van de Meent, D., 2008. Estimating overall persistence and long-range transport potential of persistent organic pollutants: a comparison of seven multimedia mass balance models and atmospheric transport models. J. Environ. Monit. 10, 1139. https://doi.org/10.1039/b803760d.

Hollander, A., Pistocchi, A., Huijbregts, M.A.J., Ragas, A.M.J., Van De Meent, D., 2009. Substance or space? The relative importance of substance properties and environmental characteristics in modeling the fate of chemicals in Europe. Environ. Toxicol. Chem. 28, 44. https://doi.org/10.1897/08-158.1.

Holmes, N.S., Morawska, L., 2006. A review of dispersion modelling and its application to the dispersion of particles: an overview of different dispersion models available. Atmos. Environ. 40, 5902–5928. https://doi.org/10.1016/j.atmosenv.2006.06.003.

Horowitz, L.W., Walters, S., Mauzerall, D.L., Emmons, L.K., Rasch, P.J., Granier, C., Tie, X., Lamarque, J.-F., Schultz, M.G., Tyndall, G.S., Orlando, J.J., Brasseur, G.P., 2003. A global simulation of tropospheric ozone and related tracers: description and evaluation of MOZART, version 2: MOZART-2 description and evaluation. J. Geophys. Res. Atmos. 108 https://doi.org/10.1029/2002JD002853 n/a-n/a.

Huang, Y., Sun, X., Liu, M., Zhu, J., Yang, J., Du, W., Zhang, X., Gao, D., Qadeer, A., Xie, Y., Nie, N., 2019. A multimedia fugacity model to estimate the fate and transport of polycyclic aromatic hydrocarbons (PAHs) in a largely urbanized area, Shanghai,

China. Chemosphere 217, 298–307. https://doi.org/10.1016/j.chemosphere.2018.10.172.
Humbert, S., Manneh, R., Shaked, S., Wannaz, C., Horvath, A., Deschênes, L., Jolliet, O., Margni, M., 2009. Assessing regional intake fractions in North America. Sci. Total Environ. 407, 4812–4820. https://doi.org/10.1016/j.scitotenv.2009.05.024.
IARC, 2010. Some non-heterocyclic polycyclic aromatic hydrocarbons and some related occupational exposures. In: International Agency for Research on Cancer-IARC Monographs on the Evaluation of Carcinogenic Risks to Humans. IARC Press ; Distributed by World Health Organization, Lyon, France: Geneva.
Imaizumi, Y., Suzuki, N., Shiraishi, F., Nakajima, D., Serizawa, S., Sakurai, T., Shiraishi, H., 2018. Development and validation of a simulation method, PeCHREM, for evaluating spatio-temporal concentration changes of paddy herbicides in rivers. Environ. Sci. Process. Impacts 20, 120–132. https://doi.org/10.1039/C7EM00517B.
Ippolito, A., Fait, G., 2019. Pesticides in surface waters: from edge-of-field to global modelling. Curr. Opin. Environ. Sustain. 36, 78–84. https://doi.org/10.1016/j.cosust.2018.10.023.
Jolliet, O., Wannaz, C., Kilgallon, J., Speirs, L., Franco, A., Lehner, B., Veltman, K., Hodges, J., 2020. Spatial variability of ecosystem exposure to home and personal care chemicals in Asia. Environ. Int. 134, 105260. https://doi.org/10.1016/j.envint.2019.105260.
Jung, J.E., Kim, Y.K., Song, J.H., Lee, D.S., 2014. Development and evaluation of a dynamic multimedia model (ECORAME) for local scale assessment of aquatic ecological exposure to chemicals originating from sources in environmental media. Sci. Total Environ 500–501. https://doi.org/10.1016/j.scitotenv.2014.08.097, 103–112.
Karl, M., Jonson, J.E., Uppstu, A., Aulinger, A., Prank, M., Sofiev, M., Jalkanen, J.-P., Johansson, L., Quante, M., Matthias, V., 2019a. Effects of ship emissions on air quality in the Baltic Sea region simulated with three different chemistry transport models. Atmos. Chem. Phys. 19, 7019–7053. https://doi.org/10.5194/acp-19-7019-2019.
Karl, M., Walker, S.-E., Solberg, S., Ramacher, M.O.P., 2019b. The Eulerian urban dispersion model EPISODE – Part 2: extensions to the source dispersion and photochemistry for EPISODE–CityChem v1.2 and its application to the city of Hamburg. Geosci. Model Dev. (GMD) 12, 3357–3399. https://doi.org/10.5194/gmd-12-3357-2019.
Kim, J.H., Kwak, B.K., Shin, C.B., Jeon, W.J., Park, H.-S., Choi, K., Yi, J., 2010. Spatial distribution multimedia fate model: numerical aspects and ability for spatial analysis. Appl. Math. Model. 34, 2279–2290. https://doi.org/10.1016/j.apm.2009.10.036.
Kim, J.H., Kwak, B.K., Shin, C.B., Jeon, W.J., Park, H.-S., Lee, S.W., Choi, K., Lee, W.G., Lee, J.H., Baek, S.H., Yi, J., 2011. Development of a local-scale spatially refined multimedia fate model (LSRMFM) for urban-scale risk assessment: model formulation, GIS-based preprocessing, and case study. Environ. Model. Assess. 16, 265–281. https://doi.org/10.1007/s10666-011-9250-x.
Kim, J., Mackay, D., Powell, D.E., 2017. Roles of steady-state and dynamic models for regulation of hydrophobic chemicals in aquatic systems: a case study of decamethylcyclopentasiloxane (D5) and PCB-180 in three diverse ecosystems. Chemosphere 175, 253–268. https://doi.org/10.1016/j.chemosphere.2017.02.050.
Kim, K.-E., Jung, J.E., Lee, Y., Lee, D.S., 2018. Ranking surface soil pollution potential of chemicals from accidental release by using two indicators calculated with a multimedia model (SoilPCA). Ecol. Indicat. 85, 664–673. https://doi.org/10.1016/j.ecolind.2017.11.010.
Kong, X., Liu, W., He, W., Xu, F., Koelmans, A.A., Mooij, W.M., 2018. Multimedia fate modeling of perfluorooctanoic acid (PFOA) and perfluorooctane sulphonate (PFOS) in the shallow lake Chaohu, China. Environ. Pollut. 237, 339–347. https://doi.org/10.1016/j.envpol.2018.02.026.
Kounina, A., Margni, M., Shaked, S., Bulle, C., Jolliet, O., 2014. Spatial analysis of toxic emissions in LCA: a sub-continental nested USEtox model with freshwater archetypes. Environ. Int. 69, 67–89. https://doi.org/10.1016/j.envint.2014.04.004.
Lammel, G., Stemmler, I., 2012. Fractionation and current time trends of PCB congeners: evolvement of distributions 1950–2010 studied using a global atmosphere-ocean general circulation model. Atmos. Chem. Phys. 12, 7199–7213. https://doi.org/10.5194/acp-12-7199-2012.
Lawrence, M.G., Butler, T.M., Steinkamp, J., Gurjar, B.R., Lelieveld, J., 2007. Regional pollution potentials of megacities and other major population centers. Atmos. Chem. Phys. 7, 3969–3987. https://doi.org/10.5194/acp-7-3969-2007.
Lee, Y., Lee, D.S., Kim, S.K., Kim, Y.K., Kim, D.W., 2004. Use of the relative concentration to evaluate a multimedia model, POPsME, for PAHs in the absence of emission estimate. Environ. Sci. Technol. 38, 1079–1088. https://doi.org/10.1021/es034792j.
Lee, Y., Cho, G., Lee, D.S., Lee, J.Y., Kim, Y.K., Kim, D.W., Kim, S.J., Kim, K., Jang, G., Choi, S., 2007. Influence of the large grid size used in a multimedia mass balance model (POPsME) on the exposure assessment of polychlorinated dibenzo- *p* -dioxins and dibenzofurans. Environ. Sci. Technol. 41, 5231–5236. https://doi.org/10.1021/es070222y.
Leelossy, Á., Molnár, F., Izsák, F., Havasi, Á., Lagzi, I., Mészáros, R., 2014. Dispersion modeling of air pollutants in the atmosphere: a review. Cent. Eur. J. Geosci. 6, 257–278. https://doi.org/10.2478/s13533-012-0188-6.
Leelossy, Á., Lagzi, I., Kovács, A., Mészáros, R., 2018. A review of numerical models to predict the atmospheric dispersion of radionuclides. J. Environ. Radioact. 182, 20–33. https://doi.org/10.1016/j.jenvrad.2017.11.009.
Li, J., 2019. A critical review of spatial predictive modeling process in environmental sciences with reproducible examples in R. Appl. Sci. 9, 2048. https://doi.org/10.3390/app9102048.
Li, Q., Wang, T., Zhu, Z., Meng, J., Wang, P., Suriyanarayanan, S., Zhang, Y., Zhou, Y., Song, S., Lu, Y., Yvette, B., 2017. Using hydrodynamic model to predict PFOS and PFOA transport in the Daling River and its tributary, a heavily polluted river into the Bohai Sea, China. Chemosphere 167, 344–352. https://doi.org/10.1016/j.chemosphere.2016.09.119.
Li, B., Wu, S., Zhou, S., Wang, T., Wang, C., 2018. Spatiotemporal distribution and dynamic modeling of atmospheric gaseous polycyclic aromatic hydrocarbons in a rapidly urbanizing city: Nanjing, China. Environ. Geochem. Health 40, 2603–2616. https://doi.org/10.1007/s10653-018-0126-8.
Li, L., Arnot, J.A., Wania, F., 2018a. Towards a systematic understanding of the dynamic fate of polychlorinated biphenyls in indoor, urban and rural environments. Environ. Int. 117, 57–68. https://doi.org/10.1016/j.envint.2018.04.038.
Li, L., Arnot, J.A., Wania, F., 2018b. Revisiting the contributions of far- and near-field routes to aggregate human exposure to polychlorinated biphenyls (PCBs). Environ. Sci. Technol. 52, 6974–6984. https://doi.org/10.1021/acs.est.8b00151.
Li, L., Arnot, J.A., Wania, F., 2019. How are humans exposed to organic chemicals released to indoor air? Environ. Sci. Technol. 53, 11276–11284. https://doi.org/10.1021/acs.est.9b02036.
Li, D., Tao, M., Vieira, J., Suh, S., 2020. The effects of incorporating non-linearity in LCA: characterizing the impact on human health. Front. Sustain. 1, 569385. https://doi.org/10.3389/frsus.2020.569385.
Li, L., Hoang, C., Arnot, J.A., Wania, F., 2020. Clarifying temporal trend variability in human biomonitoring of polybrominated diphenyl ethers through mechanistic modeling. Environ. Sci. Technol. 54, 166–175. https://doi.org/10.1021/acs.est.9b04130.
Ligaray, M., Baek, S.S., Kwon, H.-O., Choi, S.-D., Cho, K.H., 2016. Watershed-scale modeling on the fate and transport of polycyclic aromatic hydrocarbons (PAHs). J. Hazard Mater. 320, 442–457. https://doi.org/10.1016/j.jhazmat.2016.08.063.
Liu, S., Lu, Y., Wang, T., Xie, S., Jones, K.C., Sweetman, A.J., 2014. Using gridded multimedia model to simulate spatial fate of Benzo[α]pyrene on regional scale. Environ. Int. 63, 53–63. https://doi.org/10.1016/j.envint.2013.10.015.
Liu, S., Lu, Y., Xie, S., Wang, T., Jones, K.C., Sweetman, A.J., 2015. Exploring the fate, transport and risk of Perfluorooctane Sulfonate (PFOS) in a coastal region of China using a multimedia model. Environ. Int. 85, 15–26. https://doi.org/10.1016/j.envint.2015.08.007.
Lu, Q., Whitehead, P.G., Bussi, G., Futter, M.N., Nizzetto, L., 2017. Modelling metaldehyde in catchments: a River Thames case-study. Environ. Sci. Process. Impacts 19, 586–595. https://doi.org/10.1039/C6EM00527F.
Luo, Y., Yang, X., 2007. A multimedia environmental model of chemical distribution: fate, transport, and uncertainty analysis. Chemosphere 66, 1396–1407. https://doi.org/10.1016/j.chemosphere.2006.09.026.
Luo, Y., Gao, Q., Yang, X., 2007. Dynamic modeling of chemical fate and transport in multimedia environments at watershed scale—II: trichloroethylene test case. J. Environ. Manag. 83, 56–65. https://doi.org/10.1016/j.jenvman.2006.01.018.
Mackay, D., 1979. Finding fugacity feasible. Environ. Sci. Technol. 13, 1218–1223. https://doi.org/10.1021/es60158a003.
Mackay, D., 2001. Multimedia Environmental Models: the Fugacity Approach. CRC press.
Mackay, D., Diamond, M., 1989. Application of the QWASI (Quantitative Water Air Sediment Interaction) fugacity model to the dynamics of organic and inorganic chemicals in lakes. Chemosphere 18, 1343–1365. https://doi.org/10.1016/0045-6535(89)90027-1.
Mackay, D., Di Guardo, A., Paterson, S., Cowan, C.E., 1996a. Evaluating the environmental fate of a variety of types of chemicals using the EQC model. Environ. Toxicol. Chem. 15, 1627–1637. https://doi.org/10.1002/etc.5620150929.
Mackay, D., Di Guardo, A., Paterson, S., Kicsi, G., Cowan, C.E., 1996b. Assessing the fate of new and existing chemicals: a five-stage process. Environ. Toxicol. Chem. 15, 1618–1626. https://doi.org/10.1002/etc.5620150928.
Mackay, D., Di Guardo, A., Paterson, S., Kicsi, G., Cowan, C.E., Kane, D.M., 1996c. Assessment of chemical fate in the environment using evaluative, regional and local-scale models: illustrative application to chlorobenzene and linear alkylbenzene sulfonates. Environ. Toxicol. Chem. 15, 1638–1648. https://doi.org/10.1002/etc.5620150930.
Mackay, D., Celsie, A.K.D., Parnis, J.M., 2019. Kinetic delay in partitioning and parallel particle pathways: underappreciated aspects of environmental transport. Env. Sci. Technol. 53, 234–241. https://doi.org/10.1021/acs.est.8b04514.
MacLeod, M., Woodfine, D.G., Mackay, D., McKone, T., Bennett, D., Maddalena, R., 2001. BETR North America: a regionally segmented multimedia contaminant fate model for North America. Environ. Sci. Pollut. Res. 8, 156. https://doi.org/10.1007/BF02987379.
MacLeod, M., Riley, W.J., Mckone, T.E., 2005. Assessing the influence of climate variability on atmospheric concentrations of polychlorinated biphenyls using a global-scale mass balance model (BETR-Global). Environ. Sci. Technol. 39, 6749–6756. https://doi.org/10.1021/es048426r.
MacLeod, M., von Waldow, H., Tay, P., Armitage, J.M., Wöhrnschimmel, H., Riley, W.J., McKone, T.E., Hungerbuhler, K., 2011. BETR global – a geographically-explicit global-scale multimedia contaminant fate model. Environ. Pollut. 159, 1442–1445. https://doi.org/10.1016/j.envpol.2011.01.038.
Manneh, R., Margni, M., Deschênes, L., 2010. Spatial variability of intake fractions for Canadian emission scenarios: a comparison between three resolution scales. Environ. Sci. Technol. 44, 4217–4224. https://doi.org/10.1021/es902983b.
McKone, T.E., MacLeod, M., 2003. Tracking multiple pathways of human exposure to persistent multimedia pollutants: regional, continental, and global-scale models. Annu. Rev. Environ. Resour. 28, 463–492. https://doi.org/10.1146/annurev.energy.28.050302.105623.
McLachlan, M.S., Horstmann, M., 1998. Forests as filters of airborne organic pollutants: a model. Environ. Sci. Technol. 32, 413–420. https://doi.org/10.1021/es970592u.

Misaki, T., Yokomizo, H., Tanaka, Y., 2019. Broad-scale effect of herbicides on functional properties in benthic invertebrate communities of rivers: an integrated analysis of biomonitoring and exposure evaluations. Ecotoxicol. Environ. Saf. 171, 173–180. https://doi.org/10.1016/j.ecoenv.2018.12.089.

Mishra, K., Sharma, R.C., Kumar, S., 2012. Contamination levels and spatial distribution of organochlorine pesticides in soils from India. Ecotoxicol. Environ. Saf. 76, 215–225. https://doi.org/10.1016/j.ecoenv.2011.09.014.

Morselli, M., Ghirardello, D., Semplice, M., Di Guardo, A., 2011. Modeling short-term variability of semivolatile organic chemicals in air at a local scale: an integrated modeling approach. Environ. Pollut. 159, 1406–1412. https://doi.org/10.1016/j.envpol.2010.12.034.

Morselli, M., Ghirardello, D., Semplice, M., Raspa, G., Di Guardo, A., 2012. Integration of an atmospheric dispersion model with a dynamic multimedia fate model: development and illustration. Environ. Pollut. 164, 182–187. https://doi.org/10.1016/j.envpol.2012.01.039.

Morselli, M., Semplice, M., De Laender, F., Van den Brink, P.J., Di Guardo, A., 2015. Importance of environmental and biomass dynamics in predicting chemical exposure in ecological risk assessment. Sci. Total Environ. 526, 338–345. https://doi.org/10.1016/j.scitotenv.2015.04.072.

Morselli, M., Terzaghi, E., Di Guardo, A., 2018a. Do environmental dynamics matter in fate models? Exploring scenario dynamics for a terrestrial and an aquatic system. Environ. Sci. Process. Impacts 20, 145–156. https://doi.org/10.1039/C7EM00530J.

Morselli, M., Terzaghi, E., Galimberti, F., Di Guardo, A., 2018b. Pesticide fate in cultivated mountain basins: the improved DynAPlus model for predicting peak exposure and directing sustainable monitoring campaigns to protect aquatic ecosystems. Chemosphere 210, 204–214. https://doi.org/10.1016/j.chemosphere.2018.06.181.

Morselli, M., Vitale, C.M., Ippolito, A., Villa, S., Giacchini, R., Vighi, M., Di Guardo, A., 2018c. Predicting pesticide fate in small cultivated mountain watersheds using the DynAPlus model: toward improved assessment of peak exposure. Sci. Total Environ. 615, 307–318. https://doi.org/10.1016/j.scitotenv.2017.09.287.

Nassar, R., Logan, J.A., Megretskaia, I.A., Murray, L.T., Zhang, L., Jones, D.B.A., 2009. Analysis of tropical tropospheric ozone, carbon monoxide, and water vapor during the 2006 El Niño using TES observations and the GEOS-Chem model. J. Geophys. Res. 114, D17304. https://doi.org/10.1029/2009JD011760.

Nizzetto, L., Butterfield, D., Futter, M., Lin, Y., Allan, I., Larssen, T., 2016. Assessment of contaminant fate in catchments using a novel integrated hydrobiogeochemical-multimedia fate model. Sci. Total Environ. 544, 553–563. https://doi.org/10.1016/j.scitotenv.2015.11.087.

Nopmongcol, U., Koo, B., Tai, E., Jung, J., Piyachaturawat, P., Emery, C., Yarwood, G., Pirovano, G., Mitsakou, C., Kallos, G., 2012. Modeling Europe with CAMx for the air quality model evaluation international initiative (AQMEII). Atmos. Environ. 53, 177–185. https://doi.org/10.1016/j.atmosenv.2011.11.023.

Oleniacz, R., Rzeszutek, M., 2018. Intercomparison of the CALMET/CALPUFF modeling system for selected horizontal grid resolutions at a local scale: a case study of the MSWI plant in krakow, Poland. Appl. Sci. 8, 2301. https://doi.org/10.3390/app8112301.

Paumier, J.O., Burns, D.J., Perry, S.G., 1992. CTDMPLUS: a dispersion model for sources near complex topography. Part II: performance characteristics. Cover J. Appl. Meteorol. Climatol. J. Appl. Meteorol. Climatol. 31, 646–660. https://doi.org/10.1175/1520-0450(1992)031<0646:CADMFS>2.0.CO;2.

Pennington, D.W., Margni, M., Ammann, C., Jolliet, O., 2005. Multimedia fate and human intake modeling: spatial versus nonspatial insights for chemical emissions in western Europe. Environ. Sci. Technol. 39, 1119–1128. https://doi.org/10.1021/es034598x.

Perry, S.G., 1992. CTDMPLUS: a dispersion model for sources near complex topography. Part I: technical formulations. J. Appl. Meteorol. 31, 633–645.

Perry, S.G., Cimorelli, A.J., Paine, R.J., Brode, R.W., Weil, J.C., Venkatram, A., Wilson, R. B., Lee, R.F., Peters, W.D., 2005. AERMOD: a dispersion model for industrial source applications. Part II: model performance against 17 field study databases. J. Appl. Meteorol. 44, 694–708. https://doi.org/10.1175/JAM2228.1.

Pisso, I., Sollum, E., Grythe, H., Kristiansen, N.I., Cassiani, M., Eckhardt, S., Arnold, D., Morton, D., Thompson, R.L., Groot Zwaaftink, C.D., Evangeliou, N., Sodemann, H., Haimberger, L., Henne, S., Brunner, D., Burkhart, J.F., Fouilloux, A., Brioude, J., Philipp, A., Seibert, P., Stohl, A., 2019. The Lagrangian particle dispersion model FLEXPART version 10.4. Geosci. Model Dev 12, 4955–4997. https://doi.org/10.5194/gmd-12-4955-2019.

Pistocchi, A., Galmarini, S., 2010. Evaluation of a simple spatially explicit model of atmospheric transport of pollutants in Europe. Environ. Model. Assess. 15, 37–51. https://doi.org/10.1007/s10666-008-9187-x.

Pistocchi, A., Sarigiannis, D.A., Vizcaino, P., 2010. Spatially explicit multimedia fate models for pollutants in Europe: state of the art and perspectives. Sci. Total Environ. 408, 3817–3830. https://doi.org/10.1016/j.scitotenv.2009.10.046.

Pistocchi, A., Groenwold, J., Lahr, J., Loos, M., Mujica, M., Ragas, A.M.J., Rallo, R., Sala, S., Schlink, U., Strebel, K., Vighi, M., Vizcaino, P., 2011. Mapping cumulative environmental risks: examples from the EU NoMiracle project. Environ. Model. Assess. 16, 119–133. https://doi.org/10.1007/s10666-010-9230-6.

Prevedouros, K., Jones, K.C., Sweetman, A.J., 2004. European-scale modeling of concentrations and distribution of polybrominated diphenyl ethers in the pentabromodiphenyl ether product. Environ. Sci. Technol. 38, 5993–6001. https://doi.org/10.1021/es049206g.

Prevedouros, K., MacLeod, M., Jones, K.C., Sweetman, A.J., 2004. Modelling the fate of persistent organic pollutants in Europe: parameterisation of a gridded distribution model. Environ. Pollut. 128, 251–261. https://doi.org/10.1016/j.envpol.2003.08.041.

RIVM, 2004. RIVM. https://doi.org/10.1787/9789264103092-3-en. European Union System for the Evaluation of Substances 2.0 (EUSES 2.0). Background report.

Robertson, L., Langner, J., Engardt, M., 1999. An eulerian limited-area atmospheric transport model. J. Appl. Meteorol. 38, 190–210. https://doi.org/10.1175/1520-0450(1999)038<0190:AELAAT>2.0.CO, 2.

Roemer, M., Baart, A., Libre, J.M., 2005. ADEPT development of an Atmospheric Deposition and Transport model for risk assessment. TNO Rep. BO- R 2005-208 Apeldoorn.

Rosenbaum, R.K., Bachmann, T.M., Gold, L.S., Huijbregts, M.A.J., Jolliet, O., Juraske, R., Koehler, A., Larsen, H.F., MacLeod, M., Margni, M., McKone, T.E., Payet, J., Schuhmacher, M., van de Meent, D., Hauschild, M.Z., 2008. USEtox—the UNEP-SETAC toxicity model: recommended characterisation factors for human toxicity and freshwater ecotoxicity in life cycle impact assessment. Int. J. Life Cycle Assess. 13, 532–546. https://doi.org/10.1007/s11367-008-0038-4.

Russell, A., 2000. NARSTO critical review of photochemical models and modeling. Atmos. Environ. 34, 2283–2324. https://doi.org/10.1016/S1352-2310(99)00468-9.

Sala, S., Marinov, D., Pennington, D., 2011. Spatial differentiation of chemical removal rates from air in life cycle impact assessment. Int. J. Life Cycle Assess. 16, 748–760. https://doi.org/10.1007/s11367-011-0312-8.

Scheringer, M., 1996. Persistence and spatial range as endpoints of an exposure-based assessment of organic chemicals. Envirnmental Sci. Technol. 30, 1652–1659. https://doi.org/10.1021/es9506418.

Scheringer, M., Wania, F., 2003. Multimedia models of global transport and fate of persistent organic pollutants. In: Fiedler, H. (Ed.), Persistent Organic Pollutants, the Handbook of Environmental Chemistry. Springer-Verlag, Berlin/Heidelberg, pp. 237–269. https://doi.org/10.1007/10751132_9.

Scheringer, M., Wegmann, F., Fenner, K., Hungerbühler, K., 2000. Investigation of the cold condensation of persistent organic pollutants with a global multimedia fate model. Environ. Sci. Technol. 34, 1842–1850. https://doi.org/10.1021/es991085a.

Scheringer, M., Salzmann, M., Stroebe, M., Wegmann, F., Fenner, K., 2004. Long-range transport and global fractionation of POPs: insights from multimedia modeling studies. Environ. Pollut. 128, 177–188. https://doi.org/10.1016/j.envpol.2003.08.027.

Scire, J.S., Robe, F.R., Fernau, M.E., Yamartino, R.J., 1999. A User's Guide for the CALMET Meteorological Model. Earth Tech, Concord MA.

Scire, J.S., Strimaitis, D.G., Yamartino, R.J., 2000. A User's Guide for CALPUFF Dispersion Model. Earth Tech, Concord MA.

Scott, S., Mackay, D., Webster, E., 1998. Estimation of spatially variable atmospheric concentrations deduced from regional mass balance models. Chemosphere 36, 2507–2522. https://doi.org/10.1016/S0045-6535(97)10218-1.

Seigneur, C., Pun, B., Lohman, K., Wu, S.-Y., 2003. Regional modeling of the atmospheric fate and transport of benzene and diesel particles. Environ. Sci. Technol. 37, 5236–5246. https://doi.org/10.1021/es034433o.

Shankar Rao, K., 2007. Source estimation methods for atmospheric dispersion. Atmos. Environ. 41, 6964–6973. https://doi.org/10.1016/j.atmosenv.2007.04.064.

Shen, L., Wania, F., Lei, Y.D., Teixeira, C., Muir, D.C.G., Bidleman, T.F., 2005. Atmospheric distribution and long-range transport behavior of organochlorine pesticides in North America. Environ. Sci. Technol. 39, 409–420. https://doi.org/10.1021/es049489c.

Shugart, H.H., Foster, A., Wang, B., Druckenbrod, D., Ma, J., Lerdau, M., Saatchi, S., Yang, X., Yan, X., 2020. Gap models across micro- to mega-scales of time and space: examples of Tansley's ecosystem concept. For. Ecosyst. 7, 14. https://doi.org/10.1186/s40663-020-00225-4.

Sicard, P., Crippa, P., De Marco, A., Castruccio, S., Giani, P., Cuesta, J., Paoletti, E., Feng, Z., Anav, A., 2021. High spatial resolution WRF-Chem model over Asia: physics and chemistry evaluation. Atmos. Environ. 244, 118004. https://doi.org/10.1016/j.atmosenv.2020.118004.

Skov, H., Hjorth, J., Nordstrøm, C., Jensen, B., Christoffersen, C., Bech Poulsen, M., Baldtzer Liisberg, J., Beddows, D., Dall'Osto, M., Christensen, J.H., 2020. Variability in gaseous elemental mercury at villum research station, station nord, in North Greenland from 1999 to 2017. Atmos. Chem. Phys. 20, 13253–13265. https://doi.org/10.5194/acp-20-13253-2020.

Song, J.H., Lee, Y., Lee, D.S., 2016. Development of a multimedia model (POPsLTEA) to assess the influence of climate change on the fate and transport of polycyclic aromatic hydrocarbons in East Asia. Sci. Total Environ. 569 (570), 690–699. https://doi.org/10.1016/j.scitotenv.2016.06.127.

Song, S., Su, C., Lu, Y., Wang, T., Zhang, Y., Liu, S., 2016. Urban and rural transport of semivolatile organic compounds at regional scale: a multimedia model approach. J. Environ. Sci. 39, 228–241. https://doi.org/10.1016/j.jes.2015.12.005.

Stohl, A., 1998. Computation, accuracy and applications of trajectories—a review and bibliography. Atmos. Environ. 32, 947–966. https://doi.org/10.1016/S1352-2310(97)00457-3.

Stohl, A., Hittenberger, M., Wotawa, G., 1998. Validation of the Lagrangian particle dispersion model FLEXPART against large-scale tracer experiment data. Atmos. Environ. 32, 4245–4264. https://doi.org/10.1016/S1352-2310(98)00184-8.

Stohl, A., Forster, C., Frank, A., Seibert, P., Wotawa, G., 2005. Technical note: the Lagrangian particle dispersion model FLEXPART version 6.2. Atmos. Chem. Phys. 5, 2461–2474. https://doi.org/10.5194/acp-5-2461-2005.

Su, C., Song, S., Lu, Y., Wang, P., Meng, J., Lu, X., Jürgens, M.D., Khan, K., Baninla, Y., Liang, R., 2018. Multimedia fate and transport simulation of perfluorooctanoic acid/perfluorooctanoate in an urbanizing area. Sci. Total Environ. 643, 90–97. https://doi.org/10.1016/j.scitotenv.2018.06.156.

Suzuki, N., Murasawa, K., Sakurai, T., Nansai, K., Matsuhashi, K., Moriguchi, Y., Tanabe, K., Nakasugi, O., Morita, M., 2004. Geo-referenced multimedia environmental fate model (G-CIEMS): model formulation and comparison to the

generic model and monitoring approaches. Environ. Sci. Technol. 38, 5682–5693. https://doi.org/10.1021/es049261p.
Terzaghi, E., Morselli, M., Semplice, M., Cerabolini, B.E.L., Jones, K.C., Freppaz, M., Di Guardo, A., 2017. SoilPlusVeg: an integrated air-plant-litter-soil model to predict organic chemical fate and recycling in forests. Sci. Total Environ. 595, 169–177. https://doi.org/10.1016/j.scitotenv.2017.03.252.
Tesche, T.W., 1983. Photochemical dispersion modeling: review of model concepts and applications studies. Environ. Int. 9, 465–489. https://doi.org/10.1016/0160-4120(83)90004-1.
Tesche, T.W., Morris, R., Tonnesen, G., McNally, D., Boylan, J., Brewer, P., 2006. CMAQ/CAMx annual 2002 performance evaluation over the eastern US. Atmos. Environ. 40, 4906–4919. https://doi.org/10.1016/j.atmosenv.2005.08.046.
Trapp, S., Franco, A., Mackay, D., 2010. Activity-based concept for transport and partitioning of ionizing organics. Environ. Sci. Technol. 44, 6123–6129. https://doi.org/10.1021/es100509x.
Turner, D.B., 1979. A critical review. J. Air Pollut. Control Assoc. 29, 502–519. https://doi.org/10.1080/00022470.1979.10470821.
van den Brink, N.W., Arblaster, J.A., Bowman, S.R., Conder, J.M., Elliott, J.E., Johnson, M.S., Muir, D.C., Natal-da-Luz, T., Rattner, B.A., Sample, B.E., Shore, R.F., 2016. Use of terrestrial field studies in the derivation of bioaccumulation potential of chemicals. Integrated Environ. Assess. Manag. 12, 135–145. https://doi.org/10.1002/ieam.1717.
Vardoulakis, S., Fisher, B.E.A., Pericleous, K., Gonzalez-Flesca, N., 2003. Modelling air quality in street canyons: a review. Atmos. Environ. 37, 155–182. https://doi.org/10.1016/S1352-2310(02)00857-9.
Venkatram, A., Brode, R., Cimorelli, A., Lee, R., Paine, R., Perry, S., Peters, W., Weil, J., Wilson, R., 2001. A complex terrain dispersion model for regulatory applications. Atmos. Environ. 35, 4211–4221. https://doi.org/10.1016/S1352-2310(01)00186-8.
Vermeire, T.G., Jager, D.T., Bussian, B., Devillers, J., den Haan, K., Hansen, B., Lundberg, I., Niessen, H., Robertson, S., Tyle, H., van der Zandt, P.T.J., 1997. European union system for the evaluation of substances (EUSES). Principles and structure. Chemosphere 34, 1823–1836. https://doi.org/10.1016/S0045-6535(97)00017-9.
Wagner, C.C., Amos, H.M., Thackray, C.P., Zhang, Y., Lundgren, E.W., Forget, G., Friedman, C.L., Selin, N.E., Lohmann, R., Sunderland, E.M., 2019. A global 3-d ocean model for PCBs: benchmark compounds for understanding the impacts of global change on neutral persistent organic pollutants. Global Biogeochem. Cycles 33, 469–481. https://doi.org/10.1029/2018GB006018.
Wang, C., Zhou, S., He, Y., Wang, J., Wang, F., Wu, S., 2017. Developing a black carbon-substituted multimedia model for simulating the PAH distributions in urban environments. Sci. Rep. 7, 14548. https://doi.org/10.1038/s41598-017-14789-9.
Wania, F., 1996. Spatial variability in compartmental fate modelling: linking fugacity models and GIS. Environ. Sci. Pollut. Res. 3, 39–46. https://doi.org/10.1007/BF02986813.
Wania, F., Dugani, C.B., 2003. Assessing the long-range transport potential of polybrominated diphenyl ethers: a comparison of four multimedia models. Environ. Toxicol. Chem. 22, 1252–1261. https://doi.org/10.1002/etc.5620220610.
Wania, F., Mackay, D., 1993. Modelling the global distribution of toxaphene: a discussion of feasibility and desirability. Chemosphere 27, 2079–2094. https://doi.org/10.1016/0045-6535(93)90403-R.
Wania, F., Mackay, D., 1995. A global distribution model for persistent organic chemicals. Sci. Total Environ. 160–161, 211–232. https://doi.org/10.1016/0048-9697(95)04358-8.
Wania, F., Mackay, D., 1996. Tracking the distribution of persistent organic pollutants. Environ. Sci. Technol. 30, 390A–396A. https://doi.org/10.1021/es962399q.
Wania, F., Breivik, K., Persson, N.J., McLachlan, M.S., 2006. CoZMo-POP 2 – a fugacity-based dynamic multi-compartmental mass balance model of the fate of persistent organic pollutants. Environ. Model. Software 21, 868–884. https://doi.org/10.1016/j.envsoft.2005.04.003.
Wannaz, C., Fantke, P., Jolliet, O., 2018a. Multiscale spatial modeling of human exposure from local sources to global intake. Environ. Sci. Technol. 52, 701–711. https://doi.org/10.1021/acs.est.7b05099.
Wannaz, C., Fantke, P., Lane, J., Jolliet, O., 2018b. Source-to-exposure assessment with the Pangea multi-scale framework – case study in Australia. Environ. Sci. Process. Impacts 20, 133–144. https://doi.org/10.1039/C7EM00523G.
Wannaz, C., Franco, A., Kilgallon, J., Hodges, J., Jolliet, O., 2018c. A global framework to model spatial ecosystems exposure to home and personal care chemicals in Asia. Sci. Total Environ. 622 (623), 410–420. https://doi.org/10.1016/j.scitotenv.2017.11.315.
Warren, C.S., Mackay, D., Webster, E., Arnot, J.A., 2009. A cautionary note ON implications OF the well-mixed compartment assumption as applied to mass balance models OF chemical fate IN flowing systems. Environ. Toxicol. Chem. 28, 1858. https://doi.org/10.1897/08-569.1.
Webster, E., Mackay, D., Di Guardo, A., Kane, D., Woodfine, D., 2004. Regional differences in chemical fate model outcome. Chemosphere 55, 1361–1376. https://doi.org/10.1016/j.chemosphere.2003.10.061.
Wegener Sleeswijk, A., 2006. Globox – a spatially differentiated multimedia fate and exposure model. Environ. Sci. Pollut. Res. Int. 13 https://doi.org/10.1065/espr2006.02.003, 143–143.
Wegener Sleeswijk, A., Heijungs, R., 2010. GLOBOX: a spatially differentiated global fate, intake and effect model for toxicity assessment in LCA. Sci. Total Environ. 408, 2817–2832. https://doi.org/10.1016/j.scitotenv.2010.02.044.
Whitten, G.Z., Hogo, Henry, Killus, J.P., 1980. The carbon-bond mechanism: a condensed kinetic mechanism for photochemical smog. Environ. Sci. Technol. 14, 690–700. https://doi.org/10.1021/es60166a008.
Woodfine, D.G., MacLeod, M., Mackay, D., Brimacombe, J.R., 2001. Development of continental scale multimedia contaminant fate models: integrating GIS. Environ. Sci. Pollut. Res. 8, 164. https://doi.org/10.1007/BF02987380.
Yarwood, G., Kemball-Cook, S., Keinath, M., Waterland, R.L., Korzeniowski, S.H., Buck, R.C., Russell, M.H., Washburn, S.T., 2007. High-resolution atmospheric modeling of fluorotelomer alcohols and perfluorocarboxylic acids in the North American troposphere. Environ. Sci. Technol. 41, 5756–5762. https://doi.org/10.1021/es0708971.
Zannetti, P., 1990. Air Pollution Modeling. Springer US, Boston, MA. https://doi.org/10.1007/978-1-4757-4465-1.
Zannetti, P., 1992. Particle modeling and its application for simulating air pollution phenomena. In: Melli, P., Zannetti, P. (Eds.). Environmental modelling. Computational Mechanics Publications ; Elsevier Applied Science, Southampton ; Boston : London ; New York, pp. 211–242.
Zhang, Y., Horowitz, H., Wang, J., Xie, Z., Kuss, J., Soerensen, A.L., 2019. A coupled global atmosphere-ocean model for air-sea exchange of mercury: insights into wet deposition and atmospheric redox chemistry. Environ. Sci. Technol. 53, 5052–5061. https://doi.org/10.1021/acs.est.8b06205.
Zhu, Y., Price, O.R., Tao, S., Jones, K.C., Sweetman, A.J., 2014. A new multimedia contaminant fate model for China: how important are environmental parameters in influencing chemical persistence and long-range transport potential? Environ. Int. 69, 18–27. https://doi.org/10.1016/j.envint.2014.03.020.
Zhu, Y., Price, O.R., Kilgallon, J., Rendal, C., Tao, S., Jones, K.C., Sweetman, A.J., 2016. A multimedia fate model to support chemical management in China: a case study for selected trace organics. Environ. Sci. Technol. 50, 7001–7009. https://doi.org/10.1021/acs.est.5b05769.
Zhu, Y., Tao, S., Sun, J., Wang, X., Li, X., Tsang, D.C.W., Zhu, L., Shen, G., Huang, H., Cai, C., Liu, W., 2019. Multimedia modeling of the PAH concentration and distribution in the Yangtze River Delta and human health risk assessment. Sci. Total Environ. 647, 962–972. https://doi.org/10.1016/j.scitotenv.2018.08.075.

Paper II

Science of the Total Environment 845 (2022) 157190

Contents lists available at ScienceDirect

Science of the Total Environment

journal homepage: www.elsevier.com/locate/scitotenv

Predicting the regional contamination evolution of DDT for 100-years with a new gridded spatial and dynamic multimedia fate model

Parisa Falakdin [a], Elisa Terzaghi [a], Giuseppe Raspa [b], Antonio Di Guardo [a,*]

[a] Department of Science and High Technology, University of Insubria, Via Valleggio 11, 22100 Como, CO, Italy
[b] Department of Chemical Engineering, Materials, and Environment, Rome "La Sapienza" University, Via Eudossiana 18, 00184 Rome, RM, Italy

HIGHLIGHTS

- A spatiotemporal gridded fugacity-based model was developed.
- A dynamic local scale scenario was applied to evaluate the model accuracy.
- The emission of DDT was estimated using the world production trend.
- The model predicted the fate and degradation of DDT over 100 years.
- Wind direction can significantly affect the distribution of chemicals.

GRAPHICAL ABSTRACT

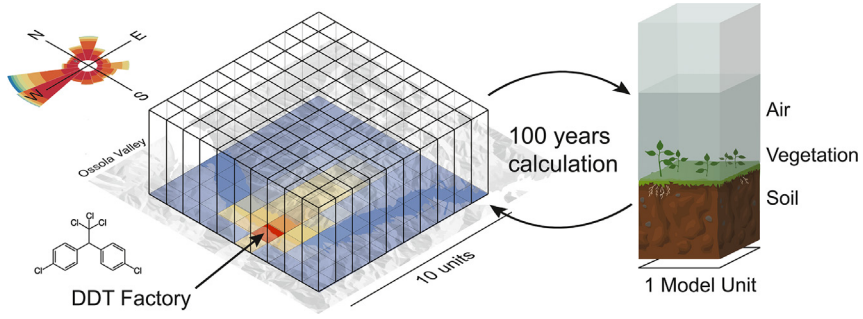

ARTICLE INFO

Editor: Damià Barceló

Keywords:
Soil and vegetation
p,p′-DDT
Contaminated site
Val d'Ossola
Pieve Vergonte
POPs

ABSTRACT

In 1996 high dichlorodiphenyltrichloroethane (DDT) concentrations were found in Lake Maggiore (Italy) fish and sediments. DDT was produced by a chemical company located in a subalpine valley (Ossola valley, Piedmont Region, Italy), and ended up in the Toce River, a tributary of Lake Maggiore. In the area surrounding the chemical plant, high DDT concentrations in soil and vegetation were found after subsequent investigations. The quantification of the release from contaminated soil and the following migration toward downwind areas, deposition to the soil, and further evaporation plays an important role in understanding future DDT trends in soil and the atmosphere. To study this phenomenon, soil, and vegetation from Ossola Valley were monitored in 2001 and 2011. The concentration values obtained (soils: 0.05 to 1 μg/g; vegetation 2–100 ng/g), allowed to reconstruct the contamination gradient in the valley and were used to develop and calibrate a spatially resolved multimedia fugacity model. The model accounts for spatial and temporal dynamicity of environmental characteristics such as wind speed and direction, variable air compartment height etc., and simulates the fate and transport of chemicals on a local scale. The dynamic emission of DDT (about 13,000 kg for the 50 y production time) to the air was estimated and utilized for a 100-year simulation (from 1948 to 2048). The results obtained allowed to understand the temporal and spatial pattern of DDT contamination for a long period at a local scale as well as the potential contribution as a source potentially affecting sites at larger distances.

1. Introduction

DDT is an insecticide widely used in the past to control the mosquito vector of malaria and to eradicate this disease (Tomlin, 1997). In the seventies, environmental concerns led to the ban of this chemical in some developed countries (WHO, 1979) and later by the Stockholm Convention on Persistent Organic Pollutants (POPs), although some limited use in developing countries is still permitted to control malaria (UNEP, 2001). In the summer of 1996, after routine monitoring of contamination in fish from one of the largest lakes in northern Italy, Lake Maggiore, DDTs were found at levels exceeding the legal threshold for food, with concentration in fish reaching up mg/kg fresh weight (f.w.) levels (Ceschi et al., 1996). The increase in DDTs concentrations in Lake Maggiore was due to the

* Corresponding author.
E-mail address: antonio.diguardo@uninsubria.it (A. Di Guardo).

http://dx.doi.org/10.1016/j.scitotenv.2022.157190
Received 31 May 2022; Received in revised form 30 June 2022; Accepted 2 July 2022
Available online xxxx

spill of this compound into a river (River Toce), flowing in Ossola Valley (Fig. 1), where a chemical plant, located in Pieve Vergonte (VB) manufactured DDT from 1948 up to 1997 (Barca, 2012).

While most of the efforts were initially devoted to the study of the evolution of the lake contamination, limited investigations were done to evaluate the contamination in the valley, in the area surrounding the chemical plant. Therefore, several monitoring campaigns were started to assess the possible effects of this DDTs rise on different environmental compartments. A project evaluated the gradient of air contamination, analyzing the bioaccumulated DDTs levels in conifer needles (Di Guardo et al., 2003). The measured concentrations of total DDTs, ranging from 1.35 to 47.7 ng/g dry weight (d.w.), indicated the existence of a pollution gradient in the air at increasing distance from the source. Additionally, the accumulation and release kinetics of DDTs were assessed in three plant species (oak, azalea, and cherry laurel) placed in a garden adjacent to the chemical factory producing DDTs (Di Guardo et al., 2008). Dynamic multimedia environmental models were also developed by this and other groups (Ghirardello et al., 2010a, 2010b; Morselli et al., 2012, 2011; Terzaghi et al., 2017; Wegmann et al., 2004) allowing for the evaluation of the fate of chemicals in a scenario including air, soil, vegetation, etc. However, these models did not allow following the fate of chemicals released into the air at a small, valley-wide, scale, with the potential of spreading to adjacent areas and regions and be deposited and accumulated in time. For this reason, although spatial and temporal models are available (Falakdin et al., 2022), a model capable of simulating the dynamic and spatial behaviour of DDT deriving from a local source was needed.

The aim of this study is therefore twofold: to investigate the spatial variability of air and soil concentrations at further distances from the industrial plant, and to develop a spatial fate model to predict the temporal and spatial dynamics of p,p′-DDT contamination in the valley (during the emission years as well as the years after the production ban), its future trends, and its potential for atmospheric transport outside the valley.

2. Materials and methods

2.1. Sampling

2.1.1. Site characterization

Ossola Valley is located at the south of the Italian Alps chain and west of Lake Maggiore, in the Province of Verbano-Cusio-Ossola in Northern Italy (Fig. 1). The flat bottom of the valley, located at 200 m above sea level, has a maximum width of 2 km and is oriented from the North-West to the South-East direction. The valley, which has a glacial origin, is surrounded by slopes that reach a height of 900 m on the Westside and 1300 m on the Eastside. River Toce flows across the valley's length, from North-West to South-East into Lake Maggiore.

The chemical plant from which the DDTs emission originated (formerly Enichem S.p.A.) is located in a small town (Pieve Vergonte), in the middle of Ossola valley which now hosts a contaminated site of national relevance (SIN Pieve Vergonte) (MITE, 2022). The plant started the production of technical DDT around 1948. This mixture contained p,p′- and o,p′-isomers of DDT, DDE and DDD, and p,p′-DDT was about 70 % (Di Guardo et al., 2003). It continued until the end of 1996 when the Italian Ministry of Environment issued the ban on DDTs production, after the discovery of Lake Maggiore contamination.

During the present study, about a hundred samples were obtained from various matrices (soil, leaves, and litter) from 61 sampling points, to evaluate the concentration gradient with distance from the industrial site.

2.1.2. Soil sampling

For the present study, 44 composite soil samples were collected in Ossola valley between July 2000 and May 2001 (later identified as “2001

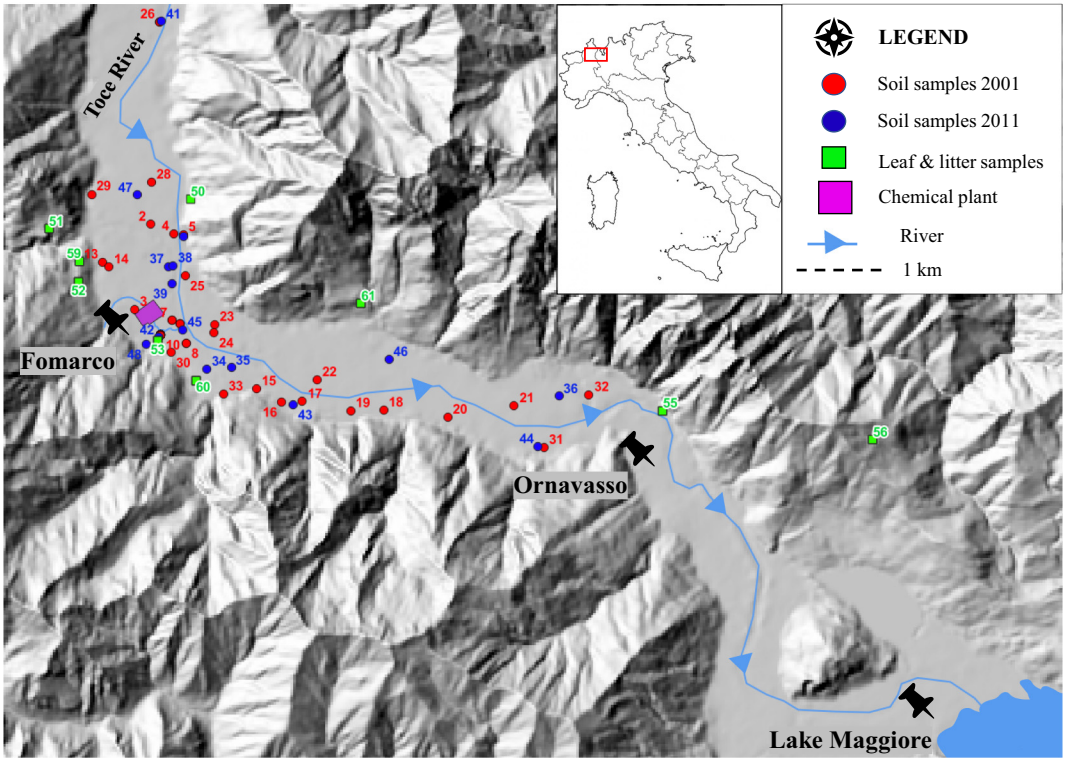

Fig. 1. Geographical position of Ossola valley in Northern Italy and the location of soil, litter, and leaf samples. Numbers represent the location ID of the samples (Appendix A.1). Fomarco and Ornavasso points are the locations of the closest meteorological stations. Map was realized using a digital elevation model obtained from Piedmont Region and elaborated in QGIS.

samples") (Table A.1). The position of each sampling point was determined using a Garmin GPS II Plus, in UTM WGS84 projection system, and later inserted in a digital map of Ossola valley (Fig. 1), created with ArcView 3.0 (Esri, Redlands CA, USA). For each soil sample, 5 surface subsamples (taken at a 0–5 cm depth) were obtained (at the four corners and the center of a square of approximately 1 m^2) with an acetone-rinsed stainless-steel corer and then mixed in order to obtain a single pooled sample. Grass turf was removed before sampling if present. All samples were stored at −30 °C (see 3.2 for more details).

In November 2011, 14 soil samples (from now on called "2011 soil samples") were collected and stored as above and analyzed by a GLP certified laboratory (ChemService s.r.l., Novate Milanese, MI, Italy).

2.1.3. Leaf and litter sampling

A total of 35 leaf samples (conifer needles of different ages) were collected from 10 locations along the valley between January 1999 and June 2000 (see Fig. 1). Some of leaf concentration data were previously published just for total DDT to examine their capability as passive air samplers (Di Guardo et al., 2003). Conifer needles were taken along Ossola Valley with increasing distance from the source during 1999. In each sampling location, spruce needles (*P. abies*) and pine (*P. nigra*) (Tables A.2, A.3) of different age classes (0 to 2 years) were collected paying attention to their relative position on the branch (Arndt et al., 1987). In nine sites, the litter samples were also collected between January to June 1999 (Table A.4). To avoid cross-contamination, clean rubber gloves were used for leaf sampling. Around 50 g of each needle age class was randomly collected at 1.5 m above ground, stored in hexane-rinsed glass jars with aluminum foil-lined lids, and kept at −30 °C until analysis (see 3.2 for more details).

2.2. Chemical analyses

Leaf, litter, and soil samples were first freeze-dried. Leaves and litter were then treated as outlined in (Di Guardo et al., 2008, 2003). Briefly, 2 g, d.w. of freeze-dried leaves or litter were extracted with hexane/acetone (9:1) (Baker, Deventer, The Netherlands) using a modified all-glass Soxtec apparatus (SER 148, Velp Scientifica, Usmate, Italy) for 6 h, then the extract was first concentrated and cleaned up using gel permeation chromatography in a 50 cm, 2.5 cm I.D. glass column with dichloromethane for residue analysis. The soil was sieved at 2 mm with a certified steel sieve and extracted in hexane/acetone (9:1) with an all-glass Soxtec apparatus for 6 h. The extracts were then digested in H_2SO_4 (on Extralut columns, Merck, Darmstadt, Germany) for 4 h in order to remove the organic fraction. Leaf, litter, and soil samples were afterward eluted and cleaned up on silica gel chromatography. The elution solvent was a mixture of hexane and toluene (65:35) (Baker, Deventer, The Netherlands). The eluted fraction was first concentrated in a rotary evaporator and then with a gentle flux of nitrogen. Internal standards ($^{13}C_{12}$ p,p′-DDT and $^{13}C_{12}$ p,p′-DDE, CIL, Boston, MA, USA) were added at extraction time. Standards of o,p′-DDT, p,p′-DDT, o,p′-DDD, p,p′-DDD, o,p′-DDE, p,p′-DDE (Riedel de Haën, 96 % purity) were used to create calibration curves. The analyses were performed with a gas chromatograph-mass spectrometer - (HP 6890-5972a) and electron impact in selected ion monitoring mode. The column used was an SGE BP10, 50 m (0.22 nm i.d., 25 μm phase thickness). More details can be found in Di Guardo et al. (2008, 2003).

2.2.1. Organic carbon measurement

Organic carbon in soil was measured using the Walkley-Black method (Gaudette et al., 1974; Walkley and Black, 1934) using 1 g of freeze-dried soil.

2.3. Quality assurance/quality control

The recovery for all the chemicals ranged from 65 to 90 % in 2001 samples. The limit of quantitation (LOQ) for each isomer was 0.1 μg/kg d.w. Procedural blanks (same solvents, glassware, and chemicals used but with no sample), were included with every five samples. The compounds were never detected in blanks above LOQ. No significant degradation of DDTs to DDDs was observed since ^{13}C-labelled standards were used as internal standards. Method reproducibility was checked by routinely analyzing a certified fish sample obtained during a previous laboratory intercalibration. Results were within 15 % of the certified values. More details on the analytical method employed can be found in (Di Guardo et al., 2008).

For the 2011 samples, analyzed by the commercial laboratory ChemService s.r.l., the limit of quantitation (LOQ) for each isomer was 10 μg/kg.

2.4. Gridded SoilPlusVeg model development

2.4.1. SoilPlusVeg model

The Gridded SoilPlusVeg (GSPV) model was built based on the SoilPlusVeg model (Terzaghi et al., 2017) which was used as a single building unit. SoilPlusVeg (SPV) is a dynamic multimedia model based on the fugacity approach (Mackay, 2001), developed to simulate the dynamic fate of chemicals in an area characterized by vegetation compartments (roots, stem, and leaves) along with different soil and atmospheric compartments: lower air, corresponding to the planetary boundary layer, and upper air. The capacity of each compartment is described in terms of *Z* values (mol/m^3 Pa), while transport and transformation processes are described using *D* values (mol/Pa h) (Ghirardello et al., 2010a; Terzaghi et al., 2017). SPV model performance was evaluated in a previous work (Terzaghi et al., 2017); moreover, an extensive sensitivity analysis was previously conducted in order to investigate the most influential parameters on concentrations in air, leaves and litter (Terzaghi et al., 2017). SPV model was developed in Visual Basic version 6.0 and integrates a GIS tool (MapWindow v. 5.6.3, MapWindow.org) to interrogate and retrieve geographical information. QuantumGIS version 3.20 (QGIS Development Team, 2018) was used for data storage, visualization, and analysis of the geospatial data.

2.5. Simulation scenario for the model evaluation

An evaluation of GSPV model performance was carried out for p,p′-DDT (Table A.5, Table A.6). The model was parameterized as shown in the following sections. GSPV was run for 49-years (1948 to 1997), period of DDTs production at the Pieve Vergonte chemical plant and for the following 51 years after the halt of production (a total of 100 years, up to the year 2048), to evaluate dissipation of DDT in time and space. The results of the simulation relating to the years 2001 and 2011 were compared to the measurements in soil, leaves, and air to evaluate the results.

2.5.1. Meteorological data

Due to the lack of hourly wind data at the Fomarco station, these data were obtained by the closest available meteorological station, for which wind direction and speed, located in Ornavasso (VB) (215 m a.s.l), about 11 km East of Pieve Vergonte (Fig. 1). Data were provided by Meteo Live Verbano Cusio Ossola and were obtained with a Davis Vantage Pro2 Weather station, installed at a height of 2 m from the ground, in an open area. Hourly data, average obtained from every half an hour, were gathered for year 2013, and used in the model as such. The wind rose from this station are shown in Fig. A.2. Wind speed in upper air ranged between 0.4 m/s to 12 m/s while that of lower air was between 0.3 m/s to 9 m/s.

Meteorological parameters such as temperature, precipitation, and solar radiation were provided by the closest regional station (Regional Agency for Environmental Protection) of year 2005 (ARPA, 2005) of the Piedmont Region for the Fomarco station (Fig. 1) on an hourly basis. Annual precipitation was 1293 mm (Fig. A.3), and the average temperature was 11 °C.

Due to the lack of locally estimated PBL heights, the planetary boundary layer (PBL) dataset of Milan (Terzaghi et al., 2017) was used, with the upper air compartment height ranging between 10 m to 2267 m and the lower air height ranging between 100 m to 3000 m, depending on the season and the diurnal temperature variations. The meteorological scenario

described above, related to one representative year, was implemented for the entire simulation time, in the lack of measured data for the simulated years.

2.5.2. Compartment parameters

The grid over the study area is composed of 100 square cells (i.e., 10 rows and 10 columns) of horizontal (x-y coordinates) sides of 1200 × 1200 m (1.44 km^2). Two types of vegetation cover were considered representative of the study area: a deciduous forest (parameterized as *Corylus avellana* (hazelnut)) (Terzaghi et al., 2013) for the mountain slopes adjacent to the two sides of the valley and a grass species (parameterized as *Festuca arundinacea*, tall fescue) along the valley (Fig. A.4), mostly characterized by agricultural and pasture use. For grass, constant biomass was considered, however, two cutting events were set: one for mid-April and one for mid-August. From the cutting events, the grass was considered to grow for one month until it reached its maximum biomass. In terms of chemical mass balance, the DDT content in grass is transferred to the soil after each cutting event.

The soil composition was set to loamy sand including 10 % clay, 10 % silt, and 80 % sand content, based on the soil textural data available (Lupato, 2001). Particulate/dissolved organic carbon (POC/DOC) in soil was set to 15 and 10 (mg/l), respectively (Terzaghi et al., 2020). The soil horizon was divided into 5 layers of 20 mm thickness. The mean organic carbon (OC) mass fraction was set to 0.0234 in soil, obtained by averaging the OC fractions measured at soil sampling sites.

2.5.3. Emission scenario

In order to run the simulation, p,p′-DDT emission in air was required. Due to the lack of information about the amount of DDT emitted from the chemical plant, an estimation was performed. The amount of hourly emitted chemicals into the air was back calculated based on the measured leaf concentrations at a certain distance from the source. Expressly, it was estimated the amount emitted into the air in one hour which could produce an air concentration equal to the available measured concentration in the same hour and at a specific distance from the source. An emission profile was then constructed for yearly emissions of the chemical plant to account for emission rise during the high productivity years, basing on the United States DDT production (WHO, 1979), which varied abruptly during the years from 1948 to 1997 (Figs. A.6 and A.7).

The yearly values were eventually broken down into hourly emission rates and fed into the model. PM10 was set to 50 (μg/m^3), representing average values for 1995–1998 for Northern Italy among those present in the AirBase & e-Reporting merged EU database (EEA, 2022).

Air background concentration at further distances from the source was estimated from leaves and litter values (Eq. (1)). Leaf concentrations (ng/g d.w.) were converted into air concentration (ng/m^3) values using plant-air partitioning coefficients according to the Nizzetto et al. (2008) (Eq. (1)).

$$log\ K_{PA} = y_0 + a\ \ log\ K_{OA} \tag{1}$$

where K_{pa} (m^3/g) and K_{oa} are the plant-air and octanol-air equilibrium partitioning coefficients, respectively, and y_0 and a are the regression parameters of the equation (Nizzetto et al., 2008). These values for spruce species were −1.75 and 0.33, respectively.

The leaf species used for this conversion were Norway spruce (*Picea abies*), black pine (*Pinus nigra*), white pine (*Pinus strobus*), Scots pine (*Pinus sylvestris*), and the European larch (*Larix decidua*).

For the points located 10 to 15 km away from the source, air concentration values vary between 0.04 and 0.06 ng/m^3. Therefore, the value of 0.05 ng/m^3 was selected for the model scenario, possibly reflecting background air concentrations outside of this scenario. Similar average concentrations in air (50–80 pg/m^3) were measured in 2008 for p,p′-DDT in air from Tuscany for urban and rural transects (Estellano et al., 2012).

2.6. Data representation

The 100-year simulation data were spatially plotted in Fig. 5 using one value for cell (center of the cell for each cell and at 10-year intervals) using the kriging interpolation method with an exponential covariance (Chilès and Delfiner, 2012). For the comparison of predicted vs. measured soil concentrations (Section 3.6), measured values were averaged within the location of a grid cell and were compared to the model results of the corresponding cell. The error bars relating to the measured data show the variation of concentration values for the nearby sample points. For the 2011 measured data, half of the limit of detection (LOQ) was considered for the samples with concentrations below LOQ (= 0.01 μg/g d.w.). For the predicted vs. measured leaf concentration comparison two years old needles were selected for comparison because these samples consistently provided valid concentration values of p,p′-DDT chemicals (among all the measured DDT components). The predicted air concentrations of Section 3.6 were calculated using K_{PA}. Given its high dependence on temperature, it was calculated for the minimum, maximum, median, first, and the third quartile of the hourly temperature of the year of the simulation scenario in order to have a range of K_{PA} values and incorporate the effect of temperature on uptake and release of chemicals between leaves and air (see also section A.4 in the Appendix).

2.7. Sensitivity and uncertainty analysis

A comprehensive sensitivity analysis for SPV was conducted in the corresponding paper (Terzaghi et al., 2017). For a gridded model, some parameters may have additional impact on the spatial distribution of chemicals. These parameters are the lower air height, windspeed and wind direction. Therefore, a sensitivity analysis was specifically conducted for these parameters to show their relevance in driving concentration in lower air, leaves, and soil for the entire grid system. These parameters were changed by 1 % one at a time and the results were assessed by calculating the absolute variations of the output to these changes using the following equation (MacLeod et al., 2002):

$$|S| = \left|\frac{\Delta O/O}{\Delta I/I}\right| \tag{2}$$

where ΔO and ΔI are the relative changes in the output and the input parameter, respectively.

A dynamic scenario in a predictive model along with limited available data can lead to the selection of a set of representative input and result in the deviation from the real scenario. Therefore, an uncertainty analysis was required to account for the uncertainty of the scenario hypotheses. The most sensitive parameters were used to perform this analysis to highlight the uncertainty of the implemented scenario on the chemical fate and transport within the grid system. Therefore, the average concentration of the entire grid was used for the comparison rather than a single cell value. An uncertainty of 30 % for PBL height and lower air windspeed was considered, accordingly, the variation of the results was assessed.

3. Results and discussion

3.1. Gridded SoilPlusVeg model

The SPV model was expanded to a 3D gridded model with a user-defined number of square-based grid cells in which each cell is one SPV unit. The originally integrated GIS tool in SPV can be now used to import site-specific information for each cell, later used in model calculations. The advective air fluxes in and out of each cell distribute the chemicals among different cells depending on the current hour wind speed and wind directions. The wind x, y velocity components for each layer (upper and lower air) were calculated depending on the wind speed, wind direction, and the angle at which wind is entering the system to account for the hourly distribution of moles between the cells (Fig. 2).

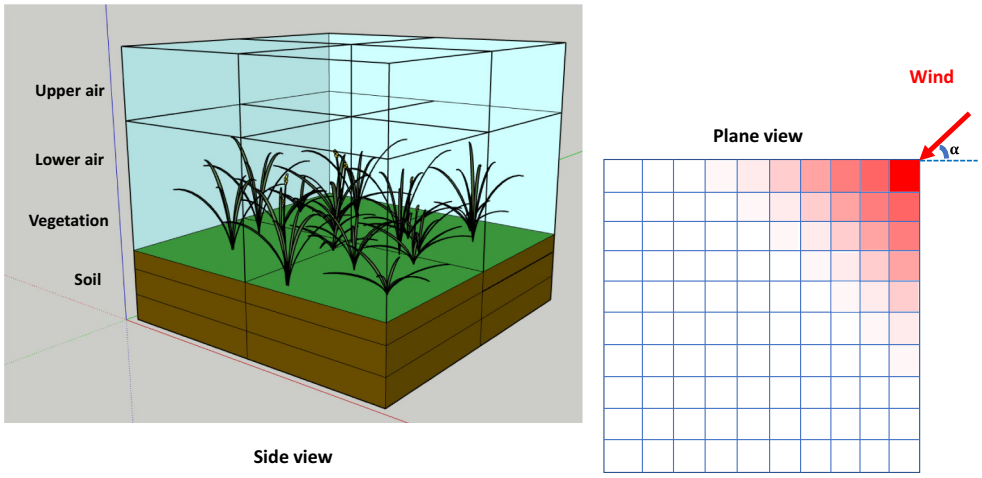

Fig. 2. Side view of the model including different environmental compartments. Plane view showing advective transport between adjacent air grid cells.

3.1.1. Approaches used in segmenting model scenario

This is the first approach in multimedia fate modeling, to our knowledge, that deals with the dynamic directional advective wind within a fine grid system (1.2 km × 1.2 km) for a small-scale scenario. Spatiotemporal multimedia fate models on small scale were mostly developed for the aquatic networks and the contribution of dynamic directional wind in the transport of chemical were either ignored and limited to the use of steady-state or dynamic hence unidirectional wind (Coulibaly et al., 2004). Additionally, the use of a fine grid for the air compartment is avoided in such models. The main reason for these choices is the numerical instability arising from the high-velocity wind and its propagation through a grid system when the transport distance of the wind within the time step is larger than the grid side length in that direction. For example, the ECORAM model (Jung et al., 2014), which is a multimedia model for exposure assessment in aquatic ecosystems at the local scale, incorporated an air grid system of 12 km × 12 km for the advective transport in order to keep the grid size larger than the wind travel distance while the spatial resolution of the watersheds was set up to 1 km^2.

Courant Fridrich Lewy (CFL) condition (de Moura and Kubrusly, 2013) indicates that the Courant number c ($=v_x\Delta t/\Delta x$) (where v_x is the wind velocity, t is time and x is distance) must be equal to or less than one in each time-step, implying that transport distance at each time-step should be smaller than the cell length.

In addition to incorporating large grid cells, another solution to keep the c number equal to or less than one is to use small time steps. This method in small-scale atmospheric models is employed by solving the advection-diffusion equation utilizing a Lagrangian approach. For example, the MATCH model is a high spatial resolution (5 km × 5 km) atmospheric model that used a limited area Eulerian approach (Robertson et al., 1999). Although a discrete approach was implemented to solve the gradient of advective flux between the two cell walls, to calculate the flux at the location of the cell walls a Lagrangian polynomial approximation was used. Nevertheless, it is not always feasible for a dynamic fate model including various environmental media to take advantage of a Lagrangian operator since it can lead to computational complexity especially when the model is aimed to simulate several decades.

3.1.2. Approach used in GSPV model

In this paper, a model composed of 100 cells is applied to a local scale (144 km^2) which includes 14 environmental compartments in each cell. In order to run the model for 100 years, a time step of 1 h is considered for the grid calculations, however, the SPV solver can calculate compartmental mass balance up to the temporal resolution of a second. Since in this simulation, the grid cells have high spatial resolution and the temporal resolution of less than 1 h can cause computational redundancy, the model requires a numerical solution to overcome the issue of advection between the small cells.

The GSPV model follows the upwind propagation method (UPM) meaning that the advective information in the grid system is only incorporated from the upstream adjacent grid (Chapra, 1997). To handle the chemical advective transport within a grid system when the wind speed is high, a solution was designed based on the sequential advection transport scheme presented by (Wu et al., 2019) in the formulation of the ICAT model. In this approach, the *c* number was always kept equal to or <1, however, a group of small queue-cells (i.e., cells with connected inflow and outflow faces) were considered within the adjacent cell and the transport and distribution of scalar (i.e., chemical) between the queue-cells were calculated. Calculation of the advection within the small queue-cells was used in GSPV to calculate the chemical distribution among the downstream cells. In the ICAT method, the number of queue-cells within the adjacent cell, *e*, was determined as N_e (Eq. (3)) and the volume of the small queue-cells was calculated as V_e^1(Eq. (4)). Eventually, the fraction of the scalar transporting to the first queue-cell, α_e, was obtained as the ratio between the volume of the small cells to the volume of the entering fluid in that time step (Eq. (5)).

$$N_e = \left[\frac{V_e}{q_e \Delta t}\right] \tag{3}$$

$$V_e^1 = V_e - (N_e - 1) q_e \Delta t \tag{4}$$

$$\alpha_e = [V_e - (N_e - 1) q_e \Delta t]/(q_e \Delta t) \tag{5}$$

where V_e is the volume of the cell, q_e is the flowrate, Δt is the time step. [] is the rounding up operator. The scalar was distributed among the queue-cells by a discrete piecewise-constant function as

$$\alpha_e . \varnothing_i + (1 - \alpha_e) \varnothing_{i-1} \tag{6}$$

where ϕ is the scalar, the first term represents the fraction of the scalar entering the cell, α_e, from the adjacent upstream queue-cell *i*, and the second term is the fraction of scalar exiting the cell, $(1 - \alpha_e)$, to the adjacent downstream queue-cell $i - 1$. In the GSPV model, the *c* number is calculated at each hour for the horizontal wind directions (i.e., along *x* and *y*). The roundup of the *c* number (i.e., *p*) can provide information about the number of cells that are getting affected by the advective wind of that hour in that direction. If the *p* number is equal one (i.e., only one adjacent cell is impacted by the wind), chemicals that exit the current cell through advection are considered as the input chemical of one neighboring cell. Otherwise, it means that the air enters and exits each cell faster than the defined time-step. For example, if the *p* number is equal to three it means that three

following cells along that direction are getting the advective wind, therefore, the amount of chemicals that are exiting the current cell will be distributed among the three following cells in the same time step using the abovementioned sequential advection transport method (Appendix B.1).

It is also assumed that at the current simulation scale, the compartmental processes occur after the advection process in that time step since the mass transfer coefficients (MTC) have an extremely lower rate compared to the advection rate. The MTC calculated for different processes varied between 10^{-6} to 6.5 m/h while the hourly wind speeds of the simulation scenario differ from 1080 to 43,200 m/h. Therefore, the wind speed is significantly faster than the compartmental processes (Appendix B.1.1). Therefore, at the end of each hour, the amount of chemicals entering each cell through advection is used for the multimedia mass balance calculations. Grid cells go through the compartmental mass-balance calculations (i.e., the SPV solver) one by one. Further details about the mass-balance calculation are described in Terzaghi et al. (2017).

The model accounts for the temporal hourly variation of meteorological data such as PBL height, wind speed, wind direction, temperature, precipitation, and solar radiation as well as site-specific vegetation type (with a user-defined cell-size resolution).

Based on available geographical information, the model will load data (i.e., average properties of the cell) from the attribute table corresponding to the shapefile of each cell. The vegetation type and parameters such as density and volume of roots and stem, stable specific leaf area (SLA), and parameters of plant-air partitioning coefficient (K_{PA}) for each cell were specified within the GIS database (Table A.7), while time-varying parameters such as dynamic SLA, leaf area index (LAI), leaf density, and wind speed at the height of the plant were fed into the model using external datasets.

3.2. Comparison between GSPV and SPV

The results of the GSPV model, calculated for one cell, were compared with the original single-cell SPV to validate the accuracy of the newly developed model. The scope of this comparison was to guarantee that each cell in the grid can produce identical results as a single cell SoilPlusVeg model when receiving similar input (i.e., chemical properties, meteorological, and environmental parameters). All concentration values for different compartments were identical. More details can be found in Appendix B.2.

3.3. Model sensitivity and uncertainty

The result of the sensitivity analysis showed that the lower air and foliage concentrations were more sensitive to the change of the tested parameters in comparison with soil ($S \sim 0$). Lower air concentration was mostly affected by the wind speed ($S \sim 1.5$). The effect of the wind direction ($S \sim 1.2$) and the height of the lower air ($S \sim 0.9$) were also considerable. Leaf concentrations however were mostly affected by the wind direction ($S \sim 1.4$). The influence of height of the lower air ($S \sim 0.9$) and windspeed ($S \sim 0.8$) on leaf concentrations were within the same range (Table B.2).

The result of the uncertainty analysis shows that with an uncertainty of 30 % for PBL height, the concentration of the lower air and leaves will change approximately 40 %. Additionally, a 30 % uncertainty for the lower air windspeed resulted in 40 % change in the foliage concentration and 80 % change in the lower air concentration (Table B.3). Concerning wind direction variability, a comparison of the data used for the 100 y simulation vs. the 10 y average for the Ornavasso station shows a relatively stable situation with the main changes in the WNW wind with a frequency which varies between of a factor of 2–3, WSW with a change of a factor of 4, and the NE of about 25 %. Additionally, in SPV model wind speed is reduced within the canopy as a function of the canopy height and cover (i.e., Leaf Area Index).

For all the above-mentioned scenarios, soil did not show a significant change of concentration. Therefore, this media can provide a more robust platform for comparison and prediction.

Additionally, for the analytical variability of the measurements, an uncertainty of 10 to 15 % was considered.

3.4. Spatial trend of DDT along the valley

Concentrations of DDTs (p, p'-DDT and isomers and metabolites) in soil (2001 and 2011), litter, and leaf (relating to the years 1997 to 2000) samples are reported in Appendix A.1 (Tables A.1, A.2, A.3, and A.4). Although these isomers and metabolites were measured, the simulation and comparison with measured data was performed for p,p′-DDT only, since the p,p′-DDT was the most abundant chemical in the technical DDT mixture produced by the chemical plant. Additionally, basing the comparison only on the parent compound would allow reducing the potential accounting of older metabolites (such as p,p′-DDE and p,p′-DDD) which could derive from local use of DDT in the past.

DDT concentrations in measured leaf and soil samples decrease with increasing distance from the chemical plant (Fig. A.1) as previously shown in Di Guardo et al. (2003). In spruce needles and back-calculated air samples, as well as soil, the p, p'-DDT concentrations reduce by about two orders of magnitude (needles: from 94 ng/g d.w. and 1.64 ng/g d.w., air from 3.95 to 0.068 ng/m^3) with distance. Soil concentrations of samples located in close vicinity of each other were averaged showing the maximum value of 0.7 μg/g d.w. in the vicinity of the chemical plant and minimum value of 0.003 μg/g d.w. 2 km northwest of the source. The soil concentration gradient varies up to 5 orders of magnitude; however, samples affected by external factors such as direct spill or washout by the river flow were excluded in the comparison predicted vs. measured values (Table A.1, PV-Red Soil 1, PV-Red Soil 2, Rio Marmazza 1, and Rio Marmazza 2 samples were excluded due to direct spill of sewage to soil. Villadossola 2 was excluded due to its vicinity to the river and flood soil washout

3.5. Importance of fluxes in driving the environmental behaviour of DDT

Basing on the assumption on chemical emission trend and calculated emission of Fig. A.6 and Fig. A.7 we calculated that the total emission in air (in the 50 years of production) was about 13,000 kg of DDT, equivalent to an average of 260 kg/y for each year of DDT production. Basing on this data and model simulations it can be estimated that the air advection out of the system is responsible of >95 % of the fluxes, in other terms <5 % of DDT is stored in soil and vegetation. This means that although an important amount of DDT is deposited to vegetation and soil (and there accumulated), nearly all DDT is exported to other areas through air movement.

Degradation is one of the most important loss fluxes in soil (up to 90 %) especially in those periods characterized by no leaching and runoff events. Degradation rates showed a seasonal variability (up to a factor of about 30) according to temperature and rainfall trend (i.e., degradation rates are updated considering Walker equation (Walker, 1974). Average degradation rate slightly varied with depth (i.e., a factor of about 1.2) while its spatial variability could not be appreciated since the same meteorological scenario was adopted for all the considered cells. The presence of vegetation generally increase the deposition fluxes to soil of about 40 % (compared to a bare soil), showing the importance of plants in capturing DDT from air and transferring it to soil (Wegmann et al., 2004). When looking at average soil loss fluxes, degradation is responsible for about 70 % of losses, infiltration, diffusion downwards and volatilization for about 10 % each while runoff is responsible for <1 %.

3.6. Comparison between GSPV simulation and measurements

GSPV model was run for the selected scenario and for 100 years, calculating concentration values of p,p′-DDT in air, leaves, and soil with respect to distance from the emission source. Simulated and measured concentrations were first compared for the years in which measurements were available (years 2001 and 2011). To evaluate the simulated/measured concentrations comparison, it should be remembered that air is a very dynamic media, and its hourly concentration highly depends on the

meteorological condition of that hour (e.g., PBL changes, affecting the air volume and concentrations, or wind speed, that can increase or reduce the chemical residence time in air). Soil instead, as a relatively immobile medium, receives chemicals deposition from air and can be used to represent the accumulation history of the chemicals in the study area.

Fig. 3 a and b shows the simulated versus measured logarithmic soil concentration values along the valley with distance from the chemical plant for the years 2001 and 2011, respectively.

The result of the comparison for soil samples shows a good agreement between the modeled and measured concentrations, with variation comprised up to one order of magnitude, but generally within a factor of five (Fig. 3). The deviation between the simulated and measured values is higher in areas further away from the chemical plant, possibly related to the uncertainty of precise meteorological conditions for the period simulated. However, considering the numerous assumptions we regard these results as a very good indication that the model could represent the historical contamination in the valley with sufficient accuracy.

Fig. 4 shows the simulated versus measured logarithmic leaf concentration values with distance from the chemical plant for years 2001 and 2011 (also available in Tables A.2, A.3; sample ID 51, 52, 53, 54, 55, 61). The result of predicted versus measured leaf concentrations indicated a satisfying agreement with the maximum measured values, within a factor of 2 (Fig. 4a). The comparison with maximum values depends on the fact that monitoring leaf samples are from evergreen species, accumulating DDT for a longer period, while simulated leaves are from deciduous species, for which accumulation takes place only for about 6 months a year.

Fig. 4b shows the measured versus the range of predicted logarithmic lower air concentration values with distance from the chemical plant. While the median predicted values show a better agreement with the measured data, the difference between the minimum and maximum simulated values is close to two orders of magnitude indicating the unstable nature of the lower air compartment (see also section B.4 in the appendix). Factors affecting these variations include the changes in planetary boundary layer height, which affects the air volume even within 24 h and results in different concentrations from one hour to another, wind speed, and wind direction which spread the chemicals in different areas at different times, resulting in very different hourly concentrations.

To fully evaluate the range of concentrations measured and predicted in this study it could be useful to show some measured values form the literature in periods for which DDT use was banned. For example, Calamari et al. (1991) studied the level of DDT metabolites in plant samples obtained from 26 sites around the world as a way to measure air contamination and global circulation of POPs. They showed that levels varied between 0.15 (ng/g d. w.) in Africa up to 77.8 (ng/g d. w.) in India (Calamari et al., 1991). More recently, soil DDT concentrations in the end of the 1990s in different measured by (Covaci et al., 2002) were 6.8, 26.2, 24.1, and 96 (ng/g d.w.) for

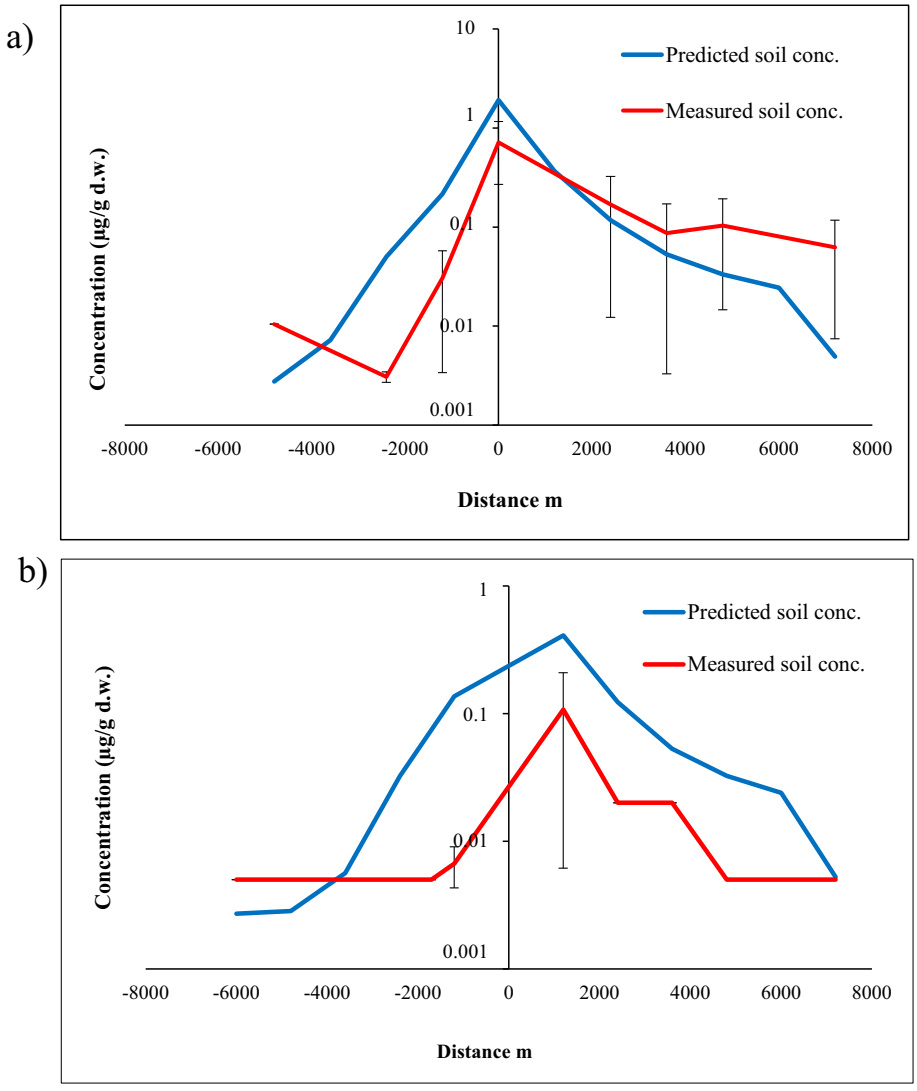

Fig. 3. Simulated and measured soil concentrations versus distance from the chemical plant. a) 2001; b) 2011. Error bars represent the standard deviation of the values of the measured samples within the cells at the different distances.

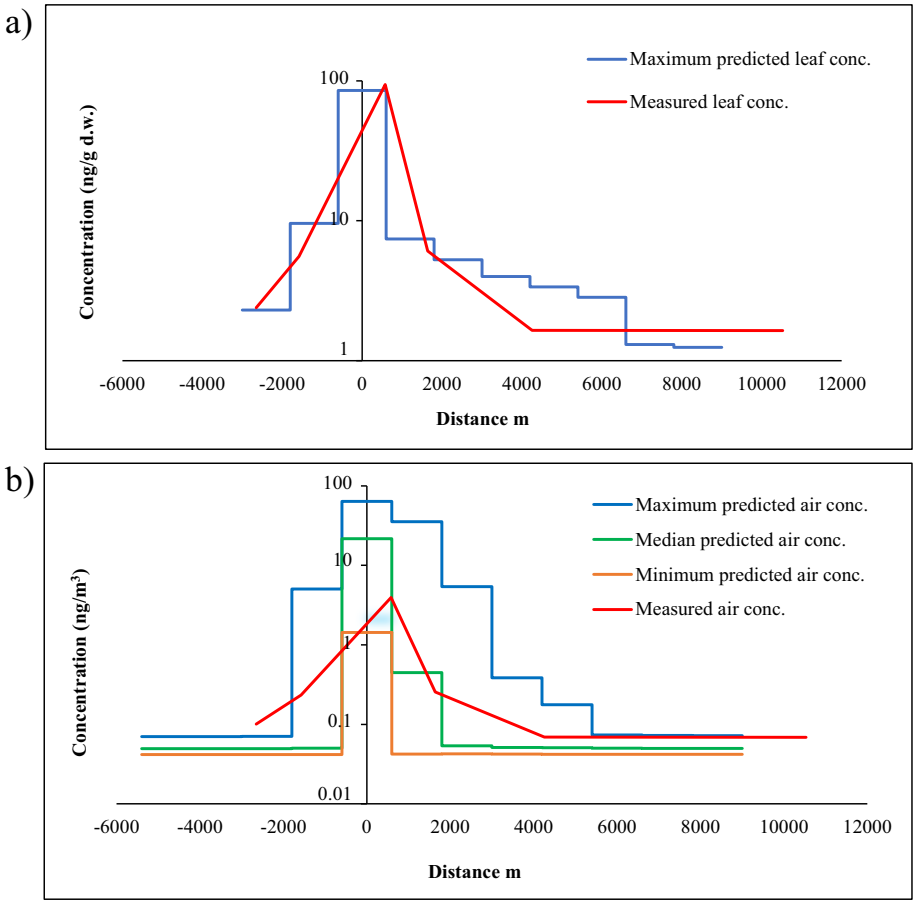

Fig. 4. a) Simulated and measured leaf concentrations versus distance from the chemical plant. b) Simulated and measured air concentrations versus distance from the chemical plant.

Belgium, Italy, Greece, and Romania, respectively. In surface agricultural soil samples from Tianjin area in China, the mean concentration of the total DDTs was 56 (ng/g d.w.) (Gong et al., 2004) and the DDT concentrations was reported by the authors as derived by the intense use of DDT between the 1960s to 1980s. Soil concentrations obtained in this study, were at least three orders of magnitude higher than those of the literature (μg/g vs. ng/g level) due to the influence of the emission source. However, at distance from the emission source concentrations in soils are closer to literature data, probably reflecting past agricultural DDT use and/or deposition from background air.

As mentioned before, soil concentrations can be used to evaluate DDT accumulation in time due to deposition from air, and specifically to focus on the effect of wind direction . For example, the concentration in soil at a location downwind of the source along the prevalent wind direction can be up to a factor of 20 higher than of a location scarcely reached by wind coming from the emission source. Fig. 5 shows the gradient of concentrations of DDT in soil from the emission point represented for 100 years at a 10 year interval, starting from the presumed production start (1948).

In each map isoconcentration lines differentiate areas characterized by soil DDT values within a factor of ten. Concentrations in soil generally vary between two to three orders of magnitude within the simulated grid, showing the intensity of deposition around the source and the dilution with distance, emission in time (with maximum emission in the '60), and the slow decrease in concentration after the production stop (1996). The maps for years 2001 and 2011 also include the corresponding measured sample points, represented with the same color range as the map predicted concentration gradients. The comparison of simulated and measured concentrations for these two sequential periods of time reveals the goodness of the simulation and be used for model benchmarking: most of the points, especially those close to the chemical plant, are in the same range (a factor of 10) of simulated concentrations. Some of the most distant points present either slightly higher or lower concentrations, probably depending on the uncertainties about the meteorological scenario in such a long simulation. However, given the uncertainties in the assumptions we regard these results as reasonably accurate to give a representation of the past and future contamination of the valley.

Overall, the results of the 100-year simulation showed that DDT accumulation in soil has involved a vast area in time. If we consider soil inventory, we calculated that the peak would be in 1971 with about 2415 kg sequestered in soil, reducing to 253 in 2021, 159 in 2031 and 99 in 2041. This last amount corresponds to <1 % of the amount emitted in the production period.

If we consider the current Italian threshold for DDT (including p,p′- and o, p'-isomers) contamination in soil for agricultural areas (0.01 μg/g d.w.) (Italian Ministry of Environment, 2019) it can be calculated that the soil surface at concentrations higher than the threshold corresponded to about 1560 ha in 1951, a maximum of 7433 ha in 1981 and currently (2021) of 3994 ha. The next 20-year simulations showed that this area will progressively reduce to 2872 ha in 2031 and 2045 ha in 2041, revealing that the long temporal burden of DDT will be still present on a large portion of the territory. It has to be underlined that agriculture has an important role in Ossola valley, with husbandry and other practices still taking place. Additionally, just adjacent to the north side of the valley lies the Val Grande National Park, and therefore, given the predicted concentrations, it might be advisable to evaluate the current and future ecosystem exposure and the potential effects in this and other areas.

While this exercise depicts DDT contamination, one should remember that DDE, the major degradation product in the soil of DDT, being more persistent

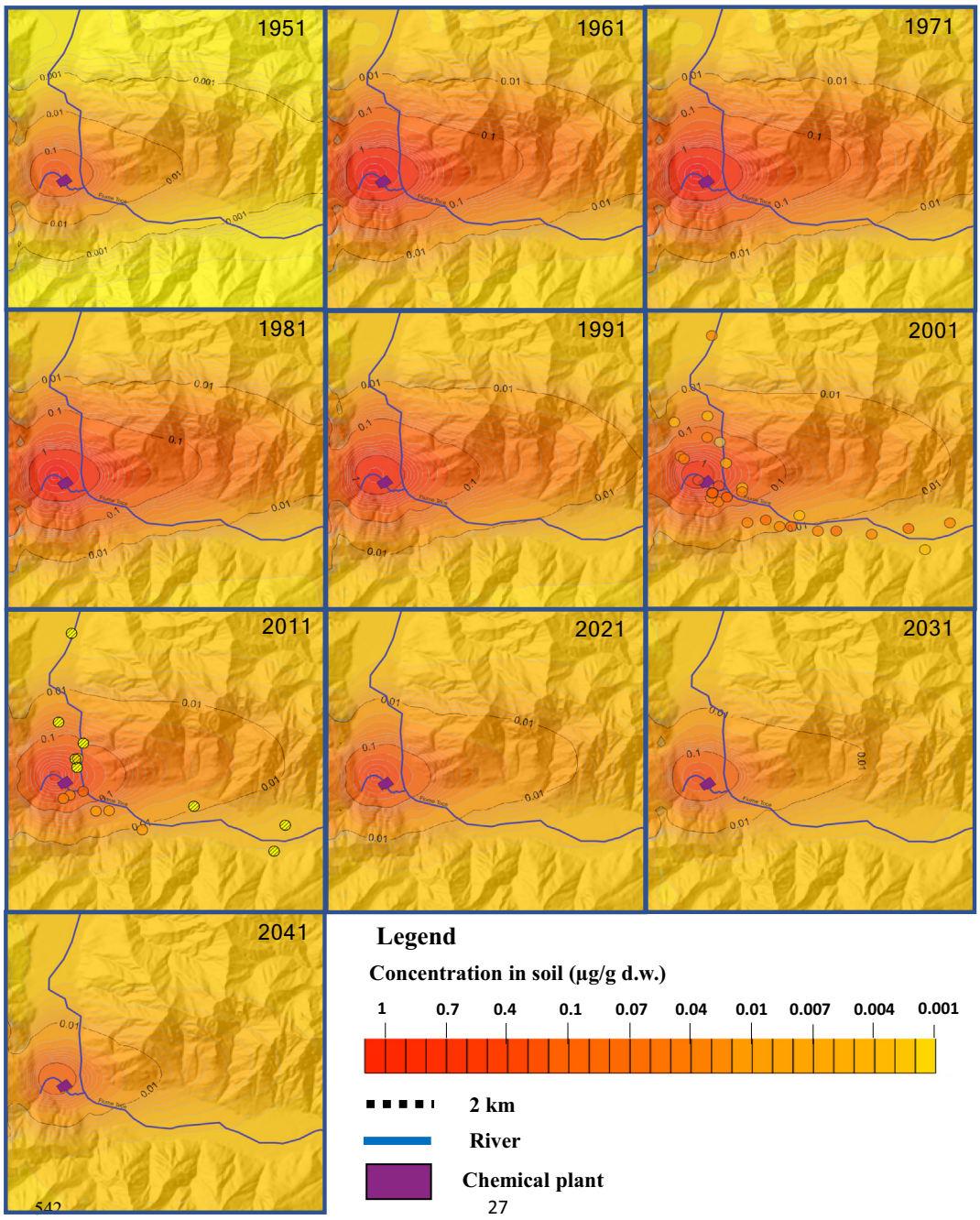

Fig. 5. Maps of the simulated soil concentrations in time. Round markers represent soil samples measured in 2001 and 2011, and their color represent the same interval of concentrations as the legend. The striped points in the 2011 map have a value lower than the limit of quantitation (LOQ) of 0.01 µg/g d.w.

(Mackay, 2001) will be probably present in the soil for additional time and contribute to the total ecotoxicity of DDTs in time. Basing on 2001 samples, DDE is about 50 % of DDT therefore, to a first approximation and as a worst case we can assume that total DDTs at each time interval will be comprised of these amounts to be added to the DDT levels depicted in Fig. 5.

3.7. Limitations

The model scenario in the simulated area was simplified to reduce complexity. However, wind direction and speed can be different along a valley shaped topography due to the canyon effect (Chen et al., 2020). In this situation, for example, the wind direction is more likely to have a coherence pattern during the years. This matter could not be hence investigated due to the lack of different meteorological stations along the valley. Higher soil concentration along the valley can be due to this fact in addition to the presence of the river, chemical can move through the suspended solids and deposit in downstream areas. The absence of a river in the simulation scenario was due to complications arising from the discretization of river segments, which was not incorporated in the current model version. However, an estimation of DDT loads reaching Lake Maggiore water and sediments was obtained previously (Di Guardo et al., 2006).

A remediation project was started in 2014 by Eni Rewind (Eni rewind, 2020). One of the activities was the removal of the contaminated soil from the internal and external areas of the industrial site. This might have reduced the chemical emissions due to evaporation from soil starting from that year. However, these activities were limited to the areas adjacent to the chemical plant, while as the results show, these chemicals seem to be accumulated in the soil of large portions of the valley.

4. Conclusions

A spatially resolved gridded model with multimedia fate model units was developed and benchmarked against >100 measured data for the Ossola valley. This allowed estimating the emission of DDT released from a local chemical plant and determining the role of the spatial meteorological and environmental parameters on the fate and transport of DDT in the valley. The simulation performed allowed to calculate DDT concentrations in different media, generally within an order of magnitude from measured data. Long term simulation results showed the spatial and temporal extent for an area contaminated by a persistent and hydrophobic chemical to clean up. Further future monitoring activities would be useful to verify the trend of contamination and model validation. In addition, further investigation should be performed to evaluate the contribution of this local DDT emission source toward the regional/continental scale.

CRediT authorship contribution statement

Parisa Falakdin: Investigation, Writing - Original draft preparation, Visualization; **Elisa Terzaghi**: Resources, Data curation, Writing - Reviewing and Editing; **Giuseppe Raspa**: Investigation; **Antonio Di Guardo**: Funding Acquisition, Resources, Writing - Reviewing and Editing, Supervision.

Declaration of competing interest

The authors declare that they have no known competing financial interests or personal relationships that could have appeared to influence the work reported in this paper.

Acknowledgments

Serena Zaccara, Elena Saporiti, Ilaria Colombo, and Alessandro Antichi are acknowledged for their help in sampling and analysis of the environmental samples; Luca Sergio (Meteo Live Verbano Cusio Ossola) is kindly acknowledged for providing the wind direction and intensity data of the Ornavasso meteorological station. Gianmaria Cetti is gratefully acknowledged for preparing the graphical abstract.

Appendix A. Supplementary data

Supplementary data to this article can be found online at https://doi.org/10.1016/j.scitotenv.2022.157190.

References

Arndt, U., Nobel, W., Schweizer, B., 1987. Bio-indikatoren: Möglichkeiten, Grenzen und neue Erkenntnisse. Eugen Ulmer GmbH & Co., Stuttgart, Germany.

Arpa, 2005. The Regional Agency for Environmental Protection, Arpa Agenzia Regionale Per La Protezione Ambientale [WWW Document]. http://www.arpa.piemonte.it/.

Barca, S., 2012. Il caso italiano: industria, chimica e ambiente. Jaca Book, Milan.

Calamari, D., Bacci, E., Focardi, S., Gaggi, C., Morosini, M., Vighi, M., 1991. Role of plant biomass in the global environmental partitioning of chlorinated hydrocarbons. Environ. Sci. Technol. 25, 1489–1495. https://doi.org/10.1021/es00020a020.

Ceschi, M., De Rossa, M., Jaggli, M., 1996. Contaminanti organici, inorganici e radionuclidi nell'ittiofauna dei laghi Ceresio e Verbano (bacini svizzeri). Trav. Chim. Aliment. Hyg. 87, 189–211.

Chapra, S.C., 1997. Surface Water Quality Modeling. McGraw-Hill, New York, NY.

Chen, T., Li, Y., Luan, D., Jiao, A., Yang, L., Fan, C., Shi, L., 2020. Study of flow characteristics in tunnels induced by canyon wind. J. Wind Eng. Ind. Aerodyn. 202, 104236. https://doi.org/10.1016/j.jweia.2020.104236.

Chilès, J.-P., Delfiner, P., 2012. Geostatistics: Modeling Spatial Uncertainty. Wiley, Hoboken, N.J., p. 699 p.

Coulibaly, L., Labib, M.E., Hazen, R., 2004. A GIS-based multimedia watershed model: development and application. Chemosphere 55, 1067–1080. https://doi.org/10.1016/j.chemosphere.2004.01.014.

Covaci, A., Manirakiza, P., Schepens, P., 2002. Persistent organochlorine pollutants in soils from Belgium, Italy, Greece, and Romania. Bull. Environ. Contam. Toxicol. 68, 97–103. https://doi.org/10.1007/s00128-001-0224-6.

de Moura, C.A., Kubrusly, C.S. (Eds.), 2013. The Courant–Friedrichs–Lewy (CFL) Condition. Birkhäuser Boston, Boston https://doi.org/10.1007/978-0-8176-8394-8.

Di Guardo, A., Ferrari, C., Infantino, A., 2006. Development of a dynamic aquatic model (DynA Model): estimating temporal emissions of DDT to Lake Maggiore (N. Italy). Environ. Sci. Pollut. Res. Int. 13, 50–58. https://doi.org/10.1065/espr2006.01.009.

Di Guardo, A., Nizzetto, L., Infantino, A., Colombo, I., Saporiti, E., Jones, K.C., 2008. Field derived accumulation and release kinetics of DDTs in plants. Chemosphere 72, 1497–1503. https://doi.org/10.1016/j.chemosphere.2008.04.072.

Di Guardo, A., Zaccara, S., Cerabolini, B., Acciarri, M., Terzaghi, G., Calamari, D., 2003. Conifer needles as passive biomonitors of the spatial and temporal distribution of DDT from a point source. Chemosphere 52, 789–797. https://doi.org/10.1016/S0045-6535(03)00256-X.

EEA, 2022. Air Quality e-Reporting (AQ e-Reporting) — European Environment Agency [WWW Document]. https://www.eea.europa.eu/data-and-maps/data/aqereporting-9 (accessed 4.18.22).

Eni rewind, 2020. Pieve Vergonte. The remediation of the site is destined to become part of Italy's environmental engineering history. [WWW Document]. https://www.eni.com/enirewind/en-IT/remediation/remediation-projects-pieve-vergonte.html.

Estellano, V.H., Pozo, K., Harner, T., Corsolini, S., Focardi, S., 2012. Using PUF disk passive samplers to simultaneously measure air concentrations of persistent organic pollutants (POPs) across the Tuscany Region, Italy. Atmos. Pollut. Res. 3 (1), 88–94. https://doi.org/10.5094/APR.2012.008.

Falakdin, P., Terzaghi, E., Di Guardo, A., 2022. Spatially resolved environmental fate models: a review. Chemosphere 290, 133394. https://doi.org/10.1016/j.chemosphere.2021.133394.

Gaudette, H.E., Flight, W.R., Toner, L., Folger, D.W., 1974. An inexpensive titration method for the determination of organic carbon in recent sediments. J. Sediment. Res. 44, 249–253. https://doi.org/10.1306/74D729D7-2B21-11D7-8648000102C1865D.

Ghirardello, D., Morselli, M., Semplice, M., Di Guardo, A., 2010a. A dynamic model of the fate of organic Chemicals in a Multilayered Air/Soil system: development and illustrative application. Environ. Sci. Technol. 44, 9010–9017. https://doi.org/10.1021/es1023866.

Ghirardello, D., Morselli, M., Semplice, M., Di Guardo, A., 2010b. A dynamic model of the fate of organic chemicals in a multilayered air/soil system: development and illustrative application. Environ. Sci. Technol. 44, 9010–9017.

Gong, Z.M., Tao, S., Xu, F.L., Dawson, R., Liu, W.X., Cui, Y.H., Cao, J., Wang, X.J., Shen, W.R., Zhang, W.J., Qing, B.P., Sun, R., 2004. Level and distribution of DDT in surface soils from Tianjin, China. Chemosphere 54, 1247–1253. https://doi.org/10.1016/j.chemosphere.2003.10.021.

Italian Ministry of Environment, 2019. Decreto 1 marzo 2019, n. 46 - Regolamento relativo agli interventi di bonifica, di ripristino ambientale e di messa in sicurezza, d'emergenza, operativa e permanente, delle aree destinate alla produzione agricola e all'allevamento. [WWW Document]. https://www.gazzettaufficiale.it/eli/id/2019/06/07/19G00052/sg (accessed 5.27.22).

Jung, J.E., Kim, Y.K., Song, J.H., Lee, D.S., 2014. Development and evaluation of a dynamic multimedia model (ECORAME) for local scale assessment of aquatic ecological exposure to chemicals originating from sources in environmental media. Sci. Total Environ. 500–501, 103–112. https://doi.org/10.1016/j.scitotenv.2014.08.097.

Lupato, J., 2001. Area forestale: Valle Ossola Piano Forestale Territoriale. Regione Piemonte. Report. https://www.sistemapiemonte.it%2Fmontagna%2Fsifor%2Fdwd%2Frelazioni%2FAF19_rel_tot.pdf.

Mackay, D., 2001. Multimedia Environmental Models: The Fugacity Approach, Second Edition. 2nd ed. CRC Press.

MacLeod, M., Fraser, A.J., Mackay, D., 2002. Evaluating and expressing the propagation of uncertainty in chemical fate and bioaccumulation models. Environ. Toxicol. Chem. 21, 700–709. https://doi.org/10.1002/etc.5620210403.

MITE, 2022. Ministero della Transizione Ecologica - SIN di Pieve Vergonte [WWW Document]. https://bonifichesiticontaminati.mite.gov.it/sin-15/ (accessed 5.27.22).

Morselli, M., Ghirardello, D., Semplice, M., Di Guardo, A., 2011. Modeling short-term variability of semivolatile organic chemicals in air at a local scale: an integrated modeling approach. Environ. Pollut. 159, 1406–1412. https://doi.org/10.1016/j.envpol.2010.12.034.

Morselli, M., Ghirardello, D., Semplice, M., Raspa, G., Di Guardo, A., 2012. Integration of an atmospheric dispersion model with a dynamic multimedia fate model: development and illustration. Environ. Pollut. 164, 182–187. https://doi.org/10.1016/j.envpol.2012.01.039.

Nizzetto, L., Pastore, C., Liu, X., Camporini, P., Stroppiana, D., Herbert, B., Boschetti, M., Zhang, G., Brivio, P.A., Jones, K.C., Di Guardo, A., 2008. Accumulation parameters and seasonal trends for PCBs in temperate and boreal Forest Plant species. Environ. Sci. Technol. 42, 5911–5916. https://doi.org/10.1021/es800217m.

QGIS Development Team, 2018. QGIS Geographic Information System. Open Source Geospatial Foundation Project. http://qgis.osgeo.org. (Accessed 15 May 2022).

Robertson, L., Langner, J., Engardt, M., 1999. An eulerian limited-area atmospheric transport model. J. Appl. Meteorol. 38, 190–210. https://doi.org/10.1175/1520-0450(1999)038<0190:AELAAT>2.0.CO;2.

Terzaghi, E., Morselli, M., Semplice, M., Cerabolini, B.E.L., Jones, K.C., Freppaz, M., Di Guardo, A., 2017. SoilPlusVeg: an integrated air-plant-litter-soil model to predict organic chemical fate and recycling in forests. Sci. Total Environ. 595, 169–177. https://doi.org/10.1016/j.scitotenv.2017.03.252.

Terzaghi, E., Vitale, C.M., Salina, G., Di Guardo, A., 2020. Plants radically change the mobility of PCBs in soil: role of different species and soil conditions. J. Hazard. Mater. 388, 121786. https://doi.org/10.1016/j.jhazmat.2019.121786.

Terzaghi, E., Wild, E., Zacchello, G., Cerabolini, B.E.L., Jones, K.C., Di Guardo, A., 2013. Forest filter effect: role of leaves in capturing/releasing air particulate matter and its associated PAHs. Atmos. Environ. 74, 378–384. https://doi.org/10.1016/j.atmosenv.2013.04.013.

Tomlin, C.D.S., 1997. The pesticide manual: a world compendium. British Crop Protection Council, 11th ed. British Crop Protection Publications, Farnham, UK.

UNEP, 2001. Stockholm Convention - Home page [WWW Document]. http://www.pops.int/ (accessed 2.27.20).

Walker, A., 1974. A simulation model for prediction of herbicide persistence. J. Environ. Qual. 3 (4), 396–401. https://doi.org/10.2134/jeq1974.00472425000300040021x.
Walkley, A., Black, I.A., 1934. An examination of the degtjareff method for determining soil organic matter, and a proposed modification of the chromic acid titration method. Soil Sci. 37, 29–38. https://doi.org/10.1097/00010694-193401000-00003.
Wegmann, F., Scheringer, M., Möller, M., Hungerbühler, K., 2004. Influence of vegetation on the environmental partitioning of DDT in two global multimedia models. Environ. Sci. Technol. 38, 1505–1512. https://doi.org/10.1021/es034262n.
WHO, 1979. DDT and Its Derivates. WHO Environmental Health Criteria. 9. World Health Organization, Geneva.
Wu, H., Fu, P., Morris, J.P., Settgast, R.R., Ryerson, F.J., 2019. ICAT: A Numerical Scheme to Minimize Numerical Diffusion in Advection-Dispersion Modeling and Its Application in Identifying Flow Channeling.

Appendix to:

Predicting the regional contamination evolution of DDT for 100-years with a new gridded spatial and dynamic multimedia fate model

Parisa Falakdin[1], Elisa Terzaghi[1], Giuseppe Raspa[2], Antonio Di Guardo[1]*

[1] Department of Science and High Technology, University of Insubria, Via Valleggio 11, 22100,Como, CO, Italy
[2] Department of Chemical Engineering, Materials, and Environment, Rome "La Sapienza" University, Via Eudossiana 18, 00184 Rome, RM, Italy

Table of Contents

* Corresponding author
E-mail address: antonio.diguardo@uninsubria.it (A. Di Guardo).

MONITORING DATA AND SIMULATION SCENARIO

A.1) Soil, leaf, and litter samples

Table A.1. Soil DDT concentrations 2001 and 2011 (µg/g d.w.)

ID	Name	o,p'-DDE	o,p'-DDD	p,p'-DDD	o,p'-DDT	p,p'-DDE	p,p'-DDT	DDTS_TOT	X_COORD	Y_COORD
Year 2001										
1	PV - Forest	0.00108	0.00033	0.00195	0.00675	0.03798	0.07663	0.12472	1444074	5094435
2	PV - L 1	0.00021	0.00071	0.00248	0.01851	0.00484	0.04928	0.07603	1443933	5096864
3	PV - L 2	0.01371	0.00051	0.03782	0.15242	0.73445	1.172	2.1109	1443608	5095150
4	PV - L 3	<0.0001	<0.0001	<0.0001	<0.0001	0.0002	0.00067	0.00087	1444391	5096674
5	PV - L 4	<0.0001	<0.0001	<0.0001	0.00023	0.00077	0.00115	0.00215	1444586	5096646
6	PV - Red Soil 1 *	0.37848	0.02644	0.03231	0.22947	1.36073	1.58163	3.60906	1444358	5094924
7	PV - Red Soil 2 *	0.14481	0.20409	0.50555	3.27714	0.63147	18.012	22.77506	1444358	5094924
8	PV - RM 5cm	0.00111	0.00076	0.01284	0.02371	0.04507	0.72208	0.80557	1444646	5094467
	PV - RM 10cm	0.00083	0.0005	0.00319	0.01546	0.05119	0.18587	0.25704	1444646	5094467
9	PV1 - L 5cm	0.01471	0.01406	0.03499	0.10375	0.39148	0.57114	1.13013	1444123	5094638
	PV1 - L 10cm	0.00739	0.00357	0.02586	0.03306	0.46288	0.81943	1.35219	1444123	5094638
	PV1 - L 15cm	0.03281	0.00246	0.01593	0.02402	0.42383	0.46127	0.96032	1444123	5094638
10	PV2 - L 5cm	0.01268	0.00672	0.02459	0.08585	0.56916	0.65314	1.35214	1444128	5094638
	PV2 - L 10cm	0.01012	0.00501	0.02563	0.0511	0.57032	0.38909	1.05127	1444128	5094638
	PV2 - L 15cm	0.01973	0.00545	0.02957	0.09426	1.08457	0.57058	1.80416	1444128	5094638
11	PV3 - L 5cm	0.01019	0.00812	0.03994	0.0571	0.49459	0.59065	1.20059	1444128	5094633
	PV3 - L 10cm	0.00454	0.0026	0.01629	0.16698	0.35743	0.19547	0.74331	1444128	5094633
	PV3 - L 15cm	0.0137	0.00556	0.02521	0.07551	0.65716	0.42472	1.20186	1444128	5094633
12	PV4 - L 5cm	<0.0001	0.009	0.05	0.102	0.895	1.191	2.247	1444122	5094633
	PV4 - L 10cm	0.01	0.005	0.026	0.037	0.632	0.342	1.052	1444122	5094633
	PV4 - L 15cm	0.028	0.02	0.044	0.09	1.554	0.646	2.382	1444122	5094633
13	Fomarco 1	0.00091	0.0003	0.00107	0.00678	0.02958	0.02927	0.06791	1442961	5096104
14	Fomarco 2	0.00137	0.0007	0.00283	0.01128	0.05569	0.07093	0.1428	1443088	5096003
15	M. Mezzo 1	0.00553	0.00271	0.00744	0.0709	0.11175	0.38755	0.58588	1446063	5093548
16	M. Mezzo 2	0.00304	0.00232	0.00629	0.01361	0.0764	0.08661	0.18827	1446567	5093289
17	M. Mezzo 3	0.00094	0.00071	0.00431	0.01113	0.04286	0.1708	0.23075	1446984	5093291
18	M. Mezzo 4	0.00063	0.00027	0.00245	0.00488	0.04764	0.22486	0.28073	1448624	5093110
19	Anzola - M. Mezzo	0.00044	0.00032	0.00165	0.01005	0.03868	0.07329	0.12443	1447959	5093107
20	Anzola	0.00022	0.00016	0.00043	0.00147	0.01221	0.01293	0.02742	1449917	5092977
21	Premosello 1	0.00068	0.00086	0.0028	0.00714	0.00577	0.13462	0.15187	1451253	5093206
22	Premosello 2	0.00012	0.00005	0.00017	0.00047	0.0024	0.00328	0.00649	1447284	5093730
23	Vogogna 1	0.00023	<0.0001	0.00053	0.00045	0.00178	0.0026	0.00559	1445208	5094845
24	Vogogna 2	0.00012	0.00007	0.00135	0.00042	0.01075	0.02168	0.03439	1445204	5094680

25	Vogogna 3	0.00012	<0.0001	0.00016	0.00043	0.00094	0.0023	0.00395	1444619	5095828
26	Villadossola 1	0.0002	0.00014	0.00046	0.0007	0.00112	0.01046	0.01308	1444100	5100945
	Villadossola 2 *	<0.0001	<0.0001	<0.0001	<0.0001	0.0004	0.00048	0.00088	1444100	5100945
27	Rio Marmazza1 *	0.27145	0.07579	0.39708	1.07591	3.49756	29.39685	34.71464	1444520	5094865
	Rio Marmazza2 *	0.00861	0.00385	0.02112	0.16918	0.20361	1.27714	1.68351	1444520	5094865
28	Piedimulera	0.00012	0.00009	0.00017	0.0004	0.00185	0.0027	0.00533	1443942	5097712
29	Moiachina	0.00012	0.00008	0.00036	0.00076	0.00316	0.00343	0.00791	1442734	5097469
30	Loro	0.00116	0.00018	0.00067	0.0033	0.04229	0.02095	0.06855	1444337	5094279
31	Gabbio	<0.0001	<0.0001	0.00011	0.00042	0.00185	0.00182	0.0042	1451855	5092358
32	Nibbio	0.00024	0.0003	0.00156	0.00169	0.00321	0.05039	0.05739	1452761	5093431
33	Rumianca	0.00127	0.00024	0.00124	0.00636	0.04619	0.03181	0.08711	1445397	5093444
Year 2011										
34	Rumianca 1	<0.01	<0.01	<0.01	<0.01	0.01	0.02	0.03	1445060	5093953
35	Rumianca 2	<0.01	<0.01	<0.01	<0.01	0.01	0.02	0.03	1445549	5093972
36	Cuzzago	<0.01	<0.01	<0.01	<0.01	<0.01	<0.01	<0.01	1452159	5093399
37	Toce 1	<0.01	<0.01	<0.01	<0.01	<0.01	<0.01	<0.01	1444287	5096008
38	Toce 2	<0.01	<0.01	<0.01	0.01	<0.01	0.01	0.02	1444374	5096029
39	Toce 3	<0.01	<0.01	<0.01	<0.01	<0.01	<0.01	<0.01	1444349	5095671
40	PV - L 1	<0.01	<0.01	<0.01	<0.01	<0.01	<0.01	<0.01	1444584	5096625
41	PV - L 2	<0.01	<0.01	<0.01	<0.01	<0.01	<0.01	<0.01	1444140	5100951
42	PV - L 3	<0.01	<0.01	0.02	0.02	0.08	0.06	0.18	1444081	5094581
43	M. Mezzo	<0.01	<0.01	<0.01	<0.01	<0.01	0.02	0.02	1446796	5093220
44	Gabbio	<0.01	<0.01	<0.01	<0.01	<0.01	<0.01	<0.01	1451735	5092381
45	PV - RM	<0.01	<0.01	0.03	0.03	0.05	0.28	0.39	1444576	5094733
46	P - Chio	<0.01	<0.01	<0.01	<0.01	<0.01	<0.01	<0.01	1448727	5094146
47	Piedimulera	<0.01	<0.01	<0.01	0.01	<0.01	<0.01	0.01	1443655	5097452
48	Loro	<0.01	<0.01	0.01	<0.01	0.1	0.07	0.18	1443836	5094443

Note: ID = Location ID, DDT-TOT= Sum of the total DDTs, PV= Pieve Vergonte, L = grass soil, RM = Rio Marmazza, M. Mezzo = Megolo Mezzo, P – Chio = Premosello Chiovenda. ***** These samples were excluded for comparison between simulated and measured in Figure 3.

Table A.2 Needle concentrations (ng/g d.w.) in spruce with ages

ID	Site (x,y)	Date	Distance* (km)	Needle Age	Tot. Lipids (%)	o,p'-DDE	p,p'-DDE	o,p'-DDD	p,p'-DDD	o,p'-DDT	p,p'-DDT
49	Altoggio (1449367.9; 5112711.6)	Jan-99	-18	< 1 y	-	<0.1	n.a	n.a	n.a	n.a	n.a
				1 y	3.03	<0.1	1.97	<0.1	<0.1	<0.1	<0.1
				2 y	3.197	0.7	2.05	<0.1	<0.1	<0.1	<0.1
50	Campo Albino (1444730.5; 5097373.4)	Jul-99	-2.5	< 1 y	4.87	<0.1	<0.1	<0.1	<0.1	<0.1	<0.1
				1 y	7.14	<0.1	1.83	<0.1	<0.1	<0.1	<0.1
				2 y	8.36	<0.1	2.48	<0.1	<0.1	<0.1	<0.1
51	Cimamulera (1441872.6; 5096771.1)	May-99	-2.5	< 1 y	4.71	<0.1	2.05	<0.1	<0.1	0.77	0.97
				1 y	4.52	<0.1	1.95	<0.1	0.08	3.79	4.42
				2 y	4.26	<0.1	2.16	0.16	0.17	1.22	2.39
52	Fomarco Chiesa (1442463.8; 5095698.7)	May-99	-1.5	< 1 y	3.68	<0.1	3.71	<0.1	<0.1	1.64	4.36
				1 y	3.88	1.65	2.25	<0.1	0.04	2.67	4.22
				2 y	5.19	3.7	6.33	<0.1	0.08	1.78	5.56
53	Pieve Vergonte (1444062.9; 5094509.8)	Jul-99	0	< 1 y	5.1	2.62	7.24	0.91	0.72	6.43	9.46
				1 y	5.81	<0.1	11.08	0.6	1.78	2.45	6.77
				2 y	6.9	<0.1	13.78	1.38	1.08	<0.1	4.19
54	Rumianca (1444835.6; 5093714.4)	Jun-99	1.5	< 1 y	4.66	1.01	1.65	<0.1	<0.1	1.55	2.06
				1 y	6.52	2.6	3.92	<0.1	<0.1	4.03	10.1
				2 y	7.58	1.98	5.71	<0.1	0.21	1.11	6.08
55	Mergozzo (1454249.9; 5093109.7)	Jan-99	10	< 1 y	n.a	n.a	n.a	n.a	n.a	n.a	n.a
				1 y	1.803	0.74	1.97	<0.1	0.14	<0.1	1.25
				2 y	4.4	1.4	2.98	<0.1	0.19	0.49	1.64
56	Alpe Ompio (1458484.5; 5092523)	Jan-99	15	< 1 y	n.a	n.a	n.a	n.a	n.a	n.a	n.a
				1 y	2.71	0.75	0.6	<0.1	<0.1	<0.1	<0.1
				2 y	4.02	0.95	1.34	<0.1	<0.1	<0.1	<0.1
57	Mottarone Base (1458802.0; 5082130.0)	Jan-00	20	1 y	n.a.	2.52	2.63	4.74	4.8	4.1	4.97
58	Mottarone Top (1457716.0; 5081243.0)	Jan-00	19.5	1 y	n.a.	<0.1	0.99	<0.1	<0.1	1.51	1.27

Note: ID = Location ID, *= distance from Pieve Vergonte; n.a = not available;

Table A.3 Needle concentrations (ng/g d.w.) in pine species.

ID	Site (x,y)	Species	Date	Distance* (km)	Needle Age	Tot. Lipids (%)	o,p'-DDE	p,p'-DDE	o,p'-DDD	p,p'-DDD	o,p'-DDT	p,p'-DDT
50	Campo Albino (1444730.5; 5097373.4)	*Pinus strobus*	Jul-99	-2.5	1 y	11.99	<0.1	4.22	<0.1	<0.1	<0.1	<0.1
59	Fomarco Alto (1442482; 5096123.7)	*Pinus nigra*	Jul-99	-2	1 y	13.03	0.52	1.17	<0.1	<0.1	<0.1	<0.1
53	Pieve Vergonte (1444062.9; 5094509.8)	*Pinus nigra*	Jan-99	0	1 y	6.39	2.42	10.22	0.23	0.27	6.24	11.62
		Pinus nigra	Jun-99	0	1 y	10.37	1.57	4.51	0.87	2.52	34.52	96.69
				0	2 y	n.a.	12.158	30.006	1.116	2.942	46.523	94.061
		Pinus nigra	Oct-99	0	1 y	8.12	4.02	13.19	2.27	2.04	35.77	91.82
		Pinus strobus	Jul-99	0	1 y	9.87	<0.1	6.69	<0.1	0.84	2.13	7.5
60	Rumianca (1444835.6; 5093714.4)	*Pinus strobus*	Jun-99	1.5	1 y	12.01	2.09	4.47	1.17	0.57	8.25	12.01
61	Colloro (1448168.1; 5095267.8)	*Pinus strobus*	Jun-99	3	1 y	11.01	<0.1	0.73	<0.1	<0.1	<0.1	<0.1
					2 y	n.a.	<0.1	5.032	<0.1	<0.1	0.539	1.647
		Pinus sylvestris	Jun-99	3	1 y	11.3	<0.1	<0.1	<0.1	<0.1	<0.1	<0.1

Note: ID = Location ID, *= distance from Pieve Vergonte;

Table A.4. Litter concentration (µg/g d.w.)

ID	SAMPLE	2,4'-DDE	2,4'-DDD	4,4'-DDD	2,4'-DDT	4,4'-DDE	4,4'-DDT	DDTS_TOT	X_COORD	Y_COORD
49	Altoggio	0.00105	<0.0001	0.00767	0.00344	0.00688	0.02637	0.04541	1449367	5112711
51	Cimamulera	0.00076	0.00068	0.00767	0.00589	0.00831	0.04118	0.06449	1441873	5096771
59	Fomarco Alto	0.00354	0.00357	0.01386	0.01688	0.00866	0.04762	0.09413	1442482	5096124
50	Campo Albino	0.00048	<0.0001	0.01175	0.00893	0.00724	0.04102	0.06942	1444731	5097373
53	Enichem	0.01572	<0.0001	0.01868	0.03739	0.0381	0.16015	0.27004	1444063	5094510
60	Rumianca	0.00521	0.00074	0.00889	0.02137	0.03763	0.1096	0.18344	1444836	5093714
55	Mergozzo	0.00053	0.00012	0.00151	0.00121	0.00519	0.00754	0.0161	1454250	5093110
56	Alpe Ompio	0.00044	0.00019	0.00066	0.00166	0.00347	0.00627	0.01269	1458484	5092523
61	Colloro	0.00155	<0.0001	<0.0001	0.00469	0.00369	<0.0001	0.00993	1448168	5095268

Note: ID = Location ID.

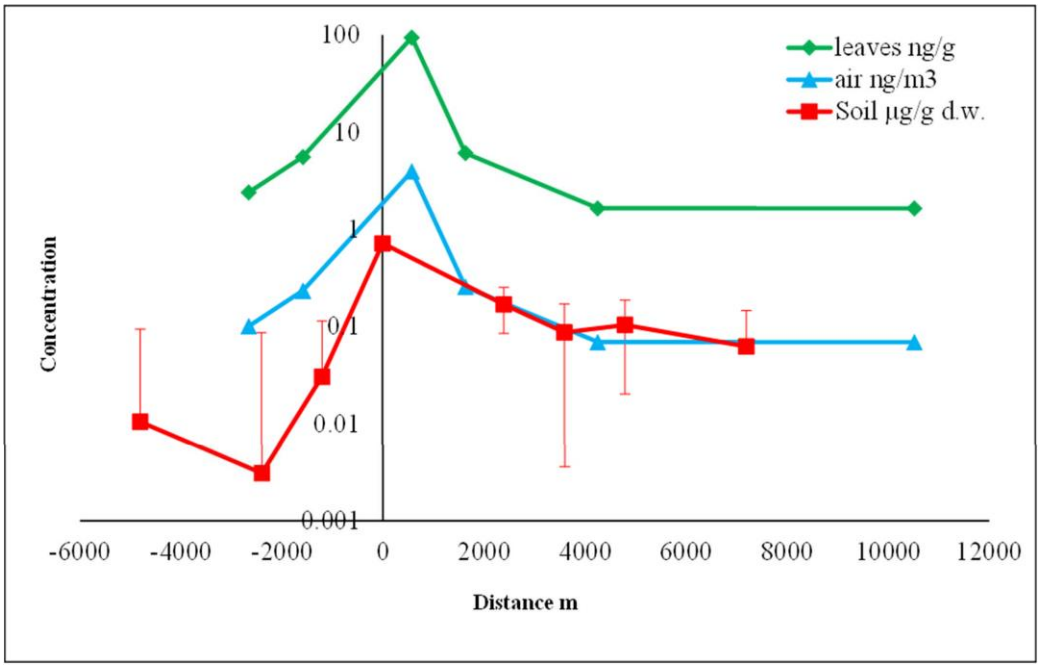

Figure A.1 p,p'-DDT concentration measured in leaves, air, and soil (2001 data) with distance from the chemical plant. Soil error bars represent the standard deviation of the corresponding points, located within 1.44 km^2.

Figure A.1 shows measured logarithmic concentration values of air, spruce needles of two years, and soil with distance from the chemical plant. The green line represents the leaf concentrations of p,p'-DDT for the points along the valley with distance from the emission source. The location of the chemical plant is set to zero distance, points located upstream/ downstream of the valley have negative/positive distances. The blue line corresponds to the estimated air concentrations. The highest concentration was observed in the vicinity of the chemical plant with a noticeable reduction at an increasing distance from the industrial plant. Additionally, in the same chart soil concentrations (2001 samples) of p,p'-DDT with distance from the chemical plant are shown. Since several samples were collected in a location corresponding to the same cell in the model scenario, the mean and standard deviation of the points within each hypothetical cell (1.44 km^2) were calculated. This information is also useful to evaluate the concentration variations

in soil with respect to distance from the location of the source, influenced by local (e.g., deposition, soil characteristics, agricultural operations, etc.) and meteorological conditions. At several points, different depths of soil were sampled (5 cm, 10 cm, and 15 cm) to evaluate the concentration gradient with depth (Table A.1; PV-RM, PV1-L, PV2-L, PV3-L, PV4-L). The concentration of p,p'-DDT with depth decreases up to 4 orders of magnitude for point PV-RM indicating the strong dependence of soil concentration contribution from the atmospheric compartments. However, only the superficial points (0- 5 cm layer) were used for comparison.

A.2) Meteorological data

The wind data for Pieve Vergonte was estimated based on Ornavasso local meteorological station which is among the nearest stations to Pieve Vergonte (Figure A.2).

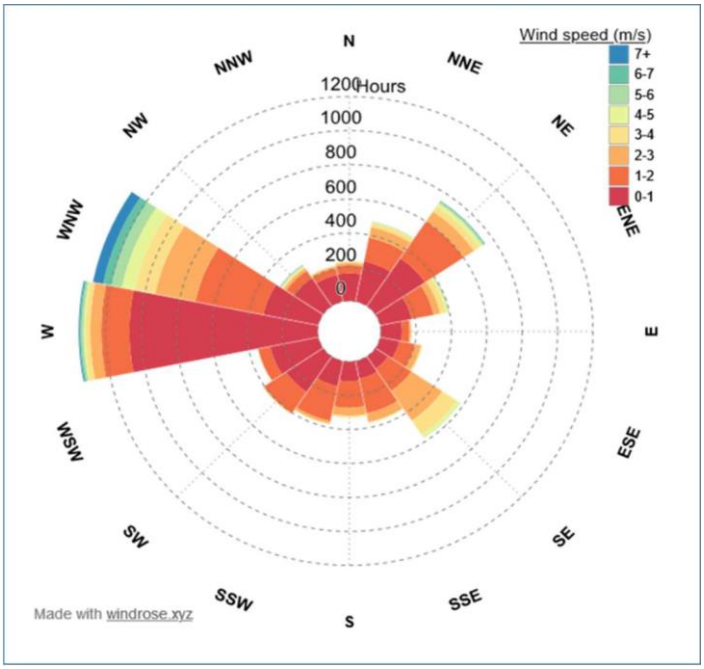

Figure A.2 - Yearly averaged wind rose at Ornavasso station

Daily precipitation values obtained from the ARPA station of Fomarco relating to the year 2005 show a number of high rain events. The two highest precipitation incidents have occurred in July and September with 153.8 and 148.6, respectively. Figure A.*3*.

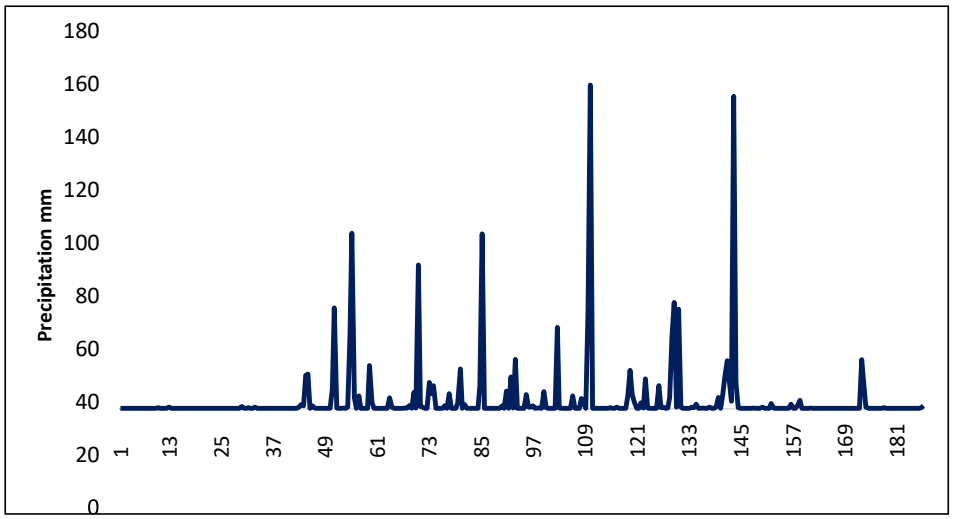

Figure A.3- Daily precipitation values for the Fomarco station used for the simulation scenario.

A.3) Model parametrization

Parameters required by the GSPV model, apart from those that are common with SPV (Terzaghi et al., 2017), are depicted in Table A.5.

Table A.5. Input parameters required by Grid SPV.

Parameter required by GSPV	**Unit**
Wind direction	
Wind angle	degree
Air emission	mol/h
Organic matter fraction	
Shapefile of the grid	

Physical-chemical properties implemented in the model simulation are expressed in Table A.6.

Table A.6. Physical-chemical properties of p,p'-DDT.

Property	Unit	p, p'-DDT
Molecular weight	g/mol	354.5
Reference temperature	°C	25
Melting point	°C	108.5
Vapor pressure	Pa	0.00002
Water solubility	g/m	0.0055
log K_{OW}		6.19
Half-life in air	d	7.083
Half-life in soil	d	10950

Note: all physical-chemical parameters and half-life in air are from (Mackay, 2006) while half-life in soilis from (Dimond and Owen, 1996).

Figure A.4.b shows the location of the grid over the study area as well as the allocation of cells as grassor forest.

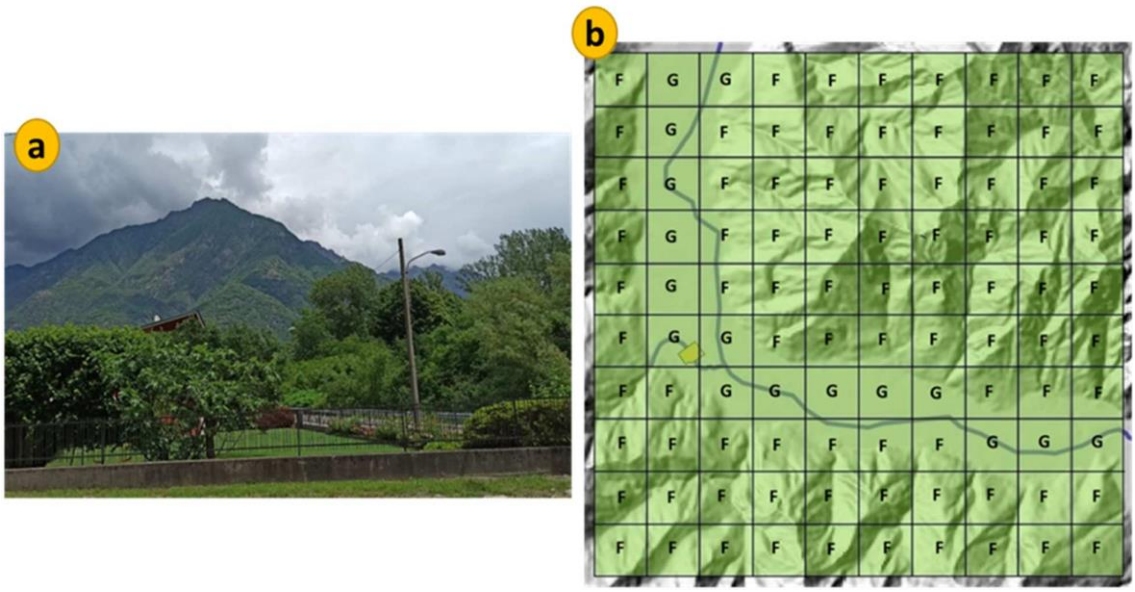

Figure A.4. a) General vegetation characteristics of Pieve Vergonte. b) Cells that are labelled with F, are the forest

Constant parameters relating to the two vegetation scenarios, that were introduced into the model through the GIS database, are illustrated in Table A.7. Moreover, hourly dynamic parameters for one year were set as an external dataset.

Table A.7. Constant vegetation parameters for Grass and Forest. * are the regression parameters of the Nizzetto et al., (2008) equation.

Vegetation Type	Root Density (g/m^3)	Stem Density (g/m^3)	SLA (m^2/g)	Minimum Canopy Height (m)	Maximum Canopy Height (m)	Root Volume (m^3)	Stem Volume (m^3)	y^*_0	a^*
Grass	180000	300000	0.01	0.1	1	15408	1008	-2.6	0.43
Forest	180000	300000	0.028	1	4	33552	44352	-3.08	0.49

A.4) Calculation of temperature-dependent K_{PA}

The plant-air partitioning coefficient was calculated for 25 ºC using the (Nizzetto et al., 2008) formula as mentioned earlier. In order to calculate the K_{PA} for an intended temperature, the Van't Hoff-type equation proposed by (Kömp and McLachlan, 1997) (Eq. A.1) was implemented. This equation requires the enthalpy of phase-change that was calculated based on the enthalpy of evaporation for PCBs (Puri et al., 2001).

$$K_{PA}(T) = K_{pa}(T_R)\exp\left[\left(\frac{1}{T} - \frac{1}{T_R}\right)\frac{\Delta H_{PA}}{R}\right] \qquad \text{Eq. (A.1)}$$

Logarithmic K_{PA} values were calculated for the minimum, median, maximum, first and the third quartile of the hourly temperature dataset of the simulation scenario. The K_{PA} varies close to 5 orders of magnitude between the minimum and maximum temperatures. The difference between the K_{PA} of the first and third quartile of the temperature dataset is also more than one order of magnitude (Figure A.5).

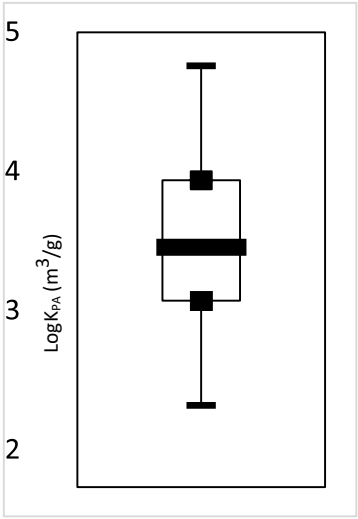

Figure A.5. Logarithmic K_{PA} values calculated for the range of hourly temperature dataset.

A.5) Simulation scenario

Emission data were estimated based on the United States DDT production trend (World Health Organization, 1979) (Figure A.6) and back-calculated based on the measured air concentrations (Figure A.7).

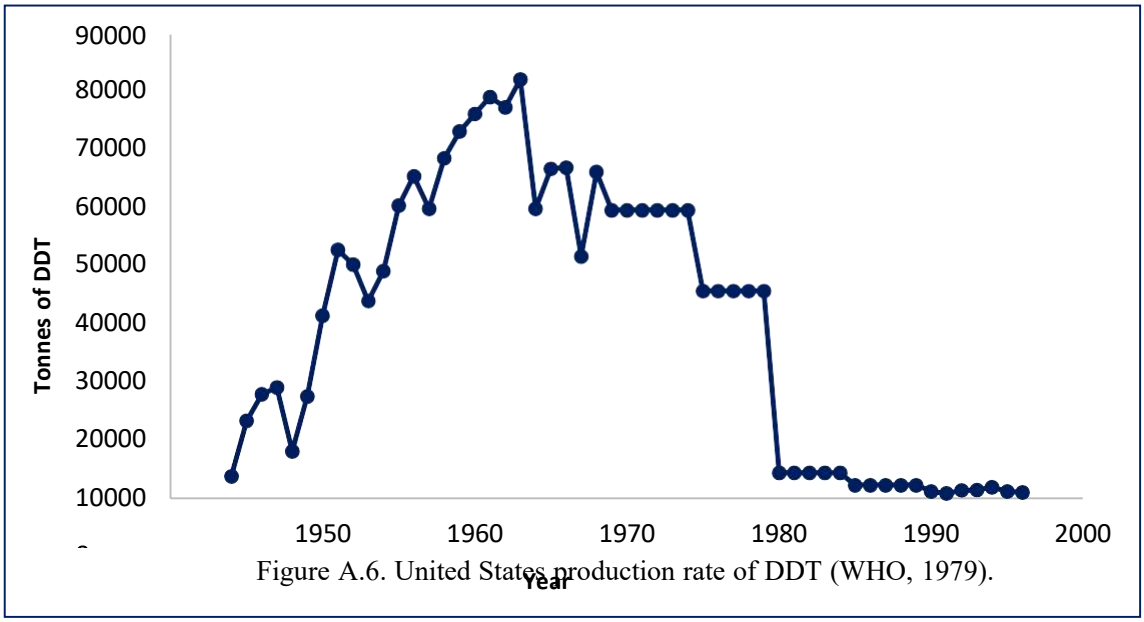

Figure A.6. United States production rate of DDT (WHO, 1979).

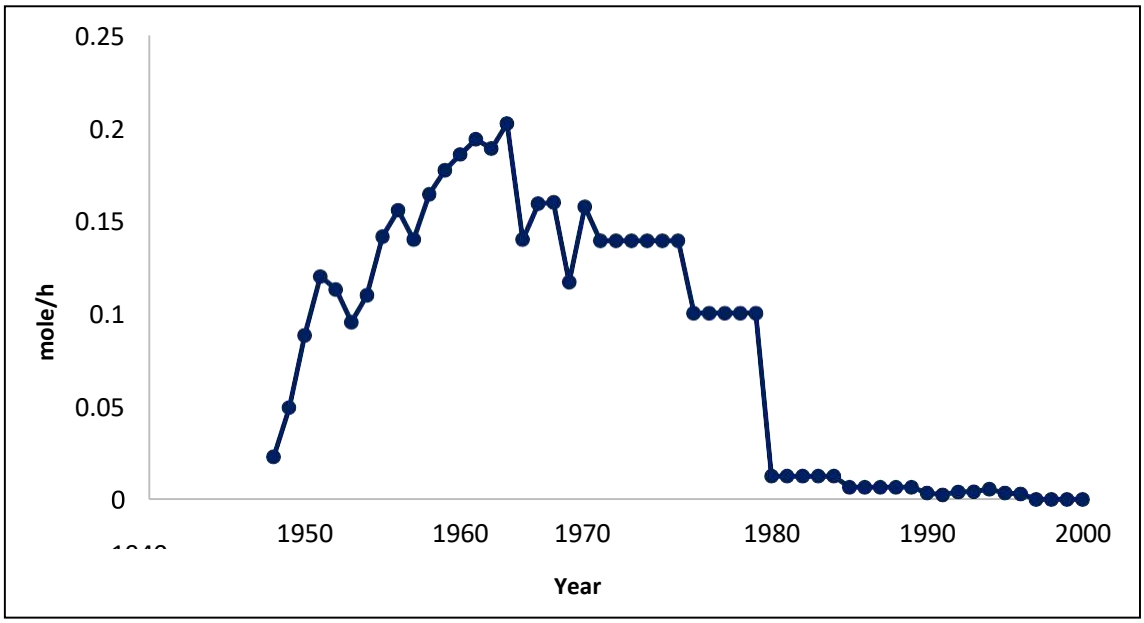

Figure A.7. Local p,p'-DDT emission estimate based on the United States production rate.

A RESULTS AND DISCUSSION

A.1) Model development

Wind propagation in the gridded system is explained in brief in this section. The same equations were applied for both lower air and upper air compartments, however, the equations relating to the lower air are shown here as an example.

Courant number is calculated along *x* and *y* directions and is used to calculate the number of cells that are getting affected by the advective wind (Eq. B.1). The calculation of chemical distribution depends on the Courant number (i.e., *c)* and wind component along that direction.

$$c = \frac{V_{LA(t)}\Delta t}{l} \qquad \text{Eq. (B.1)}$$

The numerator of the equation indicates the transport distance of wind within the one-hour time step and l is the cell length. In order to know how many cells are getting affected by wind, the round-up value of c is considered (Eq. B.2).

$$p = Roundup(c)$$

Eq. (B.2)

First, the condition of the 1D computational domain (e.g., along x-direction) is explained. Figure B.1.a shows a situation where the *p* number is equal to one. In this case, all chemicals exiting the current cell will go to the adjacent cell. This is the ideal CFL condition where the calculation of chemical distributionamong several cells is not required. When the *p* number is more than one, a discrete sequential advection transport scheme introduced by (Wu et al., 2019) was implemented to estimate the distribution of chemicals among several cells. Figure B.1.b. illustrates an example of when the *p* number is more than one (e.g., 3). In this situation, the chemical is divided among three cells A *p* number of 3 indicates that 3 cells will get affected by the advective wind at the same time step (1h), additionally, the solution is implemented in 3 steps. Step 3 shows the final cell values at the end of the current hour.

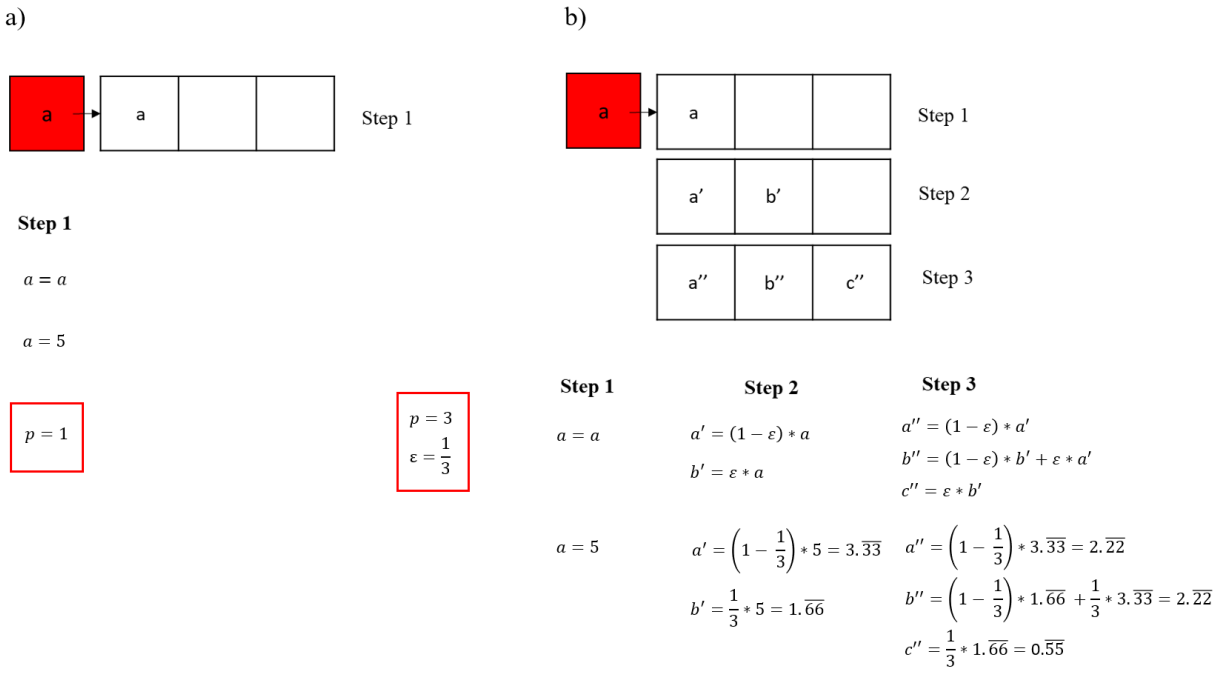

Figure B.1.a) Chemical distribution when the p-number is equal to one along the x-direction. b) chemical distribution when the p-number is equal to three along the x-direction.

In Figure B.1, a represents chemicals exiting one cell and entering the following cells during the current hour, a' and b' are temporary cell values of step 2, though, a'' and b'' are final cell values at the end of the

time step. The ε index incorporates the percentage of chemicals exiting cells at each step of the distribution, based on the p-number (Eq. B.3). This value is equal to α_e in the queue-cells calculations (Wu et al., 2019).

$$\varepsilon = \left(\frac{1}{p}\right) \qquad \text{Eq. (B.3)}$$

The second case is the 2D computational domain when the wind vector enters the study area with a non-perpendicular angle (e.g., NW, 30º). In this situation, the p numbers along the x and y directions are calculated (p_x and p_y). The 2D distribution of chemicals is performed based on the same logic as the 1D domain. However, in this case, the order of calculations along the two directions must be specified. If the p number is equal for both directions (i.e., when the wind enters the area with a 45-degree angle) the wind propagates equally in both directions, otherwise, the wind moves faster along the direction with the higher p number. In both situations, first, the minimum value between the p_x and p_y is considered as the number of steps that the wind moves in both directions. Then, the wind moves along the direction with the greater p-number by additional steps. The number of these additional steps is equal to the absolute value of the difference between the two p numbers (i.e., $|p_x - p_y|$). The entire process of wind propagation and chemical distribution is performed within the current time step. The vertical diffusion and transport of chemicals between the atmospheric compartments are performed during the SPVcalculations.

B.1.1) Mass transfer coefficients (MTC)

Table B.1. shows the transport and degradation processes for air compartment and air/soil transfer as well as their mass transfer coefficients (MTC) for the simulation scenario.

Compartment	Process	D values (mol/h Pa)	MTC
Upper air→Free atmosphere	Diffusion[(a)]	$D_{diffUAFA} = A_s . U_{UAFA} . ZB_{UA}$	U_{UAFA}: 0.01
Upper air	Degradation[(a)]	$D_{DrUA} = V_{UA} . k_{DrUA} . ZB_{UA}$	k_{DrUA}: 3.06E-06 _ 0.000688
Upper air→Lower air	Diffusion[(a)]	$D_{diffUALA} = A_s . U_{UALA} . ZB_{UA}$	U_{UALA}: 0.1
	Rain dissolution[(a)]	$D_{RDissUA} = A_s . U_R . Z_w$	U_R: 0 - 0.15
	Wet deposition[(a)]	$D_{WDepUA} = A_s . U_R . Q . u_{UAQ} . Z_Q$	U_R: 0 - 0.036
	Dry deposition[(a)]	$D_{DDepUA} = A_s . U_Q . u_{UAQ} . Z_Q$	U_Q: 1.03
Lower air → Soil	Absorption[(a)]	$D_{AbsLA} = 1/(1/D_s + 1/(D_A + D_W))$	U_{AbsLA}: 2.08
	Rain dissolution[(a*)]	$D_{RDissLA} = (f_{NotInt} + f_{Drip}) . A_s . U_R . Z_w$	U_R: 0 - 0.15
	Wet deposition[(a*)]	$D_{WDepLA} = (f_{NotInt} + f_{Drip}) . A_s . U_R . Q . u_{LAQ} . Z_Q$	U_R: 0- 0.036
	Dry deposition[(a*)]	$D_{DDepLA} = A_s . U_Q . u_{LAQ} . Z_Q . (1 - If_D)$	U_Q: 1.03
Lower air → Upper air	Diffusion[(a)]	$D_{DiffLAUA} = A_s . U_{LAUA} . ZB_{LA}$	U_{LAUA}: 0.1
Lower air	Degradation[(a)]	$D_{DrLA} = V_{LA} . k_{DrLA} . ZB_{LA}$	k_{DrLA}: 3.06E-06 - 0.0009
Rain rate Lower air → Leaves	Absorption(b)	$D_{AbsF} = 1/(1/D_{AB-F} + 1/D_C)$	U_{Abs-F}: 0.08 – 6.5 U_C: 59-1976
	Rain dissolution[(c*)]	$D_{RDissF} = (f_{Evap}) . A_s . LAI . U_R . Z_w$	U_R: 0 - 0.7
	Wet deposition[(c*)]	$D_{WDepF} = (f_{Evap}) . A_s . LAI . U_R . Q . u_{LAQ} . Z_Q$	U_R: 0 - 1.64
	Dry deposition[(c)]	$D_{DDepF} = A_s . LAI . U_{AF-P} . u_{LAQ} . Z_Q . If_D$	U_{AF-P}: 0.3 - 2.5
Leaves → LowerAir	Volatilization(b)	$D_{FLA} = -D_{absF}$	U_{Abs-F}: 0.08 – 6.5 U_C: 59-1976
Leaves	Degradation(b)	$D_{DrF} = V_F . k_{DrF} . Z_F$	k_{DrF}: 0.21
Soil → Lower air	Volatilization(a)	$D_V = -D_{AbsLA}$	U_{AbsLA}:2.08

Note: FA = free atmosphere, UA = upper air; LA = lower air; F= leaves; A_S = land surface area (m^2); LAI = Leaf Area Index (m^2/m^2); Vx = volume (m^3); Zx = Z-values (mol/m^3Pa); k_{Drx} = degradation rate constants (h^{-1}); U_{UAFA} = transfer rate fromUA to FA (m/h); U_{UALA} = transfer rate from UA to LA (m/h); U_{LAUA} = transfer rate from LA to UA (m/h); U_R = rain rate (m^3 rain/m^2 area h); U_Q = dry deposition velocity (m/h); U_{AF-P} = dry deposition particle velocity to the vegetation canopy (m/h), Gx = air advective inflow (m^3/h); f_{NotInt}, f_{Drip}, f_{Evap} = fraction of precipitation that is not intercepted by the leaves, drips and evaporates from leaves; If_D = dry particle interception factor; Q = scavenging ratio (-), Details about the formulation used for D values for the air and litter/soil compartment can be found in (Ghirardello et al., 2010; Morselli et al., 2011)

B.1.2. Sensitivity and uncertainty analysis

Table B.2 results of the sensitivity analysis for three parameters (concentration in lower air, LA, leaves, F, and soil).

	Sensitivity		
Parameter	**LA**	**F**	**Soil**
Windspeed LA	1.512480	0.770253	0.000017
PBL height	0.933518	0.898971	0.000022
Wind direction	1.161633	1.403834	0.000008

Table B.3 results of the 30% uncertainty on the concentration of the lower air and leaves.

30 % Change	Δ %	
PBL Height	LA	39.89866607
	F	38.33287116
Windspeed	LA	77.95018414
	F	37.59266105

A.2) Model evaluation: comparison between Grid SPV and Single-Cell SPV

Four simulations were performed with both single-cell and grid versions of SPV. The results of the simulations as concentration values in the atmosphere, soil, and leaves were compared between the two models where the vegetation type of the models is selected as grass or forest. Other parameters and input data required for the simulations were selected to be identical. The same emission was added to the first layer of soil in the single-cell and one of the cells within the grid system.

A.3) Lower air variations

In order to show the frequency of variation of concentration in air, lower air concentrations relating to the first year (255 consecutive hours) of the simulation were shown for the cells along the valley (Figure B.4).

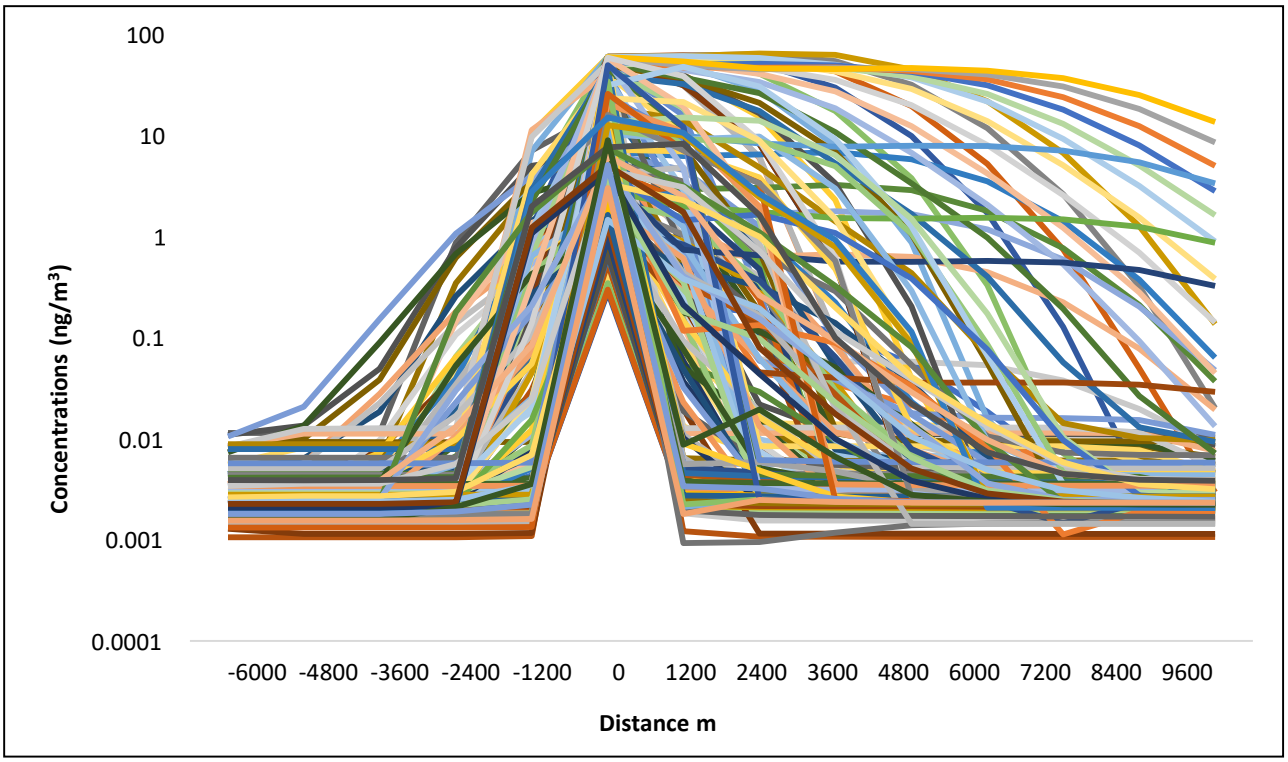

Figure B.4. Hourly lower air concentrations for the first 255 hours

Zero distance represents the location of the chemical plant. In the same direction, the concentration values of lower air vary from one hour to another. The reason is the unstable nature of air due to different factors such as the intensity of wind speed, the height of the planetary boundary, and temperature-driven evaporation and deposition.

References

Dimond, J.B., Owen, R.B., 1996. Long-term residue of DDT compounds in forest soils in Maine.
Environ. Pollut. 92, 227–230. https://doi.org/10.1016/0269-7491(95)00059-3

Ghirardello, D., Morselli, M., Semplice, M., Di Guardo, A., 2010. A Dynamic Model of the Fate of Organic Chemicals in a Multilayered Air/Soil System: Development and Illustrative Application. Environ. Sci. Technol. 44, 9010–9017. https://doi.org/10.1021/es1023866

Kömp, P., McLachlan, M.S., 1997. Influence of Temperature on the Plant/Air Partitioning of Semivolatile Organic Compounds. Environ. Sci. Technol. 31, 886–890. https://doi.org/10.1021/es960590u

Mackay, D. (Ed.), 2006. Handbook of physical-chemical properties and environmental fate for organic chemicals, 2nd ed. ed. CRC/Taylor & Francis, Boca Raton, FL.

Morselli, M., Ghirardello, D., Semplice, M., Di Guardo, A., 2011. Modeling short-term variability of semivolatile organic chemicals in air at a local scale: An integrated modeling approach. Environ. Pollut. 159, 1406–1412. https://doi.org/10.1016/j.envpol.2010.12.03

Nizzetto, L., Pastore, C., Liu, X., Camporini, P., Stroppiana, D., Herbert, B., Boschetti, M., Zhang, G., Brivio, P.A., Jones, K.C., Di Guardo, A., 2008. Accumulation Parameters and Seasonal Trends for PCBs in Temperate and Boreal Forest Plant Species. Environ. Sci. Technol. 42, 5911–5916. https://doi.org/10.1021/es800217m

Puri, S., Chickos, J.S., Welsh, W.J., 2001. Determination of Vaporization Enthalpies of Polychlorinated Biphenyls by Correlation Gas Chromatography 5.

Terzaghi, E., Morselli, M., Semplice, M., Cerabolini, B.E.L., Jones, K.C., Freppaz, M., Di Guardo, A., 2017. SoilPlusVeg: An integrated air-plant-litter-soil model to predict organic chemical fate and recycling in forests. Sci. Total Environ. 595, 169–177. https://doi.org/10.1016/j.scitotenv.2017.03.252

WHO, 1979. DDT and its Derivates. WHO Environmental Health Criteria., 9. World Health Organization, Geneva.

Wu, H., Fu, P., Morris, J.P., Settgast, R.R., Ryerson, F.J., 2019. ICAT: A numerical scheme to minimize numerical diffusion in advection-dispersion modeling and its application in identifying flow channeling.

Paper III

Predicting the contribution of a local emission source in mid-range transport of DDTs and their deposition in terrestrial and aquatic ecosystems

(Submitted to Science of the Total Environment)

Parisa Falakdin, Elisa Terzaghi, Di Guardo Antonio*

Department of Science and High Technology, University of Insubria, Via Valleggio 11, 22100, Como, CO, Italy

1. Abstract

A recently developed dynamic multiple box multimedia fate model (Gridded-SoilPlusVeg) was developed and implemented to account for the environmental variation and the effect of directional advective transport of chemicals towards different compartments and geographical locations. A chemical plant located in Pieve Vergonte in Ossola Valley produced and emitted DDTs for around 50 years. In the previous study the fate and transport of p,p'-DDT emitted from the chemical plant were evaluated in nearby areas (up to 12 km). In this paper, the Gridded-SoilPlusVeg model was run for p,p'-DDT during its production and decades after the production stop in 1996 (a total of 100 years) for a larger study area (200 km x 200 km) in order to evaluate the contribution of a local source on a larger scale. Additionally, the deposition fluxes into the lakes were calculated and were used as input into a dynamic fugacity-based aquatic model to calculate DDT concentration in water and sediments of three prealpine lakes: Lake Maggiore, Lake Como and Lake Lugano. The results of the simulations were compared with the monitoring and literature data. The results obtained from the spatial fate model, Gridded-SoilPlusVeg, allowed to estimate the atmospheric deposition fluxes and identify a potential cause for the high level of contamination in terrestrial and aquatic ecosystems on a regional scale.

Keywords: sediment; water; dynamic spatial model; fugacity model; DDT

2. Introduction

Air is an environmental medium which is highly affected by the advective forces of wind. Therefore, atmospheric compounds can be transported and deposit in areas away from the source and contaminate different environmental media such as soil, vegetation, and water. Particularly, persistent organic pollutants (POPs) with a long half-life in stable media such as soil, can be accumulated in time; additionally, as a result of further volatilization, soil can act as a secondary source of emission and contribute to the fate and transport of chemicals even years after the cease of an active emission source such as an industrial plant (Cabrerizo et al., 2011; Dalla Villa et al., 2006).

A Northern Italy chemical plant located in the town of Pieve Vergonte (VB) in the vicinity of Lake Maggiore produced Dichlorodiphenyltrichloroethane (DDT) for around 50 years until the production was ban after the discovery of Lake Maggiore pollution by DDTs in 1996 (Di Guardo et al., 2008, 2006, 2003). The pollution was attributed to the industrial plant DDT discharges in River Toce, a tributary of Lake Maggiore. In a recent work, the contribution of the emission from this local producer of DDTs to the pollution of the surrounding area (144 Ha) and the spatial and temporal extent of contamination in soil, leaves, and the air within the adjacent valley was shown (Falakdin et al., 2022). However, different levels of DDTs were found in areas further away from the source. In rain samples collected between 1985 to 1988 from different locations in North Italy such as Longone (in the vicinity of Lake Como), Brugherio (located in the North East of Milan), Monticolo (near the town of Bolzano), DDTs were found at concentrations of ng/l levels (Galassi et al., 1993). Tremolada et al., (2011) collected and analyzed several soil samples obtained in the years 2007-2008 from different altitudes in the Splugen pass of the Italian Central Alps. Due to the contribution of various factors such as organic matter content, depth of the soil layer, solar radiation, and seasonality,

measured concentrations of p,p'-DDT, varied up to one order of magnitude, and reached the level of 10 ng/g d.w. (Tremolada et al., 2011).

In the recent paper mentioned above, a spatial multimedia fate model (Gridded-SoilPlusVeg (GSPV) (Falakdin et al., 2022; Ghirardello et al., 2010; Terzaghi et al., 2017)) was developed and implemented to simulate the fate and transport of p,p'-DDT for 100 years starting from the year of the DDT production (1948) emitted from the chemical plant of Pieve Vergonte and contaminating the surrounding area. The results of the simulation showed a good agreement between the predicted concentrations versus monitoring data for soil and leaves confirming the temporal and spatial impact of a local emission source on the surrounding environment. Furthermore, it proved a potential for a larger influence on the regional environment. Multimedia fate models, coupled to a physical description of air movement (Falakdin et al., 2022; Ghirardello et al., 2010; Terzaghi et al., 2017) can be used to simulate the long term fate of contaminants by including relevant processes such as deposition and revolatilization, degradation, etc.. For this reason, they can be employed to reconstruct the chemical mass balance at different spatial and temporal extents. The objective of this work is to evaluate this contribution utilizing two fugacity-based multimedia fate models (GSPV and DynaModel, an unsteady-state lake model (Di Guardo et al., 2006; Infantino et al., 2008) to investigate whether this local but continuous emission can be responsible for the DDT concentration levels found in the farther terrestrial and aquatic environment.

3. Materials and methods

3.1. Study Area

A square-shaped area of 200 km × 200 km, partially covering parts of Italy and Switzerland, was considered (7º0 E–9º6 E, 45º1 N–46º9 N). The area includes three Italian/Swiss lakes namely Lake Maggiore, Lake Lugano, and Lake Como. It consists of different types of land use including croplands, forests, and residential areas. The chemical plant where the DDTs

production and emissions started is placed in the city of Pieve Vergonte, in the center of the study area and in the middle of Ossola valley: The site was recognized as a contaminated site of national relevance (SIN Pieve Vergonte) by the Italian authorities (MITE, 2022). Figure 1 shows the study area and the location of the industrial plant. The production of DDTs started in 1948 and continued till 1996 when due to the discovery of a high level of contamination in Lake Maggiore, the Italian Ministry of Environment issued a ban on DDTs production.

3.2. Monitoring data

Many different samples of various matrices such as soil, leaf, and litter were previously collected along Ossola valley. In the former study, samples of soil, leaf, and litter represented the concentration gradient with distance from the production source (Falakdin et al., 2022). In this paper, 15 additional soil samples, obtained in a monitoring campaign in Lombardy Region (Beone et al., 2015) and located within the study area, were used to show the relevance of DDT gradient in the regional environment (Table A.1).

3.3.Literature data

Data gathered from the literature were utilized to evaluate the level of environmental concentrations in different locations and matrices to provide insight into the contribution of DDT production and use during and after the ban of DDT in Italy as well as validation of lake simulations. Table A.2 shows the historical concentration values obtained from the literature for sediments, water, fish, and soil. Sediment data for DDTs relating to Lake Maggiore for the years from 1971 to 1996 shows the maximum value for 1996 indicating the deposition and accumulation through the years of DDTs production and the contribution from River Toce. Infact, these data are corresponding to samples collected from the inlet of Toce River which tend to have higher value than sediments of the other parts of the lake due to the received discharge. Concentration values for sediments of Lake Como (Northern Italy) vary for the years from 1978 to 1991 showing a small increase during the 1980s (Galassi et al., 1995;

Guzzella et al., 1998). (Bettinetti et al., 2016); measurements for sediment concentrations of Lake Como show levels between 30 to 95 ng/g d.w. for the years from 1970 to 2009. Water concentrations for different Italian rivers (Arno, Po, Ticino, and Toce) as well as Lake Maggiore are shown in the table for different years from 1970 to 2003. Total DDT trend generally indicate a higher value (by up to four orders of magnitude) for the years of production and use in the environment, in comparison with the subsequent years (CIPAIS, 2004, 2003, 1999). Additionally, levels of p,p'-DDT (up to ng/g lipid) were observed in the fish samples of Lake Lugano for the year 1996 indicating the bioaccumulation of these substances in the fat tissues, although fish samples from Lake Maggiore reached concentrations up to 25 ng/g lipid (Ceschi et al., 1996; Infantino et al., 2013).

For the decade after the end of production, values of p,p' DDT stated for the Italian town of Delebio, located in the vicinity of Lake Como, was 1.2 ng/g d.w. and for Splugen Pass, mountain located in the border of Italy and Switzerland and around 30 km North of Lake Como, varied between 0.05 to 10 ng/g d.w. depending on the location and the depth of soil samples (Tremolada et al., 2011, 2008). Additionally, values reported in the previous paper concerning the soil concentration of Ossola valley indicated levels up to 1 μg/g d.w. for 2001 (Falakdin et al., 2022). The complete dataset of data collected is shown in Table A2 in the supporting information.

3.4. Spatial multimedia fate model

The Gridded-SoilPlusVeg model was implemented for further validation and prediction of the long-term fate and transport of chemicals on a regional scale. The GSPV is a spatiodynamic multimedia fate model based on the fugacity approach (Mackay, 2001) including air, vegetation, and soil compartments. The grid is composed of a user-defined number of cells and each cell is a multimedia fate model unit. The cells are connected through the advective flows of air. Additionally, each cell can incorporate different land use and vegetation characteristics.

The model calculates the chemical fate processes among different environmental compartments such as deposition, volatilization, diffusion, degradation, and runoff and provides concentration values for each grid cell and each compartment on an hourly basis. Further explanation of processes, model performance, and sensitivity analysis were described in detail in the previous works (Falakdin et al., 2022; Ghirardello et al., 2010; Terzaghi et al., 2017). The model was developed in Visual Basic version 6.0 and integrates a GIS tool (MapWindow v. 5.6.3, MapWindow.org) for the incorporation of geographical information. For visualization and analysis of geographical data QuantumGIS version 3.20 (QGIS Development Team, 2018) was utilized.

3.5. Lake model

A dynamic fugacity-based water-sediment lake model (Dyna Model) (Di Guardo et al., 2006; Infantino et al., 2008), based on the QWASI Lake model (Mackay et al., 1983) was used for the simulation of Lakes Maggiore, Como, and Lugano. The model includes processes of volatilization, air deposition, inflow/outflow, sediment resuspension, sediment burial, sediment transformation, sediment-water diffusion, and water transformation. The results are provided as concentration or fugacity values. Further information concerning the model formulation, calibration, and model performance can be found in (Di Guardo et al., 2006; Infantino et al., 2013, 2008).

3.6. Simulation scenario

The first simulation was performed with GSPV to calculate the fate and transport in the terrestrial environment. The simulation area was covered by 49 square-shaped cells (i.e., 7 × 7) of each 28.5 × 28.5 km^2 (Figure 1). The results were obtained as concentration values of soil in addition to deposition fluxes of air and vegetation to the soil. The mass-balance calculation of GSPV model is performed on temporal resolution of a second, however, the gridded model can save the results up to the resolution of an hour. The presence of lakes was not considered in GSPV, nevertheless, the

deposition fluxes relating to the location of the lakes were saved for the dynamic lake model simulations. In the lake simulations, the dynamic deposition flux corresponding to each lake was used as emission input to calculate the concentration values in water and sediment compartments. Parameters and properties used for the lake simulations can be found in Table A.4.

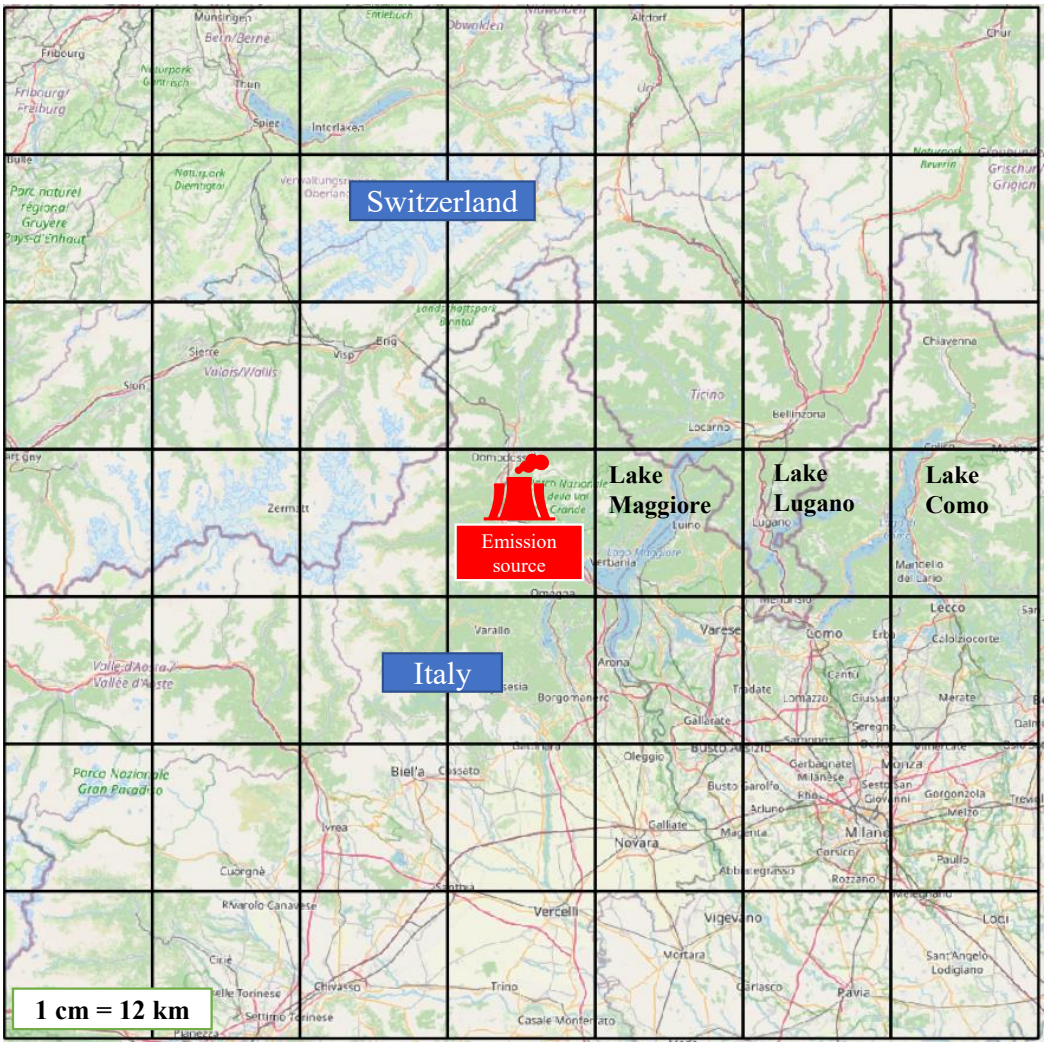

Figure 1 map of study area including the chemical plant and three lakes. Each cell corresponds to 812 km^2.

3.6.1. Chemical and environmental properties

The chemical selected for the simulations is p,p'-DDT. The physico-chemical parameters used in the simulations are shown in Table A.3. The use of p,p'-DDT as selected compound was due to the need of avoiding to evaluate further contribution of degradation and production of metabolites within each phase to the mass balance. This is the case of the DDE and DDD metabolites of DDT,

which may add up in a phase (e.g., soil, water, sediment) due to the degradation of the parent compound DDT.

Information relating to the land use and vegetation cover of the study area was extracted from the CORINE Land Cover (CLC 2018, land.copernicus.eu) database. For each cell, the dominant vegetation cover was considered and classified into three categories: crop, forest, and bare land where crop (including herbaceous vegetation), forest, and bare land (including the build-up areas) were set as tall fescue (*Festuca arundinacea*) grass, hazelnut forest, and no vegetation, respectively. The allocation of land use to the simulation cells is illustrated in Figure A.1.

Organic carbon (OC) and soil characteristics were set uniformly for the entire simulation area and equal to the data used for the simulation of Ossola valley. OC fraction value was set to 0.0234 as the average of measured values for the area surrounding Lake Maggiore. Additionally, the soil composition of loamy sand with 5 layers of each 20 mm thickness was assigned. Particulate and dissolved organic carbon in soil (POC and DOC) were set to 15 and 10 mg/l, respectively (Terzaghi et al., 2020).

The meteorological scenario was implemented as the previous simulation of Pieve Vergonte (Falakdin et al., 2022) in order to reconstruct the spread of the outgoing chemicals to the regional environment for the same period of time. Therefore, the wind data of Ornavasso (VB) local meteorological station (215 m a.s.l, about 11 km East of Pieve Vergonte) was set in addition to other meteorological parameters such as temperature, precipitation, and solar radiation imported from the Regional Agency for Environmental Protection (ARPA, 2005) of the Piedmont Region relating to the Fomarco station in the vicinity of the chemical plant.

3.6.2. Emission scenario

Hourly emission rate to the regional environment was reconstructed based on the previous study (Falakdin et al., 2022); chemicals exiting the simulation area of the former scenario through the

advective wind are now considered as the atmospheric emission on a larger scale. Then, the emission rate is calculated by multiplying the hourly advective air flowrate by the average atmospheric concentration of the corresponding hour. Since the entire study area of the previous work is located within one cell of the new grid system in this work (row: 4, column: 4), the hourly emission rate is allocated to that cell, and it is referred to as the "emission cell". Figure A.3 shows the yearly emission rates implemented for the simulation scenario.

3.6.4 Integration between GPSV and Dyna model simulations

The GSPV simulation was run for p,p'-DDT over a period of 100 years. The concentration values of the p,p' DDT isomer were obtained for soil on a monthly basis. Additionally, the deposition fluxes to soil were saved for the corresponding months. Dyna Model simulations were run for 100 years for Lake Maggiore, Lake Como, and Lake Lugano using the dynamic atmospheric deposition obtained from GSPV results. The results of these simulations were shown as yearly values of water and sediment concentrations. For Lake Como, an average incoming advective p,p'-DDT concentration (0.0015 ng/L) was also used in the simulation basing on the measurement of (Villa et al., 2011) who measured DDTs in water in the upper part of Lake Como, near to the Adda inlet, in July 2007. In this work p,p'-DDT was below LOQ (3 pg/L) and therefore the concentration value assumed was ½ of LOQ.

4. Results and discussion

4.1. Simulation uncertainty

Uncertainty and sensitivity analysis of the meteorological scenario were conducted in the previous paper (Falakdin et al., 2022).

The deposition flux of a forest cell compared to a grass cell varies up to a factor of 3, while this value for the cells without vegetation cover is significantly different since in the absence of vegetation, soil can be affected to a great extent by the environmental factors such as temperature,

therefore, soil of a bare cell for this simulation acted as a source especially during the hot seasons. However, since the area surrounding the lakes are predominantly covered by vegetation, the allocation of vegetation cover to the cells including the lakes can be more convenient. Soil concentration for a cell with forest vegetation cover compared to a bare soil with the same distance from the source for all the simulation years varies up to a factor of 1.5. However, soil concentration of a cell with grass vegetation cover in comparison with a cell without vegetation covers varies up to a factor of 2.5. The soil concentrations between a forest and a grass cell at the same distance from the source vary up to a factor of 1.5. Additionally, the estimation of atmospheric emission was based on the leaf concentrations and back-calculated using the plant-air partition coefficient (Kpa) (Nizzetto et al., 2006) which is affected by temperature, therefore, the uncertainty of meteorological data can also affect the estimated emission rates.

4.2.The spatial and temporal trend of DDT in soil

Soil concentrations in the simulation area vary depending on the location and the year of the simulation. Simulated and measured concentrations were compared for 2011 when measurements were available (Figure 2) indicated a good agreement (within the same order of magnitude) for most of the points. Since each cell covers an area of about 812 km^2 and one concentration value is calculated for each cell, an interval of concentrations was considered for comparison (i.e., ± 15% of the predicted values; similar uncertainty was considered as measurement uncertainty for the measured values). However, since each sample represents a point and the predicted values are assigned to the entire area of the cells, variations between the two values are inevitable. For 2011, minimum and maximum calculated concentrations were 0.28 and 3.80 ng/g d.w., respectively. These values for the measured concentration relating to the same year were between 0.08 and 4.87 ng/g d.w. Both measured and predicted values were adjusted for their corresponding organic matter fraction prior to comparison.

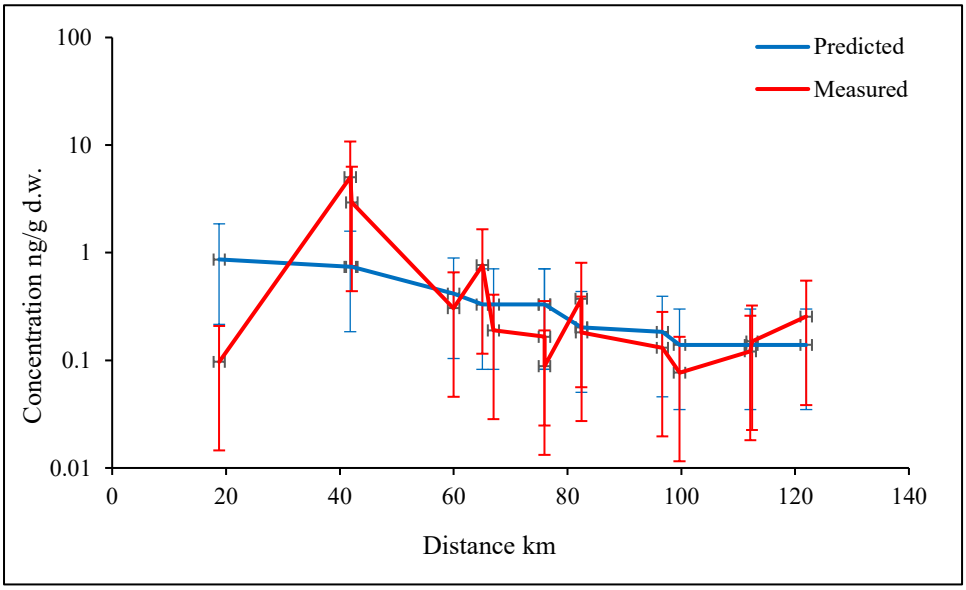

Figure 2 soil predicted concentration for with distance from the chemical plant.

The concentration of the emission cell (where the entire study area of the previous paper is located) was within the same order of magnitude for all the years in comparison with the average concentration of the entire grid of the previous work (Falakdin et al., 2022).

Figure 3 shows the predicted soil concentrations of the entire grid represented at 10 year intervals (1951-2051). Concentrations in soil vary of around one order of magnitude within the simulated grid depending on the vicinity to the source and the environmental and meteorological parameters such as vegetation cover and wind direction. The mild variation of concentration within the entire grid indicates the effect of long-term release and dispersion within a regional environment as well as the effect of background concentration. The highest soil concentration is related to the maximum production year (the 1960s) and the reduction occurs in the years after the production halt (1996). The deviation between the years of production in comparison to the following years reaches up to an order of magnitude for the corresponding locations. Each grid is representative of the month of Jun. The grid shows a higher deposition in the area covered by vegetation in comparison with the bare soil, as predicted by the Forest Filter effect (McLachlan and Horstmann, 1998).

However, apart from the effect of source strength (higher concentrations in the cells closer to the source), the organic carbon (OC) content of soil can also impact the concentrations. The map of organic carbon for the Lombardy region, obtained from (The Regional Agency for Environmental Protection, 2006) (Figure A.2), indicates that the soil OC content varies between 0.3% to 3% generally with a higher percentage in the Northern areas.

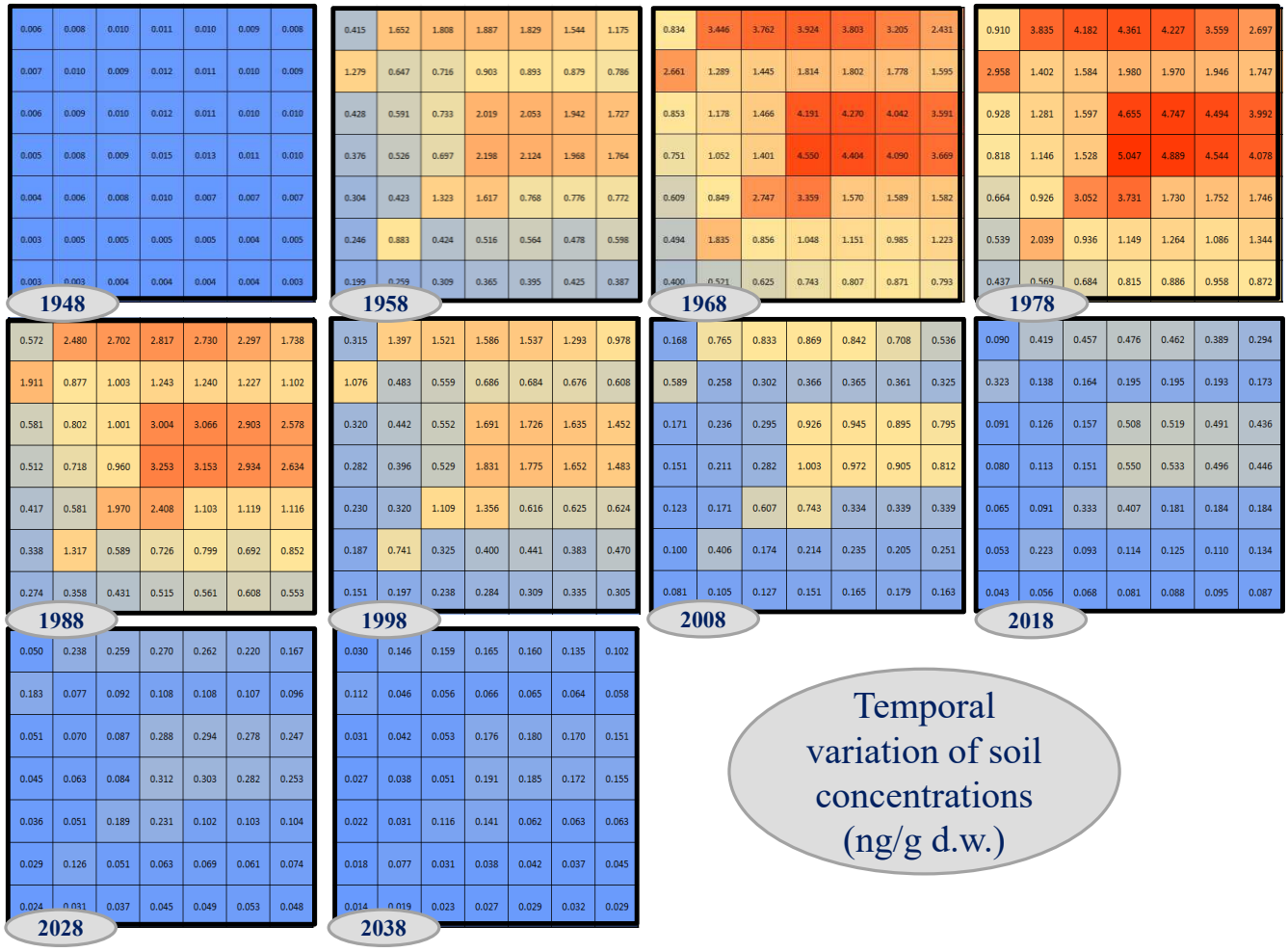

Figure 3 simulated soil concentrations with time within the entire grid.

Overall, the results agree with monitoring and literature data for the corresponding year and location. Moreover, the results of the simulation on a regional scale of about 40000 km^2 highlight the extent of chemical transport, deposition, and its evolution over 100 years. However, these results were only regarding the impact of DDT emitted from one local source and the effects of DDTs used for agricultural purposes or emitted from other producers were not considered.

However, model results show that the air deposition from an important source, such as a chemical plant can justify the concentration ranges measured throughout the investigated area.

4.3.Lake model results

DDT deposition through 100 years to the investigated lakes can be obtained from GSPV simulation. Although the simulation area does not include existing lakes, the deposition fluxes in the same area can be used to evaluate the importance of such contribution to the level of DDT in water and sediments of the regional lakes. As calculated in the previous work, more than 95% of the total emission to air during the 50 years of production (an average value of 260 kg/y) exited the local study area (here the emission cell). In this work, the calculation of grid flux showed that 14% of the exited chemicals ended up in the cells located in the East of the emission cell due to the prevalent wind direction (an area of about 1625 km^2). Approximately, the average yearly fluxes of 55.8 kg/y, 52.1 kg/y, and 17.4 kg/y were calculated for Lake Maggiore, Lake Lugano, and Lake Como, respectively. Figure 4 illustrates the variation of daily flux, on a monthly basis, for the lakes during the years of production demonstrating the same temporal trend of emission.

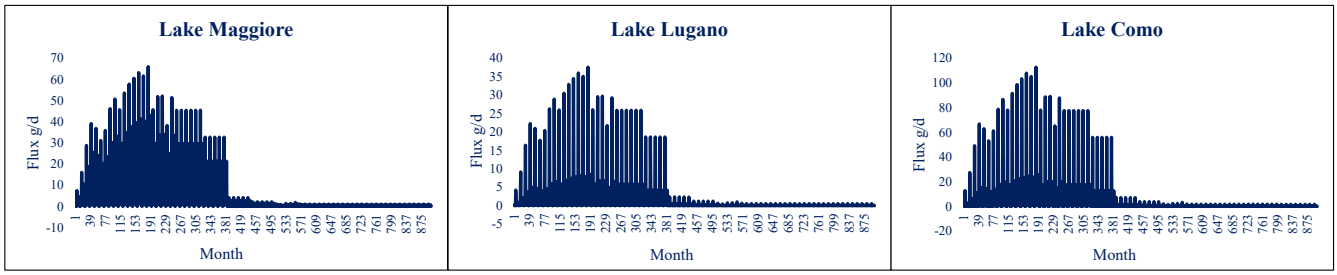

Figure 4 atmospheric deposition fluxes for Lakes Maggiore, Lugano, and Como.

The results of water and sediment concentrations obtained from the simulations were compared with concentration data from the literature (Figure 5). For all lakes, concentrations of p,p'-DDT in water and sediments indicates higher values during the 1950s to 1980s following the increase of atmospheric deposition relating to these years, due to increased production and release. Predicted values obtained for water in Lake Maggiore reach to the maximum of 0.7 ng/l which

corresponds to the year 1965. For the following years, this value drops below 0.08 ng/l. Measured water concentrations of Lake Maggiore corresponding to 2003 and 2004, represent a value lower than the detection limit for p,p'-DDT. This value however for total DDTs is up to 0.2 ng/l. Since total DDTs include the degradation products of DDT, high levels of p,p'-DDT atmospheric deposition during the production year can be a contributing source to the lake concentration. Although the dominant emission source of DDT in Lake Maggiore is the direct discharge from the Toce River (Di Guardo et al., 2006), calculations show the importance of an additional contributing contamination source that might be underestimated. This contribution is more evident in the other simulated lakes (Como and Lugano) where the direct discharge of DDT into them is less significant in comparison with Lake Maggiore. The measured p,p'-DDT concentration of sediments of Lake Maggiore from 1984 to 1996 varies between 5 to 121 ng/g (Guzzella et al., 1998). However, the predicted concentrations for the same time interval reach the maximum of 6 ng/g. The highest concentrations measured though are referred to areas close to River Toce estuary and indicate the contribution of direct discharge of DDT to river water and accumulation in sediments over time. Therefore, the prediction agrees well with the expected role of atmospheric deposition as general background contamination.

Predicted concentration values for water and sediments of Lake Como for the production years reach up to 0.08 ng/l and 26 ng/g, respectively. Literature data for sediments of Lake Como shows values within the same order of magnitude as predicted (Bettinetti et al., 2016; Galassi et al., 1995) (Table A.2). The contribution of glaciers on the concentration of Lake Como sediments was emphasized in (Bettinetti et al., 2016) which supposed that the gradually melting glaciers (storing historical DDT loading and rapidly releasing to freshwater) can act as the primary source of high levels of DDTs in sediments. DDTs deposition and accumulation on glaciers over years are due to the atmospheric transport of these contaminants, however glacier surface is considerably smaller even of the lake surface and therefore such contribution should be considered smaller than

the direct deposition to lake water surface. Additionally, model simulations and mass balance show that the constant advective inflow concentration used in the simulation, considering p,p'-DDT measured by (Villa et al., 2011) does not affect significantly model results, showing that for Lake Como direct transport and deposition of DDTs into the lake is the dominant source of the relatively high levels of DDTs in this lake.

The prediction of water and sediment concentrations for Lake Lugano also indicates that apart from other contributing sources, even atmospheric deposition over years solely can be capable of increasing the levels of concentrations up to 0.07 ng/l and 7 ng/g for water and sediments of this lake, respectively (Figure 5).

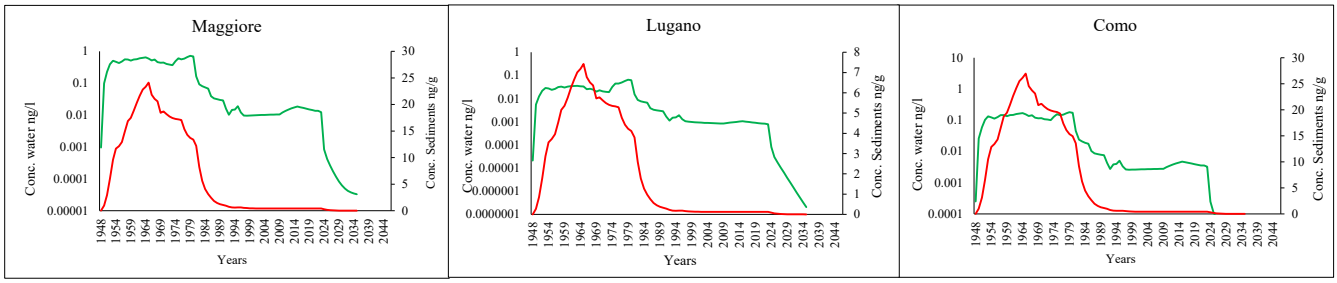

Figure 5 water and sediment predicted concentrations for Lakes Maggiore, Lugano, and Como.

5. Conclusions

In this work, different simulations were performed to estimate the impact of DDT released from a local chemical plant and determine the role of the spatial, meteorological, and environmental parameters on the fate and transport of p,p'-DDT in the regional environment. The simulations performed allowed to predict levels of DDT concentrations in different environmental media. The comparison between predictions and literature data in soil, sediments, and water showed a good agreement (within the same order of magnitude). Spatial and temporal predicted results for soil were also illustrated for 100 years indicating the extent of contamination of a persistent and hydrophobic chemical and the time required to clean up.

Additionally, levels of predicted concentration in sediments and water of Lake Maggiore, Como, and Lugano were calculated by a dynamic lake model emphasizing the potential influence of atmospheric transport and air deposition in the further area from a local contamination source. Additional monitoring of the regional environment is required to obtain levels of DDTs in different media in the following years and to further validate the predictions of spatial and lake simulations.

References

Beone, G., Cenci, R., Guidotti, L., Sena, F., Umlauf, G. (EDs), 2015. Progetto di monitoraggio ambientale su tutto il territorio della regione Lombardia (Progetto Soil): indagine conoscitiva della qualità e dello stato di salute dei suoli lombardi. (No. EUR 27161 IT). European Commission. Joint Research Centre. Institute for Environment and Sustainability. Publications Office, LU.

Bettinetti, R., Quadroni, S., Boggio, E., Galassi, S., 2016. Recent DDT and PCB contamination in the sediment and biota of the Como Bay (Lake Como, Italy). Sci. Total Environ. 542, 404–410. https://doi.org/10.1016/j.scitotenv.2015.10.099

Cabrerizo, A., Dachs, J., Jones, K.C., Barceló, D., 2011. Soil-Air exchange controls on background atmospheric concentrations of organochlorine pesticides. Atmospheric Chem. Phys. 11, 12799–12811. https://doi.org/10.5194/acp-11-12799-2011

Ceschi, M., De Rossa, M., Jaggli, M., 1996. Contaminanti organici, inorganici e radionuclidi nell'ittiofauna dei laghi Ceresio e Verbano (bacini svizzeri). Trav Chim Aliment Hyg 87, 189–211.

CIPAIS, 2004. Commissione Internazionale per la protezione delle acque italo-svizzere. Consiglio Nazionale delle Ricerche Istituto per lo Studio degli Ecosistemi.

CIPAIS, 2003. Commissione Internazionale per la protezione delle acque italo-svizzere. Consiglio Nazionale delle Ricerche Istituto per lo Studio degli Ecosistemi.

CIPAIS, 1999. Commissione Internazionale per la protezione delle acque italo-svizzere. Consiglio Nazionale delle Ricerche Istituto per lo Studio degli Ecosistemi.

Dalla Villa, R., de Carvalho Dores, E.F.G., Carbo, L., Cunha, M.L.F., 2006. Dissipation of DDT in a heavily contaminated soil in Mato Grosso, Brazil. Chemosphere 64, 549–554. https://doi.org/10.1016/j.chemosphere.2005.11.019

Di Guardo, A., Ferrari, C., Infantino, A., 2006. Development of a Dynamic Aquatic Model (DynA Model): Estimating Temporal Emissions of DDT to Lake Maggiore (N. Italy). Environ. Sci. Pollut. Res. 9.

Di Guardo, A., Nizzetto, L., Infantino, A., Colombo, I., Saporiti, E., Jones, K.C., 2008. Field derived accumulation and release kinetics of DDTs in plants. Chemosphere 72, 1497–1503. https://doi.org/10.1016/j.chemosphere.2008.04.072

Di Guardo, A., Zaccara, S., Cerabolini, B., Acciarri, M., Terzaghi, G., Calamari, D., 2003. Conifer needles as passive biomonitors of the spatial and temporal distribution of DDT from a point source. Chemosphere 52, 789–797. https://doi.org/10.1016/S0045-6535(03)00256-X

Falakdin, P., Terzaghi, E., Raspa, G., Di Guardo, A., 2022. Predicting the regional contamination evolution of DDT for 100-years with a new gridded spatial and dynamic multimedia fate model. Sci. Total Environ. 845, 157190. https://doi.org/10.1016/j.scitotenv.2022.157190

Galassi, S., Gosso, E., Tartari, G., 1993. PCBs and chlorinated pesticides in rains of Northern Italy. Chemosphere 27, 2287–2293. https://doi.org/10.1016/0045-6535(93)90139-V

Galassi, S., Provini, A., Guzzella, L., De Paolis, A., 1995. I pesticidi clorurati costituiscono ancora un problema in Italia?', Atti VI Congresso Nazionale della Società Italiana di Ecologiaw 16, 341–343.

Ghirardello, D., Morselli, M., Semplice, M., Di Guardo, A., 2010. A Dynamic Model of the Fate of Organic Chemicals in a Multilayered Air/Soil System: Development and Illustrative Application. Environ. Sci. Technol. 44, 9010–9017. https://doi.org/10.1021/es1023866

Guzzella, L., Patrolecco, L., Pagnotta, R., Langone, L., Guilizzoni, P., 1998. DDT and another organochlorine compounds in the Lake Maggiore sediments: a recent point source of contamination. Fresenius Environmental Bullettin 79–89.

Infantino, A., Morselli, M., Di Guardo, A., 2013. Integration of a dynamic organism model into the DynA Model: Development and application to the case of DDT in Lake Maggiore, Italy. Sci. Total Environ. 454–455, 358–365. https://doi.org/10.1016/j.scitotenv.2013.03.026

Infantino, A., Pereira, T., Ferrari, C., Cerejeira, M.J., Di Guardo, A., 2008. Calibration and validation of a dynamic water model in agricultural scenarios. Chemosphere 70, 1298–1308. https://doi.org/10.1016/j.chemosphere.2007.07.047

Mackay, D., 2001. Multimedia Environmental Models: The Fugacity Approach, Second Edition, 0 ed. CRC Press. https://doi.org/10.1201/9781420032543

Mackay, D., Joy, M., Paterson, S., 1983. A quantitative water, air, sediment interaction (QWASI) fugacity model for describing the fate of chemicals in lakes. Chemosphere 12, 981–997. https://doi.org/10.1016/0045-6535(83)90251-5

McLachlan, M.S., Horstmann, M., 1998. Forests as filters of airborne organic pollutants: a model. Environ. Sci. Technol. 32, 413–420.

MITE, 2022. Ministero della Transizione Ecologica - SIN di Pieve Vergonte [WWW Document]. [WWW Document]. URL https://bonifichesiticontaminati.mite.gov.it/sin-15/ (accessed 5.27.22)

Nizzetto, L., Jones, K.C., Gramatica, P., Papa, E., Cerabolini, B., Di Guardo, A., 2006. Accumulation of Persistent Organic Pollutants in Canopies of Different Forest Types: Role of Species Composition and Altitudinal-Temperature Gradient. Environ. Sci. Technol. 40, 6580–6586. https://doi.org/10.1021/es0605523

QGIS Development Team, 2018. QGIS Geographic Information System. Open Source Geospatial Foundation Project. [WWW Document]. URL http://qgis.osgeo.org

Terzaghi, E., Morselli, M., Semplice, M., Cerabolini, B.E.L., Jones, K.C., Freppaz, M., Di Guardo, A., 2017. SoilPlusVeg: An integrated air-plant-litter-soil model to predict organic chemical fate and recycling in forests. Sci. Total Environ. 595, 169–177. https://doi.org/10.1016/j.scitotenv.2017.03.252

Terzaghi, E., Vitale, C.M., Salina, G., Di Guardo, A., 2020. Plants radically change the mobility of PCBs in soil: Role of different species and soil conditions. J. Hazard. Mater. 388, 121786. https://doi.org/10.1016/j.jhazmat.2019.121786

The Regional Agency for Environmental Protection, n.d. Arpa Agenzia Regionale Per La Protezione Ambientale [WWW Document]. URL http://www.arpa.piemonte.it/

Tremolada, P., Comolli, R., Parolini, M., Moia, F., Binelli, A., 2011. One-Year Cycle of DDT Concentrations in High-Altitude Soils. Water Air Soil Pollut 13.

Tremolada, P., Villa, S., Bazzarin, P., Bizzotto, E., Comolli, R., Vighi, M., 2008. POPs in Mountain Soils from the Alps and Andes: Suggestions for a 'Precipitation Effect' on Altitudinal Gradients. Water. Air. Soil Pollut. 188, 93–109. https://doi.org/10.1007/s11270-007-9527-5

Villa, S., Bizzotto, E.C., Vighi, M., 2011. Persistent organic pollutant in a fish community of a sub-alpine lake. Environ. Pollut. 159, 932–939. https://doi.org/10.1016/j.envpol.2010.12.013

Predicting the contribution of a local emission source in mid-range transport of DDTs and their deposition in terrestrial and aquatic ecosystems – *Supplementary data*

Parisa Falakdin, Elisa Terzaghi, Di Guardo Antonio*

Department of Science and High Technology, University of Insubria, Via Valleggio 11, 22100, Como, CO, Italy

Table of Contents

A MONITORING DATA AND SIMULATION SCENARIO

A.1) Monitoring and literature data

Samples of soil, leaves, and litter values within the source area (Pieve Vergonte in Ossola Valley) were presented in the previous paper (Falakdin et al., 2022, SI). Table A.1 shows the measured concentrations of soil samples in the current study area. Table A.2 provides literature data of DDTs concentrations in different matrices within the study area.

Table A.1 Monitoring data for soil concentrations.

Soil concentration ng/g dry weight									
References	**Year**	**Location**	**ΣDDTs**	**2,4-DDT**	**4,4 DDT**	**2,4-DDD**	**4,4-DDD**	**2,4-DDE**	**4,4-DDE**
(Tremolada et al., 2008)	2003	Delebio, Italy	2.2	0.29	1.2	0.02	0.18	<0.01	0.53
(Offenthaler et al., 2008)	2004	Bagni di Masino, Italy	1.402	0.255	0.428	0.0027	0.0049	0.0088	0.8306
(Tremolada et al., 2011)	2007/2008	Spluga Pass, Swiss	1.2-58	n.a.	0.05-10	n.a.	0.14-9.4	n.a.	0.56-48
(Beone et al., 2015)	2011	Pavia, Italy	0.749	0.15	0.253	0.005	0.012	0.013	0.316
(Beone et al., 2015)	2011	Pavia, Italy	0.389	0.056	0.149	0.006	0.008	0.008	0.162
(Beone et al., 2015)	2011	Pavia, Italy	0.615	0.03	0.13	0.028	0.043	0.01	0.374
(Beone et al., 2015)	2011	Bergamo, Italy	0.4	0.036	0.12	0.005	0.018	0.005	0.217
(Beone et al., 2015)	2011	Milan, Italy	3.53	0.065	0.371	0.019	0.079	0.249	2.75
(Beone et al., 2015)	2011	Pavia, Italy	0.222	0.021	0.076	0.007	0.017	0.003	0.098
(Beone et al., 2015)	2011	Pavia, Italy	0.484	0.085	0.165	0.01	0.033	0.007	0.184
(Beone et al., 2015)	2011	Pavia, Italy	0.468	0.025	0.087	0.011	0.021	0.02	0.304
(Beone et al., 2015)	2011	Pavia, Italy	0.553	0.046	0.188	0.011	0.037	0.006	0.265
(Beone et al., 2015)	2011	Milan, Italy	2.68	0.112	0.754	0.011	0.052	0.01	1.74
(Beone et al., 2015)	2011	Lecco, Italy	0.547	0.036	0.18	0.008	0.025	0.005	0.292
(Beone et al., 2015)	2011	Como, Italy	0.634	0.068	0.302	0.005	0.027	0.004	0.227
(Beone et al., 2015)	2011	Como, Italy	9.12	0.626	2.89	0.228	0.636	0.04	4.71
(Beone et al., 2015)	2011	Varese, Italy	14.76	0.848	4.87	0.043	0.256	0.052	8.68
(Beone et al., 2015)	2011	Varese, Italy	0.32	0.043	0.095	0.01	0.041	0.003	0.129

Table A.2 Literature data concentrations of DDTs in matrices other than soil.

Sediment concentration ng/g dry weight												
Reference	**year**	**Location**	**ΣDDTs**	**ΣDDT**	**ΣDDD**	**ΣDDE**	**2,4-DDT**	**4,4-DDT**	**2,4-DDD**	**4,4-DDD**	**2,4-DDE**	**4,4-DDE**
(Galassi et al., 1993)	1986	Lake Comabbio	23.60	n.a.	n.a.	11.80	n.a.	n.a.	n.a.	n.a.	n.a.	11.80
(Galassi et al., 1993)	1986	Lake Monate	1.20	n.a.	n.a.	0.60	n.a.	n.a.	n.a.	n.a.	n.a.	0.60
(Galassi et al., 1993)	1986	Lake Varese	7.40	n.a.	n.a.	3.70	n.a.	n.a.	n.a.	n.a.	n.a.	3.70
IRSA,1995	1984	Lake Maggiore	280.00	6.00	125.00	149.00	1.00	5.00	47.00	78.00	24.00	125.00

IRSA,1995	1987	Lake Maggiore	103.00	3.00	40.00	60.00	1.00	2.00	15.00	25.00	12.00	48.00
IRSA,1995	1990	Lake Maggiore	72.00	4.00	18.00	50.00	0.00	4.00	8.00	10.00	8.00	42.00
(Guzzella et al., 1998)	1996	Lake Maggiore	32.00	7.00	11.00	14.00	1.00	6.00	4.00	7.00	3.00	11.00
(Guzzella et al., 1998)	1996	Lake Maggiore	106.00	32.00	54.00	20.00	3.00	29.00	15.00	39.00	6.00	14.00
(Guzzella et al., 1998)	1996	Lake Maggiore	146.00	104.00	29.00	13.00	1.00	103.00	10.00	19.00	2.00	11.00
(Guzzella et al., 1998)	1996	Lake Maggiore	58.00	41.00	12.00	5.00	1.00	40.00	3.00	9.00	1.00	4.00
(Guzzella et al., 1998)	1996	Lake Maggiore	136.00	12.00	54.00	70.00	1.00	11.00	20.00	34.00	15.00	55.00
(Guzzella et al., 1998)	1996	Lake Maggiore	48.00	35.00	7.00	6.00	1.00	34.00	3.00	4.00	1.00	5.00
(Guzzella et al., 1998)	1996	Lake Maggiore	213.00	49.00	119.00	45.00	3.00	46.00	43.00	76.00	12.00	33.00
(Guzzella et al., 1998)	1996	Lake Maggiore	33.00	7.00	17.00	9.00	2.00	5.00	6.00	11.00	3.00	6.00
(Guzzella et al., 1998)	1996	Lake Maggiore	222.00	124.00	69.00	29.00	3.00	121.00	23.00	46.00	5.00	24.00
(Guzzella et al., 1998)	1996	Lake Maggiore	113.00	33.00	46.00	34.00	6.00	27.00	17.00	29.00	9.00	25.00
(Guzzella et al., 1998)	1996	Lake Maggiore	1865.00	1719.00	86.00	60.00	19.00	1700.00	8.00	78.00	4.00	56.00
(Guzzella et al., 1998)	1996	Lake Maggiore	204.00	86.00	70.00	48.00	4.00	82.00	20.00	50.00	12.00	36.00
(Galassi et al., 1995)	1958	Lake Maggiore	180.00	<10	n.a.	<200	n.a.	<10	n.a.	n.a.	n.a.	<200
(Galassi et al., 1995)	1962	Lake Maggiore	430.00	<10	n.a.	430	n.a.	<10	n.a.	n.a.	n.a.	430
(Galassi et al., 1995)	1964	Lake Maggiore	1480.00	30	n.a.	1450	n.a.	30	n.a.	n.a.	n.a.	1450
(Galassi et al., 1995)	1966	Lake Maggiore	820.00	20	n.a.	800	n.a.	20	n.a.	n.a.	n.a.	800
(Galassi et al., 1995)	1968	Lake Maggiore	595.00	15	n.a.	580	n.a.	15	n.a.	n.a.	n.a.	580
(Galassi et al., 1995)	1969	Lake Maggiore	15.00	15	n.a.	<200	n.a.	15	n.a.	n.a.	n.a.	<200
(Galassi et al., 1995)	1971	Lake Maggiore	180.00	<10	n.a.	<200	n.a.	<10	n.a.	n.a.	n.a.	<200
(Galassi et al., 1995)	1978	Lake Como	18	<10	n.a.	18	n.a.	<10	n.a.	n.a.	n.a.	18
(Galassi et al., 1995)	1979	Lake Como	10	<10	n.a.	10	n.a.	<10	n.a.	n.a.	n.a.	10
(Galassi et al., 1995)	1980	Lake Como	4	<10	n.a.	4	n.a.	<10	n.a.	n.a.	n.a.	4
(Galassi et al., 1995)	1981	Lake Como	6	<10	n.a.	6	n.a.	<10	n.a.	n.a.	n.a.	6
(Galassi et al., 1995)	1982	Lake Como	17	<10	n.a.	17	n.a.	<10	n.a.	n.a.	n.a.	17
(Galassi et al., 1995)	1983	Lake Como	21	<10	n.a.	21	n.a.	<10	n.a.	n.a.	n.a.	21
(Galassi et al., 1995)	1984	Lake Como	16	<10	n.a.	16	n.a.	<10	n.a.	n.a.	n.a.	16
(Galassi et al., 1995)	1985	Lake Como	17	<10	n.a.	17	n.a.	<10	n.a.	n.a.	n.a.	17
(Galassi et al., 1995)	1986	Lake Como	18	140	n.a.	18	n.a.	n.a.	n.a.	n.a.	n.a.	18
(Galassi et al., 1995)	1987	Lake Como	19	18	n.a.	1	n.a.	18	n.a.	n.a.	n.a.	1
(Galassi et al., 1995)	1988	Lake Como	14	<10	n.a.	14	n.a.	<10	n.a.	n.a.	n.a.	14
(Galassi et al., 1995)	1989	Lake Como	10	<10	n.a.	10	n.a.	<10	n.a.	n.a.	n.a.	10

(Galassi et al., 1995)	1990	Lake Como	10	<10	n.a.	10	n.a.	<10	n.a.	n.a.	n.a.	10
(Galassi et al., 1995)	1991	Lake Como	12	<10	n.a.	12	n.a.	<10	n.a.	n.a.	n.a.	12
(CIPAIS, 2002)	2001	Lake Maggiore	27	n.a.	n.a.	n.a.	n.a.	n.a.	n.a.	n.a.	n.a.	n.a.
(CIPAIS, 2003)	2002	Lake Maggiore	10	n.a.	n.a.	n.a.	n.a.	n.a.	n.a.	n.a.	n.a.	n.a.
(CIPAIS, 2004)	2003	Lake Maggiore	10	n.a.	n.a.	n.a.	n.a.	n.a.	n.a.	n.a.	n.a.	n.a.
(Bettinetti et al., 2016)	2009	Lake Como	n.a.	n.a.	n.a.	n.a.	n.a.	30-95	n.a.	30-90	n.a.	25-75
Water concentration ng/l												
Reference	**year**	**Location**	**DDTs**	**DDT**	**DDD**	**DDE**	**2,4DDT**	**4,4DDT**	**2,4DDD**	**4,4DDD**	**2,4DDE**	**4,4DDE**
Grasso 1998	1996	River Arno	345.000	317	n.a.	28	n.a.	n.a.	n.a.	n.a.	n.a.	n.a.
Grasso 1998	1996	River Arno	31.6400	9.64	n.a.	22	n.a.	n.a.	n.a.	n.a.	n.a.	n.a.
Grasso 1998	1996	River Arno	130.9600	102.6	n.a.	28.36	n.a.	n.a.	n.a.	n.a.	n.a.	n.a.
Grasso 1998	1996	River Arno	80.4000	67.7	n.a.	12.7	n.a.	n.a.	n.a.	n.a.	n.a.	n.a.
Grasso 1998	1996	River Arno	80.4000	67.7	n.a.	12.7	n.a.	n.a.	n.a.	n.a.	n.a.	n.a.
Galassi et al.1983	1969	River Po	22.12	19.75	n.a.	2.37	n.a.	19.75	n.a.	n.a.	n.a.	2.37
Galassi et al.1983	1971	River Po	102.3	98.3	n.a.	4	n.a.	98.3	n.a.	n.a.	n.a.	4
Galassi et al.1983	1972	River Po	90	80	n.a.	10	n.a.	80	n.a.	n.a.	n.a.	10
Galassi et al.1983	1977	River Po	1.2	1.2	n.a.	n.d.	n.a.	1.2	n.a.	n.a.	n.a.	n.d.
Galassi et al.1983	1979	River Po	5.6	2	n.a.	3.6	n.a.	2	n.a.	n.a.	n.a.	3.6
Galassi et al.1983	1969	River Ticino	32.17	27.72	n.a.	4.45	n.a.	27.72	n.a.	n.a.	n.a.	4.45
Galassi et al.1983	1970	River Ticino	75	43	n.a.	32	n.a.	43	n.a.	n.a.	n.a.	32
Galassi et al.1983	1983	River Ticino	n.d.	n.d.	n.a.	n.d.	n.a.	n.d.	n.a.	n.a.	n.a.	n.d.
(CIPAIS, 1999)	1998	Toce river	n.a.	n.a.	n.a.	n.a.	0-0.08	0-1.3	n.a.	0-0.02	n.a.	0-0.6
(CIPAIS, 2003)	2002	Lake Maggiore	0.04	n.a.	n.a.	n.a.	n.a.	n.a.	n.a.	n.a.	n.a.	n.a.
(CIPAIS, 2004)	2003	Lake Maggiore	0.2	n.a.	n.a.	n.a.	n.a.	n.a.	n.a.	n.a.	n.a.	n.a.
Fish concentration ng/g lipid												
Reference	**year**	**Location**	**DDTs**	**DDT**	**DDD**	**DDE**	**2,4DDT**	**4,4DDT**	**2,4DDD**	**4,4DDD**	**2,4DDE**	**4,4DDE**
(Ceschi et al., 1996)	1993	Lake Lugano	23.40	1.60	2.70	19.10	0.50	1.10	0.40	2.30	0.00	19.10
(Ceschi et al., 1996)	1993	Lake Maggiore	630.80	21.40	30.70	578.70	14.80	6.60	15.50	15.20	6.20	572.50
(Ceschi et al., 1996)	1995	Lake Maggiore	2042.20	597.40	771.50	673.30	149.50	447.90	184.20	587.30	62.20	611.10
(Infantino et al., 2013)	1997-1998	Lake Maggiore	n.a.	n.a.	n.a.	n.a.	n.a.	590-1700	n.a.	1100-2400	n.a.	1700-9000

Note: n.a. refers to "not available".

A.2) Model parametrization

Physical-chemical properties implemented in the model simulation are expressed in Table A.3.

Table A.3 Physical-chemical properties of p.p'DDT employed in the simulation scenario.

Property	Unit	Value
Molecular weight	g mol^{-1}	354.5
Reference temperature	°C	25
Melting point	°C	108.5
Vapor pressure	Pa	0.00002
Water solubility	g m^{-3}	0.0055
log K_{OW}	-	6.19
Half-life in air	d	7.083
Half-life in soil	d	708.33
Half-life in water	d	229
Half-life in sediment	d	2292

Note: all physical-chemical parameters and half-life in air, water, and sediments are from (Mackay, 2006) while half-life in soil is from (Dimond and Owen, 1996).

Vegetation cover scenario adopted for the simulation area is shown in Figure A.1. Each grid cell represents the average predominant cover.

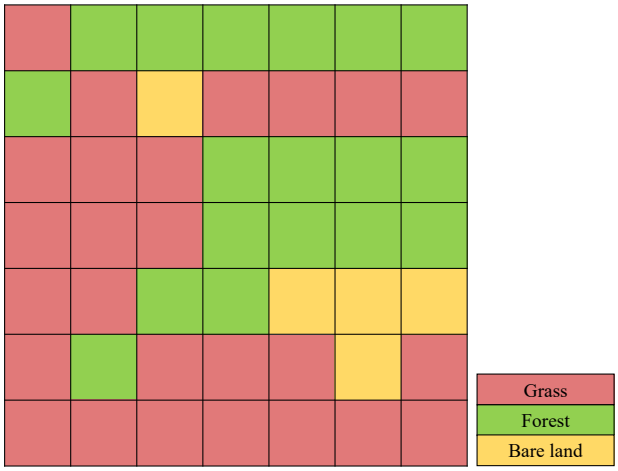

Figure A.1 Each cell is represented by its general vegetation characteristic.

Parameters relating to the vegetation types that were introduced into the model through the GIS database can be found in (Falakdin et al., 2022, SI).

Percentage of organic carbon content was imported for Lombardy region (Figure A.2) ranging from 0.28% (yellow) to 11% (green). Blue dots show the location of soil samples and their concentration (ng/g d.w.).

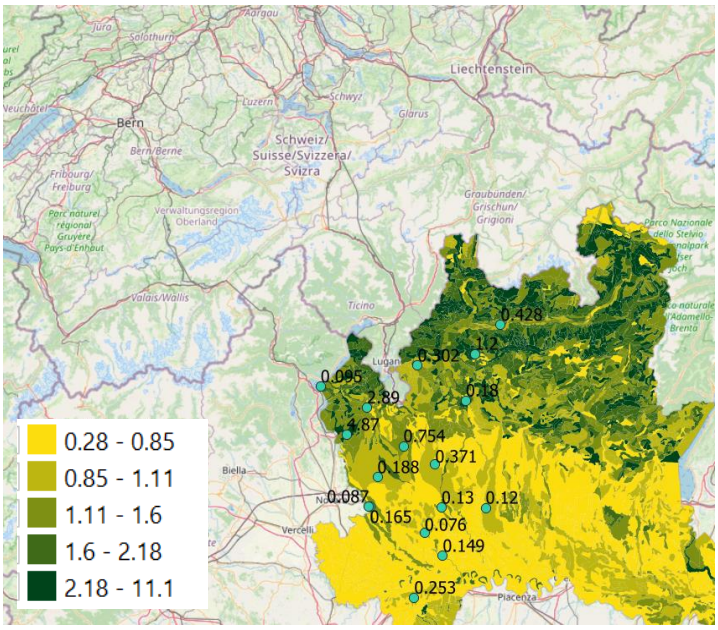

Figure A.2 map of OC content of Lombardy on the simulation area.

Table A.4 shows the parameters used for the three lake simulations.

Table A.4 Lake properties corresponding to Lakes Maggiore, Como, and Lugano **(Villa et al., 2011).**

Properties	Lake Maggiore		Lake Como		Lake Lugano	
	Value	Unit	Value	Unit	Value	Unit
Water Surface	212.5	km^2	146	km^2	48.7	km^2
Water Inflow Rate	380	m^3/s	158	m^3/s	23.6	m^3/s
Water Outflow Rate	292	m^3/s	158	m^3/s	23.6	m^3/s
Average Depth	176.5	m	154	m	134	m

A.3) Simulation scenario

Figure A.3 shows the hourly emission rate value imported to the GPSV model for each year.

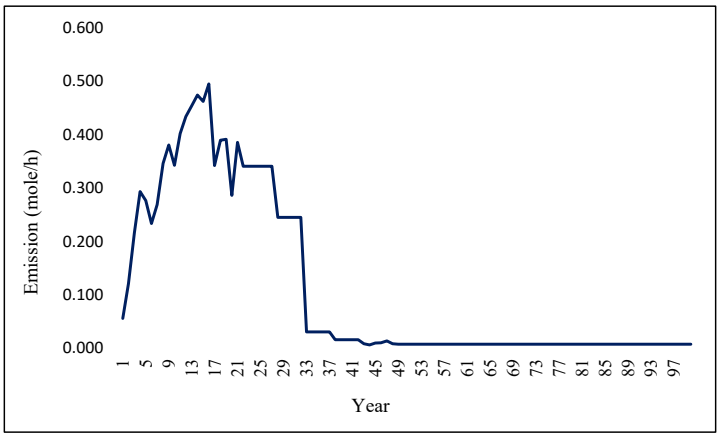

Figure A.3 Hourly emission rate by year (1948-2048) **(Falakdin et al., 2022).**

References

Beone, G., Cenci, R., Guidotti, L., Sena, F., Umlauf, G. (EDs), 2015. Progetto di monitoraggio ambientale su tutto il territorio della regione Lombardia (Progetto Soil): indagine conoscitiva della qualità e dello stato di salute dei suoli lombardi. (No. EUR 27161 IT). European Commission. Joint Research Centre. Institute for Environment and Sustainability. Publications Office, LU.

Bettinetti, R., Quadroni, S., Boggio, E., Galassi, S., 2016. Recent DDT and PCB contamination in the sediment and biota of the Como Bay (Lake Como, Italy). Sci. Total Environ. 542, 404–410. https://doi.org/10.1016/j.scitotenv.2015.10.099

Ceschi, M., De Rossa, M., Jaggli, M., 1996. Contaminanti organici, inorganici e radionuclidi nell'ittiofauna dei laghi Ceresio e Verbano (bacini svizzeri). Trav Chim Aliment Hyg 87, 189–211.

CIPAIS, 2004. Commissione Internazionale per la protezione delle acque italo-svizzere. Consiglio Nazionale delle Ricerche Istituto per lo Studio degli Ecosistemi.

CIPAIS, 2003. Commissione Internazionale per la protezione delle acque italo-svizzere. Consiglio Nazionale delle Ricerche Istituto per lo Studio degli Ecosistemi.

CIPAIS, 2002. Commissione Internazionale per la protezione delle acque italo-svizzere. Consiglio Nazionale delle Ricerche Istituto per lo Studio degli Ecosistemi.

CIPAIS, 1999. Commissione Internazionale per la protezione delle acque italo-svizzere. Consiglio Nazionale delle Ricerche Istituto per lo Studio degli Ecosistemi.

Dimond, J.B., Owen, R.B., 1996. Long-term residue of DDT compounds in forest soils in Maine. Environ. Pollut. 92, 227–230. https://doi.org/10.1016/0269-7491(95)00059-3

Falakdin, P., Terzaghi, E., Raspa, G., Di Guardo, A., 2022. Predicting the regional contamination evolution of DDT for 100-years with a new gridded spatial and dynamic multimedia fate model. Sci. Total Environ. 845, 157190. https://doi.org/10.1016/j.scitotenv.2022.157190

Galassi, S., Gosso, E., Tartari, G., 1993. PCBs and chlorinated pesticides in rains of Northern Italy. Chemosphere 27, 2287–2293. https://doi.org/10.1016/0045-6535(93)90139-V

Galassi, S., Provini, A., Guzzella, L., De Paolis, A., 1995. I pesticidi clorurati costituiscono ancora un problema in Italia?', Atti VI Congresso Nazionale della Società Italiana di Ecologiaw 16, 341–343.

Guzzella, L., Patrolecco, L., Pagnotta, R., Langone, L., Guilizzoni, P., 1998. DDT and another organochlorine compounds in the Lake Maggiore sediments: a recent point source of contamination. Fresenius Environmental Bullettin 79–89.

Infantino, A., Morselli, M., Di Guardo, A., 2013. Integration of a dynamic organism model into the DynA Model: Development and application to the case of DDT in Lake Maggiore, Italy. Sci. Total Environ. 454–455, 358–365. https://doi.org/10.1016/j.scitotenv.2013.03.026

Mackay, D. (Ed.), 2006. Handbook of physical-chemical properties and environmental fate for organic chemicals, 2nd ed. ed. CRC/Taylor & Francis, Boca Raton, FL.

Offenthaler, I., Simončič, P., Vilhar, U., 2008. MONARPOP: technichal report. Federal Ministry of Agriculture, Forestry, Environment and Water Management, Vienna.

Tremolada, P., Comolli, R., Parolini, M., Moia, F., Binelli, A., 2011. One-Year Cycle of DDT Concentrations in High-Altitude Soils. Water Air Soil Pollut 13.

Tremolada, P., Villa, S., Bazzarin, P., Bizzotto, E., Comolli, R., Vighi, M., 2008. POPs in Mountain Soils from the Alps and Andes: Suggestions for a 'Precipitation Effect' on Altitudinal Gradients. Water. Air. Soil Pollut. 188, 93–109. https://doi.org/10.1007/s11270-007-9527-5

Villa, S., Bizzotto, E.C., Vighi, M., 2011. Persistent organic pollutant in a fish community of a sub-alpine lake. Environ. Pollut. 159, 932–939. https://doi.org/10.1016/j.envpol.2010.12.013

Characterization of microplastics in atmospheric and foliage samples

Parisa Falakdin[1], Adrian Lopez-Rosales[2], Jose Andrade[2], Elisa Terzaghi[1], Antonio Di Guardo[1], Soledad Muniategui[2]

[1] Department of Science and High Technology, University of Insubria, Via Valleggio 11, 22100 Como, Italy

[2] Grupo Química Analítica Aplicada (QANAP), Instituto Universitario de Medio Ambiente (IUMA), Universidade da Coruña, Campus da Zapateira, E-15071 A Coruña, Spain

ABSTRACT

The growing trend of plastic production in recent years and the inadequate disposal of related waste has raised concerns regarding microplastic-related environmental issues. Microplastic particles disperse by means of transport and deposition processes to different ecosystems and enter food chains. In this paper airborne and foliage samples were collected and analysed for the quantity and identity of microplastics (MPs). This work presents preliminary methodology to treat the samples and subsequently identify MPs using a quantum cascade laser IR spectrometer. Airborne sample treatment involved filtration, extraction, concentration, and transfer onto reflective slides. Foliage treatment involved washing, extraction, concentration, and transference of putative MPs onto reflective slides. Fibres and fragments were differentiated automatically according to their physical features (size, width, height, etc.) and some derived characteristics, as circularity and solidity. The results suggested good agreement between the amounts of atmospheric-deposited and foliage-retained MPs.

KEY WORDS

Foliage; atmospheric microplastics; LDIR

1. INTRODUCTION

Plastic waste increased as a result of population growth and excessive use of polymers and inadequate waste management. Plastics are among the most convenient commodity materials, and they are utilized hugely for the production of disposable products. When spilled in the environment, these residues degrade due to erosion, solar radiation, weathering, and microorganisms and break into smaller particles. Additionally, microplastic particles (MPs) might be released directly into the environment from primary sources, such as personal care products, synthetic textiles, and tyres (Boucher and Friot, 2017).

Increasing concerns about MPs rocketed over the last decade and they dragged attention to their identification and quantitation in different environmental compartments. MPs can be defined as solid plastic particles insoluble in water with dimensions between 1 μm and 1 000 μm (=1 mm) (ISO, 2020) whose composition is dominated by carbon, hydrogen, and heteroatoms like oxygen, nitrogen, sulfur, and chlorine.

The presence of MPs in marine environments, some organisms and soils and sediments has been broadly studied (Hernandez-Gonzalez et al., 2018; Novillo et al., 2020; Thompson et al., 2004). However, fewer studies focused on atmospheric microplastics (AMPs) despite it is already known that they can be transported over long distances in the form of suspended atmospheric particles (Allen et al., 2019). Therefore, they may contribute to terrestrial and vegetation contamination and, ultimately, reach the breathing organs of animals. Hence, there is a growing demand for validated analytical procedures devoted to the identification of AMPs and for studying their presence in terrestrial vegetation. The issue of microplastics in marine vegetables (algae) and plankton has already been considered (López-Rosales et al., 2021, 2022b).

Before characterization, sample treatment protocols are needed and their implementation constitutes an important challenge as they ideally should be reliable (validated), fast, and yield maximum analyte recovery (López-Rosales et al., 2022a). Since the investigation of atmospheric and foliage MPs constitutes a relatively new field there is room for research on this topic. Luo et al., (2022) provided a recent review on the availability of procedures for the different working stages: sampling, sample treatment, particle identification, and modeling of AMPs. Another general review was conducted by Shao et al., (2022) on the possible sources of AMPs and their spatial and temporal distribution. It turned out that population density and industrialization are important factors to explain the distribution of AMPs. Thus, a higher level of AMPs was seen in urban environments when compared to rural areas. Also, more plastic fibers and particles were found indoors than outdoors (Shao et al., 2022). A recent study focused on finding atmospheric sources of MPs (Munyaneza et al., 2022) evaluated different pathways such as households, industry, traffic, and landfill as responsible for a potential threat to humans due to inhalation of MPs. The study demands urgent methodological developments and standardization of sampling and analysis (Munyaneza et al., 2022).

On the other hand, the leaves of terrestrial vegetation can act as passive air samplers. Indeed, a variety of studies demonstrated the capability of leaves to accumulate organic chemicals depending on the plant/air partitioning coefficient (Giráldez et al., 2022; Kömp and McLachlan, 1997; Nizzetto et al., 2008). Terzaghi et al., (2013) evaluated the processes involved in atmospheric particulate matter deposition, along with the semi-volatile organic compounds (SVOCs) captured by vegetation.

To the best of the author's knowledge, there is no investigation so far regarding the interaction between airborne and foliage MPs. Hence, this paper presents a preliminary study to develop

protocols for sampling, sample treatment, and identification of airborne-based MPs deposited on leaves. Some guidelines are also given to determine AMPs using a quantum cascade laser-based infrared spectrometer. Some previous results obtained for atmospheric samples using passive samplers and two species of leaves revealed the same general patterns.

2. Materials and methods

2.1. Apparatus

The relatively novel instrumental technique based on the use of quantum cascade laser in the IR spectral region (8700 LDIR from Agilent Technologies, USA) working in 1800-600 cm^{-1} mid-IR region along with reflective slides (MiRR, Kevley Technologies, Chesterland, USA) offered a suitable means to characterize MPs, although some instrumental parameters require some ad-hoc optimization. A number of physical parameters derived from measurement over the particles, such as aspect ratio, circularity, and solidity were used to automatically categorize the MPs as fibers or particles.

A Syncore-Plus® automated evaporation system, equipped with a V-800/805 vacuum controller and an R-12 vacuum line, and 12 dedicated glass containers (residual volume 1.0 mL), from Büchi, Switzerland were employed. A Rotabit P incubation system (Selecta, Spain), with adjustable temperature and trembling controls, and a Pobel vacuum filtration system equipped with a Millipore vacuum pump (Millipore, Ballerica, MA model WP6122050) were used as well.

2.2. Reagents and materials

The reagents for the treatment were KOH (100 % purity, Emsure®), and Triton X-100 (Sigma-Aldrich) and NaClO 6-14% active chloride from Emplura®. 96 % ethanol was from Ensure®. Ultrapure MilliQ-type water (18 MΩ•cm-1 resistivity) was from a Direct-Q 3-V Millipore (Molsheim, France) device, collected and used daily. The 20 μm mesh size (open bore, square weave mesh type) metallic filters were from Bopp & Co. A.G: (Switzerland) and the 1000 μL pipette tips were from Eppendorf (Hamburg, Germany).

A 8700 IR quantum cascade laser-based Agilent system (LDIR, Laser Direct Infrared) working in the 1800-600 cm-1 mid-IR region and using flat reflective slides (MiRR, Kevley Technologies, Chesterland, USA), was used. The same parameters were set for all samples, including the blanks. A measuring manual size range was set from 20 μm to 5000 μm, sensitivity was set to 3 (Agilent Clarity 1.0. version). These parameters were fixed after preliminary tests carried out to optimise their use.

An automatic evaporation system composed of a V-800/805 vacuum controller, Vacuum line and R-12 analyst Syncore Plus® Line plus dedicated glass containers (residual volume 1.0 mL) (Büchi, Switzerland); a Rotabit P incubation system (Selecta, Spain), with temperature and agitation controls; a Pobel vacuum filtration system combined with a Millipore vacuum pump (Millipore, Ballerica, MA, model WP6122050); a 3000867 Selecta ultrasonic bath (Barcelona, Spain). Further, a Leitz Wetzlar stereomicroscope (10x ocular and manual adjustment of the objective zoom up to 5x, total magnification 50x) was employed to spike samples.

2.3. Atmospheric microplastic sampling

Several samples were collected in January 2022 in an air monitoring station located close to the city of A Coruña (Instituto Universitario de Medio Ambiente). The location and geographical

coordinates of the sampling site are shown in Figure 1. This corresponds to a semi-urban location.

Two equal passive samplers were placed at a height of 2.5 m on top of the air monitoring station, and they were retrieved after a month in order to determine the total atmospheric deposition of January 2022. The passive samplers are constituted by 22 mm diameter (0.038 m^2) stainless steel funnels and 10 L ISO standardized glass collecting bottles, surrounded by a Teflon shield (they are commercialized by LAbService Analytica as "Depobulk" samplers). Figure 2 illustrates the atmospheric samplers used for this experiment.

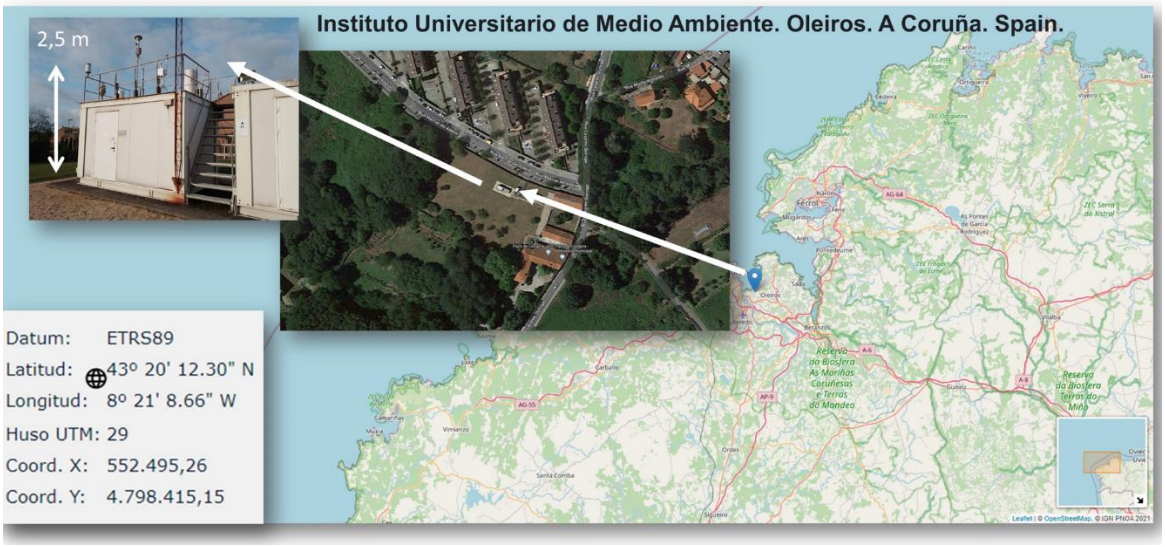

Figure 1: Location of the atmospheric sampling site, in a semi-urban location, close to the city of A Coruña, NW Spain.

Figure 2: Atmospheric passive samplers employed in this work –see text for details.

2.4. Leaf sampling

Adult and undamaged leaf samples of two species, *Hedra Helix* and *Photinia glabra* were collected in the vicinity of the Faculty of Sciences. This location corresponds to a semiurban site with some hourly peaks of traffic vehicles although low traffic density during the day. On the weekends the amount of traffic is negligible. A relevant point is that the collection site is at the top of a little hill SW of the city and wind blows frequently from the city to that point.

For each species, five to six leaves were sampled from different parts of the plants and at different locations. Figure 3 depicts the leaves collected to determine MPs on them.

Figure 3: Photographs of the two species of vegetables sampled for leaves in this work.

2.5. Sample treatment methods

2.5.1. Atmospheric samples

Atmospheric bulk samplers containing one-month deposition of organic matter and atmospheric particles were washed with MilliQ water toroughly and the solution was filtered through 20 µm stainless steel filters. The resulting filters were washed directly into dedicated Büchi glass tubes using 40 mL of 98 % ethanol. Particles were released from the surface of the filters using an ultrasonic bath (30 min, with different frequencies: 37 and 80 kHz, 15 min each; temperature < 35 °C).

The suspensions thus obtained were located into an automatic evaporation Syncore system and evaporated until ca. 2 mL. Since MPs can degrade with high temperatures, the evaporation process must be done gently and so evaporation extended overnight. The 2 mL remains were transferred onto reflective slides required for the LDIR system. The Büchi evaporation glass tubes were washed twice with ethanol, concentrated in the Syncore and the remaining volume was transferred onto the slide. The slides were kept in a closed fume hood at room temperature until completely dried prior to their measurement (Figure 4).

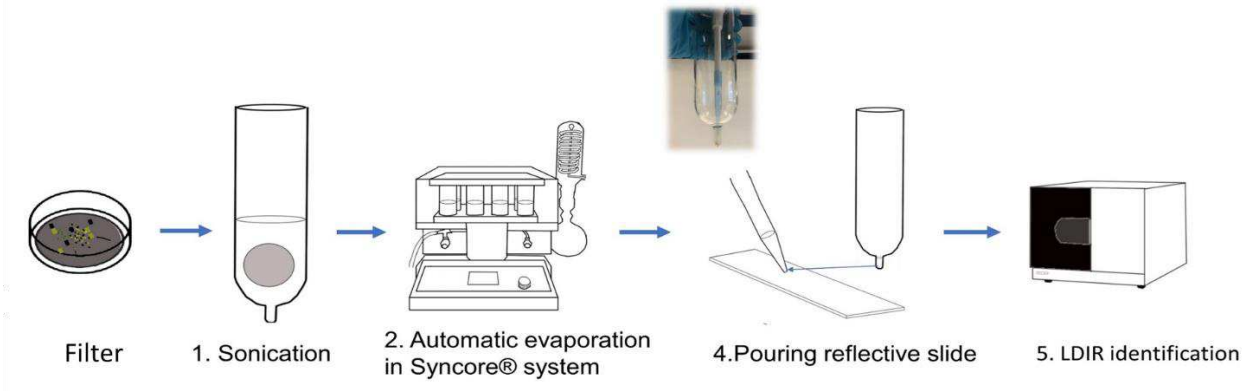

Figure 4: Scheme of the main steps to treat airborne-deposited samples.

2.5.2. Foliage samples

The procedure for the foliage samples implied washing the leaves over a beaker using 500 mL of surfactant (Tritón X-100 0,1%) and 500 mL of MilliQ water. The resulting suspension (1 L) was vacuum-filtered through a 20 μm stainless steel filter. To release the particles from the metallic filters, they were washed thoroughly using 50 mL of 98 % ethanol over a Büchi glass tube. The filter is afterwards submerged in the suspension and ultrasonicated for 30 min at different frequencies (37 and 80 kHz, 15 min each) and at < 35 °C. Then, the filter is removed and washed again with 25 mL of ethanol. Subsequent steps to reduce the volume of the suspension using a Syncore system and its final withdrawal were as for the airborne samples. Finally, the contents of the Büchi tubes were evaporated to ca. 1 mL, and the final remains were transferred to the reflective slides for their measurement.

2.5.3. Quality control

All glassware was washed with alkaline soap (Extran ® MA01) for 48 h and rinsed with abundant tap and MiliQ water. All reflectance slides were pre-cleaned with ethanol. Glassware and other materials used during the analysis were covered with aluminium foil during storage and use. The entire experiment was performed inside a fume hood. During operation, cotton clothing was used to prevent contamination by microplastic fibers. Two procedural blanks were considered along with each sample batch, according to procedures proposed elsewhere (Hermsen et al., 2018).

3. Results and Discussion

3.1. Setting the criterion for polymer identification

The QCL-based LDIR system scans the surface of the horizontal, flat, highly reflective slides and gets a spectrum from each and every detected particle. Detection is carried out automatically

by the built-in software after imaging the surface of the slide and identifying pixels different from the background. Therefore, the measurement time per slide varies depending on the number of particles deposited over it. For 1000 particles the system needs about 5 h. For each particle on the slide, a transflectance spectrum is registered and compared to the spectral libraries to match it to the most probable known material.

In our experience, a match (or correlation) index higher than 90 % must be set to consider that he identification of the unknown particle is reliable. Figure 6 shows an example of a particle whose match index = 95.4 % and, so, it was identified as polymethyl methacrylate (PMMA). Some other authors relaxed this value to 65 or 70 % but this led to too many false positives. However, the complex spectra of the tyres made us to consider a positive identification of a particle as of tyres only when the match index was around 95 % or higher. Figure 7 shows the identification of an unknown particle as a tyre, with a match index of 95.3 %. After identification, the plastic particles considered as MPs were categorized as particles or fibers according to their size and type, as addressed in the next section.

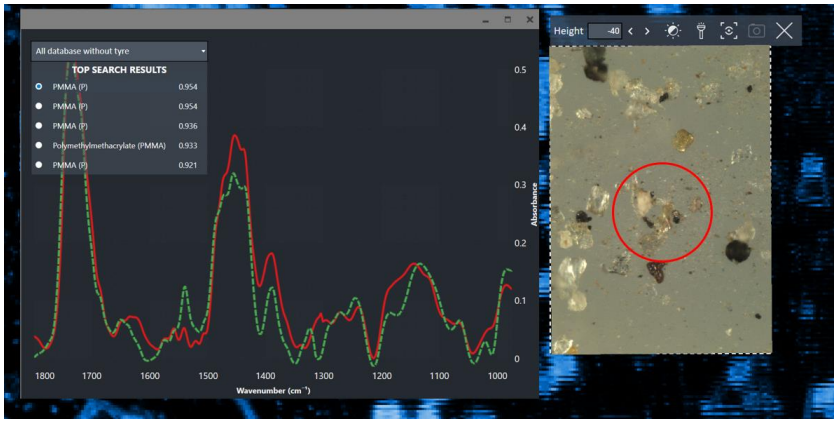

Figure 1: Example of a PMMA spectral identification with a match index of 95.4 %.

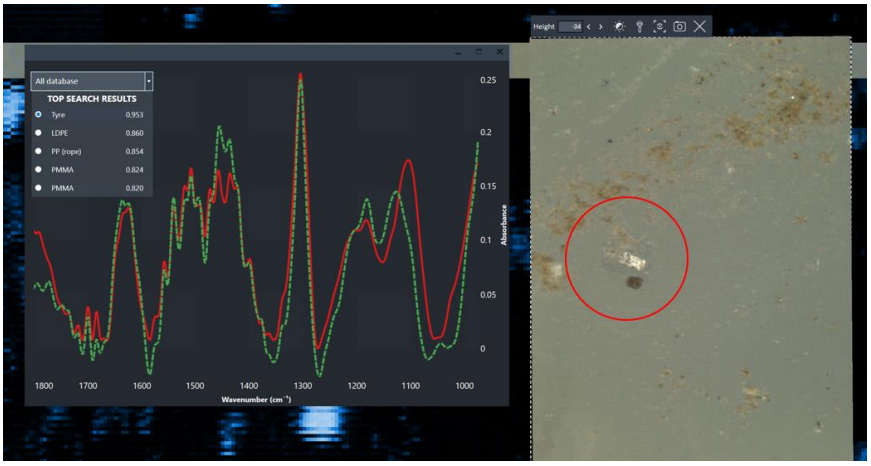

Figure 2: Example of a tyre identification with a match index of 95.3 %.

3.2. Microplastics in air and foliage

Microplastic particles and fibers were counted after the raw values were blank-corrected (i.e., the number of each kind of MP in the procedural blanks subtracted from the raw countings). AMPs were counted per sample and referred to daily deposition rate (MPs/m^2/day) by dividing the number of MPs by the circular area of the funnel and the number of the days of the sampling period (here, 31 days for January). Calculation of MPs "concentration" on leaves referred to their total surface area (MPs/m^2).

Figure 8 shows the distribution of the polymer forms (fiber or particle) by size, both for AMPs and leaves. Tyres were excluded from the figure as their values are clearly much higher (up to 60) (see Table 1) than those for the other polymers and they would obscure the general picture.

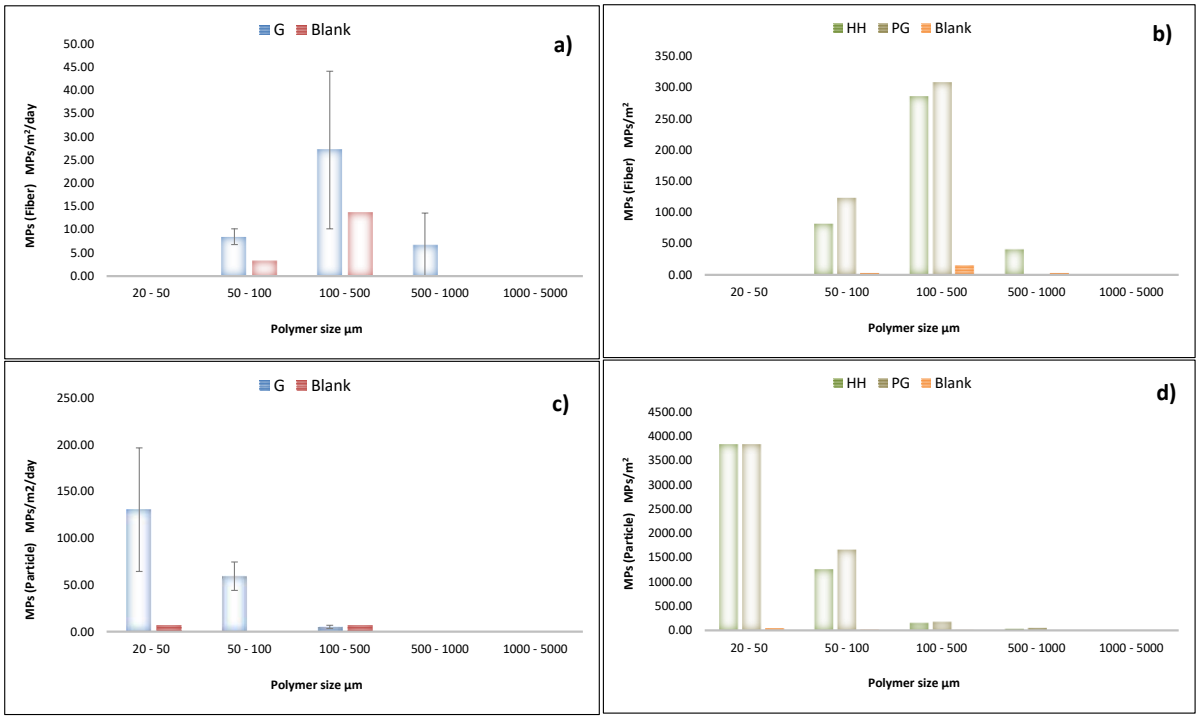

Figure 3: Distribution of fibers (a and b) and particles (c and d) by size and collection system: G: bulk sampler (average value of G1 and G2 with error bars indicating the standard deviations), HH: leaf sample of Hedra helix, PG: leaf sample of Photinia glabra.

In both atmospheric and leaf samples, the concentration of particles is higher than that of fibers, by up to two orders of magnitude. Particle and fiber distributions on leaf surface reflect those in air: the number of fibers is greater in the medium size range (100 to 500 µm) (Figures 3a and 3b), while small particles (20 to 50 µm) are the most abundant (Figures 3c and 3d). Small particles (20 – 100 µm) are more abundant in air since they tend to remain suspended in the air while the coarser and heavier ones tend to settle down (Munyaneza et al., 2022). Similarly, big particles deposited on leaves could be more susceptible to wind resuspension and rain wash off. Comparing the air deposition rates (MP/m^{2}day) and leaf concentrations (MP/m^2) and assuming a similar spatial and temporal MP distribution in the air of the two sampling sites, particle accumulation on leaf surface seems to be slower (up to 30 days) than fiber uptake

(maximum 10 days), suggesting a higher affinity and retention capacity of plant leaves for fiber than for particles. Considering the MP distribution on leaf surfaces a species-specific behaviour does not appear.

With regard to the total number of particles identified as MPs (Figure 4), they were very similar and ranged between 53 and 111, for air samples, and 86 and 117, for leaves. Although the samples analyzed in this study were intended mostly to test the analytical methodologies and not to find specific trends, those results can provide a preliminary insight into what can be expected of leaves when it comes to microplastics.

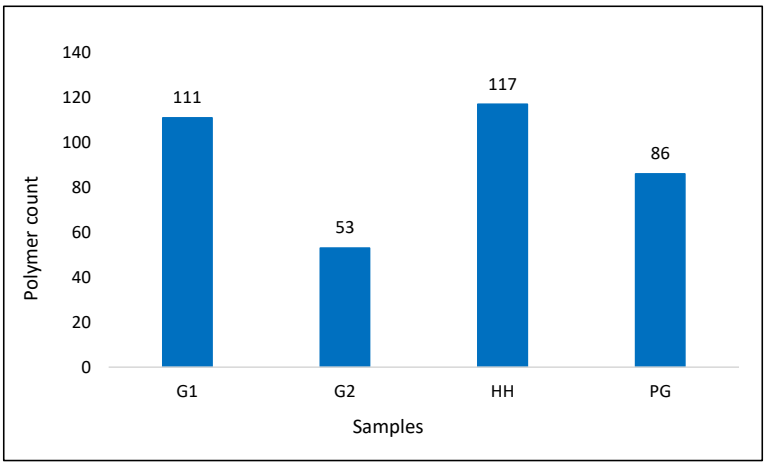

Figure 4: Number of total polymers found in each sample.

Table 1 indicates that, aside from tyre, the predominant polymers in all samples (except for HH) are PET, PP, and PE. PVC and PP were the most abundant polymers in the HH sample. All these polymers are of common use and they constitute the basis of the primary production of many commodities (Khalid et al., 2021) that can erode and/or degrade while in use or after their spillage.

The number of particles identified as tyres in PG, and HH samples was high (Table 1). This might be explained by the closeness of the leaves to nearby roads (ca. 5-10 m

distance) and their accumulation capability thanks to the hydrophobic nature of their surfaces (Di Guardo et al., 2003) although other effects like airborne transportation cannot be rejected. Curiously, this effect was not observed for the samplers, but that might be caused by the different locations of the samplers and leaves.

Table 1 Types (*), physical appearance (fiber vs particle) and and number of identified polymers found in atmospheric and leaf samples.

	G1	
Fibres	**Polymer**	**Count**
	PET	12
	PP	1
	PE	2
	PS	1
Particles	**Polymer**	**Count**
	PET	7
	PP	24
	PE	28
	PVC	6
	PMMA	2
	PS	8
	EVA	3
	PA	2
	Alkyd Varnish	2
	Tyre	4

	G2	
Fibres	**Polymer**	**Count**
	PET	6
	PE	2
	PVC	1
Particles	**Polymer**	**Count**
	PS	3
	PA	3
	PE	4
	PMMA	2
	PVC	6
	PET	3
	PP	12
	Tyre	5

	PG	
Fibres	**Polymer**	**Count**
	PET	4
	PP	2
	PE	1
	PVC	1
	PU	1
	Tyre	1
Particles	**Polymer**	**Count**
	PP	14
	PE	8
	PA	5
	PU	1
	PET	3
	PS	2
	Alkyd Varnish	1
	PVC	13
	Tyre	60

	HH	
Fibres	**Polymer**	**Count**
	PP	1
	PVC	1
	PU	1
	PET	2
	Tyre	1
Particles	**Polymer**	**Count**
	PP	9
	PET	3
	PE	3
	PA	4
	PVC	13
	PS	2
	PU	1
	Alkyd Varnish	1
	Tyre	57

** PET (polyethylene tetra phthalate), PP (polypropylene, LDPE/ HDPE (low/high-density polyethylene together considered as PE), PS (polystyrene), PVC (polyvinyl chloride), PMMA (polymethyl methacrylate), EVA (ethylene vinyl acetate), PU (polyurethane), PA (polylactic acid).*

Airborne MP measurement has just recently been addressed and very few research works are available about MP leaf uptake (Campanale et al., 2022; Li et al., 2020; Mateos-Cárdenas et al., 2021), therefore an in-depth literature comparison is not feasible. However, it has recently been pointed out that airborne MP share many common features with air particulate matter (PM) (e.g., shape, size, aerodynamic properties, etc.) and therefore the knowledge about PM uptake/release by plant leaves can be used to assess MP-leaves interactions (Bi et al., 2020). For example, it is well known that leaf characteristics (e.g., roughness, hairiness, petiole length, etc.), cuticle chemical composition (e.g., quantity and quality of waxes) and cuticle structure (e.g., thickness, morphologies.) influence the removal efficiency of PM from air by different plant species (Chen et al., 2017; Dzierżanowski et al., 2011; Liu et al., 2018; Sæbø et al., 2012). Concerning PM distribution on leaf surface, PM10 (< 10 μm) is generally the most abundant (Teper, 2009; Terzaghi et al., 2013, 2013; Wang et al., 2006); bigger particles (>10 μm) are easily washed off during rain events and resuspended by wind, while and PM2.5 (<2.5 μm) represents the fraction that can be encapsulated in the leaf cuticle and therefore hardly removed by rain and wind (Dzierżanowski et al., 2011; Terzaghi et al., 2013). PM were also shown to mediate the transfer of organic contaminants to the leaf cuticle (Terzaghi et al., 2013); similarly MP found in the aquatic ecosystems can adsorb several environmental contaminants acting as *"Trojan horse"* carrier of these compounds to aquatic organisms (Akdogan and Guven, 2019; Katsumiti et al., 2021). Finally comparing PM size distribution in air and on leaf, plant leaf surfaces seem to act

also as aggregation surface for smaller particles (< 1 μm) that represent the most abundant fraction in air. This might also happen for air nanoplastics (NP) that as MP have recently attracted increasing attention representing a pathway of contaminant transfer to crop (Sun et al., 2021).

Although MP and PM could share similar behaviors, their different physical characteristic (e.g., more lipophilic surface), composition (e.g., organic substances) and shape (e.g., fibers) can differently affect their fate. Therefore, further studies are necessary to identify the driving factors in influencing leaf uptake and release of MP and therefore their environmental fate, including their transfer from air to soil through the forest filter effect, their degradation and accumulation in terrestrial food web.

4. CONCLUSIONS

This study provides an initial preliminary approach to treat leaf samples in order to determine the number and type of microplastics present on their surface. This may constitute an indicator for the presence of this type of pollutants in the atmosphere. In fact, we found a similar total number of particles identified as microplastics in leaves and in the atmospheric deposition (a passive Depobulk sampler, deployed for a month). However, the number of fibers was higher in the 100-500 μm size range whereas particles were more abundant in the 20-50 μm sizes. In our view, the procedure proposed for leaf washing provides a good way to face the issue of determining microplastics in leaves. However, there are still challenges to address. For example, how to perform reasonable evaluations of the analytical recoveries, as there is no

reference material, or how to match the periods of atmospheric collection and the accumulation time of the leaves.

ACKNOWLEDGEMENTS

This research was partially supported by the LAnd-Based Solutions for PLAstics in the Sea Project (LABPLAS Project), Grant Agreement No. 101003954, under the European Union's Horizon 2020 research and innovation programme, and the Integrated approach on the fate of MicroPlastics (MPs) towards healthy marine ecosystems Project (MicroplastiX project), Grant PCI2020-112145, supported by the JPI_Oceans Program and by MCIN/AEI/10.13039/501100011033 and the European Union "Next Generation EU/PRTR". The Program 'Consolidación e Estructuración de Unidades de Investigación Competitivas" of the Galician Government (Xunta de Galicia) is also acknowledged (Grant ED431C 2021/56).

References

Akdogan, Z., Guven, B., 2019. Microplastics in the environment: A critical review of current understanding and identification of future research needs. Environ. Pollut. 254, 113011. https://doi.org/10.1016/j.envpol.2019.113011

Allen, S., Allen, D., Phoenix, V.R., Le Roux, G., Durántez Jiménez, P., Simonneau, A., Binet, S., Galop, D., 2019. Atmospheric transport and deposition of microplastics in a remote mountain catchment. Nat. Geosci. 12, 339–344. https://doi.org/10.1038/s41561-019-0335-5

Bi, M., He, Q., Chen, Y., 2020. What Roles Are Terrestrial Plants Playing in Global Microplastic Cycling? Environ. Sci. Technol. 54, 5325–5327. https://doi.org/10.1021/acs.est.0c01009

Boucher, J., Friot, D., 2017. Primary microplastics in the oceans: A global evaluation of sources. IUCN International Union for Conservation of Nature. https://doi.org/10.2305/IUCN.CH.2017.01.en

Campanale, C., Galafassi, S., Savino, I., Massarelli, C., Ancona, V., Volta, P., Uricchio, V.F., 2022. Microplastics pollution in the terrestrial environments: Poorly known diffuse sources and implications for plants. Sci. Total Environ. 805, 150431. https://doi.org/10.1016/j.scitotenv.2021.150431

Chen, L., Liu, C., Zhang, L., Zou, R., Zhang, Z., 2017. Variation in Tree Species Ability to Capture and Retain Airborne Fine Particulate Matter (PM2.5). Sci. Rep. 7, 3206. https://doi.org/10.1038/s41598-017-03360-1

Dzierżanowski, K., Popek, R., Gawrońska, H., Sæbø, A., Gawroński, S.W., 2011. Deposition of Particulate Matter of Different Size Fractions on Leaf Surfaces and in Waxes of Urban Forest Species. Int. J. Phytoremediation 13, 1037–1046. https://doi.org/10.1080/15226514.2011.552929

Giráldez, P., Aboal, J.R., Fernández, J.Á., Di Guardo, A., Terzaghi, E., 2022. Plant-air partition coefficients for thirteen urban conifer tree species: Estimating the best gas and particulate matter associated PAH removers. Environ. Pollut. 315, 120409. https://doi.org/10.1016/j.envpol.2022.120409

Hermsen, E., Mintenig, S.M., Besseling, E., Koelmans, A.A., 2018. Quality Criteria for the Analysis of Microplastic in Biota Samples: A Critical Review. Environ. Sci. Technol. 52, 10230–10240. https://doi.org/10.1021/acs.est.8b01611

Hernandez-Gonzalez, A., Saavedra, C., Gago, J., Covelo, P., Santos, M.B., Pierce, G.J., 2018. Microplastics in the stomach contents of common dolphin (Delphinus delphis) stranded on the Galician coasts (NW Spain, 2005–2010). Mar. Pollut. Bull. 137, 526–532. https://doi.org/10.1016/j.marpolbul.2018.10.026

ISO, 2020. Plastics — Environmental aspects — State of knowledge and methodologies [WWW Document]. URL https://www.iso.org/obp

Katsumiti, A., Losada-Carrillo, M.P., Barros, M., Cajaraville, M.P., 2021. Polystyrene nanoplastics and microplastics can act as Trojan horse carriers of benzo(a)pyrene to mussel hemocytes in vitro. Sci. Rep. 11, 22396. https://doi.org/10.1038/s41598-021-01938-4

Khalid, N., Aqeel, M., Noman, A., Khan, S.M., Akhter, N., 2021. Interactions and effects of microplastics with heavy metals in aquatic and terrestrial environments. Environ. Pollut. 290, 118104. https://doi.org/10.1016/j.envpol.2021.118104

Kömp, P., McLachlan, M.S., 1997. Interspecies Variability of the Plant/Air Partitioning of Polychlorinated Biphenyls. Environ. Sci. Technol. 31, 2944–2948. https://doi.org/10.1021/es970141

Li, L., Luo, Y., Peijnenburg, W.J.G.M., Li, R., Yang, J., Zhou, Q., 2020. Confocal measurement of microplastics uptake by plants. MethodsX 7, 100750. https://doi.org/10.1016/j.mex.2019.11.023

Liu, J., Cao, Z., Zou, S., Liu, H., Hai, X., Wang, S., Duan, J., Xi, B., Yan, G., Zhang, S., Jia, Z., 2018. An investigation of the leaf retention capacity, efficiency and mechanism for atmospheric particulate matter of five greening tree species in Beijing, China. Sci. Total Environ. 616–617, 417–426. https://doi.org/10.1016/j.scitotenv.2017.10.314

López-Rosales, A., Andrade, J., Fernández-González, V., López-Mahía, P., Muniategui-Lorenzo, S., 2022a. A reliable method for the isolation and characterization of microplastics in fish gastrointestinal tracts using an infrared tunable quantum cascade laser system. Mar. Pollut. Bull. 178, 113591. https://doi.org/10.1016/j.marpolbul.2022.113591

López-Rosales, A., Andrade, J.M., Grueiro-Noche, G., Fernández-González, V., López-Mahía, P., Muniategui-Lorenzo, S., 2021. Development of a fast and efficient method to analyze microplastics in planktonic samples. Mar. Pollut. Bull. 168, 112379. https://doi.org/10.1016/j.marpolbul.2021.112379

López-Rosales, A., Andrade, J.M., López-Mahía, P., Muniategui-Lorenzo, S., 2022b. Development of an analytical procedure to analyze microplastics in edible macroalgae using an enzymatic-oxidative digestion. Mar. Pollut. Bull. 183, 114061. https://doi.org/10.1016/j.marpolbul.2022.114061

Luo, X., Wang, Z., Yang, L., Gao, T., Zhang, Y., 2022. A review of analytical methods and models used in atmospheric microplastic research. Sci. Total Environ. 828, 154487. https://doi.org/10.1016/j.scitotenv.2022.154487

Mateos-Cárdenas, A., van Pelt, F.N.A.M., O'Halloran, J., Jansen, M.A.K., 2021. Adsorption, uptake and toxicity of micro- and nanoplastics: Effects on terrestrial plants and aquatic macrophytes. Environ. Pollut. 284, 117183. https://doi.org/10.1016/j.envpol.2021.117183

Munyaneza, J., Jia, Q., Qaraah, F.A., Hossain, M.F., Wu, C., Zhen, H., Xiu, G., 2022. A review of atmospheric microplastics pollution: In-depth sighting of sources, analytical methods, physiognomies, transport and risks. Sci. Total Environ. 822, 153339. https://doi.org/10.1016/j.scitotenv.2022.153339

Nizzetto, L., Pastore, C., Liu, X., Camporini, P., Stroppiana, D., Herbert, B., Boschetti, M., Zhang, G., Brivio, P.A., Jones, K.C., Di Guardo, A., 2008. Accumulation Parameters and Seasonal Trends for PCBs in Temperate and Boreal Forest Plant Species. Environ. Sci. Technol. 42, 5911–5916. https://doi.org/10.1021/es800217m

Novillo, O., Raga, J.A., Tomás, J., 2020. Evaluating the presence of microplastics in striped dolphins (Stenella coeruleoalba) stranded in the Western Mediterranean Sea. Mar. Pollut. Bull. 160, 111557. https://doi.org/10.1016/j.marpolbul.2020.111557

Sæbø, A., Popek, R., Nawrot, B., Hanslin, H.M., Gawronska, H., Gawronski, S.W., 2012. Plant species differences in particulate matter accumulation on leaf surfaces. Sci. Total Environ. 427–428, 347–354. https://doi.org/10.1016/j.scitotenv.2012.03.084

Shao, L., Li, Y., Jones, T., Santosh, M., Liu, P., Zhang, M., Xu, L., Li, W., Lu, J., Yang, C.-X., Zhang, D., Feng, X., BéruBé, K., 2022. Airborne microplastics: A review of current perspectives and environmental implications. J. Clean. Prod. 347, 131048. https://doi.org/10.1016/j.jclepro.2022.131048

Sun, H., Lei, C., Xu, J., Li, R., 2021. Foliar uptake and leaf-to-root translocation of nanoplastics with different coating charge in maize plants. J. Hazard. Mater. 416, 125854. https://doi.org/10.1016/j.jhazmat.2021.125854

Teper, E., 2009. Dust-particle migration around flotation tailings ponds: pine needles as passive samplers. Environ. Monit. Assess. 154, 383–391. https://doi.org/10.1007/s10661-008-0405-4

Terzaghi, E., Wild, E., Zacchello, G., Cerabolini, B.E.L., Jones, K.C., Di Guardo, A., 2013. Forest Filter Effect: Role of leaves in capturing/releasing air particulate matter and its associated PAHs. Atmos. Environ. 74, 378–384. https://doi.org/10.1016/j.atmosenv.2013.04.013

Thompson, R.C., Olsen, Y., Mitchell, R.P., Davis, A., Rowland, S.J., John, A.W.G., McGonigle, D., Russell, A.E., 2004. Lost at Sea: Where Is All the Plastic? Science 304, 838–838. https://doi.org/10.1126/science.1094559

Wang, L., Liu, L., Gao, S., Hasi, E., Wang, Z., 2006. Physicochemical characteristics of ambient particles settling upon leaf surfaces of urban plants in Beijing. J. Environ. Sci. 18, 921–926. https://doi.org/10.1016/S1001-0742(06)60015-6

Paper V

Science of the Total Environment 762 (2021) 144184

Contents lists available at ScienceDirect

Science of the Total Environment

journal homepage: www.elsevier.com/locate/scitotenv

Estimating temporal and spatial levels of PAHs in air using rain samples and SPME analysis: Feasibility evaluation in an urban scenario

Elisa Terzaghi [a], Parisa Falakdin [a], Elena Fattore [b], Antonio Di Guardo [a,*]

[a] Department of Science and High Technology (DiSAT), University of Insubria, via Valleggio 11, 22100 Como, Italy
[b] Department of Environmental Health Sciences, Istituto di Ricerche Farmacologiche "Mario Negri" IRCCS, Via Mario Negri 2, 20156 Milan, Italy

HIGHLIGHTS

- Rainfall was collected at 30 min interval to estimate PAHair concentrations.
- Three sites at different traffic intensity were investigated in Como, Italy.
- SPME extraction allowed to collect small amounts of samples.
- The results outlined spatial and temporal variability of selected PAHs in air.

GRAPHICAL ABSTRACT

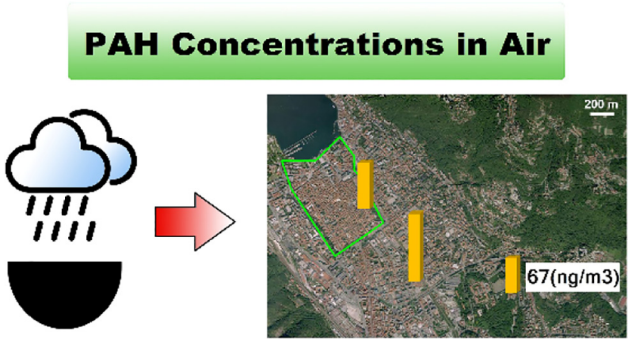

ARTICLE INFO

Article history:
Received 30 October 2020
Received in revised form 28 November 2020
Accepted 28 November 2020
Available online 17 December 2020

Editor: Damia Barcelo

Keywords:
Como
Northern Italy
Air pollution
High resolution measurement
PBL
Fate models

ABSTRACT

There is a growing interest in evaluating the role of concentration changes of contaminants in temporal and spatial gradients. This is often relevant for fast moving environmental phases such as air and water. In this paper, small volumes of rainwater were sampled as proxy for air concentrations of Polycyclic Aromatic Hydrocarbons (PAHs): rain was collected in three sampling sites (high traffic, restricted traffic and a low traffic zone) in Como. Solid phase micro extraction (SPME) was used for the extraction to reduce required sample volumes, allowing the acquisition of more samples in time. Rain samples highlighted a spatial and temporal variability along a traffic gradient in the Como city, especially for the most abundant PAH, e.g. phenanthrene. Air concentrations were then estimated from rain concentrations. The results show that this is a cheap and promising method, although requiring rainfall/snowfall conditions, that can be used to perform monitoring campaign of air concentrations at a higher temporal and spatial resolution than the adopted standard methods (e.g. high-volume air samplers). The results could be employed for evaluation of the exposure, emission profiles and calibration of fate models.

1. Introduction

There is a growing interest in assessing the spatial and temporal variability of contaminant concentrations (Di Guardo et al., 2018; Di Guardo and Hermens, 2013), especially in mobile phases such as air (Gasic et al., 2009; Lammel et al., 2010a; Morselli et al., 2011, 2012) and water (De Laender et al., 2015; Morselli et al., 2014, 2015, 2018), as well as soil (Ghirardello et al., 2010; Terzaghi et al., 2019); such knowledge would be of particular relevance to assess the realistic exposure of humans and ecosystems to atmospheric pollutants (e.g., occurrence, magnitude and duration of exposure peaks).

Recent works have underlined the relevance of the air compartment change in affecting the diel variation of concentrations of contaminants (Morselli et al., 2011, 2012, 2018). For example, the changes of the planetary boundary layer (PBL) height could affect air concentration

* Corresponding author.
E-mail address: antonio.diguardo@uninsubria.it (A. Di Guardo).

https://doi.org/10.1016/j.scitotenv.2020.144184
0048-9697/

variations (Oke, 2009; Stull, 1988) on an hourly basis since it would affect the mixing layer height, the level of the lower part of the troposphere in which pollutant are diluted. This implies that air concentration of constantly ground level emitted contaminants can vary significantly during the day/night cycle. Given such amplitude it would be desirable to provide a tool or technique to efficiently monitor (temporally and spatially) those hourly variations in order to be capable to evaluate the extent of environmental and human health risk during peaks of concentrations to possibly reduce or mitigate emissions (Di Guardo and Hermens, 2013). However, due to sampling cost limitations and available techniques, the investigation of air concentrations is usually limited to daily averages for specific contaminants or particulate matter in air.

PAHs are ubiquitous contaminants, typically deriving from incomplete combustion of anthropogenic sources (fossil fuels, industrial sources, wood combustion in domestic heating, etc.) although they could also derive from natural sources such as forest fires and volcanic eruptions (Baek et al., 1991). PAH are important for their toxicological (Kim et al., 2013) and ecotoxicological (Jensen and Sverdrup, 2003; Sverdrup et al., 2002) properties and their semivolatility which allows them to be mobile in air, being transported to longer distances and considered long range transport pollutants (Halsall et al., 2001). Traffic is an important contribution to PAH pollution (Nielsen et al., 1996; Prevedouros et al., 2004) with the contribution of diesel and gasoline fuelled cars (especially at low speed after a cold start), although the use of catalytic converters has reduced the emissions (Ravindra et al., 2008).

Moreover, urban areas with congested traffic conditions and vehicles traveling short journeys could enhance the emission of PAHs (Ravindra et al., 2008). In many European cities low or restricted traffic areas are present, and it was shown that these areas, including also parks, presented lower PAH concentration in respect to heavy traffic roads (Nielsen et al., 1996). Some authors have measured variability of PAH concentrations during the day and in different sites (e.g. urban vs. rural) (Gaga et al., 2012; Lammel et al., 2010a; Morville et al., 2011). Nevertheless, the need of high-volume samplers employed in these studies limits the availability of replicates and simultaneous measurements to process data in a statistically robust way. Even when high volume samplers are employed, the presence of sample artifacts cannot be avoided, such as the adsorption of gaseous PAHs on the filter and or on the particle phase sampled (Li et al., 2016).

Solid phase micro extraction (SPME) is an extraction technique which necessitates small volume of sample (e.g. 30–40 mL of water) and was used to measure PAH in surface water (Doong et al., 2000) and rainwater (Guidotti et al., 2000). For this reason, it can be employed o analyze rainwater also deriving from short duration rain events and/or to study the variability of concentrations during each event.

The aim of this work was therefore to investigate the use of small amounts of rain samples (<50–100 mL) and SPME analysis as a tool to explore the spatial and short term variability of atmospheric levels of PAHs in a city using rain as proxy of air concentrations. The water concentration data can be converted to air concentrations using air/water partition coefficients and used to compare the levels in the different areas, showing the potential use of relatively rapid and simple method for simultaneously obtaining and comparing PAH concentrations in air. For example, this can be used to explore the emission profiles of chemicals with time and space, with the limitations imposed by the need of rainfall/snowfall conditions to obtain a water sample. The results could be later employed for evaluation of the human and ecosystem exposure, source apportionment, and calibration of fate models.

2. Materials and methods

2.1. Rain sampling

Three sampling sites (Fig. 1) were chosen to evaluate the spatial variability at a local scale in an urban environment and to estimate the short-term variability (i.e. half-hour) of concentrations. The rain sampling campaign was performed in Como (Lombardy Region, Northern Italy), a town of about 85,000 inhabitants, on Dec 20, 2013. The city lies at an elevation of 201 m a.s.l. and is located at the end of the south-west branch of the Lake, about 40 km north of Milan. The first site (A) was located on the side of a high-traffic road, next to a traffic light (about 2400 car/h). The second site (B) was located in the Como historical city centre, a restricted traffic zone where only authorized vehicles can circulate (less than 10 car/h), while the third site (C) was located in the middle of a park, a semi-urban area (less than 10 car/h but about 300 m away from a medium traffic road, about 1000 car/h) where previous measurements of PAH in air, particulate matter, leaves and impervious surfaces were taken (Terzaghi et al., 2013, 2015a, 2015b). Rain samples were simultaneously collected in triplicates at each site (S1, S2, S3 for site A; S4, S5, S6 for site B; S7, S8, S9 for site C) (for a total of 27 individual rain samples) by means of 9 large stainless-steel containers (salad bowls) with a diameter of 0.5 m positioned on the ground, at the vertexes of a triangle (at 10 m distance). The samplers were thoroughly washed with soap and water and, when dry, were rinsed three times with pesticide grade hexane, acetone, and MilliQ water. They were carried to the sampling areas (and back) individually wrapped in new polyethylene bags. Rain samples (50–100 mL) were collected for 30 min, and then were transferred into solvent rinsed aluminum bottles by means of solvent washed steel funnels. Then the samplers were exposed again, after being rinsed with MilliQ water. Three rainfall samples were therefore collected for each container, simultaneously in all sites, from 9:00 to 9:30 am, from 9:30 to 10:00 am and from 10:00 to 10:30 am. Total sampling time was 1:30 h. Rainwater samples were stored at −30 °C until analysis.

2.2. Meteorological and population statistics data

Precipitations and temperature data for the rainfall sampling (Fig. A7) were obtained by Regional Protection Agency (ARPA Lombardia, 2018). Planet boundary layer height was estimated from a previous dataset (Morselli et al., 2012).

2.3. Chemicals

Acenaphthene (ACE), acenaphthylene (ACY) fluorene (FLUO), phenanthrene (PHE), anthracene (ANTH), fluoranthene (FLUOT), pyrene (PYR), benz[*a*]anthracene (B[*a*]ANTH), chrysene (CHR), benzo[*b*]fluoranthene (B[*b*]FLUOT), benzo[*a*]pyrene (B[*a*]PYR), benzo[*g,h,i*]perylene (B[*ghi*]PER), indeno[*c,d*]pyrene (I[*cd*]PYR), were purchased from Supelco (QTM PAH mix, 2000 ng/μL in methylene chloride). Perylene (PER) was purchased from Sigma-Aldrich (purity 99.7%). Deuterated internal standards (Acenaphthene-d10, Phenanthrene-d10, Chrysene-d12, Perylene-d12) were purchased from Supelco (Semivolatile Internal Standard mix, 2000 ng/ μL in methylene chloride). Solvents used were acetone, hexane (pesticide-grade, Fluka analytical) and toluene for analysis of dioxins, furans and PCB, (purity ≥ 99.7%, Riedel-de Haën).

2.4. Extraction

Manual SPME holder equipped with a 100-μm polydimethylsiloxane (PDMS) non-polar fiber was used (Supelco, Sigma Aldrich). Before use and at the beginning of every working day, fibers were conditioned at 250 °C for 30 min in the GC injection port. Water samples were transferred in 40 mL amber glass vials, minimizing headspace, and capped and sealed using Teflon-lined septa. Vials were previously cleaned in a muffle furnace at 450 °C for 8 h and further washed before use with hexane and acetone to minimize sample cross contamination. The direct immersion mode was chosen to improve the sensitivity of the method. Extractions were performed at a temperature of 60 °C for 40 min under constant stirring (1000 rpm). These conditions were optimized running extraction test at different temperatures and sampling times, basing on

Fig. 1. Location of the three sampling sites in the city of Como. A = high traffic zone, B = restricted traffic zone, C = low traffic zone. The green line delimits the restricted traffic zone in Como. Satellite image from Google Maps, 2019. The green dot in the small map in the left bottom corner shows the location of the town of Como within Lombardy Region and Italy.

literature results (Doong et al., 2000; Rianawati and Balasubramanian, 2009; Yan et al., 2012). More information can be found in the Appendix section. The thermal desorption of the analytes took place in the GC injector port, at a temperature of 280 °C, for 2 min. The fiber was then left in the injector port for 1 min to ensure complete desorption and avoid carryover.

Internal calibration approach using spiked water was used to quantify the samples. Calibration standard solutions in deionized water were prepared in the range of 1 ng/L to 100 ng/L adding non labelled and deuterated standards at 20 ng/L. The same amount of deuterated standard (i.e., 0.8 ng) was added to each sample prior to extraction.

2.5. Instrumental analysis

Analyses were performed using an HP 6890 Series gas chromatograph coupled to a 5972A mass detector (Agilent Technologies), and equipped with a J&W DB-35MS capillary column (60-m, internal diameter 0.25 mm, phase thickness 0.25 μm). Helium was used as carrier gas. The injection was performed in splitless mode and the injector port temperature was set to 280 °C. Oven temperature program was started at 110 °C, raised to 155 °C at a rate of 5.00 °C/min, then to 335 °C at a rate of 6.25 °C/min, and finally held at 335 °C for 23 min. Carrier gas flow was kept constant (0.8 mL/min). The mass spectrometer was operated in Selected Ion Monitoring (SIM) mode. Retention times, ions and groups selected for MS analysis for each investigated chemical, as well the correspondence between measured compounds and their internal standards are reported in Table A1.

2.6. QA/QC

All analytical procedures were monitored using strict quality assurance and control measures. Analytical blanks consisted in field blanks and laboratory blanks. They were extracted by washing them with deionized (MilliQ) water. Field and laboratory blank samples were taken by washing three rain samplers with deionized water; they were subjected to the same storage, extraction and analytical procedures as those used for environmental samples. An additional blank was obtained with deionized water. Concentrations reported were blank corrected. Method detection limits (MDLs) were calculated as blank concentration plus three times the standard deviation of the blank (Muir and Sverko, 2006). Table A.2 shows MDL values for rain samples. In addition, peaks were integrated only when the signal-to-noise ratio was ≥3. Reproducibility and other details of method validation are also available in the appendix section.

2.7. PAH air concentration estimation

Air concentrations were calculated for each chemical by assuming that rainfall samples were in equilibrium with the atmosphere and therefore Henry's Law could be used to define the equilibrium partitioning (Shahpoury et al., 2015). Since the partitioning depends on temperature (Mackay, 2001; Shahpoury et al., 2015) a dimensionless air/water partition coefficient (Kaw) was calculated at each sampling temperature for each chemical, starting from vapour pressure and water solubility (Mackay et al., 2006) and using the heat of vaporization and solubilization reported in (Ghirardello et al., 2010).

$$C_{a(g)} = Kaw * C_{w(d)} * 1000 \quad (1)$$

where: $C_{a(g)}$ = gaseous concentration in air (ng/m^3), $C_{w(d)}$ = dissolved concentration in rainfall (ng/L), 1000 is a conversion factor (from ng/m^3 to ng/L).

2.8. Statistical analyses

Analysis of Variance (ANOVA), regression and PCA analyses were performed with the XLSTAT software (Addinsoft SARL, Version 2020.3.1, Boston, USA). The data subjected to ANOVA ($\alpha = 0.05$) passed the normality and equal variance tests. Tukey test was applied for pairwise comparisons. Fisher test was used to assess the significance of the linear regression ($\alpha = 0.05$). For principal component analysis (PCA), individual concentration data were normalized to the total concentration in the sample. Concentration values < MDL were assumed to be zero.

Table 1
Concentration of selected PAHs in air and rainfall from the literature.

	Date	Location and Reference	Type	Season	ACE	FLUO	PHE	ANTH	FLUOT	PYR	B[*a*]ANTH	CHR	B[*b*]FLUOT	B[*a*]PYR	B[*ghi*]PER	I[*cd*]PYR	TOTAL PAH
AIR (ng/m^3)	1990	Rorvik, Swedish West Coast (Brorström-Lundén et al., 1994)	R*	Winter - Spring			[3.2]	[0.07]	[1.6]	[1.5]	[0.34]	[0.94]	[0.84]	[0.3]	[0.4]	[0.6]	[9.2]
	1991–92	London, UK (Halsall et al., 1994)	U*	Yearly	[3.4][a]	[22]	[79]	[5.8]	[10]	[9.5]	[1.3]	[2.3]	[1.4]	[0.8]	[4.9]		[140]
	1991–92	Manchester, UK (Halsall et al., 1994)	U*	Yearly	[2.5]	[21]	[46]	[3.7]		[8.9]	[1.7]	[2.2]	[1.3]	[1.5]	[2.1]		[91]
	1991–94	Rorvik, Nidinqen (Brorström-Lundén, 1996)	U	Yearly			[1.5]	[0.08]	[0.78]	[0.34]	[0.06]	[0.15]	[0.18]	[0.07]	[0.09]	[0.11]	[3.36]
	2000–01	Petrana, Greece (Terzi and Samara, 2004)	R [b]	Yearly			2.03/0.17[a]	0.1/0.03	0.6/0.09	0.2/0.08	0.04/0.03	0.03/0.05	0.008/0.08	0.003/0.05	0.006/0.07	0.008/0.09	3/0.74
	2000–01	Vegoritis, Greece (Terzi and Samara, 2004)	CS	Yearly			9.7/0.2	0.9/0.16	2.4/0.17	1.8/0.16	0.13/0.25	0.13/0.2	0.03/0.4	0.01/0.2	0.01/0.4	0.01/0.4	15/2.6
	2000–01	Kozani, Greece (Terzi and Samara, 2004)	U	Yearly			13/0.2	1.3/0.13	3.5/0.14	4.8/0.12	0.4/0.05	0.3/0.1	0.03/0.3	0.009/0.1	0.006/0.05	0.01/0.3	23/1.5
	2003–04	Zaragoza, Spain (Callén et al., 2011)	U	Yearly			[2.3]	[0.5]	[1.1]	[1.1]	[0.3]	[0.4]	[0.5]	[0.3]	[1.0]		[7.5]
	2007	Como, Italy (Terzaghi et al., 2015a, 2015b)	SU*	22 Mar - 12 Apr	0.22/<0.002	1.7/0.013	9.8/0.21	0.33/0.017	1.8/0.3	1.5/0.32	0.05/0.12	0.093/0.23	0.015/0.42	<0.002/0.14	<0.004/<0.004	<0.006/0.36	15/2.3
	2007	Como, Italy (Terzaghi et al., 2015a, 2015b)	SU*	12 Apr - 7 Jun	0.19/<0.002	0.63/0.011	5.7/0.12	0.2/0.0086	1/0.12	0.71/0.13	0.053/0.03	0.1/0.064	0.06/0.11	0.05/0.018	0.037/<0.004	0.043/<0.006	8.8/0.8
	2009–10	Paris, France (Ringuet et al., 2012)	U	Summer		−/0.04	−/0.68	- /0.1	−/1.32	−/2.14	- /0.52	- /0.33	- /0.25	- /0.16	- /0.25	- /0.13	- /5.9
	2009–10	Paris Area, France (Ringuet et al., 2012)	SU	Summer			- /0.06		- /0.15	−/0.07	- /0.02	- /0.03	- /0.05	- /0.02	- /0.04	- /0.04	- /0.48
	2010	Birmingham, UK (Alam et al., 2014)	U	Winter			0.82/0.28	0.09/0.07	0.23/0.12	0.1/0.065	0.04/0.04	0.02/0.05	0.1/0.068	0.003/0.024	0.001/0.014	0.0025/0.018	1.4/0.75
	2010	Birmingham, UK	U	Summer			0.64/0.18	0.068/0.062	0.18/0.088	0.08/0.046	0.015/0.03	0.012/0.03	0.058/0.053	- /0.021	- /0.007	- /0.0011	1/0.5

		(Alam et al., 2014)															
	2011–14	Prague, Czech Republic (Shahpoury et al., 2015)	U	Yearly	0.3/0.011	2.7/0.11	4.7/0.8	0.13/0.063	1.3/1.3	0.6/1.1	0.014/0.5	0.06/0.7	0.013/0.7	0.0087/0.4		0.0072/0.5	9.8/6.1
RAIN (ng/L)	1994–96	Tihany (Lake Balaton), Hungary (Kiss et al., 1997)	U & R	Winter		[37]	[230]	[3.9]	[190]	[190]	[<1]	[29]	[19]	[4.6]	[24]		[727]
	1996–97	Imathia, Northern Greece (Manoli et al., 2000)	R*	Yearly			[56]	[10]	[4.1]	[7.7]	[1.3]	[4.4]	[1.9]	[1.1]	[2.1]	[1.1]	[89]
	2001	Le Havre, Paris (Motelay-Massei et al., 2002)	U	Yearly	[2.1]	[3.2]	[20]	[0.61]	[24]	[21]	[5.0]	[14]	[13]	[5.8]	[12]	[5.9]	[127]
	2001	Evreux, France (Motelay-Massei et al., 2002)	R	Yearly	[0.68]	[2.3]	[17]	[0.62]	[16]	[11]	[2.0]	[4.5]	[5.0]	[2.3]	[4.3]	[2.5]	[68]
	2001	Rouren, France (Motelay-Massei et al., 2002)	U	Yearly	[1.0]	[2.4]	[8.0]	[0.3]	[9.1]	[6.8]	[1.8]	[3.8]	[3.3]	[1.7]	[2.7]	[1.1]	[42]
	2001	Notre-Dame deGravenchon, France (Motelay-Massei et al., 2002)	U	Yearly	[0.56]	[1.9]	[7.1]	[0.2]	[6.0]	[5.2]	[0.98]	[3.1]	[2.6]	[1.1]	[2.0]	[1.4]	[32]
	2003–04	Lake Maggiore, Italy (Olivella, 2006)	U	Summer-Autumn	1.65/0.75	3.4/1.5	3.8/6	0.27/0.75	0.69/13	6.2/19	0.69/11	0.55/4.7	0.14/4.7		0.14/3.8	0.0027/3.8	17/66
	2006	France, Paris (Bourdat-Deschamps et al., 2007)	SU*	Yearly		4.5/ -	17/ -		16/ -	15/ -			4/ -	2.1/ -	3/ -		62/ -
	2006–08	Brno-Bohunice, Czeck (Škrdlíková et al., 2011)	SU	Spring	0.58/0.15	1.4/0.42	10/4.7	2/1	13/10	10/6.5	1.5/2.1	1.5/3.5	2.2/7.5	0.52/2.8	0.17/1.9	0.12/2.5	43/38
	2011–14	Prague, Czech Republic (Shahpoury et al., 2015)	U	Yearly	[1.0]	[6.0]	[23.5]	[1.1]	[61.4]	[17.7]	[3.1]	[9.1]	[6.5]	[2.3]		[3.6]	[135]
	2017	Moskow, Russia (Polyakova et al., 2018)	U	Spring	[20]	[11]	[84]	[5.0]	[87]	[55]	[12]	[85]	[82]	[18]	[36]	[50]	[540]

Data processing: When an asterisk (*) is present in the Type field, it indicates that we averaged values of the series present in the manuscript. When calculating those average values, for values smaller than the detection limits, half of the detection limit values were considered. Abbreviations: U (Urban), SU (Suburban), R (Rural), CS (Coastal Site), ACE (acenaphthene), FLUO (fluorene), PHE (phenanthrene), ANTH (anthracene), FLUOT (fluoranthene), PYR (pyrene), B[*a*]ANTH (benz[*a*]anthracene), CHR (chrysene), B[*b*]FLUOT (benzo[*b*]fluoranthene), B[*a*]PYR (benzo[*a*]pyrene), B[*ghi*]PER (benzo[*ghi*]perylene), I[*cd*]PYR (indeno[1,2,3-*cd*]pyrene), TOT PAH (Total PAH).

[a] Values in square brackets represent the total (or bulk) PAH concentrations, values on the left side of the slash represent the gaseous (or dissolved) concentrations and values on the right side show the particle associated concentrations.

[b] The continental background sampling site Petrana is located close to two power plants.

3. Results and discussion

3.1. Rainfall data

Total PAH concentrations in Como rain ranged from 81 ng/L to 132 ng/L depending on the site and the sampling time. These results are comparable to literature data for other European countries, especially for the most recent data (Table 1), although it is important to note that the Como rain data were measured at a single event while generally integrated sample results (e.g. weekly or more) are often reported in the literature; however, while the samples in Como are collected and preserved right after the rain event (within half an hour), when longer time sampling are employed the relevance of chemical loss phenomena (such as volatilization, degradation, etc.) might have been larger, potentially altering the true rain concentration. In order to investigate the spatial variability of PAH in Como rain, the concentrations measured in the three replicates of each site were averaged according to the sampling time interval (Fig. 2). Intra-site variability was about 20% on average. The three sites significantly differed for PHE levels which showed a decreasing trend from the site A to the site C during all the three sampling events. Other three chemicals showed lower concentrations in the high traffic site with respect to the low traffic site but just during one sampling event (i.e, FLUOT in the third sampling event while B[*ghi*]PER and I[*cd*]PYR in the third sampling event). Acenaphthylene and dibenz(*a*,*h*)anthracene were never found above MDL. The other PAHs showed the same levels in all sites. For this reason, a real spatial distinction among sites could be appreciated only with respect to PHE concentrations.

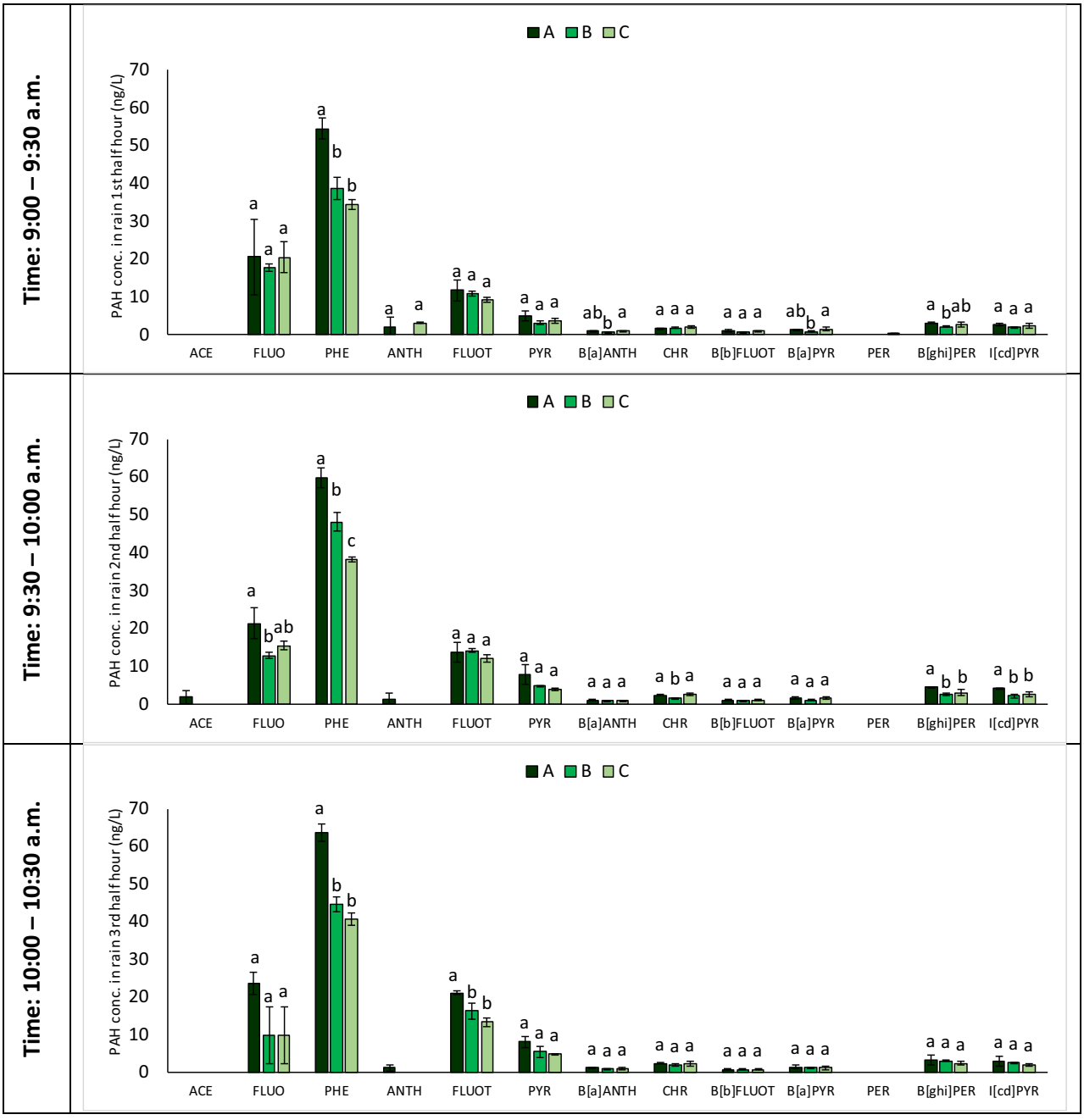

Fig. 2. Spatial variability of PAH concentration during the three sampling time intervals (9:00 to 9:30, top chart; 9:30–10:00, middle chart; 10:00–10:30, lower chart). Capital letters indicate sample zone (A: High traffic; B: Medium traffic; C: Low traffic). All values are in ng/L. Whiskers represent standard deviation of the 3 individually sampled replicates. Small letters over the bars indicate results of the ANOVA analysis. Samples with the same small letter are not statistically different ($\alpha = 0.05$).

When looking at the temporally different results (comparing the same site at different times, Fig. 3), PHE showed also a statistically significant increase form the 1st to the 3rd sampling event in all the three sites. In site A it raised up to 17% during the 1.5 h of sampling, while it was 16% and 18% for site B and C. The same trend can be also appreciated for FLUOT (+ 79% in site A, + 50% in site B and + 45% in site C), CHR in site A (+ 41%), B[*ghi*]PER and similarly, I[*cd*]PYR in site B and PYR in site C. This short-term temporal variability could be ascribed to short term variations in emission or source type (Lee et al., 1998), revolatilization from soils or surfaces given the increase in temperature during the day (Fig. A.7) (Lammel et al., 2010b).

Additionally, the increase can also be due to the change in precipitation regime (rain rate changed from 0.6 to 0.8 mm/h) or to the observed decrease in wind speed (Fig. A.7), which might have lowered the ventilation coefficient (product of wind speed and height of the PBL) (Gaga et al., 2012). Such reduction has the effect of increasing the concentrations in the mixing layer since it reduces the effect of the incoming and diluting cleaner air.

The results presented here, using the internal calibration approach (Poerschmann et al., 1997), are referred to total (bulk) concentration of PAHs in rainwater, including dissolved, particulate phase adsorbed, and dissolved organic matter (DOM) adsorbed chemicals.

However, the analysis of water samples with SPME using an external calibration has the advantages of measuring the truly dissolved fraction of the chemical in the water phase (Cui et al., 2013; Urrestarazu Ramos et al., 1998; Vitale et al., 2019; Vitale and Di Guardo, 2019); therefore using SPME with external calibration to extract PAHs from the precipitation samples is equivalent to measuring the water dissolved fraction captured by rain droplets

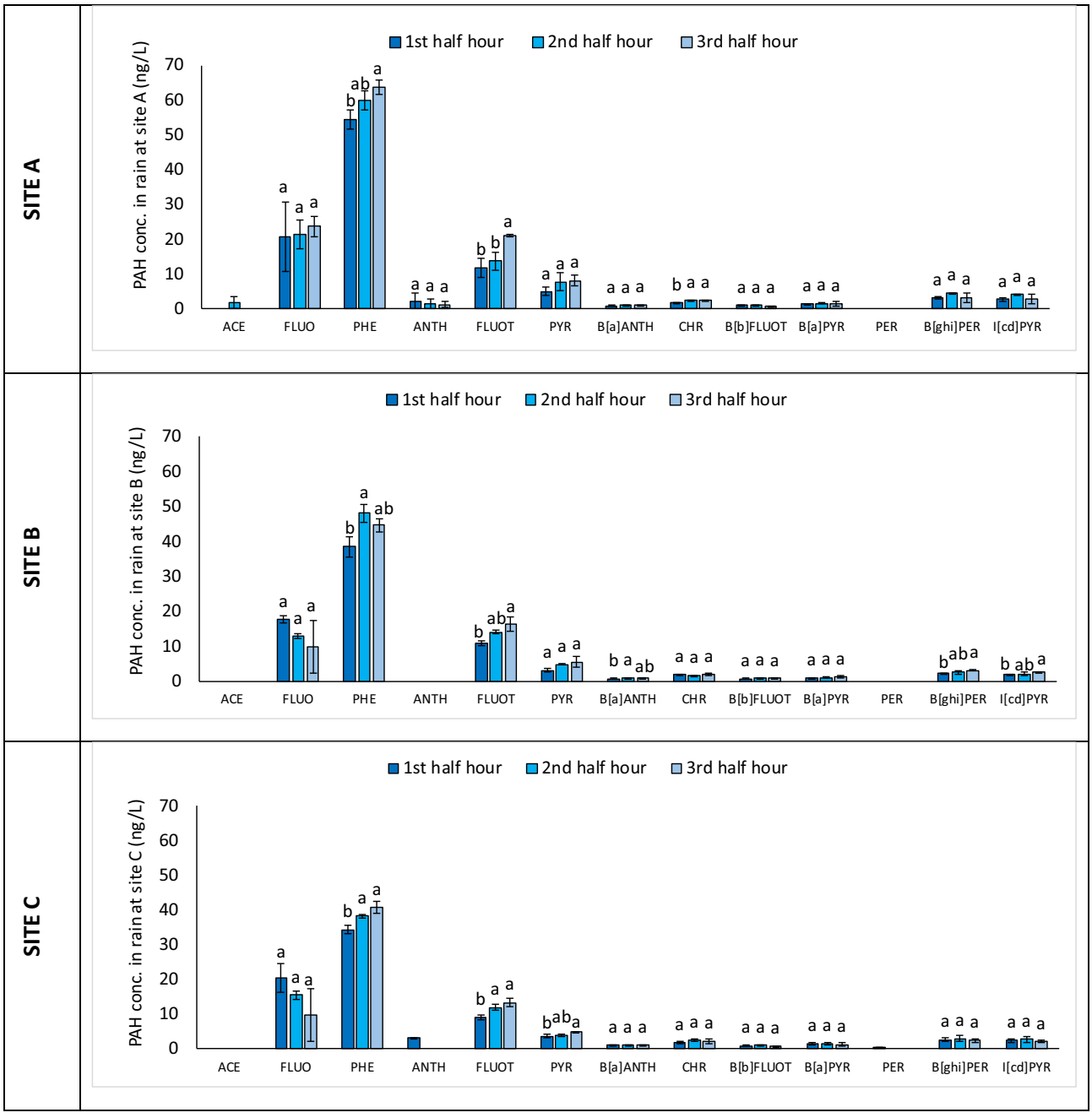

Fig. 3. Temporal variability of PAH concentration in rain at different sampling sites (A: High traffic; B: Medium traffic; C: Low traffic). All values are in ng/L. Whiskers represent standard deviation of the 3 individually sampled replicates. Small letters over the bars indicate results of the ANOVA analysis. Samples with the same letter are not statistically different ($\alpha = 0.05$).

equilibrating with air during their travel to the ground (sometimes called gaseous wet deposition or gaseous washout) (Mackay, 2001). This has the effect of separating the gaseous fractions of PAHs from the particle associated fraction, considering that the latter is usually predominant for large molecular weight PAHs and at lower temperatures. Additionally, this reduces the artifacts involved in separating the gaseous and particle associated fractions in other methods (Škrdlíková et al., 2011). On the other hands, it has the disadvantages of neglecting the information of the particle associated PAH. Care must therefore be given when comparing values obtained in different studies. For this reason, dissolved and bulk fractions (dissolved plus particle associated) are given for comparison, when available, in Table 1.

3.2. Air concentration estimates

Gaseous concentrations of PAHs were obtained assuming equilibrium between rain and air at the environmental temperatures. This was assumed to provide a first estimation of PAH concentration in air for comparative reasons and to show the potential of using rainwater to estimate air concentrations at short time intervals. While this would reflect the general uncertainty of such estimates, usually employed in many fate models (Mackay, 2001), it may lead to errors when dealing with the PAH fraction associated with air particles. In order to improve such estimate, SPME with external calibration can be used to measure the truly dissolved concentrations in water (Poerschmann et al., 1997). This would allow a better estimation of the gaseous concentrations since it would also exclude the competing effects of very tiny particles (such as black carbon) in the gaseous concentration determination (Li et al., 2016).

Although it is outside the aims of this paper, SPME can theoretically be also employed to derive the air particulate phase concentrations, if the internal standard calibration method (Poerschmann et al., 1997) is used for measuring the total (bulk) rainfall concentration ($C_{w(b)}$, ng/L) and the external calibration for the dissolved fraction.

From $C_{w(b)}$, the particle associated fraction in rain ($C_{w(p)}$) can be obtained subtracting the dissolved fraction ($C_{w(d)}$) measured with the external calibration method:

$$C_{w(p)} = C_{w(b)} - C_{w(d)} \quad (2)$$

A scavenging ratio (Wt, unitless) can then be used to derive the particulate phase air concentrations, using for example the ratios measured by Shahpoury et al. (2015), in different atmospheric conditions. The scavenging ratio can be expressed as follows (Shahpoury et al., 2015):

$$Wt = \frac{\mathrm{Cw(b)} \times 10^3}{Ca(g) + Ca(p)} \quad (3)$$

where Ca (g) and Ca(p) are the air concentrations of the gaseous and the particulate fraction (ng/m^3) of a chemical at a given temperature and 10^3 accounts for conversion from ng/L to ng/m^3. Rearranging Eq. (3) and using the gaseous concentration obtained above one could calculate the concentration in the particulate phase:

$$Ca(p) = \frac{\mathrm{Cw(b)} \times 10^3}{Wt} - Ca(g) \quad (4)$$

However, these additional measurements were not performed in this work and therefore the quality, including precision and accuracy of this estimate cannot be evaluated here and will necessitate further work.

The concentration values predicted in this study generally well agree with the range of high-volume PAH air concentrations previously measured in Como by our group (Terzaghi et al., 2015a, 2015b), although a full comparison cannot be performed since these concentrations were not simultaneously measured to the rainfall (Table 1 and Table A.4). However, when the high-volume data and the air concentration data derived from the rain sampling are analyzed using PCA in order to perform a comparison of their fingerprint, (Fig. 4 and Fig. A.8) it can be

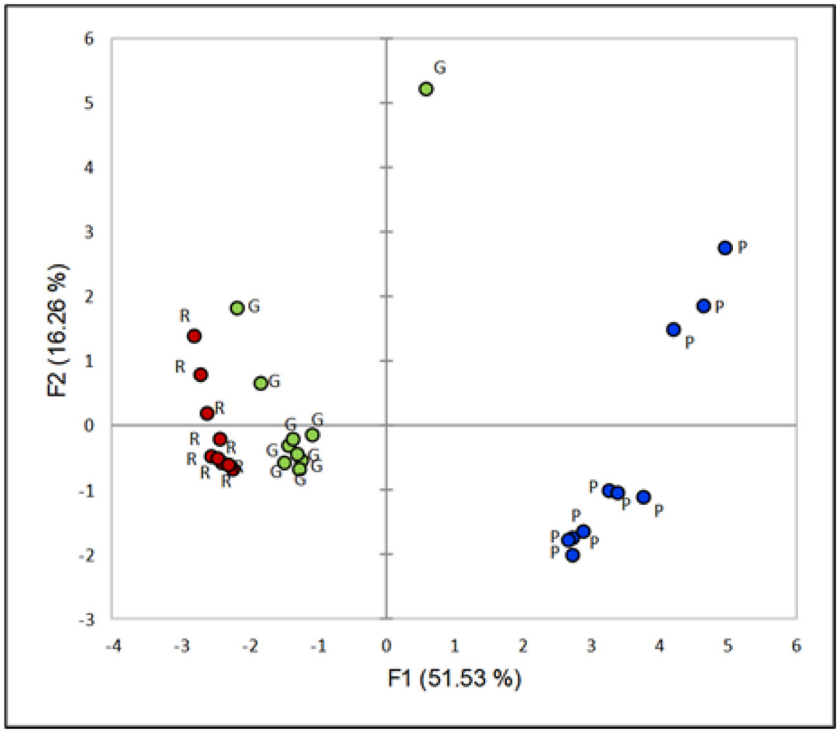

Fig. 4. PCA of PAH air concentrations measured in Como. Red dots (marked with "R") represent concentrations estimated from rain (this work), green dots (marked with "G") and blue dots (marked with "P") represent respectively gaseous and particle associated air concentrations measured in (Terzaghi et al., 2015a, 2015b).

observed that gaseous and particle Hi-Vol measured concentrations do separate on the first component (responsible for about 51% of the variability). Air data estimated from rain are closer to the gaseous measured data and separate only on the second component of the PCA, (responsible for only 16% of the variability). The data for the air estimated from rain samples and gaseous PAH concentration do lie very close and seem to possess a similar variability on the 2nd component, showing a very close relationship in fingerprint, confirming the same pattern in terms of emission source.

The air concentration data estimated from rain do lie also with the most recent data for the PAHs in urban areas in winter. From Table 1 it can be observed a general historical decrease of PAH concentrations in air with time, which reflects a change of fossil fuels employed in combustions (coal to oil derived fuels, such heating oil for domestic and industrial processes and diesel and gasoline for transportation) and the improvement in process reduction of emission (such as the implementation of catalytic converters) (European Environment Agency, 2019; ISPRA, 2016).

When looking at the predicted air concentration data averaging the temporal variations and looking at the different sites, (Fig. 5), it appears that FLUO and PHE represent about the 90% of total PAHs measured. In a previous study (Khalili et al., 1995) the fingerprint of the major sources of PAHs in a metropolitan area was evaluated and it was showed that phenanthrene was among the most abundant PAH in traffic samples, including diesel and gasoline engines. According to a recent paper, this could represent a marker of PAH traffic emission. In fact, a study (de Souza and Corrêa, 2016) reported that FLUO and PHE (together with naphthalene, not measured in the current study) were the most abundant gas phase PAH measured in diesel exhaust. It was also reported (Ravindra et al., 2008), that most of the available studies showed that the emissions from vehicle exhaust (diesel, leaded and unleaded gasoline) were the largest contributors of PAHs in urban areas. The private transport fleet (cars) of the entire province of Como in 2013 was more than 350,000 vehicles (ACI, 2019), mainly with gasoline (about 66%) rather than diesel (about 31%) engines. The cars in the town of Como account for about the 15% of the overall amount (more than 50,000 cars (2 cars every 3 people) indicating the importance of traffic contribution to PAH air emission.

Although official data for domestic heating in Como cannot be found, data for Lombardy Region (available for the year 2011) (ISTAT, 2019) show that the domestic heating sources of energy are: 87% methane, 7.2% biomasses, 3.3% heating oil, 1.5% liquefied petroleum gas and 1% electricity.

Further, the data of Fig. 5 also show a significant difference for PHE and FLUO (and for some of the higher molecular weight compounds) between the high traffic zone (A) and the restricted traffic zones (B and C), up to 35% for PHE and 37% for FLUO. This gives statistical evidence (since sampling was done simultaneously and therefore the emission in the different areas can be compared) that when implementing reduced traffic areas and/or when in presence of a park at even a relative distance from the emission points the exposure can be reasonably limited and in other terms puts the attention on traffic sources as emitters of PAHs.

It must be remembered though that the data estimated from rainfall were measured on the 20th of December (during the heating season) while the hi-vol data (Terzaghi et al., 2015a, 2015b) were obtained during spring (from the end of March to June), when the heating season is over (heating must be generally off in Como by April 15). The similarity of the fingerprints between the rain derived air concentrations and the hi vol measured seems to suggest a stable pattern, not probably depending on domestic heating and other types of non-transport related emissions. The difference in concentrations may therefore depend on change of PBL between the seasons (diluting PAHs in air) and possibly a traffic intensity change. However, further investigations and longer series of monitoring data are needed to verify such assumptions, possibly with a comparison covering the higher molecular weight compounds.

4. Conclusions

The analysis of small volume precipitation samples allowed to evaluate the levels of PAHs in the different sites at different times. Rain samples highlighted a temporal and a spatial variability along a traffic gradient in the town of Como, especially for the most abundant PAH, e.g. PHE. These trends were reflected in air concentrations derived from rain measurements, highlighting the importance of reduced traffic zones and parks in lowering the exposure for these chemicals.

The preliminary data obtained in this study, although possibly requiring further confirmations for different sampling times and locations, suggest that the estimation of PAH air concentrations from concentrations measured in rainwater is a cheap and promising tool to assess short time variations and possibly spatial variability among sites. Sampling can be performed at the same time in several places (depending on the availability of personnel and/or dedicated samplers) and given the small rainfall volumes required can produce information on hourly variations or longer time averages simply measuring water collected for, e.g., a few hours. Such frequent and easy sampling could be relevant to evaluate, for example, emission profiles with time and space. For example, this approach could allow the evaluation of temporal changes of air concentrations due to emission changes (e.g. a new source, such the change of traffic composition with heavy vs. light duty engines), environmental changes (the change of PBL height at different times of the day or night) or different air masses coming because of wind direction changes. This is not usually possible with the high-

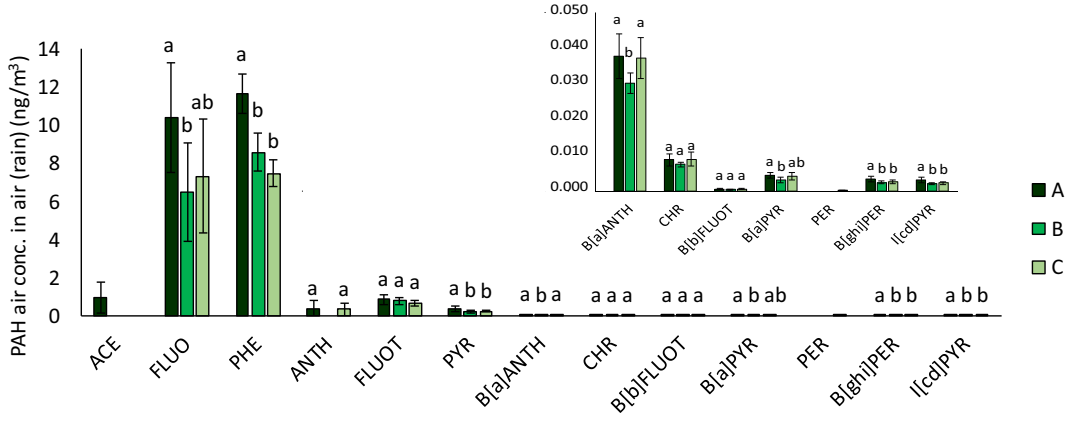

Fig. 5. PAH concentration in air estimated from rain at different sampling sites (A: High traffic; B: Medium traffic; C: Low traffic). All values are in ng/m^3. Samples with the same small letter are not statistically different ($\alpha = 0.05$).

volume air samplers due to their cost, the need of power supply and surveillance: for these reasons spatial and temporally resolved air samples are not generally available. The information on emissions, their importance and their variations obtained with this new approach can be relevant to evaluate patterns and calibrate multimedia fate models.

However, additional studies are needed to confirm these findings, better calibrate the results in different environmental conditions (especially for particle associated PAHs in different seasons) and fully evaluate the comparability of the data measured with conventional methods. This should be done coupling and comparing simultaneous short term rain measurements (an hour long or less) and, for example, high volume sampling for several rain episodes and possibly, in different environmental scenarios, characterized by different levels of gaseous and particle associated PAHs.

CRediT authorship contribution statement

The authors have all equally contributed to the manuscript preparation and finalization.

Declaration of competing interest

The authors declare that they have no known competing financial interests or personal relationships that could have appeared to influence the work reported in this paper.

Acknowledgements

Federica Tagni, Melissa Morselli, Francesca Frascoli, Sonia Ullucci, Antonella Zichella are acknowledged for participating to the rainfall sampling. The University of Insubria is acknowledged for the Post Doc salary of ET and the PhD salary of PF.

Appendix A. Supplementary data

Supplementary data to this article can be found online at https://doi.org/10.1016/j.scitotenv.2020.144184.

References

ACI, 2019. Autoritratto 2014 [WWW Document]. Automob. Club Ital. URL http://www.aci.it/laci/studi-e-ricerche/dati-e-statistiche/autoritratto/autoritratto-2014.html (accessed 12.9.19).

Alam, M.S., Delgado-Saborit, J.M., Stark, C., Harrison, R.M., 2014. Investigating PAH relative reactivity using congener profiles, quinone measurements and back trajectories. Atmos. Chem. Phys. 14, 2467–2477. https://doi.org/10.5194/acp-14-2467-2014.

Baek, S.O., Field, R.A., Goldstone, M.E., Kirk, P.W., Lester, J.N., Perry, R., 1991. A review of atmospheric polycyclic aromatic hydrocarbons: sources, fate and behavior. Water Air Soil Pollut. 60, 279–300. https://doi.org/10.1007/BF00282628.

Bourdat-Deschamps, M., Daudin, J.-J., Barriuso, E., 2007. An experimental design approach to optimise the determination of polycyclic aromatic hydrocarbons from rainfall water using stir bar sorptive extraction and high performance liquid chromatography-fluorescence detection. J. Chromatogr. A 1167, 143–153. https://doi.org/10.1016/j.chroma.2007.08.025.

Brorström-Lundén, E., 1996. Atmospheric deposition of persistent organic compounds to the sea surface. J. Sea Res. 35, 81–90. https://doi.org/10.1016/S1385-1101(96)90737-6.

Brorström-Lundén, E., Lindskog, A., Mowrer, J., 1994. Concentrations and fluxes of organic compounds in the atmosphere of the Swedish west coast. Atmos. Environ. 28, 3605–3615. https://doi.org/10.1016/1352-2310(94)00194-P.

Callén, M.S., de la Cruz, M.T., López, J.M., Mastral, A.M., 2011. PAH in airborne particulate matter. Fuel Process. Technol. 92, 176–182. https://doi.org/10.1016/j.fuproc.2010.05.019.

Cui, X., Mayer, P., Gan, J., 2013. Methods to assess bioavailability of hydrophobic organic contaminants: principles, operations, and limitations. Environ. Pollut. 172, 223–234. https://doi.org/10.1016/j.envpol.2012.09.013.

De Laender, F., Morselli, M., Baveco, H., Van den Brink, P.J., Di Guardo, A., 2015. Theoretically exploring direct and indirect chemical effects across ecological and exposure scenarios using mechanistic fate and effects modelling. Environ. Int. 74, 181–190. https://doi.org/10.1016/j.envint.2014.10.012.

de Souza, C.V., Corrêa, S.M., 2016. Polycyclic aromatic hydrocarbons in diesel emission, diesel fuel and lubricant oil. Fuel 185, 925–931. https://doi.org/10.1016/j.fuel.2016.08.054.

Di Guardo, A., Hermens, J.L., 2013. Challenges for exposure prediction in ecological risk assessment. Integr. Environ. Assess. Manag. 9, e4–e14. https://doi.org/10.1002/ieam.1442.

Di Guardo, A., Gouin, T., MacLeod, M., Scheringer, M., 2018. Environmental fate and exposure models: advances and challenges in 21st century chemical risk assessment. Environ Sci Process Impacts 20, 58–71. https://doi.org/10.1039/C7EM00568G.

Doong, R., Chang, S., Sun, Y., 2000. Solid-phase microextraction for determining the distribution of sixteen US Environmental Protection Agency polycyclic aromatic hydrocarbons in water samples. J. Chromatogr. A 879, 177–188. https://doi.org/10.1016/S0021-9673(00)00347-2.

European Environment Agency, 2019. Air Quality in Europe: 2019 report.

Gaga, E.O., Ari, A., Döğeroğlu, T., Emel Çakırca, E., Machin, N.E., 2012. Atmospheric polycyclic aromatic hydrocarbons in an industrialized city, Kocaeli, Turkey: study of seasonal variations, influence of meteorological parameters and health risk estimation. J. Environ. Monit. 14, 2219. https://doi.org/10.1039/c2em30118k.

Gasic, B., Moeckel, C., MacLeod, M., Brunner, J., Scheringer, M., Jones, K.C., Hungerbühler, K., 2009. Measuring and modeling short-term variability of PCBs in air and characterization of urban source strength in Zurich, Switzerland. Environ. Sci. Technol. 43, 769–776.

Ghirardello, D., Morselli, M., Semplice, M., Di Guardo, A., 2010. A dynamic model of the fate of organic chemicals in a multilayered air/soil system: development and illustrative application. Environ. Sci. Technol. 44, 9010–9017.

Guidotti, M., Giovinazzo, R., Cedrone, O., Vitali, M., 2000. Determination of organic micropollutants in rain water for laboratory screening of air quality in urban environment. Environ. Int. 26, 23–28. https://doi.org/10.1016/S0160-4120(00)00074-X.

Halsall, C.J., Coleman, P.J., Davis, B.J., Burnett, Victoria, Waterhouse, K.S., Harding-Jones, Peter, Jones, K.C., 1994. Polycyclic aromatic hydrocarbons in U.K. urban air. Environ. Sci. Technol. 28, 2380–2386. https://doi.org/10.1021/es00062a024.

Halsall, C.J., Sweetman, A.J., Barrie, L.A., Jones, K.C., 2001. Modelling the behaviour of PAHs during atmospheric transport from the UK to the Arctic. Atmos. Environ. 35, 255–267. https://doi.org/10.1016/S1352-2310(00)00195-3.

ISPRA, 2016. Qualità dell'ambiente urbano (No. XII Rapporto (2016) ISPRA Stato dell'Ambiente (67/16), ISPRA Stato dell'Ambiente. (ISPRA Istituto Superiore per la Protezione e la Ricerca Ambientale).

ISTAT, 2019. Consumi energetici delle famiglie : Impianto riscaldamento - disponibilità, tipo e fonte [WWW Document]. ISTAT - 'Istituto Naz. Stat. - Dati Censimento 2011. URL http://dati.istat.it/Index.aspx?QueryId=22803 (accessed 12.9.19).

Jensen, J., Sverdrup, L.E., 2003. Polycyclic aromatic hydrocarbon ecotoxicity data for developing soil quality criteria, in: Reviews of Environmental Contamination and Toxicology, Reviews of Environmental Contamination and Toxicology. Springer, New York, NY, pp. 73–97. doi:https://doi.org/10.1007/0-387-21731-2_3.

Khalili, N.R., Scheff, P.A., Holsen, T.M., 1995. PAH source fingerprints for coke ovens, diesel and, gasoline engines, highway tunnels, and wood combustion emissions. Atmos. Environ. 29, 533–542. https://doi.org/10.1016/1352-2310(94)00275-P.

Kim, K.-H., Jahan, S.A., Kabir, E., Brown, R.J.C., 2013. A review of airborne polycyclic aromatic hydrocarbons (PAHs) and their human health effects. Environ. Int. 60, 71–80. https://doi.org/10.1016/j.envint.2013.07.019.

Kiss, G., Gelencsér, A., Krivácsy, Z., Hlavay, J., 1997. Occurrence and determination of organic pollutants in aerosol, precipitation, and sediment samples collected at Lake Balaton. J. Chromatogr. A 774, 349–361. https://doi.org/10.1016/S0021-9673(97)00265-3.

Lammel, G., Klánová, J., Ilić, P., Kohoutek, J., Gasić, B., Kovacić, I., Lakić, N., Radić, R., 2010a. Polycyclic aromatic hydrocarbons in air on small spatial and temporal scales – I. Levels and variabilities. Atmos. Environ. 44, 5015–5021. https://doi.org/10.1016/j.atmosenv.2010.07.034.

Lammel, G., Klánová, J., Ilić, P., Kohoutek, J., Gasić, B., Kovacić, I., Lakić, N., Radić, R., 2010b. Polycyclic aromatic hydrocarbons in air on small spatial and temporal scales – I. Levels and variabilities. Atmos. Environ. 44, 5015–5021. https://doi.org/10.1016/j.atmosenv.2010.07.034.

Lee, R.G., Hung, H., Mackay, D., Jones, K.C., 1998. Measurement and modeling of the diurnal cycling of atmospheric PCBs and PAHs. Environ. Sci. Technol. 32, 2172–2179.

Li, P., Wang, Y., Li, Y., Wai, K., Li, H., Tong, L., 2016. Gas-particle partitioning and precipitation scavenging of polycyclic aromatic hydrocarbons (PAHs) in the free troposphere in southern China. Atmos. Environ. 128, 165–174. https://doi.org/10.1016/j.atmosenv.2015.12.030.

ARPA Lombardia, 2018. Meteorologia | ARPA Lombardia - Richiesta dati misurati [WWW Document]. ARPA Lomb. Lomb. Reg. Environ. Agency. URL https://www.arpalombardia.it/Pages/Meteorologia/Richiesta-dati-misurati.aspx (accessed 12.6.19).

Mackay, D., 2001. Multimedia Environmental Models: The Fugacity Approach. CRC press.

Mackay, D., Shiu, W.Y., Ma, K.-C. (Eds.), 2006. Handbook of Physical-chemical Properties and Environmental Fate for Organic Chemicals - Vol 2, 2nd ed. ed. CRC/Taylor & Francis, Boca Raton, FL.

Manoli, E., Samara, C., Konstantinou, I., Albanis, T., 2000. Polycyclic aromatic hydrocarbons in the bulk precipitation and surface waters of northern Greece. Chemosphere 41, 1845–1855. https://doi.org/10.1016/S0045-6535(00)00134-X.

Morselli, M., Ghirardello, D., Semplice, M., Di Guardo, A., 2011. Modeling short-term variability of semivolatile organic chemicals in air at a local scale: an integrated modeling approach. Environ. Pollut. 159, 1406–1412. https://doi.org/10.1016/j.envpol.2010.12.034.

Morselli, M., Ghirardello, D., Semplice, M., Raspa, G., Di Guardo, A., 2012. Integration of an atmospheric dispersion model with a dynamic multimedia fate model: development and illustration. Environ. Pollut. 164, 182–187. https://doi.org/10.1016/j.envpol.2012.01.039.

Morselli, M., Semplice, M., Villa, S., Di Guardo, A., 2014. Evaluating the temporal variability of concentrations of POPs in a glacier-fed stream food chain using a combined modeling approach. Sci. Total Environ. 493, 571–579. https://doi.org/10.1016/j.scitotenv.2014.05.150.

Morselli, M., Semplice, M., De Laender, F., Van den Brink, P.J., Di Guardo, A., 2015. Importance of environmental and biomass dynamics in predicting chemical exposure in ecological risk assessment. Sci. Total Environ. 526, 338–345. https://doi.org/10.1016/j.scitotenv.2015.04.072.

Morselli, M., Terzaghi, E., Di Guardo, A., 2018. Do environmental dynamics matter in fate models? Exploring scenario dynamics for a terrestrial and an aquatic system. Environ Sci Process Impacts https://doi.org/10.1039/C7EM00530J.

Morville, S., Delhomme, O., Millet, M., 2011. Seasonal and diurnal variations of atmospheric PAH concentrations between rural, suburban and urban areas. Atmospheric Pollut. Res. 2, 366–373. https://doi.org/10.5094/APR.2011.041.

Motelay-Massei, A., Ollivon, D., Garban, B., Chevreuil, M., 2002. Atmospheric deposition of toxics onto the Seine Estuary, France: example of polycyclic aromatic hydrocarbons. Atmospheric Chem. Phys. Discuss. 2, 1351–1369. https://doi.org/10.5194/acpd-2-1351-2002.

Muir, D., Sverko, E., 2006. Analytical methods for PCBs and organochlorine pesticides in environmental monitoring and surveillance: a critical appraisal. Anal. Bioanal. Chem. 386, 769–789. https://doi.org/10.1007/s00216-006-0765-y.

Nielsen, T., Jørgensen, H.E., Larsen, J.Chr, Poulsen, M., 1996. City air pollution of polycyclic aromatic hydrocarbons and other mutagens: occurrence, sources and health effects. Sci. Total Environ. Highway and Urban Pollution 189–190, 41–49. https://doi.org/10.1016/0048-9697(96)05189-3.

Oke, T.R., 2009. Boundary Layer Climates, 2. ed., reprinted. ed. Routledge, London.

Olivella, M.À., 2006. Polycyclic aromatic hydrocarbons in rainwater and surface waters of Lake Maggiore, a subalpine lake in northern Italy. Chemosphere 63, 116–131. https://doi.org/10.1016/j.chemosphere.2005.07.045.

Poerschmann, J., Kopinke, F.-D., Pawliszyn, J., 1997. Solid phase microextraction to study the sorption of organotin compounds onto particulate and dissolved humic organic matter †. Environ. Sci. Technol. 31, 3629–3636. https://doi.org/10.1021/es970377d.

Polyakova, O.V., Artaev, V.B., Lebedev, A.T., 2018. Priority and emerging pollutants in the Moscow rain. Sci. Total Environ. 645, 1126–1134. https://doi.org/10.1016/j.scitotenv.2018.07.215.

Prevedouros, K., MacLeod, M., Jones, K.C., Sweetman, A.J., 2004. Modelling the fate of persistent organic pollutants in Europe: parameterisation of a gridded distribution model. Environ. Pollut. 128, 251–261. https://doi.org/10.1016/j.envpol.2003.08.041.

Ravindra, K., Sokhi, R., Vangrieken, R., 2008. Atmospheric polycyclic aromatic hydrocarbons: source attribution, emission factors and regulation. Atmos. Environ. 42, 2895–2921. https://doi.org/10.1016/j.atmosenv.2007.12.010.

Rianawati, E., Balasubramanian, R., 2009. Optimization and validation of solid phase micro-extraction (SPME) method for analysis of polycyclic aromatic hydrocarbons in rainwater and stormwater. Phys. Chem. Earth Parts ABC 34, 857–865. https://doi.org/10.1016/j.pce.2009.07.003.

Ringuet, J., Albinet, A., Leoz-Garziandia, E., Budzinski, H., Villenave, E., 2012. Diurnal/nocturnal concentrations and sources of particulate-bound PAHs, OPAHs and NPAHs at traffic and suburban sites in the region of Paris (France). Sci. Total Environ. 437, 297–305. https://doi.org/10.1016/j.scitotenv.2012.07.072.

Shahpoury, P., Lammel, G., Holubová Šmejkalová, A., Klánová, J., Přibylová, P., Váňa, M., 2015. Polycyclic aromatic hydrocarbons, polychlorinated biphenyls, and chlorinated pesticides in background air in central Europe – investigating parameters affecting wet scavenging of polycyclic aromatic hydrocarbons. Atmos. Chem. Phys. 15, 1795–1805. https://doi.org/10.5194/acp-15-1795-2015.

Škrdlíková, L., Landlová, L., Klánová, J., Lammel, G., 2011. Wet deposition and scavenging efficiency of gaseous and particulate phase polycyclic aromatic compounds at a central European suburban site. Atmos. Environ. 45, 4305–4312. https://doi.org/10.1016/j.atmosenv.2011.04.072.

Stull, R.B., 1988. An Introduction to Boundary Layer Meteorology. Springer, Dordrecht.

Sverdrup, L.E., Nielsen, T., Krogh, P.H., 2002. Soil ecotoxicity of polycyclic aromatic hydrocarbons in relation to soil sorption, lipophilicity, and water solubility. Environ. Sci. Technol. 36, 2429–2435. https://doi.org/10.1021/es010180s.

Terzaghi, E., Wild, E., Zacchello, G., Cerabolini, B.E.L., Jones, K.C., Di Guardo, A., 2013. Forest filter effect: role of leaves in capturing/releasing air particulate matter and its associated PAHs. Atmos. Environ. 74, 378–384. https://doi.org/10.1016/j.atmosenv.2013.04.013.

Terzaghi, E., Scacchi, M., Cerabolini, B., Jones, K.C., Di Guardo, A., 2015a. Estimation of polycyclic aromatic hydrocarbon variability in air using high volume, film, and vegetation as samplers. Environ. Sci. Technol. 49, 5520–5528. https://doi.org/10.1021/es5056929.

Terzaghi, E., Zacchello, G., Scacchi, M., Raspa, G., Jones, K.C., Cerabolini, B., Di Guardo, A., 2015b. Towards more ecologically realistic scenarios of plant uptake modelling for chemicals: PAHs in a small forest. Sci. Total Environ. 505, 329–337. https://doi.org/10.1016/j.scitotenv.2014.09.108.

Terzaghi, E., Vitale, C.M., Salina, G., Di Guardo, A., 2019. Plants radically change the mobility of PCBs in soil: role of different species and soil conditions. J. Hazard. Mater. 121786. https://doi.org/10.1016/j.jhazmat.2019.121786.

Terzi, E., Samara, C., 2004. Gas-particle partitioning of polycyclic aromatic hydrocarbons in urban, adjacent coastal, and continental background sites of western Greece. Environ. Sci. Technol. 38, 4973–4978. https://doi.org/10.1021/es040042d.

Urrestarazu Ramos, E., Meijer, S.N., Vaes, W.H.J., Verhaar, H.J.M., Hermens, J.L.M., 1998. Using solid-phase microextraction to determine partition coefficients to humic acids and bioavailable concentrations of hydrophobic chemicals. Environ. Sci. Technol. 32, 3430–3435. https://doi.org/10.1021/es980274a.

Vitale, C.M., Di Guardo, A., 2019. Predicting dissolved organic carbon partition and distribution coefficients of neutral and ionizable organic chemicals. Sci. Total Environ. 658, 1056–1063. https://doi.org/10.1016/j.scitotenv.2018.12.282.

Vitale, C.M., Sjøholm, K.K., Di Guardo, A., Mayer, P., 2019. Accelerated equilibrium sampling of hydrophobic organic chemicals in solid matrices: a proof of concept on how to reach equilibrium for PCBs within 1 day. Chemosphere 124537. doi:https://doi.org/10.1016/j.chemosphere.2019.124537.

Yan, L., Li, X., Chen, J., Wang, X., Du, J., Ma, L., 2012. Source and deposition of polycyclic aromatic hydrocarbons to Shanghai, China. J. Environ. Sci. 24, 116–123. https://doi.org/10.1016/S1001-0742(10)60638-9.

Paper VI

Environmental Pollution 293 (2022) 118507

Contents lists available at ScienceDirect

Environmental Pollution

journal homepage: www.elsevier.com/locate/envpol

Bioaccumulation of PCBs and their hydroxy and sulfonated metabolites in earthworms: Comparing lab and field results☆

Jessica Palladini [a], Renzo Bagnati [b], Alice Passoni [b], Enrico Davoli [b], Alessia Lanno [b], Elisa Terzaghi [a], Parisa Falakdin [a], Antonio Di Guardo [a,*]

[a] Department of Science and High Technology (DiSAT), University of Insubria, Via Valleggio 11, 21100, Como, Italy
[b] Department of Environmental Health Sciences, Istituto di Ricerche Farmacologiche "Mario Negri" IRCCS, Via Mario Negri 2, 20156, Milan, Italy

ARTICLE INFO

Keywords:
Hydroxy-PCBs
Sulfonated PCBs
Hydroxy-sulfonated PCBs
Log D
Log K_{OW}
Ecological realism

ABSTRACT

Sulfonated and hydroxy-sulfonated PCBs were recently discovered by our group as new PCB soil contaminants, constituting about 1% of their parent compounds in soil. Here we investigate for the first time the bioaccumulation of these metabolites as well as hydroxy-PCBs and native PCBs in earthworms. A sequence of three experiments, at increasing complexity and ecological realism, were performed with four different earthworm species (*Eisenia foetida* Savigny, *Lumbricus terrestris* L, *Allolobophora chlorotica* Savigny and *Aporrectodea caliginosa* Savigny) exposed to contaminated soils. The first experiment confirmed that when exposing earthworms to soil contaminated with a single hexa-chlorinated congener (PCB 155), no formation of polar metabolites in earthworms could be detected. This allowed to plan the following two experiments, using a soil from a PCB contaminated site and rich in relatively high levels (10–130 μg kg^{-1}) of hydroxy-, sulfonated-, and hydroxy-sulfonated-PCBs. Bioaccumulation factors (BAFs) and bioconcentration factors (BCFs) were then obtained in the second and third experiments, to compare the accumulation behavior of these chemicals in laboratory and natural conditions. Regressions between BAF/BCF and Log Kow/Log D, produced a variety of results, being generally significant between BCF and PCBs and not significant in the other cases. In general, the metabolites accumulated in earthworms with detectable concentrations in their tissues (8–115 μg kg^{-1}), although sulfonated and hydroxy-sulfonated PCBs showed BAF and BCF values lower (up to two orders of magnitude) than those calculated for the parent PCBs, given their lower lipophilicity.

1. Introduction

Polychlorinated biphenyls (PCBs) are persistent organic pollutants produced and extensively used in the past in many industrial applications (Breivik et al., 2002). Their production was banned in the 1980s in many countries, but they still persist in the environment due to their low degradation rates (Paasivirta and Sinkkonen, 2009). Due to their hydrophobic nature, (i.e., Log Kow > 4) PCBs bioaccumulate in aquatic and terrestrial food webs (Campbell et al., 2003; McLachlan, 1995; Vermeulen et al., 2010), moreover, their semi-volatility enables them to move through long distances (Ockenden et al., 2003). Many studies demonstrated that human and ecosystem exposure to PCBs is correlated to a wide range of toxic effects (IARC, 2015). Although today PCBs are well studied chemicals, information about their metabolites is still lacking. For example, while Log Kow measured values for PCBs are available in several compilations, even for single congener (Mackay et al., 2006; Paasivirta and Sinkkonen, 2009), no measured data are available for PCB metabolites and therefore they must be estimated. In the last few decades, the study of the environmental fate of PCB metabolites had received increasing attention focusing not only on metabolites produced by microorganism degradation but also on those derived from plants, humans, and wildlife metabolism (including earthworms) and other environmental reactions. For example, several classes of metabolites were mainly identified in human serum and wildlife, and were shown to contain hydroxy group (-OH) (hydroxylated PCB) also found in plants such as poplar, and in earthworms, methoxy group (-OCH_3) (methoxy PCB), sulfur such as –SCH_3 (methylthio PCB), –SO_2CH_3 (methylsulfonyl PCB) and –OSO_3 (sulfate PCB) (Grimm et al., 2015; Haraguchi, 2004; He et al., 2018; Karasek et al., 1985; Marek et al., 2013; Rezek et al., 2007; Sun et al., 2016; Tehrani and Van Aken,

☆ This paper has been recommended for acceptance by Eddy Y. Zeng.

* Corresponding author.
E-mail address: antonio.diguardo@uninsubria.it (A. Di Guardo).

https://doi.org/10.1016/j.envpol.2021.118507
Received 5 August 2021; Received in revised form 8 November 2021; Accepted 13 November 2021
Available online 17 November 2021

2014; Ueno et al., 2007; Zhai et al., 2013). Additionally, two new PCB metabolite classes i.e., sulfonated-PCBs (-SO_3H) and hydroxy-sulfonated- PCBs (−OH, –SO_3H) were recently discovered in a heavily PCB contaminated site located in Northern Italy, as well as in background contaminated areas (Bagnati et al., 2019), at concentrations of approximately 1% of native PCBs. For these metabolites no information on their toxicity or ecotoxicity is available since the lack of congener level identification hinders their accurate measurements in environmental media but also the measurement of their physico-chemical properties. While some information exist on the presence of sulfonated PCBs in biota (Liu et al., 2018) and feces of PCB administered mice (Li et al., 2021), no or scarce data are available for the environmental degradation half-lives, as well as bioaccumulation in earthworms of hydroxy, sulfonated and hydroxy-sulfonated PCBs.

Earthworms are invertebrates which are commonly found in natural and agricultural soils, and they are known for their potential of investigating soil depth and interacting with contaminants. Earthworms need to ingest large amounts of soil due to their low assimilation efficiency of nutrients (EC, 2010). It is estimated that temperate geophagous species have typically soil consumption rates of 1.0–2.5 g dry mass g^{-1} fresh mass d^{-1} (Curry and Schmidt, 2007), therefore they have the capability of efficiently recycle large amounts of soil. When the ingested soil passes through the gastrointestinal tract, it undergoes physical and chemical changes (Rodriguez-Campos et al., 2014) and is expelled as casts. Earthworms are able to bioaccumulate hydrophobic organic chemicals, including PCBs, absorbing them from the soil pore water by passive diffusion through the body wall, or from the ingested soil by the passive diffusion through the gut wall (Belfroid et al., 1995; Hallgren et al., 2006; He et al., 2018; Jager et al., 2005; Krauss et al., 2000; Matscheko et al., 2002; Shang et al., 2013; van der Wal et al., 2004). However, studies about bioaccumulation of PCB metabolites in earthworms are not available yet. For these reasons, in the current work, the bioaccumulation of three classes of PCB metabolites (hydroxy-, sulfonated and hydroxy-sulfonated-PCBs) in earthworms was investigated for the first time, as well as their parent compound PCBs. More specifically, three experiments were performed: a) a preliminary experiment to investigate the timeframe and variability of PCB uptake and the potential production of hydroxy, sulfonated and hydroxy-sulfonated PCB metabolites in earthworm tissues; b) a lab experiment to investigate PCBs and PCB metabolites bioaccumulation by “clean” earthworms in a soil with detectable concentrations of a larger array of PCBs and metabolites; c) a field experiment to evaluate field bioaccumulation of PCBs and PCB metabolites in earthworms living in a contaminated soil.

2. Materials and methods

2.1. Experimental design and setup

Preliminary experiment. Grassland topsoil (0–20 cm) and adult earthworms (*Eisenia foetida* Savigny.*)* (Fig. A1) were obtained from a background site located in Como, Italy. Earthworms were kept in the background soil for 3 weeks to acclimatize before exposure without being additionally fed. Soil was sieved at 2 mm and spiked with PCB 155 at 1000 ng g^{-1} fresh weight (fw) following the suggestions reported in (Northcott and Jones, 2000; Reid et al., 1998) for spiking hydrophobic organic compounds into soil. See Appendix A1 for more details on the soil spiking procedure. Earthworms (*Eisenia foetida*) were removed from the incubation background soil, rinsed with deionized water, and purged on a wet filter paper in clean Petri dishes for 3 h before exposure. Individual glass jars (250 mL) were filled with 260 g fw of PCB 155 spiked soil and 10 earthworms (about 3 g fw), after the addition of 15 mL deionized water. Control jars were also set up (spiked soil without earthworms). All jars were weighed and stored in a temperature-controlled chamber at 18 °C ± 2, kept in the dark, maintaining a water content of 30%. The experiment lasted for 30 days: three sampling times were set up: 0 (T0), 15 (T1) and 30 days (T2). The experiment was performed in triplicate. Earthworms were not additionally fed neither in the incubation period nor during the whole exposure time. At each sampling time soil samples were collected from each jar with the JSC procedure and kept at −20 °C until analysis. Earthworms were rinsed with deionized water and allowed to purge their gut content on a moist filter paper for 48 h. After purging, the earthworms were weighed and stored at −20 °C until use. Unspiked soil and not exposed earthworms were also collected and analyzed to assess the respective PCB background levels.

Lab bioaccumulation experiment. Soil was collected from a heavily PCB contaminated site located in Northern Italy, the SIN Brescia-Caffaro (SIN, stands for “Sito di Interesse Nazionale” or National Priority Site) (Di Guardo et al., 2020, 2017) (Fig. A2). The soil was sampled in permanent grassland fields up to a depth of about 40 cm and extensively homogenized to reduce the heterogeneity of naturally weathered soil. Several mixing steps were followed, in field through mechanical mixing of a large volume of soil and in laboratory according to the one-dimensional Japanese Slab-Cake (JSC) technique (ITRC, 2012). Before JSC, soil was dried and sieved at 2 mm. The soil investigated was a loamy soil according to the US Department of Agriculture classification (Maidment, 1993), with 1.8% of organic carbon (Terzaghi et al., 2019). The same “clean” earthworm species of experiment 1 were used. Six earthworms (*Eisenia foetida*) (2 g fw) were exposed for 27 days to 250 g fw of contaminated soil in a 250 mL beaker, in similar exposure conditions of experiment 1.50 mL of deionized water were added to the beaker to reach a water content of around 30%. At the end of the experiment, earthworms and soil were collected as reported for experiment 1.

Field bioaccumulation experiment. Grassland topsoil (0–30 cm) and earthworms were sampled in two highly contaminated area (field A and B, Figure A2) of the same SIN Brescia-Caffaro, characterized by a similar PCB fingerprint. Adult earthworms of three different species were collected: *Aporrectodea caliginosa* Savigny (from field A), and *Lumbricus terrestris* L. and *Allolobophora chlorotica* Savigny (both from field B). Soil samples were kept at −20 °C until analysis. Being based on the field collection of soil and earthworms, the only operation relevant for this section was gut purging. Earthworms were first rinsed with deionized water and then later allowed to purge their gut content on a moist filter paper for 48 h. After purging, the earthworms were weighed and stored at −20 °C until analysis.

2.2. Chemicals and reagents

PCB analysis. Cyclohexane was purchased from Merck (Darmstadt, Germany) while ethylacetate from Fluka Analytical (Sigma-Aldrich, St. Louis, MO, U.S.A). All solvents were pesticide residue grade. Anhydrous sodium sulfate was purchased from Sigma-Aldrich (St. Louis, MO, U.S.A) and Florisil (0.150–0.250 mm) from Merck (Darmstadt, Germany). PCB standards were purchased from Wellington Laboratories (Guelph, ON, Canada): an 82 native PCB solution (PCB-PAR-H in nonane, purity >98%) was used for PCB congener identification and quantitation, while a mass labelled (^{13}C) 10 PCB solution (MBP-GC in nonane/toluene, purity >98% and isotopic purity ≥99%) was used as internal standard. Mass labelled PCB 37, PCB 162 and PCB 208 (MBP-37, MBP-162, MBP-208 in nonane/toluene purity >98% and isotopic purity ≥99%) were also used as recovery standards. PCB 155 and 136 were purchased from AccuStandard (New Haven, CT, U.S.A.) whereas PCB 101 from Chem-Service (West Chester, U.S.A.). PCB 136 and PCB 101 were used as internal and recovery standard respectively in experiment 1.

PCB metabolite analysis. Dichloromethane (ACS reagent. ≥ 99.8%) was obtained from Sigma-Aldrich. HPLC solvents and reagents were of pesticide or LC-MS grade: water (in house Milli-Q apparatus), acetonitrile, acetone, formic acid and ammonium acetate (Carlo Erba Reagents). Standards of OH-PCBs (4-hydroxy-2,3,3′,4′,5-Pentachlorobiphenyl, OH-PCB-107; 4-hydroxy-2,2′,3,4′,5,5′,6-heptachlorobiphenyl, OH-PCB-187; 3-hydroxy-2,2′,3′,4,4’,5-

Hexachlorobiphenyl, OH-PCB-138 and $^{13}C_{12}$-4-hydroxy-2,2′,3,4′,5,5′,6-heptachlorobiphenyl, $^{13}C_{12}$-OH-PCB-187) were purchased from Wellington Laboratories (Guelph, ON, Canada).

2.3. Extraction and analysis of PCBs

Soil and earthworm samples were extracted with a sonicator with a 100 mL of a mixture cyclohexane:ethylacetate 1:1 for 1 h and analyzed with a single quadrupole GC-MS (Agilent 7890–5977). Several PCB congeners, covering all chlorination classes (PCB 3, 15, 28/31, 52, 90/101, 138/158, 153/168, 155, 180/193, 194, 206, 209) were determined. For more details on the analytical method please see Appendix A1.

2.4. Extraction and analysis of PCB metabolites

The extraction of soil and earthworm samples was performed with a sonicator for 30 min using 4 mL of acetone:water (95:5%. V/v) containing 1% formic acid and repeated with dichloromethane (4 mL). Acetonitrile (600 μL) was used to reconstitute the samples. Analysis of the extracts was performed by HPLC-HRMS, using a LC system coupled to an Orbitrap Q Exactive mass spectrometer. More details on the extraction and analytical procedures are given in Appendix A1.

2.5. Quality assurance/quality control (QA/QC)

The quality of the whole analytical procedure for PCB analysis was assessed using recovery standards, instrumental, and method blanks and a certified reference material. See Appendix A1 for more details such as LOQs, certified reference material, recovery and blanks. Analytical variability for PCB analyses was 10%. For the analysis of PCB metabolites, no reference materials were available yet and the quality of the analytical procedures relied on the use of instrumental and method blanks and on the availability of some reference and synthesized standards. The results for the PCB metabolites are presented as sum of congener chlorination classes. Since the percent relative standard deviation in the response of the three OH-PCBs used as reference standards (OH-PCB-107, OH-PCB-138 and OH-PCB-187) was about ±60%, we assumed a similar variability for the measurement of all congener classes of PCB metabolites. For the sulfonated metabolites the variability may be probably higher.

2.6. Bioaccumulation factor calculation

The earthworm/soil bioaccumulation factor (BAF) was determined for PCBs and metabolites according to the following equation (1) (Belfroid et al., 1993; Hallgren et al., 2006):

$$BAF = \frac{Cew}{Cs} \quad (1)$$

Where BAF is the bioaccumulation factor (dimensionless), Cew is the congener concentration in earthworm (μg kg^{-1} fw) and Cs is the congener concentration in soil (μg kg^{-1} dry weight, dw).

The biota to soil accumulation factor (BSAF), normalized for lipid fraction of the earthworm and organic carbon in soil is reported in Appendix A1, together with the relative analytical methods.

2.7. Bioconcentration factor calculation

The bioconcentration factor (BCF) was determined for PCBs and metabolites according to the following equation (2):

$$BCF = \frac{Cew}{Cw_{(free)}} \quad (2)$$

where BCF is the bioconcentration factor in L kg^{-1} fresh weight (fw), Cew is the congener concentration in earthworm (μg kg^{-1} fw) and $Cw_{(free)}$ is the congener freely dissolved concentration in soil pore water (μg L^{-1}). Soil pore water concentration was estimated as reported in Appendix A1. Standard deviation was calculated propagating the variability of the concentrations using Monte Carlo simulations.

2.8. Log K_{OW} determination for PCB metabolites

The Log K_{OW} values for PCB metabolites were estimated with the fragment constant method of Hansch and Leo (Lyman et al., 1990). For simplicity and in lack of additional information it was assumed that in hydroxy-sulfonated-PCBs the –OH and –SO_3H groups were not present on the same benzene ring in the biphenyl. Log K_{OW} values for PCBs were obtained from (Paasivirta and Sinkkonen, 2009) and the metabolites corresponding values were estimated subtracting 0.48 for the –OH group and 3.16 for the –SO_3H group (Lyman et al., 1990).

2.9. pKa and log D determination for PCB metabolites

pKa values for PCB metabolites were estimated using the SPARC platform (http://archemcalc.com/sparc-web/calc/#/pka; accessed on July 27, 2021) selecting the single pKa type. Log D (at pH = 7) was calculated with the same platform. Log D is the apparent Log K_{OW} value at the experimental pH, calculated as the ratio of the sum of the concentrations of all forms of the compound (ionized and un-ionized) in each of the two phases. As such, Log D is pH dependent.

2.10. Statistical analyses

Statistical analyses were performed with the XLSTAT software by Addinsoft SARL (Version, 2021.2.1, 205 Boston, USA). Linear regression was used to model the relationship between Log BAF or Log BCF and Log K_{OW} for each species, employing the concentrations of single PCB congeners in earthworms, and soil or soil pore water. Log K_{OW} values for each PCB congener were taken from the literature (Paasivirta and Sinkkonen, 2009) while those of metabolites were estimated as explained in 2.9. The Analysis of Covariance, ANCOVA ($\alpha = 0.05$) and Tukey test ($\alpha = 0.05$) were used to verify

Whether the regression lines were different from each other in either slope or intercept.

3. Results and discussion

3.1. Estimation of selected physico-chemical properties for PCB metabolites

Log K_{OW} of metabolites were estimated starting from a selected properties compilation (Paasivirta and Sinkkonen, 2009) and using the fragment constant method, resulting from slightly different values from those listed in our previous publication on these metabolites (Bagnati et al., 2019). Due to this new starting dataset, the Log K_{OW} of metabolites were generally much lower than reported in (Bagnati et al., 2019). These data, together with estimated pKa and Log D are listed in Table 1. Although not all metabolite classes were found in earthworms/soil, we calculated the entire dataset that highlighted how the addition of the sulfonated group considerably decrease the Log K_{OW} and pKa. While Hydroxy-PCBs are only slightly affected by hydroxy group presence in reducing Log K_{OW} and pKa, the coexistence of hydroxy and sulfonated groups additionally lowers both Log K_{OW} and pKa. Moreover, the effect of lowering pKa is more pronounced for the sulfonated metabolites when the number of chlorine atoms on the biphenyl is higher than 5. As evident from the pKa values, the metabolites present in the soil solution at a pH around 7, as in the experimental soils, are generally fully dissociated, except for hydroxy-PCBs (apart from nona and in part octa and hepta). Given the range of pKa of the metabolites, which are generally dissociated at environmental pH (pH~7), it is important to

Table 1
Log K_{OW}, pKa and Log D (at pH = 7) values for PCBs and PCB metabolites.

Families	PCBs	Hydroxy-PCBs			Sulfonated-PCBs			Hydroxy-sulfonated-PCBs		
	Log K_{OW}	Log K_{OW}	pKa	Log D	Log K_{OW}	pKa	Log D	Log K_{OW}	pKa	Log D
Mono	4.67 [a]	4.19	9.81	4.54	1.51	0.56	−2.11	1.03	0.56	−2.74
Di	5.02 [b]	4.54	9.75	5.17	1.86	0.56	−1.36	1.38	0.56	−1.90
Tri	5.50 [c]	5.02	9.70	5.80	2.34	0.56	−0.60	1.86	0.56	−1.05
Tetra	6.03 [d]	5.55	9.64	6.46	2.87	0.56	0.18	2.39	0.56	−0.44
Penta	6.40 [e]	5.92	9.54	7.25	3.24	0.56	1.03	2.76	0.52	0.57
Hexa	6.99 [f]	6.51	8.00	7.63	3.83	0.52	1.97	3.35	0.55	1.55
Hepta	7.36 [g]	6.88	7.37	8.08	4.20	0.54	2.86	3.72	0.53	2.50
Octa	7.92 [h]	7.44	6.51	8.22	4.76	0.53	3.82	4.28	0.48	3.44
Nona	8.07 [i]	7.59	4.97	7.71	4.91	0.48	4.80	–	–	–
Deca	8.22	–	–	–	–	–	–	–	–	–

Note: Log Kow values for PCBs were from (Paasivirta and Sinkkonen, 2009). [a] Referred to PCB 3; [b] Referred to PCB 15; [c] Referred to PCB 28; [d] Referred to PCB 52; [e] Referred to PCB 101; [f] Referred to PCB 138 and 153; [g] Referred to PCB 180; [h] Referred to PCB 194; [i] Referred to PCB 206.

calculate the octanol-water distribution coefficient accounting for dissociated and undissociated species (Log D) for these compounds (Table 1). The Log D values should coincide with Log K_{OW} when the chemical is not dissociated. However, since Log D values were calculated with an estimation platform (SPARC) their values for undissociated compounds do not necessarily match the Log K_{OW} values obtained above. However, the obtained Log D can be used to compare the partitioning among the different classes and chemicals with different pKa. Hydroxy-PCBs, given their pKa, are not significantly dissociated, except for the nona-chlorinated congener. For this reason, Log D are very close to Log K_{OW}, generally rising with chlorination, except for the nona-chlorinated-hydroxy PCBs, with a value smaller than the octa-ones. This depends on the pKa of the nona-hydroxy PCBs (4.97), showing that this chemical, at pH 7, is dissociated >99%. The situation is slightly different for the sulfonated- and the hydroxy-sulfonated PCBs: given their low pKa (always <1), they are always dissociated at environmental pHs, being strong acids. Log Ds for sulfonated-and hydroxy-sulfonated PCBs are significantly smaller than the corresponding Log K_{OW}, especially for lower chlorinated congeners. Given the lack of precise congener identity and analytical standards for such metabolites, it was not possible to reliably quantify the uncertainty associated to these estimations. However, the authors of the fragment constant method (Hansch and Leo, 1995) estimate that the typical deviation of log Kow is ±0.5 for 8000 reliably measured Log Kow values. Also considering the fact that the structure of the precise chemical is unknown, the uncertainties might be higher.

3.2. Preliminary experiment

This experiment was conducted to evaluate the pattern of PCB uptake and the potential level of production of metabolites during the experiment, using background remote soil spiked with PCB 155 (a hexa-chlorinated congener) and "clean" earthworms (Table A1) not coming from the contaminated site. The soil was spiked with PCB 155 at a level which was about two orders of magnitude above the background total PCB concentration in the soil. The resulting initial concentration of PCB 155 was 861 ± 61 ng g^{-1} dw, comparable to the levels of other hexa-chlorinated PCBs present in SIN Brescia-Caffaro soil. Organic carbon content is reported in Table A2. PCB 155 was selected because is a hexa-chlorinated congener, representing the most abundant chlorination class present in SIN Brescia-Caffaro soil. Although PCB 155 was not present either in Brescia-Caffaro soil or in the background soil used for this experiment it is similar in terms of metabolization class to PCB 153, one of the most abundant congener (Boon et al., 1997). classified the affinity for enzymatic metabolism (an index of metabolic capability for PCB degradation) in seals and other organisms, obtaining several metabolic groups, according to the resistance to degradation. PCB 155 and PCB 153 can be classified as being part of group I (the most resistant to biotransformation).

The results of the experiment showed that PCB 155 bioaccumulated with time (Fig. 1), apparently reaching the steady state within the period of the experiment (30 d), similarly to other PCB uptake experiments (Belfroid et al., 1995). During the period of the experiment, no production of detectable metabolites in earthworms could be shown, confirming that at this parent compound concentration the presence of polar metabolites in earthworm tissues could be due to only bioaccumulation of metabolites present in soil.

Similar accumulation in earthworms (*E. foetida* Savigny) were observed by He and coworkers (He et al., 2018) in a comparable experiment using PCB 95 and PCB 149, a penta- and an hexa-chlorinated congener. Although the authors found the formation of OH-PCBs at increasing concentrations in earthworms, these metabolites were only about 0.1% of the soil PCB concentration and limited to the penta congener. PCB 149 is a Boon group V metabolite (more easily metabolized than group I), so it could have been expected that some metabolite formation would have taken place. However, He and collaborators showed that only some penta-chlorinated metabolites could be produced by earthworms and therefore caution should be exercised when evaluating whether concentration of PCB metabolites in earthworm tissues depend on bioaccumulation or metabolic production from parent PCBs, especially for lower chlorinated congeners. An indication of probable bioaccumulation of metabolites (instead of *in-situ* formation) could be a significant correlation between the ratio of earthworm and soil concentrations (BAF) vs. a hydrophobicity parameter such as Log K_{OW}.

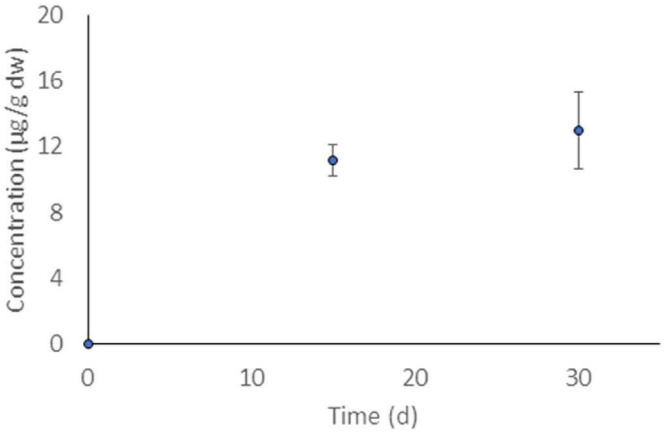

Fig. 1. Uptake of PCB 155 with time in *Eisenia foetida.* Bars show the standard deviation. The point at time 0 of the experiment corresponds to PCB 155 concentration < LOQ.

3.3. Lab bioaccumulation experiment

In this experiment "clean" earthworms were exposed to contaminated soil coming from the SIN Brescia-Caffaro. This soil shows relevant levels of PCBs and metabolites as can be seen from Fig. 2 and was chosen as a suitable test soil given the lack of sulfonated and hydroxy-sulfonated PCB standards for soil spiking and measurement. Fig. 2 shows the fingerprints for PCB and metabolite concentrations in both *Eisenia foetida*

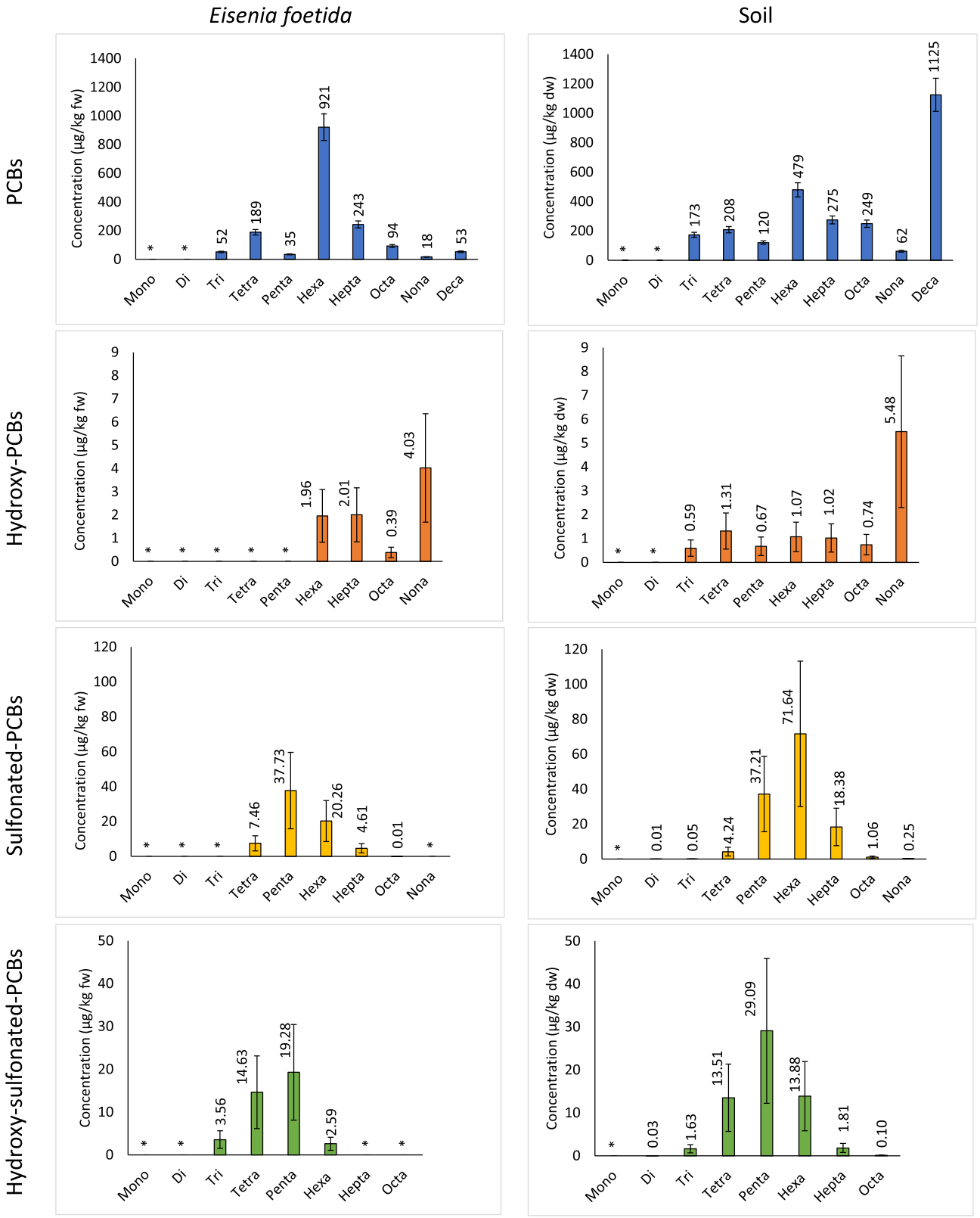

Fig. 2. PCB and PCB metabolite concentrations in earthworm (µg/kg fw) and soil (µg/kg dw) referred to each family of congeners measured in the experiment 2. Asterisks (*) refer to values below LOQs. Bars show the analytical variability.

(fw) and soil (dw), with the reported analytical variability. The most important PCB congener class present in soil was the deca-chlorinated (PCB 209), while the most accumulated class in earthworms was the hexa-chlorinated. Caffaro factory in Brescia (Italy) was the largest producer of PCBs and other chlorinated compounds in Italy. PCB were produced for more than 50 years as mixtures known as Apirolio and Fenclor. PCB 209 was a peculiar product, not part of other mixtures, also known as Fenclor DK (Di Guardo et al., 2017). When looking at the hydroxy-PCBs, the nona-chlorinated was the most abundant in both soil and earthworms, followed by hexa- and hepta-. No hydroxylated metabolites appeared for penta- and lower number of chlorine classes in earthworms. For sulfonated PCBs there is a shift in most abundant chlorinated class between soil and earthworms: the largest amount could be found for hexa-in soil and penta-in earthworms. No shift appeared instead for hydroxy-sulfonated metabolites, being the penta-chlorinated the most abundant class.

Concentration data were first plotted as BAF (bioaccumulation factor, a common metric for evaluating the capability of earthworms to accumulate chemicals), against Log K_{OW} (Figure A3, also expressed on a dw to dw basis, and Table A4). Generally, with increasing Log K_{OW} the bioaccumulation factor seemed to decrease for both PCBs and PCB metabolites, with the exclusion of tri to hepta-PCBs, although the regressions for PCBs were not significant. Only for sulfonated and hydroxy-sulfonated-PCBs was the linear regression statistically significant ($p < 0.05$) (Table A4). The decreasing bioaccumulation values for the most hydrophobic PCBs was also reported by (Hallgren et al., 2006) who exposed earthworms (*Eisenia foetida*) to a soil artificially contaminated with PCBs for 10 days. In both experiments, the earthworm uptake decreased for the most hydrophobic chemicals, probably due to their strong affinity for the soil organic fraction and the slow desorption kinetics, that occur especially in aging soils and determine their bioavailability (Pignatello and Xing, 1996). For PCB metabolites, the BAF in earthworms decreased with Log K_{OW}. As reported above (section 3.2) the present correlation of BAF with Log K_{OW} could be an indication of bioaccumulation rather than *in-situ* formation of PCB metabolites or the scarce relevance of metabolic products compared to the bioaccumulated ones. Fig. A4 in the appendix, reports the biota to soil accumulation factor (BSAF), normalized for lipid fraction of the earthworm and organic carbon in soil for comparison (Table A3). However, BSAFs do not introduce additional information than BAFs.

Accumulation data were also plotted as BCF (L/kg), obtained as concentrations in earthworms and soil pore water concentration ratios. Log BCF is first shown against Log K_{OW}, to be compared to the literature, and later to Log D (only for metabolites), to account for the dissociation of the different metabolite classes. The use of Log BCF vs. Log K_{OW} is a common metric used to evaluate the potential for uptake of non-polar chemicals considering their bioavailability in soil water (Di Guardo and Hermens, 2013). For this reason, the soil porewater concentration was estimated using an equation (Vitale et al., 2019) obtained measuring bioavailable concentrations of PCBs using a SPME technique. While BCF plots for single classes are shown in the appendix (Fig. A5), together with the predictive equations, including the statistical parameters (Table A5), an overall comparison of BCFs for all classes is shown in Fig. 3.

For PCBs and OH-PCBs (Fig. 3 and A5) the bioconcentration factor increases with the Log Kow, but only for PCBs this trend is statistically significant ($p < 0.05$) (Table A5). The best significant correlation was obtained among PCB classes from tri-to hepta-chlorinated. This is comparable to the equation obtained by (Belfroid et al., 1993) who exposed a similar species (*Eisenia andrei* Bouché) to a mixture of chlorobenzenes with Log K_{OW} ranging between 4.2 and 5.7 in an aqueous static test system. Also Van Der Wal and coworkers (van der Wal et al., 2004) used an experimental setup similar to our work utilizing the species *Eisenia andrei* and *Aporrectodea caliginosa* and three different contaminated soil in a lab experiment. They also measured bioavailable concentrations in soil water using SPME and later developed a linear bioconcentration relationship with Log K_{OW} up to their most hydrophobic PCB (PCB 180). These two experiments from the literature were, however, conceived for a relatively narrow range of hydrophobicity. Looking at the most hydrophobic classes measured in the experiment of the present work (octa-, nona-, and deca-PCBs) (Fig. A5, red points in the top graph) the BCF, even using bioavailable concentrations in pore water, dropped dramatically. This behavior can be probably explained by a non-equilibrium state (not enough time to reach equilibrium for these chemicals) and/or a third phase effect or slow kinetic in partitioning (Mackay et al., 2019). On the other hand, sulfonated and hydroxy-sulfonated-PCBs seemed to be independent of Log K_{OW}. The Log BCF oscillated around 2 for the sulfonated-PCBs while it appeared slightly smaller for hydroxy-sulfonated-PCBs (around 1.6), although a precise comparison is difficult due to the uncertainty in the measurements and the lack of precise congener identity and standards. As seen previously for BAFs, these highly polar metabolites were very poorly bioaccumulated compared to the parent compounds. Although not many studies are available on polar chemical uptake in earthworms (Gobas et al., 2016), a similar range of BCF (Log BCF = 1.33) was obtained by (Carter et al., 2014). They described the properties of diclofenac, a polar pharmaceutical (Log K_{OW} = 4.02, pKa = 4.12) with the similar hydrophobicity of hexa-chlorinated sulfonated-PCBs (Table 1) and a pKa which shows a practically complete dissociation at pH around 7. (Fig. A5)

BCF was also plotted against Log D for the metabolites (Table 1) and the results are shown in Fig. A6. Log BCFs values were generally smaller (except for hydroxy-PCBs) since the calculation of the concentration of metabolites in pore water ($Cw_{(free)}$) would be much higher when the chemical is dissociated, depending on chemical pKa and environmental pH. The values for Log D for hydroxylated-PCBs are also in a similar range to the Log K_{OW} values with an important exception: the nona-chlorinated hydroxy-PCBs, given their pKa have a Log D value at pH 7 which is smaller than octa- and hepta-. This fact, together with the higher concentration in pore water due to the large dissociation also resulted in the lowest BCF for these classes. The BCF - Log D plot (see Table A6 for significance of regression) for sulfonated and hydroxy-sulfonated PCBs shows much lower BCFs compared to those in Fig. 3 and A5 and also Log D values which are much smaller than the corresponding Log K_{OW} values, evidencing again the importance of the larger dissociated fraction in water.

3.4. Field bioaccumulation experiment

The third experiment was designed to verify whether field based and lifetime uptake of PCBs and metabolites in earthworms was comparable to the lab experiment, conducted with a soil with similar levels and fingerprint of PCBs and metabolites. While in laboratory the experimental conditions can be standardized to reduce variability, no additional information on field bioaccumulation behaviour of wild species can be obtained. For example, in field, species with preferable niches, such as depth living range can be found. This preferential behavior will be reflected in a potential large difference in exposure conditions: for example, the contaminated soils of the SIN Brescia-Caffaro showed a strong gradient of PCB concentrations with depth. In a recent paper, Di Guardo et al. (Di Guardo et al., 2020) showed that PCB concentrations of mono to deca chlorinated congener families can vary up to 2 orders of magnitude in the first 1 m; while concentrations are, as expected, rather homogeneous in the plow layer, they substantially drop in the following 70 cm. Therefore, epigeic (living and feeding in the litter layer) and endogeic earthworm species (living in the top soil) (EC, 2010) are probably exposed to the largest concentrations. Among epigeic species we can find *Eisenia* spp. and among endogeic we can find *Aporrectodea caliginosa*, *Allolobophora chlorotica* (Thakuria et al., 2010). On the other hand, anecic species, such as *Lumbricus terrestris*, may spend a considerable amount of their time in deep mineral soil layers by digging vertical borrows up to 1–2 m and, generally reaching the soil surface at

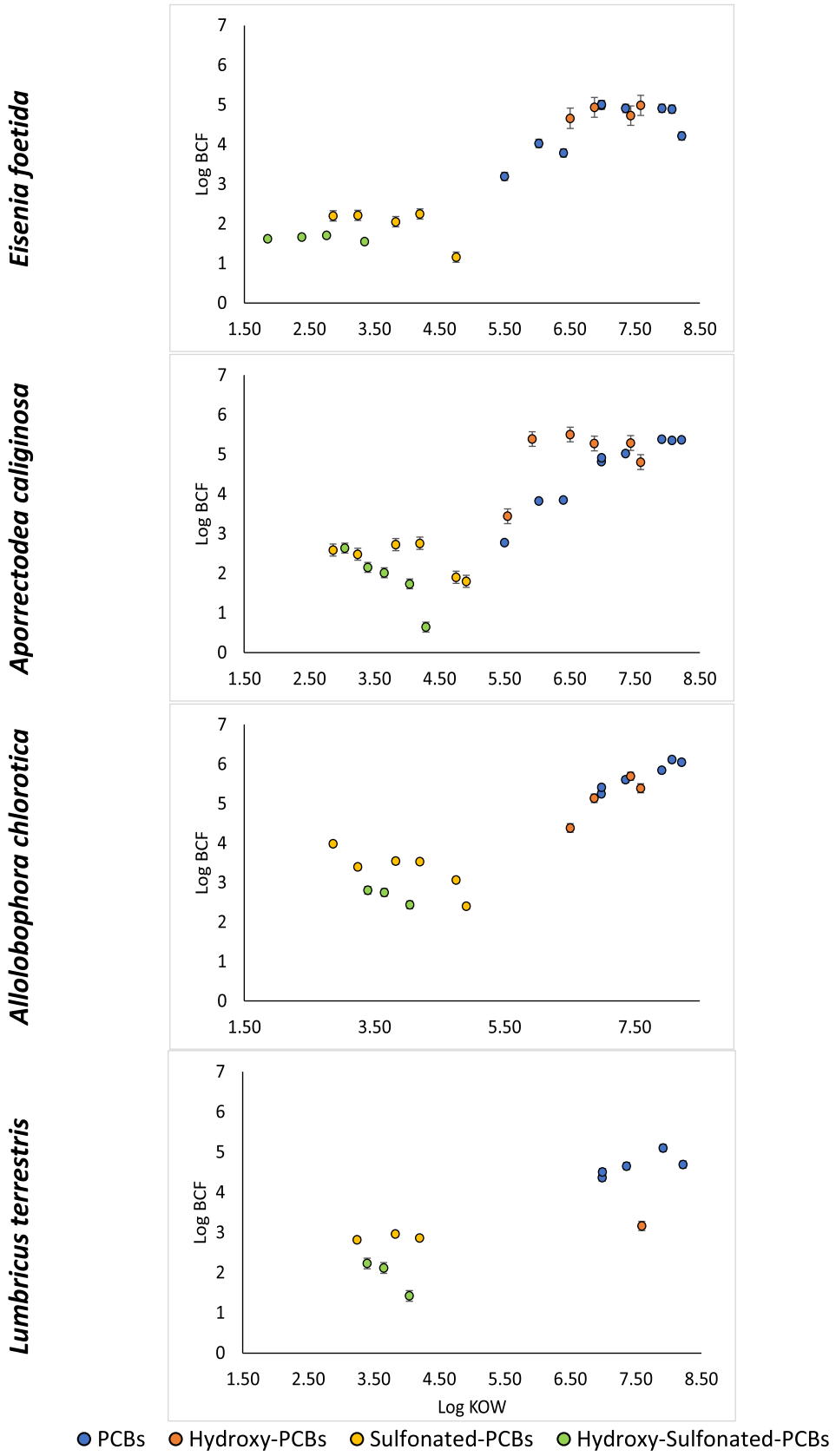

Fig. 3. Log BCF of PCB and polar metabolite (L/kg) vs Log K_{OW} for the lab (first on top) and field experiments. Whiskers represent standard deviation.

night to feed (Brown et al., 2000; Curry and Schmidt, 2007). For these reasons, anecic species may escape from contaminated surface layer (Blouin et al., 2013; EC, 2010), accumulating PCBs when they feed in the top soil layers, and depurating while they move to bottom layers.

More polar chemicals (such as lighter PCBs, e. g. mono to tri-PCBs) do move to higher depths, while more hydrophobic congeners are generally restricted to more superficial layers due to their soil-water partition coefficient (Di Guardo et al., 2020). PCB metabolites, such as those investigated in the present work, have a more polar nature than the corresponding parental chlorinated family, potentially reaching

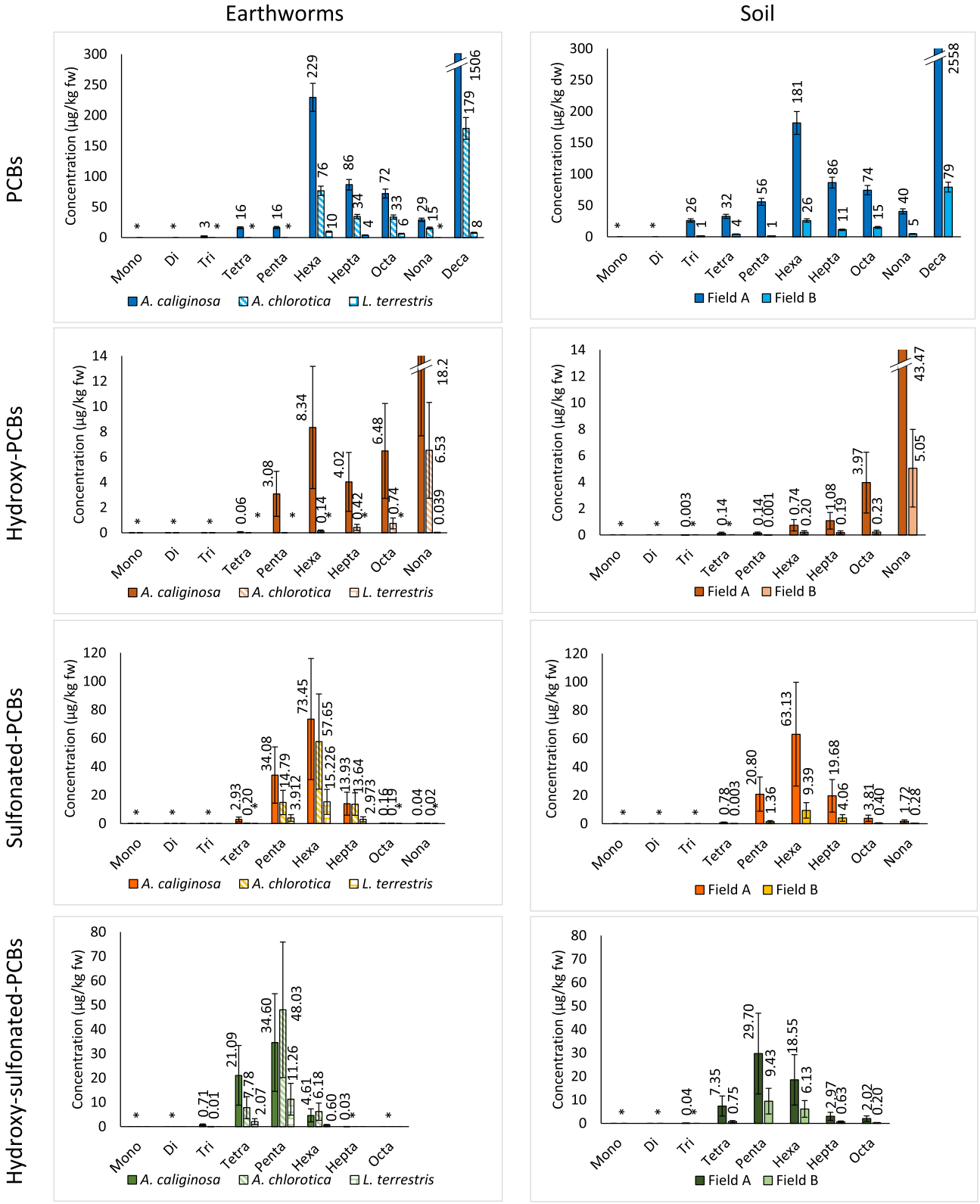

Fig. 4. PCB and PCB metabolite concentrations (µg/kg) referred to each family of congeners measured in the experiment 3. Asterisks (*) refer to values below LOQs. Bars represent the analytical variability.

higher depths. The polarity and their moving ability increase from hydroxy to sulfonated and to hydroxy-sulfonated-PCBs given their properties (Table 1).

The concentrations in earthworms and soil (Fig. 4), although different between field A and B seem to generally match more in terms of abundance and fingerprint between earthworms and soil especially for *Aporrectodea caliginosa* and *Allolobophora chlorotica*. BAFs of PCBs and metabolites for this experiment are shown in Fig. A7and A8 (expressed on a dw to dw basis), while the corresponding regression are in Table A7. The data suggest similar consideration of the experiment 2 for *A. caliginosa* and *A. chlorotica* although a different behavior could be observed for the anecic species (*Lumbricus terrestris*), where for example only one BAF for nona-hydroxy-PCBs can be found. Regressions of Log BAF vs. Log K_{OW} were significant only for *A. caliginosa* (PCBs, sulfonated-PCBs and hydroxy-sulfonated-PCBs), *A. chlorotica* (sulfonated-PCBs). Fig. A9 reports BSAFs for this experiment, which do not introduce additional information than BAF as for the lab experiment.

The BCFs calculated for the field experiment are shown in Fig. 3 (for a comparative picture) and Fig. A10 and Table A8 (for single chemical class and species), plotted as before against Log K_{OW}, and later against Log D (Figure A11). In the Log BCF-Log K_{OW} plot, when comparing PCBs, we observe that for field accumulating earthworms (with the exclusion of *Lumbricus terrestris*) the accumulation is linear also for the most chlorinated classes with $R^2 > 0.90$ and a p-value < 0.005. This probably depends on the longer time available for the accumulation of these very highly hydrophobic classes which shows the importance of kinetics in accumulation and the need of field-based experiment to verify lab experiment assumptions. The anecic species (*L. terrestris*) shows instead a different accumulation from *A. chlorotica* (ANCOVA, $p = 0.01$), but not from *A. caliginosa* (ANCOVA, $p = 0.923$). *L. terrestris* also shows a lack of lighter congener accumulation which probably depends on the fact that it transiently feeds or gets in contact with the most contaminated top layers. In a recent paper (Di Guardo et al., 2020) it was shown that in the same field where the samples of this experiment were taken, the concentration with depth dropped between two to three orders of magnitude from top layers (0–30 cm) to deeper layers (70–100 cm). The lack of correlation between PCB BCF and Log K_{OW} for this species probably depends on the traveling activity depicted above. Going to the metabolites, it appears instead that the accumulation behavior is similar to those seen in experiment 2 for the sulfonated and hydroxy-PCBs. The regression for sulfonated-PCBs was steeper for *A. chlorotica* than the one for *E. foetida* (lab experiment) (ANCOVA, $p < 0.0001$). Although a full explanation of this behavior cannot be given with the present knowledge it can be hypothesized that the longer contact time allows for this different accumulation.

BCF was also plotted against Log D for *A. caliginosa* as an example (see Table A9 for the significance of the regressions). The results (Fig. A11) are very similar to those shown for the lab experiment (Fig. A6) with the only difference that, given the highest concentrations in the soil and the long exposure time some more chlorination classes were present.

4. Conclusions

This is the first paper, to our knowledge, reporting the accumulation of highly hydrophobic PCBs (from hepta-to deca-chlorinated), hydroxy-PCBs, and of the recently discovered sulfonated and hydroxy-sulfonated PCBs in earthworms. By comparing chemicals with such a large span of chemical domain (Log K_{OW} and/or Log D) and polarity (as shown by the pKa) this study allows to evaluate the accumulation of poorly investigated chemicals (Di Guardo and Hermens, 2013; Gobas et al., 2016). The results obtained showed a reduced accumulation of highly hydrophobic PCBs in earthworms (Log $K_{OW} > 7$). The accumulation of hydroxy PCBs increased with Log K_{OW}, while the accumulation of sulfonated and hydroxy-sulfonated was markedly reduced with the increase of polarity of the metabolite, given to the low pKas. The exploitation of BCFs vs. Log D correlation allowed to evaluate the potential bioaccumulation in earthworms of chemical classes possessing both a hydrophobic nature (related to the increasing number of chlorine substituent) and a very polar fraction depending on the acidic dissociation at environmental pHs. Further studies are needed to evaluate, for example, the extent of degradability of PCBs in earthworms and their potential metabolic conversion rate to sulfonated compounds and/or their derivation from hydroxylated-PCBs, metabolites also found in earthworms (He et al., 2018). In order to perform these experiments, laboratory standards of sulfonated metabolites of PCBs will be needed to more accurately quantify the bioaccumulation and the potential additional conversion, as well as the experimental determination of soil-water partition coefficients.

Author statement

Jessica Palladini: Investigation, Writing – original draft preparation, Visualization; **Renzo Bagnati**: Methodology, Writing – review & editing; **Alice Passoni**: Investigation; **Enrico Davoli**: Resources; **Alessia Lanno**: Investigation; **Elisa Terzaghi**: Resources, Data curation, Writing – review & editing; **Parisa Falakdin**: Investigation; **Antonio Di Guardo**: Funding acquisition, Resources, Writing – review & editing, Supervision

Declaration of competing interest

The authors declare that they have no known competing financial interests or personal relationships that could have appeared to influence the work reported in this paper.

Acknowledgements

The Department of Science and High Technology of University of Insubria is acknowledged for funding ET salary. Stefano Armiraglio (Municipality of Brescia), Simone Anelli (ERSAF Brescia) and Pierino Antonioli (Brescia) are acknowledged for the help during field work. Giovanni Palmisano and Paola Gramatica of University of Insubria are kindly acknowledged for the useful discussions on chemical features and properties.

Appendix A. Supplementary data

Supplementary data to this article can be found online at https://doi.org/10.1016/j.envpol.2021.118507.

References

Bagnati, R., Terzaghi, E., Passoni, A., Davoli, E., Fattore, E., Maspero, A., Palmisano, G., Zanardini, E., Borin, S., Di Guardo, A., 2019. Identification of sulfonated and hydroxy-sulfonated polychlorinated biphenyl (PCB) metabolites in soil: new classes of intermediate products of PCB degradation? Environ. Sci. Technol. 53, 10601–10611. https://doi.org/10.1021/acs.est.9b03010.

Belfroid, A., van den Berg, M., Seinen, W., Hermens, J., van Gestel, K., 1995. Uptake, bioavailability and elimination of hydrophobic compounds in earthworms (*Eisenia andrei*) in field-contaminated soil. Environ. Toxicol. Chem. 14, 605–612. https://doi.org/10.1002/etc.5620140408.

Belfroid, A., Vanwezel, A., Sikkenk, M., Vangestel, K., Seinen, W., Hermens, J., 1993. The toxicokinetic behavior of chlorobenzenes in earthworms (Eisenia andrei): experiments in water. Ecotoxicol. Environ. Saf. 25, 154–165. https://doi.org/10.1006/eesa.1993.1014.

Blouin, M., Hodson, M.E., Delgado, E.A., Baker, G., Brussaard, L., Butt, K.R., Dai, J., Dendooven, L., Peres, G., Tondoh, J.E., Cluzeau, D., Brun, J.-J., 2013. A review of earthworm impact on soil function and ecosystem services: earthworm impact on ecosystem services. Eur. J. Soil Sci. 64, 161–182. https://doi.org/10.1111/ejss.12025.

Boon, J.P., Meer, J. van der, Allchin, C.R., Law, R.J., Klungsøyr, J., Leonards, P.E.G., Spliid, H., Storr-Hansen, E., Mckenzie, C., Wells, D.E., 1997. Concentration-dependent changes of PCB patterns in fish-eating mammals: structural evidence for induction of cytochrome P450. Arch. Environ. Contam. Toxicol. 33, 298–311. https://doi.org/10.1007/s002449900257.

Breivik, K., Sweetman, A., Pacyna, J., Jones, K., 2002. Towards a global historical emission inventory for selected PCB congeners — a mass balance approach1. Global

production and consumption. Sci. Total Environ. 290, 181–198. https://doi.org/10.1016/S0048-9697(01)01075-0.
Brown, G.G., Barois, I., Lavelle, P., 2000. Regulation of soil organic matter dynamics and microbial activityin the drilosphere and the role of interactionswith other edaphic functional domains. Eur. J. Soil Biol. 36, 177–198. https://doi.org/10.1016/S1164-5563(00)01062-1.
Campbell, L.M., Muir, D.C.G., Whittle, D.M., Backus, S., Norstrom, R.J., Fisk, A.T., 2003. Hydroxylated PCBs and other chlorinated phenolic compounds in lake trout (*Salvelinus namaycush*) blood plasma from the great lakes region. Environ. Sci. Technol. 37, 1720–1725. https://doi.org/10.1021/es026225m.
Carter, L.J., Garman, C.D., Ryan, J., Dowle, A., Bergstroem, E., Thomas-Oates, J., Boxall, A.B.A., 2014. Fate and uptake of pharmaceuticals in soil-earthworm systems. Environ. Sci. Technol. 48, 5955–5963. https://doi.org/10.1021/es500567w.
Curry, J.P., Schmidt, O., 2007. The feeding ecology of earthworms – a review. Pedobiologia 50, 463–477. https://doi.org/10.1016/j.pedobi.2006.09.001.
Di Guardo, A., Hermens, J.L., 2013. Challenges for exposure prediction in ecological risk assessment: challenges in Exposure Prediction. Integr. Environ. Assess. Manag. 9, e4–e14. https://doi.org/10.1002/ieam.1442.
Di Guardo, A., Raspa, G., Terzaghi, E., Vergani, L., Mapelli, F., Borin, S., Zanardini, E., Morosini, C., Anelli, S., Nastasio, P., Sale, V.M., Armiraglio, S., 2020. PCB vertical and horizontal movement in agricultural soils of a highly contaminated site: role of soil properties, cultivation history and PCB physico-chemical parameters. Sci. Total Environ. 747, 141477. https://doi.org/10.1016/j.scitotenv.2020.141477.
Di Guardo, A., Terzaghi, E., Raspa, G., Borin, S., Mapelli, F., Chouaia, B., Zanardini, E., Morosini, C., Colombo, A., Fattore, E., Davoli, E., Armiraglio, S., Sale, V.M., Anelli, S., Nastasio, P., 2017. Differentiating current and past PCB and PCDD/F sources: the role of a large contaminated soil site in an industrialized city area. Environ. Pollut. 223, 367–375. https://doi.org/10.1016/j.envpol.2017.01.033.
Ec, 2010. European Atlas of Soil Biodiversity, Atlas Series. Published by the Publications Office of the European Union, Luxembourg.
Gobas, F.A., Burkhard, L.P., Doucette, W.J., Sappington, K.G., Verbruggen, E.M., Hope, B.K., Bonnell, M.A., Arnot, J.A., Tarazona, J.V., 2016. Review of existing terrestrial bioaccumulation models and terrestrial bioaccumulation modeling needs for organic chemicals: terrestrial Bioaccumulation Models. Integr. Environ. Assess. Manag. 12, 123–134. https://doi.org/10.1002/ieam.1690.
Grimm, F.A., Hu, D., Kania-Korwel, I., Lehmler, H.-J., Ludewig, G., Hornbuckle, K.C., Duffel, M.W., Bergman, A., Robertson, L.W., 2015. Metabolism and metabolites of polychlorinated biphenyls. Crit. Rev. Toxicol. 45, 245–272. https://doi.org/10.3109/10408444.2014.999365.
Hallgren, P., Westbom, R., Nilsson, T., Sporring, S., Björklund, E., 2006. Measuring bioavailability of polychlorinated biphenyls in soil to earthworms using selective supercritical fluid extraction. Chemosphere 63, 1532–1538. https://doi.org/10.1016/j.chemosphere.2005.09.007.
Hansch, C., Leo, A., 1995. Exploring QSAR, ACS Professional Reference Book. American Chemical Society, Washington, DC.
Haraguchi, K., 2004. Comparative metabolism OF polychlorinated biphenyls and tissue distribution OF persistent metabolites IN rats, hamsters, and Guinea pigs. Drug Metab. Dispos. 33, 373–380. https://doi.org/10.1124/dmd.104.002444.
He, Z., Xu, Y., Wang, W., Liu, X., 2018. Stereoselective bioaccumulation and elimination of chiral PCBs 95 and 149 in earthworm Eisenia fetida. Chemosphere 212, 497–503. https://doi.org/10.1016/j.chemosphere.2018.08.075.
IARC, 2015. Polychlorinated Biphenyls and Polybrominated Biphenyls. International Agency for Research on Cancer.
ITRC, 2012. Incremental Sampling Methodology. (No. ISM-1). Interstate Technology & Regulatory Council, Incremental Sampling Methodology Team, Washington, D.C.
Jager, T., van der Wal, L., Fleuren, R.H.L.J., Barendregt, A., Hermens, J.L.M., 2005. Bioaccumulation of organic chemicals in contaminated soils: evaluation of bioassays with earthworms. Environ. Sci. Technol. 39, 293–298. https://doi.org/10.1021/es035317o.
Karasek, F.W., Hutzinger, O., Safe, S., 1985. Mass Spectrometry in Environmental Sciences.
Krauss, M., Wilcke, W., Zech, W., 2000. Availability of polycyclic aromatic hydrocarbons (PAHs) and polychlorinated biphenyls (PCBs) to earthworms in urban soils. Environ. Sci. Technol. 34, 4335–4340. https://doi.org/10.1021/es001137s.
Li, X., Liu, Y., Martin, J.W., Cui, J.Y., Lehmler, H.-J., 2021. Nontarget analysis reveals gut microbiome-dependent differences in the fecal PCB metabolite profiles of germ-free and conventional mice. Environ. Pollut. 268, 115726. https://doi.org/10.1016/j.envpol.2020.115726.
Liu, Y., Richardson, E.S., Derocher, A.E., Lunn, N.J., Lehmler, H.-J., Li, X., Zhang, Y., Cui, J.Y., Cheng, L., Martin, J.W., 2018. Hundreds of unrecognized halogenated contaminants discovered in polar bear serum. Angew. Chem. Int. Ed. 57, 16401–16406. https://doi.org/10.1002/anie.201809906.
Lyman, W.J., Reehl, W.F., Rosenblatt, D.H., 1990. Handbook of Chemical Property Estimation Methods: Environmental Behavior of Organic Compounds. American Chemical Society, Washington, DC.
Mackay, D., Celsie, A.K.D., Parnis, J.M., 2019. Kinetic delay in partitioning and parallel particle pathways: underappreciated aspects of environmental transport. Environ. Sci. Technol. 53, 234–241. https://doi.org/10.1021/acs.est.8b04514.
Mackay, D., Shiu, W.Y., Ma, K.-C. (Eds.), 2006, Handbook of Physical-Chemical Properties and Environmental Fate for Organic Chemicals -, second ed., vol. 2. CRC/Taylor & Francis, Boca Raton, FL.
Maidment, D.R., 1993. Handbook of Hydrology. McGraw-Hill Education.
Marek, R.F., Martinez, A., Hornbuckle, K.C., 2013. Discovery of hydroxylated polychlorinated biphenyls (OH-PCBs) in sediment from a lake Michigan waterway and original commercial aroclors. Environ. Sci. Technol. 47, 8204–8210. https://doi.org/10.1021/es402323c.
Matscheko, N., Tysklind, M., de Wit, C., Bergek, S., Andersson, R., Sellström, U., 2002. Application of sewage sludge to arable land-soil concentrations of polybrominated diphenyl ethers and polychorinated dibenzo- *p* -dioxins, dibenzofurans, and biphenyls, and their accumulation in earthworms. Environ. Toxicol. Chem. 21, 2515–2525. https://doi.org/10.1002/etc.5620211201.
McLachlan, M.S., 1995. Bioaccumulation of hydrophobic chemicals in agricultural food chains. Environ. Sci. Technol. 30, 252–259.
Northcott, G.L., Jones, K.C., 2000. Spiking hydrophobic organic compounds into soil and sediment: a review and critique of adopted procedures. Environ. Toxicol. Chem. 19, 2418–2430. https://doi.org/10.1002/etc.5620191005.
Ockenden, W.A., Breivik, K., Meijer, S.N., Steinnes, E., Sweetman, A.J., Jones, K.C., 2003. The global re-cycling of persistent organic pollutants is strongly retarded by soils. Environ. Pollut. 121, 75–80. https://doi.org/10.1016/S0269-7491(02)00204-X.
Paasivirta, J., Sinkkonen, S.I., 2009. Environmentally relevant properties of all 209 polychlorinated biphenyl congeners for modeling their fate in different natural and climatic conditions. J. Chem. Eng. Data 54, 1189–1213. https://doi.org/10.1021/je800501h.
Pignatello, J.J., Xing, B., 1996. Mechanisms of slow sorption of organic chemicals to natural particles. Environ. Sci. Technol. 30, 1–11. https://doi.org/10.1021/es940683g.
Reid, B.J., Northcott, G.L., Jones, K.C., Semple, K.T., 1998. Evaluation of spiking procedures for the introduction of poorly water soluble contaminants into soil. Environ. Sci. Technol. 32, 3224–3227. https://doi.org/10.1021/es9800941.
Rezek, J., Macek, T., Mackova, M., Triska, J., 2007. Plant metabolites of polychlorinated biphenyls in hairy root culture of black nightshade Solanum nigrum SNC-9O. Chemosphere 69, 1221–1227. https://doi.org/10.1016/j.chemosphere.2007.05.090.
Rodriguez-Campos, J., Dendooven, L., Alvarez-Bernal, D., Contreras-Ramos, S.M., 2014. Potential of earthworms to accelerate removal of organic contaminants from soil: a review. Appl. Soil Ecol. 79, 10–25. https://doi.org/10.1016/j.apsoil.2014.02.010.
Shang, H., Wang, P., Wang, T., Wang, Y., Zhang, H., Fu, J., Ren, D., Chen, W., Zhang, Q., Jiang, G., 2013. Bioaccumulation of PCDD/Fs, PCBs and PBDEs by earthworms in field soils of an E-waste dismantling area in China. Environ. Int. 54, 50–58. https://doi.org/10.1016/j.envint.2013.01.006.
Sun, J., Pan, L., Su, Z., Zhan, Y., Zhu, L., 2016. Interconversion between Methoxylated and Hydroxylated Polychlorinated Biphenyls in Rice Plants: an Important but Overlooked Metabolic Pathway. https://doi.org/10.1021/acs.est.6b00266 [WWW Document].
Tehrani, R., Van Aken, B., 2014. Hydroxylated polychlorinated biphenyls in the environment: sources, fate, and toxicities. Environ. Sci. Pollut. Res. 21, 6334–6345. https://doi.org/10.1007/s11356-013-1742-6.
Terzaghi, E., Vergani, L., Mapelli, F., Borin, S., Raspa, G., Zanardini, E., Morosini, C., Anelli, S., Nastasio, P., Sale, V.M., Armiraglio, S., Di Guardo, A., 2019. Rhizoremediation of weathered PCBs in a heavily contaminated agricultural soil: results of a biostimulation trial in semi field conditions. Sci. Total Environ. 686, 484–496. https://doi.org/10.1016/j.scitotenv.2019.05.458.
Thakuria, D., Schmidt, O., Finan, D., Egan, D., Doohan, F.M., 2010. Gut wall bacteria of earthworms: a natural selection process. ISME J. 4, 357–366. https://doi.org/10.1038/ismej.2009.124.
Ueno, D., Darling, C., Alaee, M., Campbell, L., Pacepavicius, G., Teixeira, C., Muir, D., 2007. Detection of hydroxylated polychlorinated biphenyls (OH-PCBs) in the abiotic environment: surface water and precipitation from ontario, Canada. Environ. Sci. Technol. 41, 1841–1848. https://doi.org/10.1021/es061539l.
van der Wal, L., Jager, T., Fleuren, R.H.L.J., Barendregt, A., Sinnige, T.L., van Gestel, C.A.M., Hermens, J.L.M., 2004. Solid-phase microextraction to predict bioavailability and accumulation of organic micropollutants in terrestrial organisms after exposure to a field-contaminated soil. Environ. Sci. Technol. 38, 4842–4848. https://doi.org/10.1021/es035318g.
Vermeulen, F., Covaci, A., D'Havé, H., Van den Brink, N.W., Blust, R., De Coen, W., Bervoets, L., 2010. Accumulation of background levels of persistent organochlorine and organobromine pollutants through the soil–earthworm–hedgehog food chain. Environ. Int. 36, 721–727. https://doi.org/10.1016/j.envint.2010.05.006.
Vitale, C.M., Knudsmark Sjøholm, K., Di Guardo, A., Mayer, P., 2019. Accelerated equilibrium sampling of hydrophobic organic chemicals in solid matrices: a proof of concept on how to reach equilibrium for PCBs within 1 day. Chemosphere 237, 124537. https://doi.org/10.1016/j.chemosphere.2019.124537.
Zhai, G., Lehmler, H.-J., Schnoor, J.L., 2013. Sulfate metabolites of 4-monochlorobiphenyl in whole poplar plants. Environ. Sci. Technol. 47, 557–562. https://doi.org/10.1021/es303807f.